*Author:*
**Ituarte, Lia S**

*Title:*
**Exploring differential erosion patterns using volcanic edifices as a proxy in South America**

# Exploring differential erosion patterns using volcanic edifices as a proxy in South America

Lia S. Ituarte

A dissertation submitted to the University of Bristol in accordance with the requirements for award of the degree of Master by Research in the Faculty of Science, School of Earth Sciences, October 2020.

61425 words

# Abstract

Porphyry Copper Deposit (PCD) exploration faces a challenging future, since promising areas for exploration are buried. PCDs form at kilometres depth, while volcanoes are the surface expression of extensive magmatic systems. Although not all volcanoes generate PCDs, it may be that all PCDs formed under a volcanic centre. As there are no complete magmatic-volcanic profiles available, I study the distribution of the exposed magmatic-volcanic portions. In this study, I compile eruption, volcano and PCD data for the Andes and then develop a tool to identify favourable areas for finding porphyries close to the surface. This methodology, however, does not distinguish enriched from barren porphyries, nor detect the intensity of the mineralization.

My results show when exploring for PCDs, high prospectivity areas are the eroded and remaining edifices of inactive stratovolcanoes. They also show that volcano erosion and PCD exposure in the Andes depend strongly on climate. There is a negative correlation between height and more humid climate for Pre-Quaternary edifices and, as the number of volcanoes drops with wetter conditions, the numbers of mineralised deposits rise. This trend of reduced number and height of edifices continues towards extreme latitudes, as well as close to the current Chilean coastline, the Intermediate depression and Precordillera. This suggests a strong erosion gradient increasing towards the south and west of the Andes.

The Arica Bend region and the Precordillera are areas of great importance, since they reflect the greatest exhumation in the Andes by exposing mineralised intrusions, therefore it becomes enormously relevant distinguishing these regions of high-erosion (South Peruvian Cordillera) from low-erosion (Altiplano plateau). Geomorphology is a promising tool for finding PCDs, since paleosurfaces could protect and preserve mineralised intrusions, while coupled mechanisms (tectonic uplift and climate) may facilitate the exposure of PCDs by river incision or rotational landslides.

# Dedication

To my family,
without whom none of my achievements would have been possible.

# Acknowledgements

I want to thank BHP for the financial support and the information provided during the database creation stage, also to Thiago Oliveira (BHP) and Cam McCuaig (BHP) for their collaboration, constant feedback and enthusiasm on my results.

I would also like to thank Laura Evenstar and Anne Mather for plenty of discussions and for showing me how to fall in love of Geomorphology. Especial thanks to Laura, who reviewed some chapters of my thesis.

Finally, I am profoundly grateful to my supervisor, Alison Rust, who went far and beyond her responsibilities, motivated me with her extensive knowledge in volcanology during these years and encouraged me to finish this work.

# Author’s declaration

I declare that the work in this dissertation was carried out in accordance with the requirements of the *University's Regulations and Code of Practice for Research Degree Programmes* and that it has not been submitted for any other academic award. Except where indicated by specific reference in the text, the work is the candidate's own work. Work done in collaboration with, or with the assistance of, others, is indicated as such. Any views expressed in the dissertation are those of the author.

SIGNED: ..... DATE: .....

# Table of Contents

*Exploring differential erosion patterns using volcanic edifices as a proxy in South America....1*

*Abstract....2*

*Dedication....3*

*Acknowledgements....4*

*Author's declaration....5*

*1 Chapter 1: Introduction....13*

1.1 Comparing PCDs against modern volcanoes....14
1.1.1 Eruptive and fertile periods versus dormancy and barren epochs....22
1.1.2 Timing: PCD development and volcanic activity....24
1.1.3 Distribution of volcanoes and PCDs....26

1.2 The Andes....26
1.2.1 Evolution of the Andes: tectonics, climate, erosion and magmatism....26
1.2.2 Magmatism....28
1.2.3 Tectonics....30
*1.2.3.1 Uplift during Eocene to Oligocene....31*
*1.2.3.2 Uplift during Oligocene to present day....32*
*1.2.3.3 The Bolivian Orocline....33*
*1.2.3.4 Precordillera region....34*
*1.2.3.5 Tectonic Segments....35*
*1.2.3.6 Sediment control on subduction plate speeds....35*
*1.2.3.7 Crust Destruction and Mass Wasting....39*
1.2.4 Climate....39
*1.2.4.1 Summary of the climate control in the Andes....39*
*1.2.4.2 Summary of the climate in the western Andes....40*
*1.2.4.3 Summary of the climate in the eastern Andes....41*
1.2.5 Erosion....42
1.2.6 Surface evolution of volcano edifices....49
*1.2.6.1 Stratovolcanoes morphometric model....49*
*1.2.6.2 Evolution model for the degradation for Central Andean volcanoes....50*
1.2.7 Porphyry deposits in the Andes....52
*1.2.7.1 PCDs exhumation....52*
*1.2.7.2 PCDs types and relation to depth of formation....53*

1.3 Summary....54

*2 Chapter 2: Database creation and basic analysis....57*

2.1 Dataset of volcanoes and eruptions....57
2.1.1 Database compilation....57
2.1.2 Database design....62

2.2 Appendix III: Dataset of Porphyry Copper Deposits (PCDsDB)....66

2.3 Dataset combination of volcanoes, eruptions and PCDs and AVEDB subsets....66
2.3.1 Appendix IV: Dataset of volcanoes, eruptions and PCDs....66
2.3.2 Appendix V: AVEDB subsets....67

*3 Chapter 3: Descriptive Statistical Analysis of the AVEDB....68*

3.1 Introduction....68

3.2 Methodology....69

3.3 Initial analysis: Understanding raw data. ..... 70
3.3.1 Valid, missing and non-valid values ..... 70
3.4 Results for Volcanic edifices ..... 71
3.4.1 Descriptive analysis for volcano parameters ..... 72
3.5 Results for Volcanism ..... 91
3.5.1 Descriptive analysis for eruption parameters ..... 91
3.6 Results for Tectonics and Morphotectonic provinces ..... 95
3.6.1 Descriptive analysis for Tectonic parameters ..... 95
3.6.2 Morphotectonic provinces ..... 98
3.7 Conclusions ..... 102
*4 Chapter 4: Assessing erosional patterns in the Andes ..... 103*
4.1 Scope of this study ..... 103
4.2 Methodology ..... 105
4.3 Spatial distribution of volcanoes and PCDs depending on time epochs ..... 106
4.3.1 Cretaceous volcanoes and PCDs ..... 106
4.3.2 Palaeocene volcanoes and PCDs ..... 107
4.3.3 Eocene volcanoes and PCDs ..... 112
4.3.4 Oligocene volcanoes and PCDs ..... 116
4.3.5 Miocene volcanoes ..... 119
4.3.6 Pleistocene and Holocene ..... 119
4.3.7 Variation in edifice height with spatial location ..... 121
4.3.8 Differential erosion related to climate ..... 130
4.4 Discussion ..... 134
4.4.1 Spatial distribution of volcanoes and PCDs depending on time epochs ..... 134
4.4.2 Variation in edifice height depending on spatial location ..... 137
4.4.3 Differential erosion related to climate ..... 140
4.5 Conclusions ..... 145
*5 Chapter 5: Summary and further work ..... 148*
*6 References ..... 151*
*7 Appendices ..... 166*
7.1 Appendix I ..... 166
7.1.1 Database design ..... 166
7.2 Appendix II ..... 196
7.3 Appendix III ..... 196
7.3.1 Database design ..... 196
7.4 Appendix IV ..... 199
7.5 Appendix V ..... 199

# List of tables

Table 2-1: Summary of sources of data on volcanoes and eruptions included in AVEDB. ..... 57
Table 2-2: Volcano type classification. ..... **Error! Bookmark not defined.**

Table 2-3: Volcano size classification of Castruccio (2017). .....**Error! Bookmark not defined.**
Table 2-4: Erosion status classification for volcanoes edifices (De Silva et al., 1991).....**Error! Bookmark not defined.**
Table 2-5: Rock name classified as per composition.....**Error! Bookmark not defined.**
Table 2-6: Eruption age recalculations.....**Error! Bookmark not defined.**
Table 2-7: Age classes and age periods.....**Error! Bookmark not defined.**
Table 2-8: Dating methods and codes. .....**Error! Bookmark not defined.**
Table 2-9: Tectonic settings and margins.....**Error! Bookmark not defined.**
Table 2-10: Climate classification following a determined Annual precipitation rate.....**Error! Bookmark not defined.**
Table 3-1. Descriptive statistics for volcanic edifice height (m). .....73
Table 3-2. Descriptive statistics for Cone Diameter (km). .....77
Table 3-3. H/D ratio outliers and age estimation.....79
Table 3-4. Descriptive statistics for Volcano volume (km3). .....80
Table 3-5. Descriptive statistics for Crater Diameter (km).....82
Table 3-6. Percentiles and the minimum value to be an upper outlier for the Volcano parameters considered for the multiple correlation analysis. .....86
Table 3-7. Descriptive statistics for the Volcano parameters values considered for the multiple correlation analysis. .....86
Table 3-8. Correlation matrix showing the relationship between variables. .....87
Table 3-9. Multiple correlation models with the volcano height (m) as the dependent variable, where each model will progressively include an independent variable. .....90
Table 3-10. Multiple correlation models, where each model will progressively include an independent variable. .....91
Table 3-11. Descriptive statistics for eruption parameters. .....91
Table 4-12: ANOVA analysis for volcanic edifices height grouped by morphotectonic provinces. .....123
Table 4-13: Multiple comparisons for volcanic edifice height and Morphotectonic provinces, using the Tukey test. .....124

# List of figures

Figure 1-1. a. Grasberg igneous complex in Indonesia, showing the dimension and shape of the complex, the presence of volcaniclastics, shales dipping to the centre of the complex and rhyodacitic intrusions (modified from Patterson and Cloos, 2005). b. Distribution of plutonic bodies, stocks and dikes in the Farallón Negro complex, Argentina (from Llambías, 1972). .....15
Figure 1-2. Satellite images from Google Earth showing crater diameters for: a. El Chaitén volcano in Chile (Simmon R., 2010) and b. Cerro Machín in Colombia (Google Earth image). c. Satellite images showing the location of caldera rims, lava domes and landslides from the NASA's Earth Observatory for El Chaitén volcano and Mount St Helens (Simmon R., 2010). .....17
Figure 1-3. Figure from Sillitoe, 1973, showing a simple cross-section across the Farallón Negro volcanic-intrusive complex, including a reconstructed volcanic edifice on top. .....19
Figure 1-4. a. Geological model of El Teniente copper porphyry in northern Chile, showing the upper connections of a hypabyssal body in the form of stocks (from Vry et al., 2010). b. Reconstructed map (A) and cross- section (B) of Yerington batholith and porphyry System in Nevada, USA, showing the distribution of the intrusive units and mineralized areas (from Schöpa et al., 2018). .....22
Figure 1-5. a. Figure from Druitt et al. (2002) showing the changes in explosion repeat interval over time for the Soufrière Hills volcano eruption in Montserrat (September-October 1997). Horizontal axis represents the number of explosions during the eruptive event. b. Mount St Helens eruptive history from 1400 AD to 1990 (USGS, n.d.). c. Map of the Cascade volcanic arc, Canada and USA (NASA Black Tusk, 2008). d. Eruptive history for the Cascades during the last 4000 years (Myers B., 2008).....23
Figure 1-6. Figure from Tsang et al. (2018) showing a compilation of published U–Pb, Ar–Ar and Re–Os ages for mineralised porphyries in northern Chile for different metallogenic belts. Error bars are not shown on the plot. .....24
Figure 1-7. a. Thermal modelling showing intrusion scenarios in time for the Yerington intrusive complex in Nevada, USA, comprising the main mineralised intrusions, McLeod monzodiorite, Bear monzonite and Luhr Hill granite. Simulations were performed by increasing magma injection rates and inducing different repose periods, showing that PCD intrusion could take less than 100 ky (from Schöpa et al. (2017)). b. Simplified volcanological and geological map of the Aucanquilcha volcanic cluster in northern Chile showing volcanic edifices and vents fed by the same source in the last 11 My (modified from Grunder et al. (2008)). .....25
Figure 1-8. Summary of the main tectonic, climate, erosional events, arc formation and migration in the Andes, from 40 My up to the present time.....27
Figure 1-9. Figure from Trumbull et al. (2006) showing the limits of the principal morphotectonic units of the central Andes, which include: Altiplano and Puna Plateaus, Western Cordillera (WC), Eastern Cordillera (EC), Subandean Ranges (SA), Sierras Pampeanas (SP). .....28
Figure 1-10. Figures from Oncken et al. (2006) showing: a. Average shortening rates of the main active structural domains and phases of deformation in the Central Andes over the last 50 My. b. Number of isotopically dated volcanoes in red, gathered within a 3 My sliding windows, between 19° S and 22° S, superposed is the average shortening rates (black solid line), based on summing minimum and maximum shortening rates from Figure 1.10a., rollback fluctuation (black dotted line), and flat slab subduction proposed period (orange box; from Mahlburg Kay et al., (1999)). c. Shows the global climate tendency of δ18O data (Zachos et al., 2001) superposed with average shortening rate (black solid line) and slab rollback fluctuation (black

dotted line); in the box at the top, local climate evolution in northern Chile (Alpers and Brimhall, 1988; Gaupp et al., 1999; Hartley and Chong, 2002).....29
Figure 1-11. Large-scale 2D structure of the Andes (from Armijo et al., 2015). The black arrow indicates westwards Nazca plate direction and speed rate. At the top, a topographic profile with vertical exaggeration of ~5 is shown. Horizontal coloured bars (red, orange and yellow) represent the age (My) of main deformation periods for the different geomorphologic domains in the Andes (Sempere et al. (1990); Maksaev and Zentilli (1999); McQuarrie et al. (2005); Oncken et al. (2006); Barnes and Ehlers (2009); Charrier et al. (2013)). Yellow arrows represent areas where deformation has propagated in the last 10 My. Grey question marks are placed where uncertainty is considerable. Red box shows the approximate location for the Precordillera region.....31
Figure 1-12. Figure from Sobolev et al. (2006) showing the model of surface topography evolution of the Central Andes in the last 30 My. Each profile represents the changes in the Andes topography every 10 My. .....32
Figure 1-13. Figure from Oncken et al. (2006) showing the cumulative shortening rates (mm/a) in the last 50 My, for four active structural domains (Precordillera, Western Altiplano, Central and Eastern Altiplano) in the Central Andes, the bold line indicates average shortening rate. .....33
Figure 1-14. Figure from Hu et al. (2016) showing the variation in the trench profile for the last 45 My. The red lines show the active and deformable trench contour for each episode (Arriagada et al., 2008), and the black lines indicate the current trench geometry for comparison. .....34
Figure 1-15. a. Figure from Vietor and Echtler (2006) showing a shaded topographic image of the subduction zone in the Andes. Yellow triangles indicate the location of Holocene volcanoes (Smithsonian Institution, Global Volcanism Program). Red contour lines indicate the depth to the Wadati Benioff zone in km, from Creager et al. (1995). On the right panel, the grey area shows the latitudinal trench infill thickness variation (Hoffmann-Rothe et al. 2006) and the blue area indicates the annual precipitation along the coast (New et al., 2002). b. Figure from Vietor and Echtler (2006) showing the main three factors that influence if, and how much, the overriding of the upper plate leads to upper plate shortening or slab rollback. Cartoons at the bottom panel present two scenarios that could occur between plates: positive (right) and negative (left) feedback. .....37
Figure 1-16. a. Figure from Behr et al. (2018) showing how much plate velocity varies when plate interface shear zone viscosity increases, for a variety (blue: 2km, orange: 5km and yellow: 10km wide) of shear zone widths (δw). Due to higher viscosity originated by dominant mafic rocks in the plate interface, the slab should subduct slower compared to slabs lubricated with sediments. b. Figure from Oncken et al. (2006) showing an estimated range of trench fill thickness (green bold line represents maximum and minimum), comprising the present-day average thickness (green box; Kudrass et al., 1998; von Huene and Ranero, 2003) and superposed is the expected trend of sediment thickness (dotted grey line), assuming that the plate interface strength has an inverse correlation with sediment supply into the trench. .....38
Figure 1-17. Figure from Evenstar et al. (2020) presents a simple sedimentary basin overview of the Longitudinal Valley showing the principal geomorphic surfaces (AS5, AS4, DS3 and DS2). On the right panel, the climatic variations and pulses for the last 30 My are also shown for Longitudinal Valley (Jordan et al., 2014; Evenstar et al., 2017). On the rightest panel, two possible uplift events: one in the Late Miocene uplift (black solid line) and another during the Early Miocene (dashed line).....41
Figure 1-18. Figures from Montgomery et al. (2001). a. It shows three environments that would create three distinctive normalized hypsometric curves along the Andes; curve colour identifies the location of each environment: northern (red), central (yellow), and southern (blue) Andes. b. 'A: Volume of Andes above sea level calculated from 1º latitude bins. B: Excess erosion rate, relative to largest 1º bin, is required to explain volume difference under uniform tectonic convergence. Latitudinal variation in erosion rates under constant tectonic convergence by calculating missing mass above sea level in each 1º latitude bin as VXSα/At, where VXS is excess volume in given bin compared to largest bin (14º–15ºS), A is bin area, t is time (taken to be 25 My.), and α=ρc/( ρm- ρc), where ρc= 2.7 g·cm-3 and ρc=3.3 g·cm-3. Note that because of the selection of strictly east-trending bins for analysis, the region between 13ºS and 17ºS, where range trends northwest rather than north, has anomalously large volume in each bin. C: Mean annual precipitation. D: Mean erosion intensity index value' (Montgomery et al. 2001, p.581). .....43
Figure 1-19. Modified figure from Montgomery et al. (2001) showing: a. mean annual precipitation (m/yr), on top of a shaded-relief map of South America. b. cross-range asymmetry indicating which are the areas in the Andes draining to the Atlantic Ocean. .....44
Figure 1-20. Figures a and b from Oncken et al. (2006) showing: a. The yellow solid line represents the erosion and sedimentation rates in the Chilean Precordillera and Longitudinal Valley. b. Estimated values of integrated erosion and sediments supply for the North Chilean Precordillera and fore-arc basins. c. Figure from Evenstar et al. (2017) showing regional deposition configurations from the Late Oligocene to the Late Pliocene.....47
Figure 1-21. Figures from Margirier et al. (2015). a. SRTM numerical elevation model on top of a Landsat image showing a regional view of the Chuquibamba region and the principal detachment scarps, debris-flow deposits, rotational landslides and faults. b. Cartoon showing the rotational landslide evolution triggered by the Ouki climatic event showing how landslides allow large remobilization on material. .....48
Figure 1-22. Figure from Karátson et al., (2011) showing the negative correlation between edifice height and degree of denudation. .....49
Figure 1-23. Figures from Karátson et al. (2011). a. Mean circularity vs. degree of denudation for Central Andean stratovolcanoes. b. Contour line for Central Andean stratovolcanoes based on the mean circularity. .....50
Figure 1-24. Figure from Karátson et al. (2011) showing degree of denudation (%) against the age of Central Andean stratovolcanoes and the climatic conditions in place, as well as their location within the orogen. .....51
Figure 1-25. Cartoon showing the connectivity between volcanic edifices and porphyries. Depending on the depth of intrusion and cooling, these mineralised bodies will experience diverse pressure and temperature ranges. In consequence, different types of mineralization may occur. Gold- rich porphyries (yellow star) form between 1-2 km depth, Cu- rich PCDs

(orange star) between 2-3km depth, while porphyries with Cu and Mo mineralization (purple star) occur in deeper parts of the crust, over 3 km depth.....53
Figure 1-26. Cartoons showing the different causes for erosion and PCD exposure in the Andes. a. On the left, an active stratovolcano and PCD formation underneath the volcanic edifice. On the right panel, uncovered PCD due to interaction between uplift pulses, exhumation and high erosion rates. b. Formation of rotational landslide that remove massive amount of sediments exposing a PCD. The formation of the landslide occurs because of the interaction between faulting and high precipitation rates during wet seasons. c. Uplift pulses increases the energy in active fluvial systems, which in return create deeper incisions and valleys, assisting on the exposure of porphyries, but also on the drop on volcanic edifices' height.....55
Figure 2-1. Modified volcano diagram (Oxford University Press, 2021) showing how volcanic edifice height was measured when constructing the AEVDB. Volcano height is calculated firstly, by identifying the maximum break in the slope of the edifice (base of the edifice). Secondly, estimating the altitude at the base and at the summit of the edifice, using a DEM (digital elevation model). Finally, using the following formula:.....62
Figure 2-2. Magmatic (volcanic and plutonic) arcs from Cretaceous to Pliocene time. a. Cretaceous magmatic arc with Cretaceous PCDs on top (green stars). b. Palaeocene magmatic arc with Palaeocene PCDs on top (pink stars). c. Eocene magmatic arc with Eocene PCDs on top (blue stars). d. Oligocene magmatic arc with Oligocene PCDs on top (purple stars). e. Miocene-Pliocene magmatic arc with Miocene PCDs (yellow stars) and Pliocene PCDs (orange stars) on top.....66
Figure 3-1. Bar plot showing valid, missing and non-valid values for the Volcano and Eruption dataset, classified into different general parameters. .....71
Figure 3-2. Bar plot showing number of values for the Volcano dimension categories classified by Volcano type. .....72
Figure 3-3. a. Box whisker for Volcanic edifice heights classified by Volcano type. Boxes represent the range of the 25th and 75th percentiles with the dividing line being the median. Whiskers represent the minimum and maximum values. Circles outside the boxes represent outliers and asterisks are extreme outliers (values more than three times the height of the boxes. b. Histograms and normal distribution curves for volcanic edifices classified by Volcano type. .....74
Figure 3-4. a. Box plot showing the variation in volcanic edifices height (m) through time from Cretaceous to present time. Boxes represent the range of the 25th and 75th percentiles with the dividing line being the median. Whiskers represent the minimum and maximum values. Circles outside the boxes represent outliers. b. Pie chart showing the percentages of values classified by epochs from Miocene to Holocene time.....74
Figure 3-5. a. Histogram of volcanoes heights showing the distribution of the values in different epochs. b. Kernel density plots of volcanoes heights showing the distribution of the values in different epochs.....76
Figure 3-6. a. Box whisker for Cone diameter classified by Volcano type. Boxes represent the range of the 25th and 75th percentiles with the dividing line being the median. Whiskers represent the minimum and maximum values. Circles outside the boxes represent outliers and asterisks are extreme outliers (values more than three times the height of the boxes. b.c. d. Histograms for Cone diameter classified by Volcano type, which were plotted in separated charts because of diameter scale differences. .....78
Figure 3-7. Box whisker for H/D ratio classified by Epochs. Boxes represent the range of the 25th and 75th percentiles with the dividing line being the median. Whiskers represent the minimum and maximum values. Circles outside the boxes represent outliers. .....79
Figure 3-8. a. Box whisker for Volcano volume classified by Volcano type. Boxes represent the range of the 25th and 75th percentiles with the dividing line being the median. Whiskers represent the minimum and maximum values. Circles outside the boxes represent outliers and asterisks are extreme outliers (values more than three times the height of the boxes. b. c. d. Histograms for Volcano volume classified by Volcano type, note Y axis (Frequency) in log scale and they were plotted in separated charts because of volume scale differences.....81
Figure 3-9. a. Box whisker for Crater diameter classified by Volcano type. Boxes represent the range of the 25th and 75th percentiles with the dividing line being the median. Whiskers represent the minimum and maximum values. Circles outside the boxes represent outliers Note Y axis in log scale. b. c. Histograms for Crater diameter classified by Volcano type, note Y axis (Frequency) in 10 based log scale. .....83
Figure 3-10. Scatter plots showing differences in volcano types for Edifice height (m) against a. Volcano volume (log scale) and b. Cone diameter (log scale). Markers are coloured by volcano size. Vertical lines represent Volume limit (50 and 100km3) and Cone diameter (14 and 24km), and horizontal ones show Height limits (1800 and 2000m).....86
Figure 3-11. Correlation matrix showing Height(m) as the dependent variable, against Volcano volume(km3), Crater and Cone diameter (km) for the valid 1058 records in the AVEDB. Black lines are linear regression lines that fit the whole population (all volcano types included). .....87
Figure 3-12. a. Correlation matrix showing Height(m) as the dependent variable, against Volcano volume (km3), Crater and Cone diameter(km). Coloured markers stand for different volcano types and the line represents a linear regression line for the whole population. a. shows stratovolcanoes and breached cones, which have been plotted together because they show the same trend and are part of the same volcanic system. b. Same as plot a, but grouped for the rest of the volcano types and its deposits. .....89
Figure 3-13. a. Frequency distribution for Eruption parameters, showing histograms (note Frequencies in Log scale) and bell curves. a and f. histograms showing high frequencies in low values and unimodal, asymmetrical and strongly positively skewed bell curves for Deposit diameter and Flow length. b. Magnitude histogram and bell curve, showing a normal distribution. c, d and e. Unimodal, asymmetrical and strongly positively skewed bell curves and histograms for Bulk volume, Bulk DRE volume and Deposit area. .....93
Figure 3-14. Box whisker for Eruption parameters classified by Volcano type. Boxes represent the range of the 25th and 75th percentiles with the dividing line being the median. Whiskers represent the minimum and maximum values. Circles outside the boxes represent outliers and asterisks are extreme outliers (values more than three times the height of the boxes). Note Y axis (Frequency) in log scale. .....95

Figure 3-15. Histograms of volcanic edifices classified by a. Location within areas with differential continental crust thickness. b. Volcanic zones in the Andes. Note Frequency in log scale. ....97
Figure 3-16. Histograms of volcanic edifices classified by location within different tectonic settings in the Andes. Note Frequency (y left axis) in log scale. ....97
Figure 3-17. Histograms of volcanic edifices classified by location within different morphotectonic provinces in the Andes. Note Frequency (y left axis) in log scale. ....98
Figure 3-18. Histograms of volcanic edifices classified by location within regions with differential denudation rates. Ranges from Denudation rate to match Karátson et al. (2011). Note Frequency (y left axis) log scale. ....99
Figure 3-19. Histograms of volcanic edifices classified by present climate. Note Frequency (y left axis) in log scale.....100
Figure 3-20. a. Histogram of volcanic edifices showing slope degree values. b. Box whisker for Slope degrees classified by Volcano type. Boxes represent the range of the 25th and 75th percentiles with the dividing line being the median. Whiskers represent the minimum and maximum values. Circles outside the boxes represent outliers and asterisks are extreme outliers (values more than three times the height of the boxes). ....101
Figure 4-1. Map of northern Chile and southern Peru showing morphotectonic provinces in the background, Cretaceous volcanoes classified by climate and Cretaceous PCDs. ....107
Figure 4-2. Map of northern Chile and southern Peru showing morphotectonic provinces in the background, Palaeocene volcanoes classified by climate (triangles), Palaeocene PCDs (circles) and tectonic segments (Sillitoe, 1984) on top. .....109
Figure 4-3. a. Map of northern Chile and the Arica inflexion showing paleosurfaces (Evenstar et al., 2017) in the background, Palaeocene volcanoes classified by height, Palaeocene PCDs and tectonic segments (Sillitoe, 1984) on top. b. Map of southern Peru showing main faults, Palaeocene volcanoes classified by height, Palaeocene PCDs and tectonic segments (Sillitoe, 1984) on top. ....111
Figure 4-4. Map of northern Chile and southern Peru showing morphotectonic provinces in the background, Eocene volcanoes classified by climate, Eocene PCDs, epithermal deposits and tectonic segments (Sillitoe, 1984) on top. Coloured boxes highlight regions with different level of exposure, where red boxes represent Cu PCDs, purple boxes show Mo-Cu rich deposits and epithermal deposit are shown inside light-blue boxes. Black arrows show increasing erosion and exhumation pattern. ....113
Figure 4-5. a. Map of northern Chile – southern Peru and the Arica inflexion showing Eocene volcanoes classified by climate, Eocene PCDs, tectonic segments (Sillitoe, 1984) and main fault systems, the Incapuquio fault. b. Map of southern Peru, Arequipa region, showing main faults, Eocene volcanoes classified by height, Eocene PCDs and tectonic segments (Sillitoe, 1984) on top. Coloured boxes highlight regions with different level of exposure and light blue circle show the location of Constancia mine....115
Figure 4-6. a. Map of northern Chile – southern Peru showing morphotectonic regions with Oligocene volcanoes classified by climate and Oligocene PCD on top. b. Zoom in on the map in a., southern Peru and the Arica inflexion, showing Oligocene volcanoes classified by climate and Oligocene PCDs. ....118
Figure 4-7. Scatter plot for Pleistocene and Holocene volcanic edifice heights against Elevation (m). ....120
Figure 4-8. a. Scatter plot for Pleistocene and Holocene volcanic edifice heights against climate, classified by morphotectonic provinces (right Y axis). b. Frequency bar plot of Pleistocene and Holocene volcanic edifices classified by climate and morphotectonic provinces. ....121
Figure 4-9. Box whisker for Volcanic edifice heights classified by Geomorphological areas in the Andes, from west to east. Boxes represent the range of the 25th and 75th percentiles with the dividing line being the median. Whiskers represent the minimum and maximum values. Circles outside the boxes represent outliers (calculated as 25th and 75th percentile ± 1.5*interquartile range (25th percentile-75th percentile). a. The figure shows height ranges that characterise different morphotectonic regions in the Andes. b. This figure shows height ranges for different morphotectonic regions, but in this case, it distinguishes between volcanoes that have been dated from the ones with an assigned age depending on their location in the Andes. ....122
Figure 4-10. a. Box whisker for Volcanic edifice heights classified by Epoch (right Y axis) and regions (X axis) in the Andes. Boxes represent the range of the 25th and 75th percentiles with the dividing line being the median. Whiskers represent the minimum and maximum values. Circles outside the boxes represent outliers (calculated as 25th and 75th percentile ± 1.5*interquartile range (25th percentile-75th percentile)). b. Histogram of volcanic edifice height classified by morphotectonic provinces....126
Figure 4-11. Scatter plots of PCDs and volcanoes height values against a. Latitude (decimal degrees); b. Longitude (decimal degrees). For both plots the data has been classified by time period, and dotted black lines represent flat slab areas (Central Chile and Peruvian) formed during Miocene times. ....127
Figure 4-12. Scatter plot for dated (brown triangle; purple circle) and non-dated (green triangle) volcanic edifice heights, dated PCDs (red circle) and elevation in metres above sea level (X axis), classified by Epoch (right Y axis). Dotted grey line marks 2000 m.a.s.l. ....128
Figure 4-13. a. Economic deposits classified by deposit type and geomorphologic regions where they are located. b. Volcanoes from Cretaceous to Pliocene time, showing elevation above current sea level against longitude. ....130
Figure 4-14. a. Scatter plot for Volcanic edifice heights against Annual precipitation rate (mm) classified by Climate showing decreasing height with wetter climate. b. Scatter plot for Volcanic edifice heights against Annual precipitation rate (mm) for different time epochs. ....131
Figure 4-15. Bar plot for volcanic edifices and PCDs against present climate (X axis) comparing units' percentages for defined time epochs. Each panel represents 100% total for the units (volcanoes + PCDs) present in that specific time period. ....132
Figure 4-16. a. Bar plot for volcanic edifices and PCDs against present climate (X axis) and Morphotectonic provinces and time epochs. a. Compares units' percentage, where each panel represents 100% total for the categories (volcanoes + PCDs)

present in that specific time period. b. Bar plot showing frequency of volcanic edifices and PCDs against present climate (X axis) and Morphotectonic provinces for defined time epochs. ..... 134
Figure 4-17. Map of Constancia open pit mine showing three intensely eroded volcanic edifices in the surroundings and fault system affecting the deposit and information on reserves and resources (Hudbay internal report, 2017). ..... 136
Figure 4-18. Scatter plot for Volcanic edifice showing heights (right Y axis) against Latitude (m) (X axis), classified by Epoch (coloured dots). a. Cretaceous and Palaeocene volcanoes. b. Eocene and Oligocene volcanoes. ..... 143
Figure 4-19. Scatter plot for Volcanic edifice showing heights (right Y axis) against Latitude (m) (X axis), classified by Epoch (coloured dots). a. Miocene and Pliocene volcanoes. b. Holocene and Pleistocene volcanoes. Figure in in the background (grey) extracted from Montgomery et al., 2001 (for more details see Figure 4-18). ..... 144
Figure 7-1. Histogram showing 4 categories for "Unit filter" field. ..... 167
Figure 7-2. Histogram showing "Country" categories and the number or records. ..... 168
Figure 7-3. a. Volcano classification modified from Volcanoes of the World, Siebert et al. (2010). b. Histogram showing "Volcano type" categories. ..... 171
Figure 7-4. Histogram showing the volcanic activity status records. ..... 172
Figure 7-5. Cartoon from Castruccio et al. (2017), showing two size of volcano and the implication in their plumbing system: a) large volcanoes are fed by a deep overpressured magma source and b) smaller volcanoes only connected to shallow magma chambers. ..... 174
Figure 7-6. Erosion status histogram and its categories ..... 175
Figure 7-7. Figure from Crosweller et al. (2012). Box and whisker plot of VEI classification versus Magnitude for global and historic eruptions in the LaMEVE database, the boxes represent a range between 5th and 95th percentiles, median is represented by the dividing line within the boxes. Whiskers indicate minimum/maximum values and 'n' inside the boxes stands for the number of eruption records at that VEI. ..... 176
Figure 7-8. Histogram plot of dominant rock composition of the different eruptive events. ..... 178
Figure 7-9. Comparison between the number of registers with ages from literature against ages assigned by the location within magmatic arcs. a. Histogram of age classes coming from different sources. b. Histogram of the age periods for datapoints located in different magmatic arcs. ..... 182
Figure 7-10. Histogram showing categories of Data uncertainty field. ..... 185
Figure 7-11. Figure from Thorpe (1984) showing a map of western South America indicating the tectonic plates configuration related to active volcanism and the thickness of the crust.- - active calc-alkaline basalt-andesite, dacite volcanoes (MacDonald, 1972); - - some alkaline volcanoes; - - volcanic areas. The location of crust with thickness over 50 km is shown by a dotted line. ..... 187
Figure 7-12. a. Schematic of the basin types generated under the two main tectonic settings. Modified from Edlmann K. et al., 2015. b. Histogram of Tectonic settings where volcanoes and its deposits are spatial distributed. ..... 188
Figure 7-13. Volcanic zones and flat slab areas present in the Andes showed in a. map of South America and b. histogram. ..... 190
Figure 7-14. a. Volcanic segments defined by Wood et al. (1987). b. Tectonic segments in the Andes, outlined by Sillitoe (1974). ..... 191
Figure 7-15. Morphotectonic provinces in the Andes. a. Showed in a map modified from Ross J. L. S., 2015 and b. Histogram showing the distribution of the datapoints. ..... 192
Figure 7-16. Denudation rates mapped in ArcGIS from Karátson et al. (2011). ..... 193
Figure 7-17. a. CHELSA raster image showing modern annual precipitation (mm). b. Histogram of climate distribution according to the location of datapoints. ..... 194
Figure 7-18. a. Plane used to calculate slope where a 3 by 3 cell (elevation value) is fitted around each processing cell. b. Slope calculated raster image for South America. ..... 195

# 1 Chapter 1: Introduction

Porphyry Copper Deposit (PCD) exploration faces a challenging future because the areas that have already been extensively explored are unlikely to contain more high-quality ore deposits, and promising unexplored areas are covered by colluvial, alluvial and volcanic layers (e.g., ignimbrites). PCDs form at kilometres depth in the crust but to be economically feasible to mine them, they must be exposed or have been exhumed to more shallow levels.

Volcanoes are just the surface expression of extensive magmatic systems below ground. Although not all volcanic centres generate PCDs, it may be that all PCDs formed under a volcanic centre. The aim of this project is to develop a practical tool to use volcanic edifice dimensions and erosion patterns to find porphyry copper deposits close to the surface. The timing and location of magmatism in arcs are key factors for the formation of both porphyry copper deposits (PCDs) and volcanic centres. As there are no complete magmatic-volcanic profiles available, the only remaining option is to study the distribution of the exposed magmatic-volcanic portions, with the understanding, of course, that the record is incomplete.

To develop a case study for using volcanic edifice patterns to explore for PCDs, I chose the area with the maximum amount of available reliable information where PCDs have been discovered: the Andes. I first focussed on northern Chile and Argentina and southern Peru, expanding later to the rest of the Andes, where PCDs are mainly found in five arc-parallel metallogenic belts. These belts are related to the eastward migration of the magmatic arc through time: the late Carboniferous- early Permian, late Cretaceous, Palaeocene- early Eocene, late Eocene- early Oligocene and middle Miocene- early Pliocene belts.

This project has three main pillars: database creation, visual spatial distribution and statistical analysis. The first step was assembling databases of porphyry copper deposits, volcanic edifices and volcanic eruptions. The second stage includes the use of visual analysis software (ArcGIS) to find patterns and clustering in the data. For context, I also delimited tectonic provinces, regional trends, geological settings and the magmatic arcs through time, and the modern climate conditions. Thirdly, I address whether the frequency of the data is evenly distributed, trying to understand the reason for any gaps. Then, I explore differential erosion trends in diverse regions in the Andes, using volcanic edifice geometry, in particular volcanic edifice height, as a proxy. I examine height as a function of time, spatial location (in given periods) and relate it to modern climate and morphotectonic provinces, but also to the elevation where volcanoes are located today.

This thesis includes five chapters. In this introductory chapter, I review the main factors that may influence the erosion of volcanic edifices and the exposure of mineralised deposits in the Andes. The review starts by comparing volcanoes and PCDs and finding similar features that may suggest that these two geological environments are part of the same system; I am simply looking into different depths. As part of the background evaluation, I consider the evolution of the Andes, mainly from the Cretaceous up to the Miocene. I focused on the tectonic regimes affecting different regions in the Andes, such as Precordillera and the Bolivian Orocline. Also, I examined how the variation between uplift, crustal shortening, subduction plate speed and crust destruction had a crucial role in the erosion of volcanic edifices and conservation of mineralised porphyries. Moreover, I reflected on the impact that pulses in volcanism and magmatism may

have on the frequency of volcanoes and PCDs, and the depths where they could be found. Finally, I consider the potential impact that climate variations in South America may have on the geometries of volcanic edifices.

The second chapter explains how I created the Andean Volcanoes and Eruptions database (AVEDB) and where the information was gathered from. The third chapter presents a statistical analysis where I use histograms, box and whisker diagrams, density and scatter plots for performing an exploratory data analysis (EDA) of all the volcano and eruption parameters in the AVEDB. Then, I studied in more detail the key parameters for Chapter 4: volcanic edifice height, cone and crater diameter, and volcano volume. I end Chapter 3 by showing how these parameters correlate to each other. The ultimate research is presented in Chapter 4. It expands on the volcanic edifice height statistical analysis in Chapter 3, and then considers how climate, tectonics and timing may influence the variation of volcanic edifice height and PCDs exhumation. It also discusses how to use volcanic edifice dimensions and erosional patterns to delineate prospective areas where PCDs, if present, are likely closer to the surface or nearly exposed, and so indicate areas worth exploring.

## 1.1 Comparing PCDs against modern volcanoes

I start by comparing examples of well-studied PCDs in order to find common features that allow us to characterise them. Figure 1-1 shows two PCDs: the Grasberg igneous complex in Indonesia and Farallón Negro in Argentina. The very young Grasberg igneous complex (~3 My) has a central rhyodacitic intrusion within a roughly circular zone consisting of different igneous and volcanic lithofacies (Dalam Fm): andesite flows (DA), fragmental intrusive breccias (DV, DF) and bedded volcaniclastic deposits (Tvs) (Patterson and Cloos, 2005). The alteration pattern is concentric around the central intrusion and fine-grained shales at the margins dip towards the centre (Figure 1-1a).

The second PCD example, Farallón Negro, was extensively studied by Llambías (1972) and other authors (Sillitoe, 1973) and has similar features to Grasberg. Magmatism in the Farallón Negro district commenced in the late Tertiary with production of extrusive, and some intrusive, igneous breccias and tuffs of andesitic composition. These are contemporaneous with the emplacement of andesite domes around the periphery of the complex, perhaps on the margin of a caldera, along with dikes, sills, and flows of andesite and basalt (Sillitoe, 1973). The next event in the Farallón Negro porphyry was the emplacement of a monzonite intrusion. Subsequent porphyry copper-type mineralization accompanied a stock of granodiorite porphyry associated with ring dikes, a radial dike swarm of andesitic to dacitic composition, and a NW-SE-trending belt of small stocks and dikes ranging in composition from quartz andesite to dacite and rhyodacite (Llambías, 1972) (Figure 1-1b).

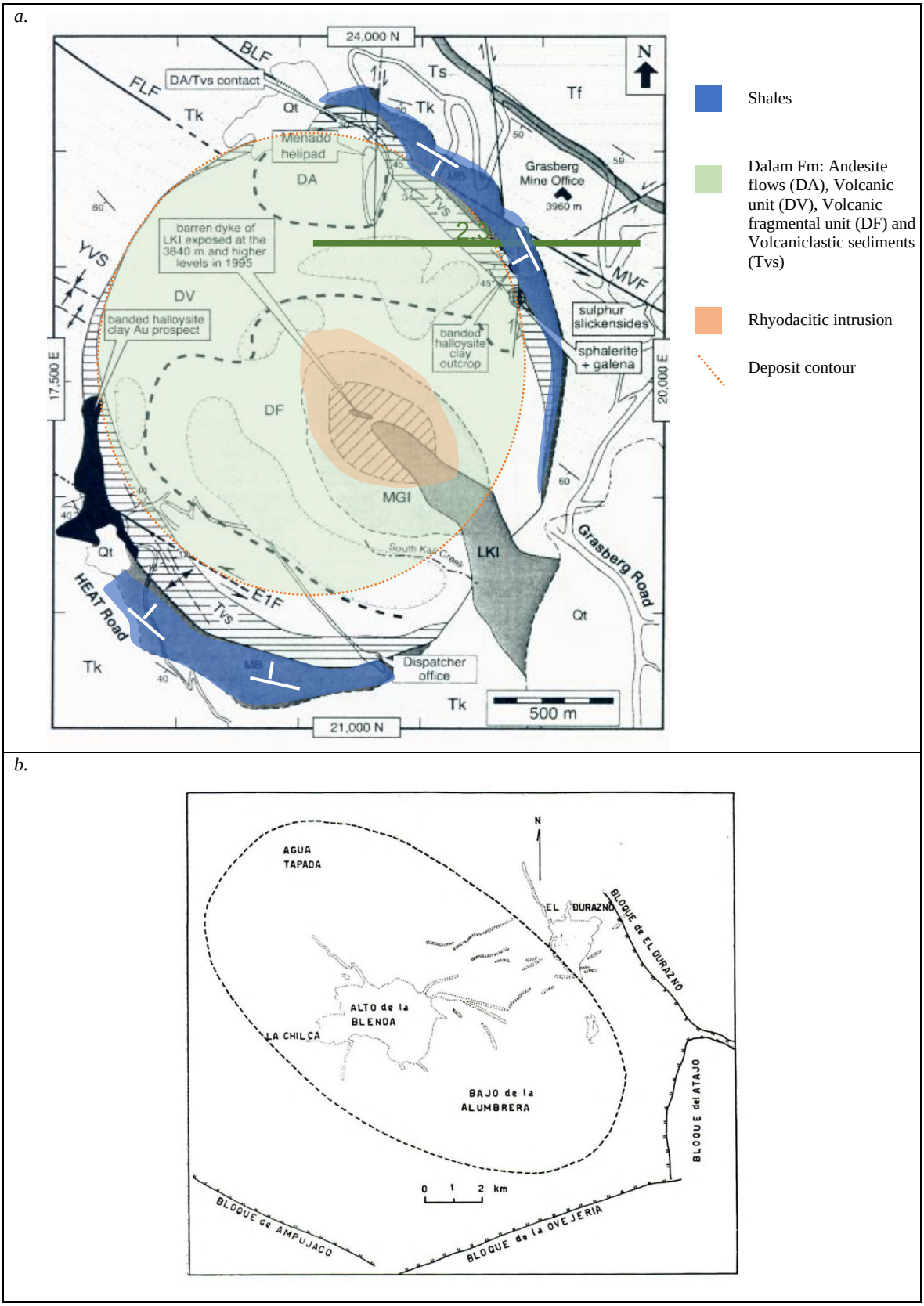


*Figure 1-1. a. Grasberg igneous complex in Indonesia, showing the dimension and shape of the complex, the presence of volcaniclastics, shales dipping to the centre of the complex and rhyodacitic intrusions (modified from Patterson and Cloos, 2005). b. Distribution of plutonic bodies, stocks and dikes in the Farallón Negro complex, Argentina (from Llambías, 1972).*

Several authors have suggested the presence of a volcanic edifice above PCDs when they formed. For example, Richards (2003) shows a schematic cross-section of a porphyry in a volcanic–magmatic system with advanced argillic alteration within the volcanic edifice. Other examples are late Cenozoic PCDs (*Farallón Negro*, Argentina (Sillitoe, 1973); *Namosi*, Fiji (Rodda, 1976); *Dizon*, Philippines) which all present diorite to quartz diorite porphyries that intruded at depth between 2-3 km, during the final construction stages of complex andesitic stratovolcanoes (Sillitoe and Bonham, 1984). The possible presence of a volcanic edifice is also discussed in the context of several specific PCDs. These include a Cu porphyry in *Cave Peak*, Texas (Audétat, 2010), a Cu-Mo-Au PCD in *Bingham Canyon* (Gruen et al., 2010) and *Bajo La Alumbrera*, Argentina (Sillitoe, 1973). Some other examples are the *Henderson* porphyry molybdenum deposit (USA), the second-largest known in the world (Seedorff and Einaudi, 2004) and the *Climax* mine (USA), the largest known porphyry molybdenum deposit (Worcester, 1935). All of these ore deposits are inferred to have developed under stratovolcanoes.

It is not common for volcanic edifices to be preserved during the unroofing process of PCDs. However, some examples exist of remaining portions of stratovolcanoes preserved on top of mineralised porphyries, such as the Marte porphyry Au deposit, northern Chile (Vila et al., 1991) or Grasberg, Indonesia, where parts of its original depositional slopes are still preserved (Sillitoe and Bonham, 1984).

Further evidence for the link between stratovolcanoes and PCDs is the resemblance in the alteration assemblages in PCDs and in drill core from depths between 600-1200m from several stratovolcanoes, typically drilled for geothermal energy (Sillitoe and Bonham, 1984). In particular, they both have pyrite-rich advanced argillic alteration (Chen, 1970; Nakamura et al., 1970; Ward, 1979; Sillitoe and Bonham, 1984) suggesting similar physical and chemical formation conditions. Despite the fact that no porphyry deposit has been intersected when drilling a geothermal system up to 2.5 km depth, the opportunity still remains open.

Richards (2003) discuss that magma of intermediate compositions (andesitic-low silica content dacite) have the capability to lose volatiles, by degassing through the volcanic edifice vent more easily than more acidic magmas. These volatiles reach the surface either in the form of fumaroles or get in contact with ground water. Hedenquist et al. (1998) proposed the alteration assemblage (hypogene advanced argillic alteration) found at the top of PCDs represents the same shallow level of degassing found in fumaroles.

Moreover, alteration found in fumaroles at the surface may indicate the presence of a deeper seated magmatic-hydrothermal activity, with the potential to host a porphyry-type ore formation. Sillitoe (1995) defined *lithocaps* as units that: "consist of vuggy residual quartz and advanced argillic alteration formed at shallow depths and potentially related to porphyry copper-bearing intrusions at depth". Several authors (e.g., Hedenquist et al., 1998, 2000; Heinrich et al., 2004; Heinrich, 2005) discuss that lithocaps are formed in low pressure environments, which makes the capability of fluids (vapour) to transport metals insignificant. Ascent of these vapours close to the surface results in extremely acidic fluids that are unlikely to precipitate any economic mineralisation. Indeed, lithocaps are mostly barren. However, the similarities between the lithocap environment and fumaroles seems hard to refute. Despite all this evidence, the genetic link between PCDs and volcanic edifices remains poorly understood because most studies consider these systems individually, and not as part of a whole.

I now compare three modern volcanic centres in order to find similarities between them, but also to find analogous features with PCDs. Figure 1-2 shows El Chaitén in Chile, Cerro Machín in Colombia and Mount St Helens in USA. All of them have similar crater diameters (2-3 km) and a lava dome in the centre (Figure 1-2a and Figure 1-2b). These examples all have volcaniclastic layers filling the crater that can be attributed to pyroclastic flows and dome talus. Volcaniclastic units are heavily altered by concentric patterns of fumaroles around central domes. There can also be moats around the inner crater edge, where standing bodies of water can deposit fine grained sediments that could later subside. Calderas like El Chaitén develop during a catastrophic eruptive event where the ejection of magma and rock causes the remaining volcanic edifice to collapse downwards, developing a crater (Figure 1-2a). On Mount St. Helens, rising magma generated an increase in the pressure that affected the northern side of the volcano, resulting in a disproportionated growth that triggered a flank eruption in 1980. The northern flank collapsed in a short period of time, resulting in a sideways explosion and an extensive landslide that propagated 27 kilometres to the north (NASA Earth Observatory, n.d.) (Figure 1-2c).

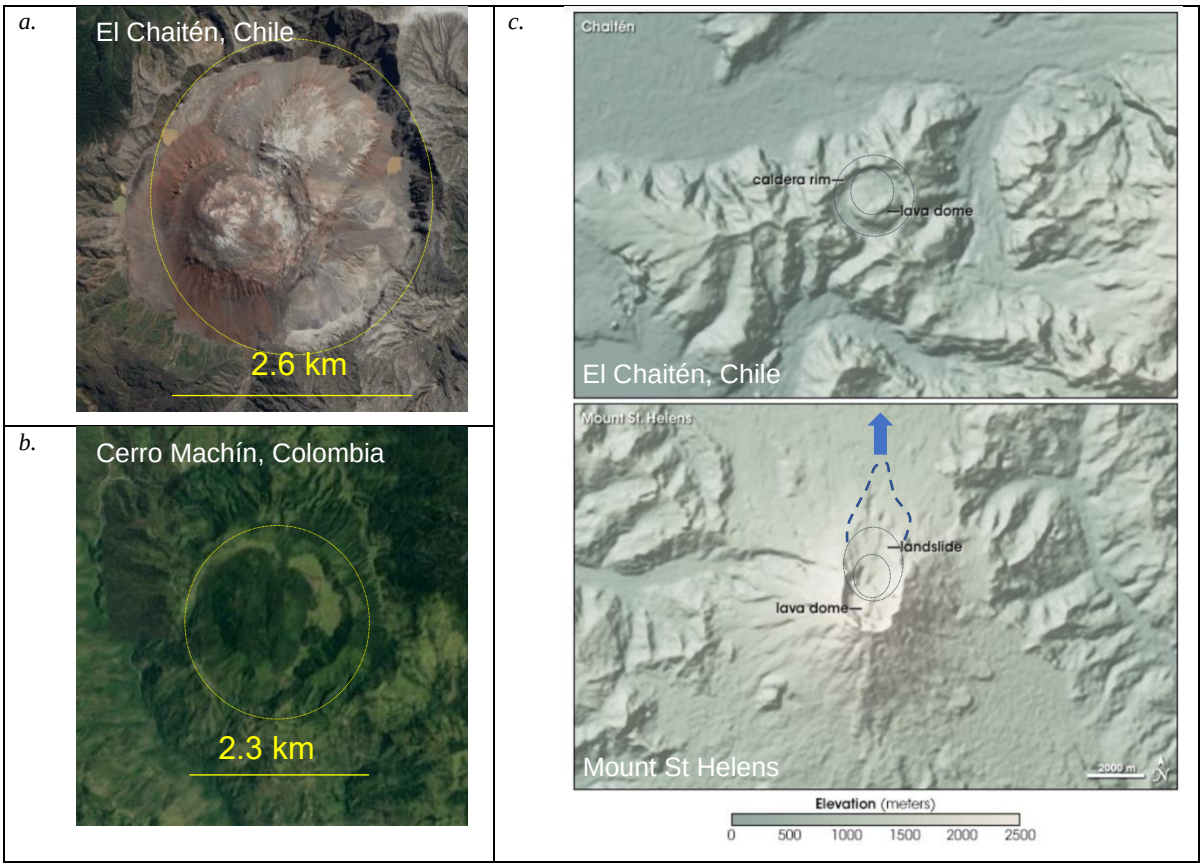


*Figure 1-2. Satellite images from Google Earth showing crater diameters for: a. El Chaitén volcano in Chile (Simmon R., 2010) and b. Cerro Machín in Colombia (Google Earth image). c. Satellite images showing the location of caldera rims, lava domes and landslides from the NASA's Earth Observatory for El Chaitén volcano and Mount St Helens (Simmon R., 2010).*

All three of these volcanoes have Holocene records of alternating periods of repose and large explosive eruptions emerging from the same conduit system. Eruptive deposits have a silicic composition: rhyolite for El Chaitén and rhyodacite for Cerro Machín. In contrast, eruption deposits at Mount St Helens can be

distinguished between the *Old Mount St Helens* from the *Modern Mount St Helens* based on composition. The former existed until about 2500 years ago as a silicic volcano (dacite and silicic andesite), and the modern volcano began with the eruption of predominantly mafic magma shortly after 2,500 years ago. However, not all magma erupted by the modern volcano is mafic. Even after the mafic magma appeared, dacitic composition deposits continued to be erupted intermittently, producing tephra, pyroclastic flows, and domes (Mullineaux, 1996) and the recent eruptions are dacitic.

Although not all volcanoes can have economic ore deposits forming below them, I now have a clear view of the main features that characterise volcanoes and porphyries and how much these systems resemble each other. Firstly, El Chaitén, Mount Saint Helens and Cerro Machín have crater shapes and dimensions which are similar to the distribution of volcanic deposits found in the upper portions of PCDs. Richards (2003) hypothesises that in the majority of systems, volcanic activity ceases before the formation of a mineralised porphyry starts. However, fairly minor eruptive activity, such as dome emplacement, may alternate with or even accompany the ascent of the mineralizing magmatic aqueous fluids, as inferred in Bingham (USA) and Yanacocha (Peru) PCDs (Deino and Keith, 1997; Longo and Teal, 2005).

Secondly, the three volcanoes considered above, are currently occupied by lava domes with silicic compositions, while the Grasberg igneous complex and Farallón Negro have rhyodacitic and monzonite intrusions respectively. These intrusions may form deeper, during or before the lava dome development. Francis et al., (1981) suggest that the only ore deposits related to dome complexes are mostly precious and base metal veins, stockworks and breccia fillings (i.e., deposits at Oruro, Bolivia). PCDs have generally not been related with flow-dome complexes in the economic geology literature (Sillitoe, 1984). The economic geology community believe this may be because the magmas that form domes represent the devolatilised and highly viscous material remaining after an eruption, which must have low volatile content in order to reach the surface (Burnham, 1967). Contrary to PCD forming magmas, which need to have: i) high water content (>~4 wt %) in order to become saturated and be able to carry metals, and ii) high oxidation states which avoids sulphur precipitation, since these minerals could sequester metals before they could partition in the aqueous phase (Burnham and Ohmoto, 1980; Candela and Holland, 1986; Dilles, 1987; Cline and Bodnar, 1991; Candela, 1992; Candela and Piccoli, 2005; Richards, 2005). However, from a modern volcanology perspective, not all these assumptions are considered to be true. Similarities between PCDs and domes are plenty. Firstly, both may form from magmas with intermediate-composition (andesites and lower silica dacites) or alternatively and less common, by the evolution of these intermediate magmas into more acidic compositions. Secondly, PCD forming magmas need to have high water content and high oxidation state, although these conditions are not exclusive to PCDs, they can also be present in dome-forming magmas, especially if those domes are forming in subduction settings, such as the Andes. However, there is a fundamental difference between PCDs and domes, which is the speed of magma ascension and the retention of volatiles during this process. Mineralised porphyries suffer decompression during fast magma ascension, which causes magma to freeze (e.g., Cashman and Blundy, 2000). This phenomenon of crystallization and cooling of hydrous arc magmas occurs in the shallow levels of the crust (Whitney, 1975; Burnham, 1979; Eichelberger, 1995; Castruccio et al., 2017) and allow for volatiles to be retained in the

magma, avoiding volatile degassing. On the contrary, dome formation is characterised by the slow ascent of magma, which allow volatiles to escape into the atmosphere throughout the edifice vent. As magmatic volatile exsolution is one of the essential steps in the formation of porphyry Cu deposit, domes show that this environment is definitely not favourable for PCDs generation. Although, it might occur that domes form during or later in time. If that is case, evidence of domes above porphyries would be challenging to obtain. Contrary to stratovolcanoes, preserving domes when the unroofing process of a porphyry has taken place seems rather difficult, because they are much smaller in volume (Sillitoe, 1984).

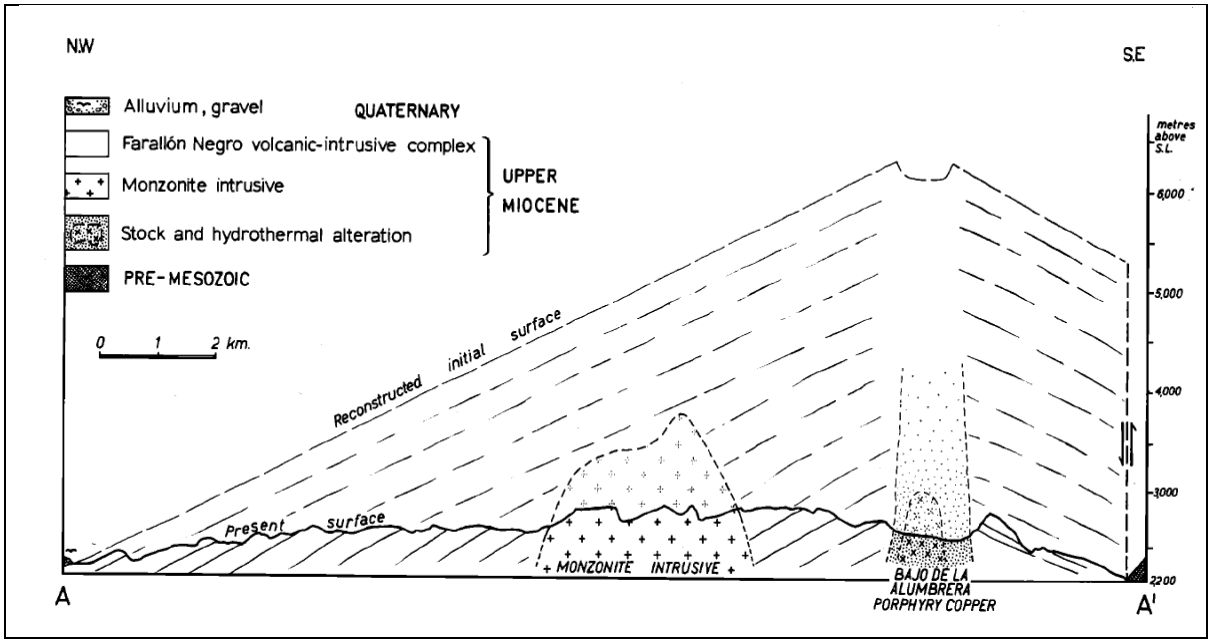


*Figure 1-3. Figure from Sillitoe, 1973, showing a simple cross-section across the Farallón Negro volcanic-intrusive complex, including a reconstructed volcanic edifice on top.*

Thirdly, volcanoes have volcaniclastic layers filling the crater that can be attributed to pyroclastic flows and dome talus. The examples that I have provided for PCDs also show a roughly circular zone consisting of different volcanic and volcaniclastic lithofacies. These facies are heavily altered in concentric patterns of fumaroles around central domes in volcanoes, and similar concentric alteration pattern occurs in PCDs around the central intrusion. Furthermore, volcanic deposits tend to be coeval with intrusions (PCDs) and lava domes formation (Sillitoe, 1973; Patterson and Cloos (2005); Audétat, 2010; Gruen et al., 2010). Plutons in arc terranes (including porphyry Cu-forming plutons) are commonly intruded at the base of a coeval volcanic pile or at the basement-supracrustal contact, because the overlying volcanic and sedimentary rocks are typically weak and of lower density than andesitic-dacitic magmas (Richards, 2003). Fourthly, my volcano examples contain moats around the inner crater edge, where standing bodies of water can form fine grained sediment similar to the fine-grained shales at the margins of the crater dipping into the centre of the Grasberg complex. These shales may represent lithified fine-grained sediments that have been tilted due to a subsidence collapse, which is very likely to have occurred during past explosive eruptions. Lastly, there is compelling evidence that upper portions of PCDs and stratovolcanoes present the same alteration assemblages and therefore similar formation conditions should be expected.

For all these reasons, I agree with Sillitoe's (1973) reconstruction of a volcanic edifice on top of PCDs, suggesting volcanoes and porphyries are part of the same magmatic complex but they represent portions at different depth (Figure 1-3).

The presence of sulphur and base metals in gas emissions from modern volcanoes indicates metal-enriched magmas below the surface, implying a correlation between PCDs and volcanoes. Ivanov (1959) and White and Waring (1963) both note the presence of base metals in high temperature fumarolic products. Roedder (1971) suggests that accumulations of alkali chlorides and sulphates around fumarolic orifices may correspond to the composition of mineralizing fluids present in the potassium silicate alteration zone, as inferred from fluid inclusion and mineralogic evidence (e.g., abundance of anhydrite). Sillitoe (1973) states that large accumulations of native sulphur are common near the vents of andesitic stratovolcanoes, along with abundant pyrite deposits beneath the surface. Hedenquist and Lowenstern (1994) and Williams-Jones and Heinrich (2005) suggest that aqueous fluid of magmatic origin is an essential medium for metals transportation in ore deposits.

The transportation of dissolved metals by magmas, metal sequestration in ore deposits and metal escape into the surface by outgassing during volcanic eruptions are responsible for a significant portion of the metal cycle of Earth in the crust (Edmonds et al., 2018). Data from the plumes of active basaltic volcanoes (e.g., Allard et al., 2000, Moune et al., 2010; Gauthier and Le Cloarec, 1998; Gauthier et al., 2016; Mather et al., 2012) show that volcanoes are releasing fluxes of metals to the environment of similar scale to those from large industrial smelters (Hong et al., 2013) and those building crustal ore deposits (Hedenquist and Lowenstern 1994; Allard et al., 2000). This shows that basaltic volcanoes are an invaluable source of metals in the atmosphere and oceans (Edmonds et al., 2018). Finally, I agree with Sillitoe (1973)'s suggestion that fumarolic, solfataric and hot-spring activity are the surficial manifestation of one or more subjacent magma chambers, and of the interaction between forcefully released magmatic fluids and convectively circulating ground waters.

So far, I have discussed the relation between subvolcanic intrusions and their possible superficial representation, i.e., volcanic edifices. Now, I focus on the connectivity between those two parts of the volcanic–magmatic system, and the deeper regions where PCDs are developed.

The shape of mineralised intrusions is controversial; they are often described as "pencil porphyries" or "finger stocks". Several authors represent PCDs as a forcefully emplaced "blind" intrusion that have no connexion with the surface. These authors (e.g., Shannon et al., 1982; Lowenstern and Sinclair, 1996; Sinclair, 2007) state that there is no evidence of unidirectional flow textures in phenocrysts at the top of the intrusions, at least in some porphyries, suggesting that magmatic fluids do not reach the surface utilising a single large volcanic vent. In contrast, they propose that magmatic fluid is released intermittently from a deeper source (e.g., Shinohara et al., 1995; Schöpa et al., 2018) and stalled in the crust for a period of time before cooling down and exhumated to the surface. However, some researchers consider these interpretations to be implausible. They suggest it is unlikely that pencil-shaped magma bodies (tens to a few hundred metres in diameter) could be forcefully intruded to produce stress fields of lateral extent, generating radial and concentric dike and vein fracture patterns (Roman and Jaupart, 2014) in several deposits. It is perhaps more

likely that these mineralised pencil style intrusions are conduits that end at the (now eroded) volcanic vent like the model proposed by Sillitoe (1973) and later on, modified by Richards (2001). Figure 1-4 shows cross- sections for two porphyries, El Teniente, in Chile, which illustrate how a porphyry may be connected to the surface according to the "pencil porphyry" model. Yerington pluton in Nevada, USA, in the other hand, is a classic example of PCDs connected to a deeper source, where a tilted batholith is connected to an inferred volcanic dome complex by swarms of dykes, hosting mineralised bodies in shallower depths.

*a.*

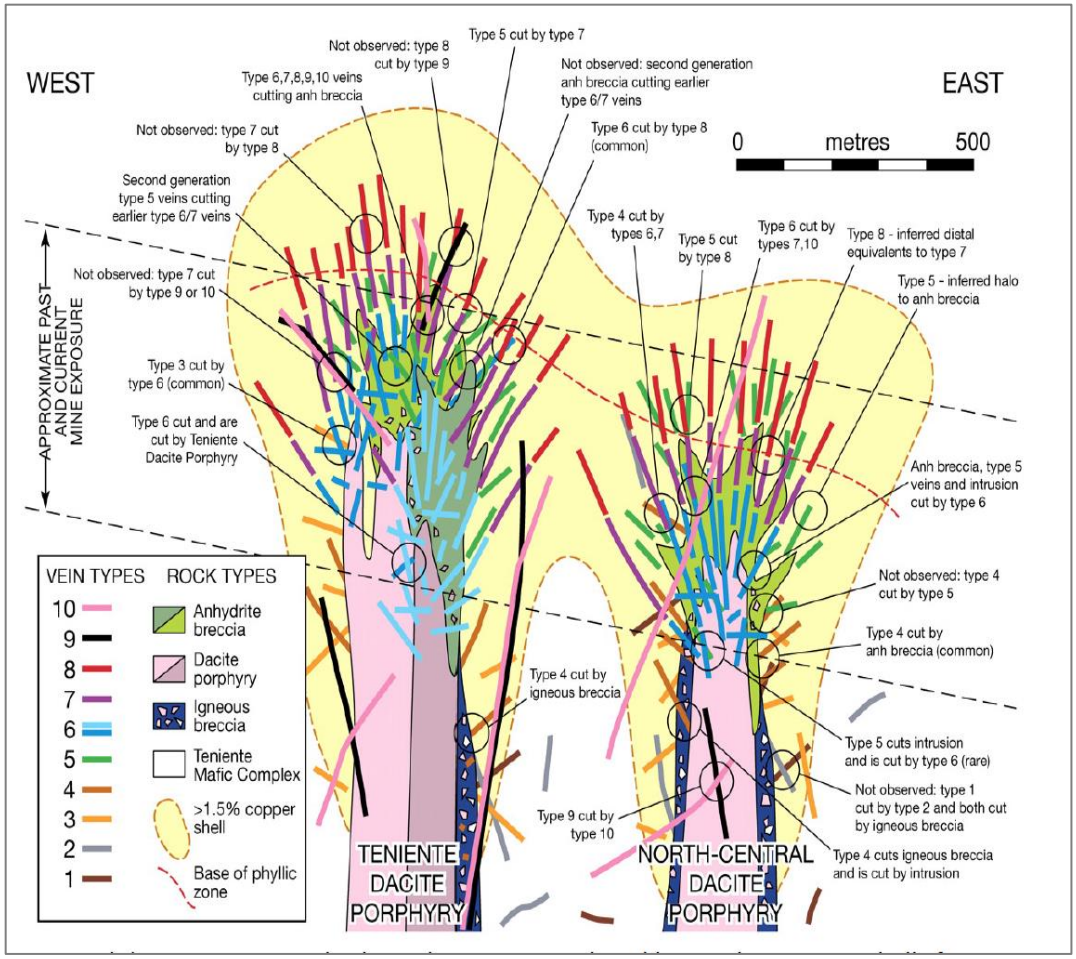


*b.*

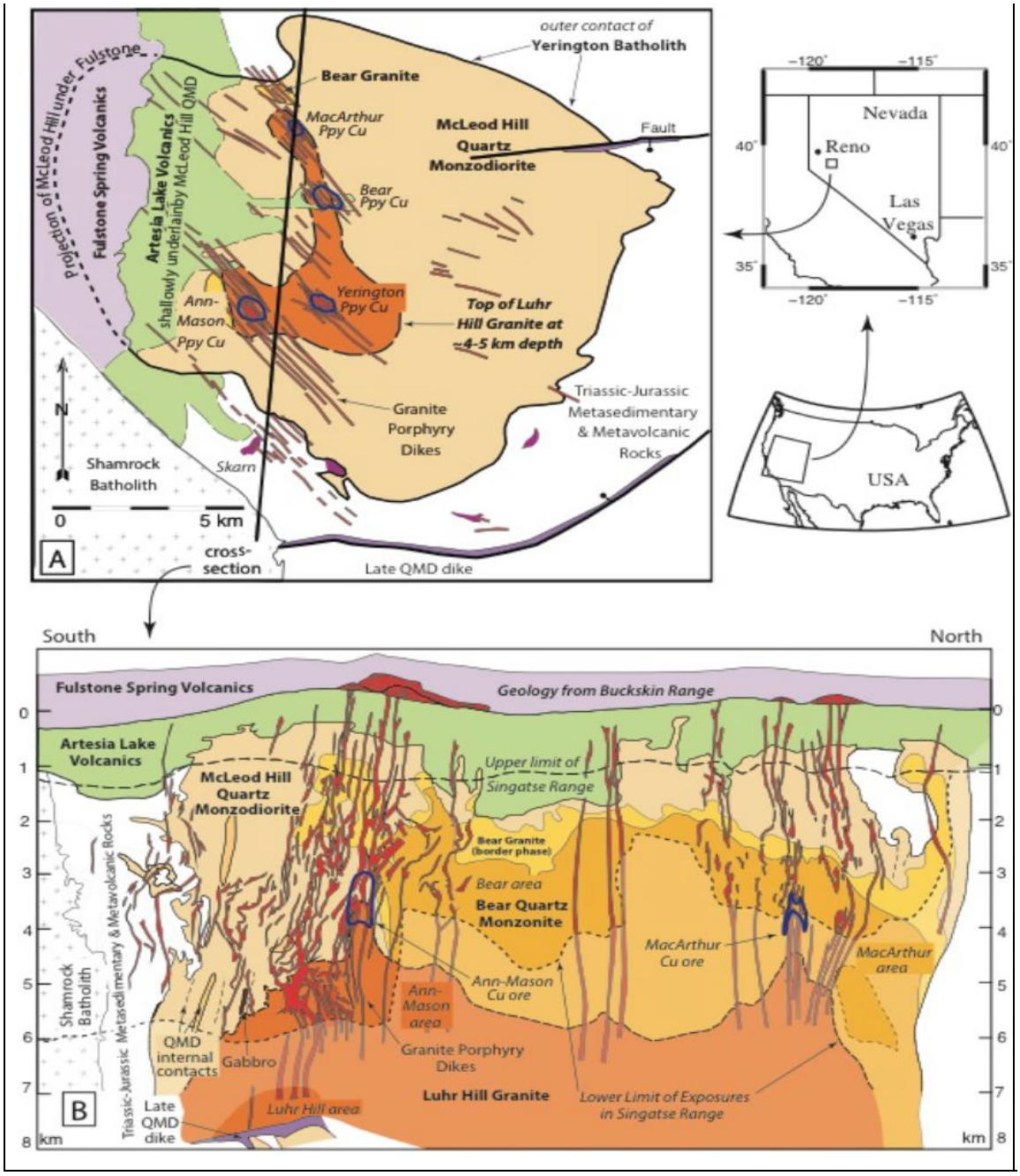


*Figure 1-4. a. Geological model of El Teniente copper porphyry in northern Chile, showing the upper connections of a hypabyssal body in the form of stocks (from Vry et al., 2010). b. Reconstructed map (A) and cross- section (B) of Yerington batholith and porphyry System in Nevada, USA, showing the distribution of the intrusive units and mineralized areas (from Schöpa et al., 2018).*

### 1.1.1 Eruptive and fertile periods versus dormancy and barren epochs

There are similarities in the timings for the generation of PCDs and the episodicity of volcanic activity. During the lifetime of a volcano, there are periods of dormancy and eruptivity. Figure 1-5a shows the explosion interval for one eruptive event for the Soufrière Hills volcano in Monserrat. At Mount St Helens, there are again periods where the volcano has been active and dormant on a timescale of 500 years (Figure

1-5b). Looking at a cluster of volcanoes, such as the Cascades (Figure 1-5c and d), again there is variation in the level of volcanic activity, alternating between activity and dormancy, over the last 4000 years.

The fertile periods for PCDs in Chile, show a similar timing distribution to volcanoes. There are certain periods of time, such as the Palaeocene - Early Eocene, where copper porphyry generation thrives compared to other epochs. There is also a similar tendency in a smaller scale. At district scale, the same porphyry complex shows different mineralization events, e.g., Escondida (Chile). PCDs only form by intermittent and rapid emplacement of plutons (Schöpa et al., 2017). None of these data require that PCDs form under volcanic edifices but they do suggest similar patterns for volcanoes and mineralised intrusive bodies, which is consistent with shared underlying magmatic processes.

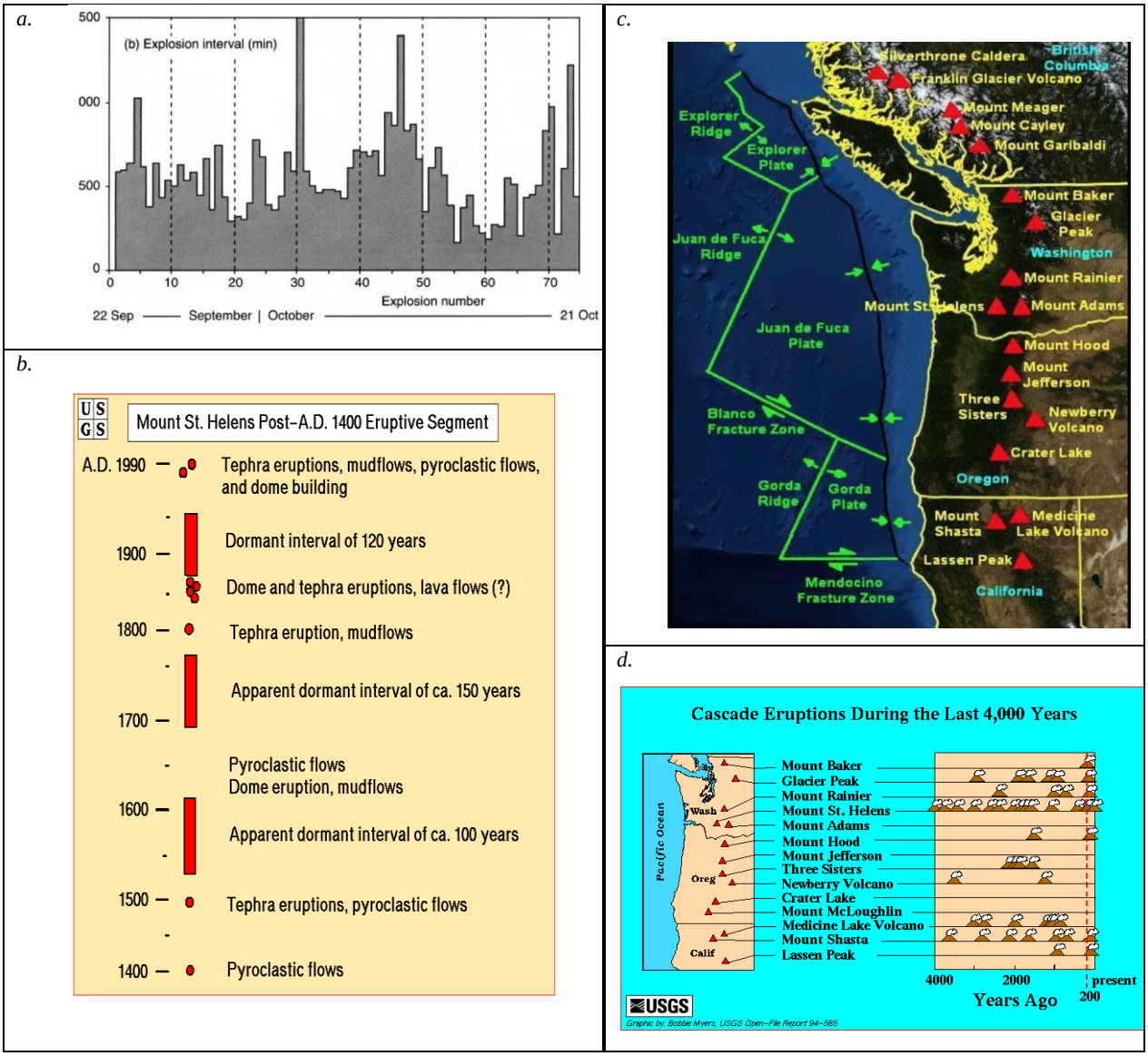


*Figure 1-5. a. Figure from Druitt et al. (2002) showing the changes in explosion repeat interval over time for the Soufrière Hills volcano eruption in Montserrat (September-October 1997). Horizontal axis represents the number of explosions during the eruptive event. b. Mount St Helens eruptive history from 1400 AD to 1990 (USGS, n.d.). c. Map of the Cascade volcanic arc, Canada and USA (NASA Black Tusk, 2008). d. Eruptive history for the Cascades during the last 4000 years (Myers B., 2008).*

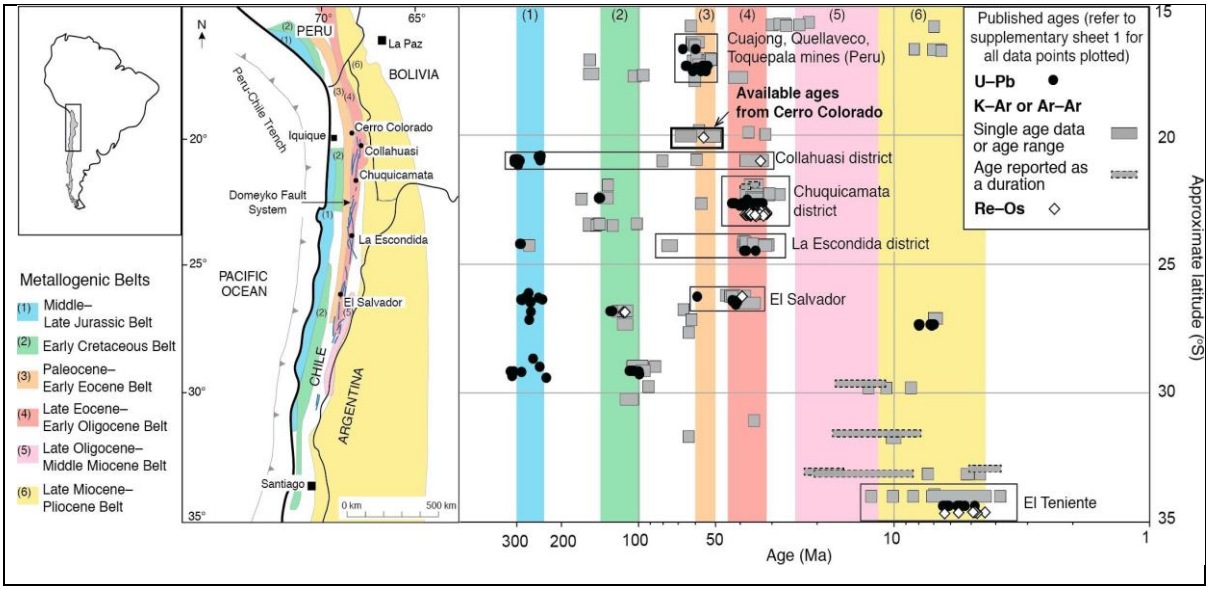


*Figure 1-6. Figure from Tsang et al. (2018) showing a compilation of published U–Pb, Ar–Ar and Re–Os ages for mineralised porphyries in northern Chile for different metallogenic belts. Error bars are not shown on the plot.*

### 1.1.2 Timing: PCD development and volcanic activity

Mineralised porphyries are generated by fast and episodic emplacement of plutons, whereas barren granitoids could be explained by excessively slow emplacement rates. The latter do not accumulate melts and likely they do not generate cupolas that keep volatiles before releasing them early during emplacement (Schöpa et al., 2017).

Figure 1-7a shows different scenarios of thermal modelling of the Yerington intrusive complex, where the magma injection rates and repose times vary with time. From all the possibilities, scenario III seems to be the most likely to generate a mineralised PCD, as it is characterised by fast emplacement rate and long repose periods. The elevated rates of emplacement cause the accumulation of large volumes of magma to happen in short periods of time, where elevated melt fractions and magma volume growth are common. The volume of magma accumulation decreases with each intrusion, as the intrusion dimensions are smaller. According to Schöpa (2017) the precursor pluton forms in less than 1My. Recent geochronological data in mine sites located in northern Chile, such as Spence (Bunker et al., In prep) and CMCC (Compañía Minera Cerro Colorado) (Tsang et al., 2018) mines, constrain the hypabyssal intrusions in PCD formation to a period of <100 ky, probably >4000 years. This is a revealing conclusion, proposing that these intrusive complexes could form faster than previously thought. Nevertheless, geochronological resolution is currently insufficient to resolve timing on the thousand years scale.

Many volcanic complexes are built and remain active for specific periods of time and are fed by the same magma source. These sites (i.e., Aucanquilcha volcanic cluster in Chile and the Cascade arc in western North America) may have similar formation times to mineralised intrusive complexes (Roman and Jaupart, 2014; Grunder et al. 2008). Figure 1-7b shows a simplified geological map of the Aucanquilcha volcanic cluster,

which comprises at least 19 volcanic centres of an area of ~700 km$^2$. The active Aucanquilcha stratovolcano is shown in the purple area. Centres of the other 18 volcanic edifices were constructed over the past 11 Ma. The cause of the many vent re-locations is an interesting research problem in relation to regional and local variations in stress regime over time. Most of these volcanic centres were constructed over a period of several hundred thousand years, fed by the same deep plumbing system and magma source. This shows continuous activity from the same source, but locally it suggests that individual portions of the volcanic system have a shorter lifespan (<1 My), comparable to PCDs and precursor plutons.

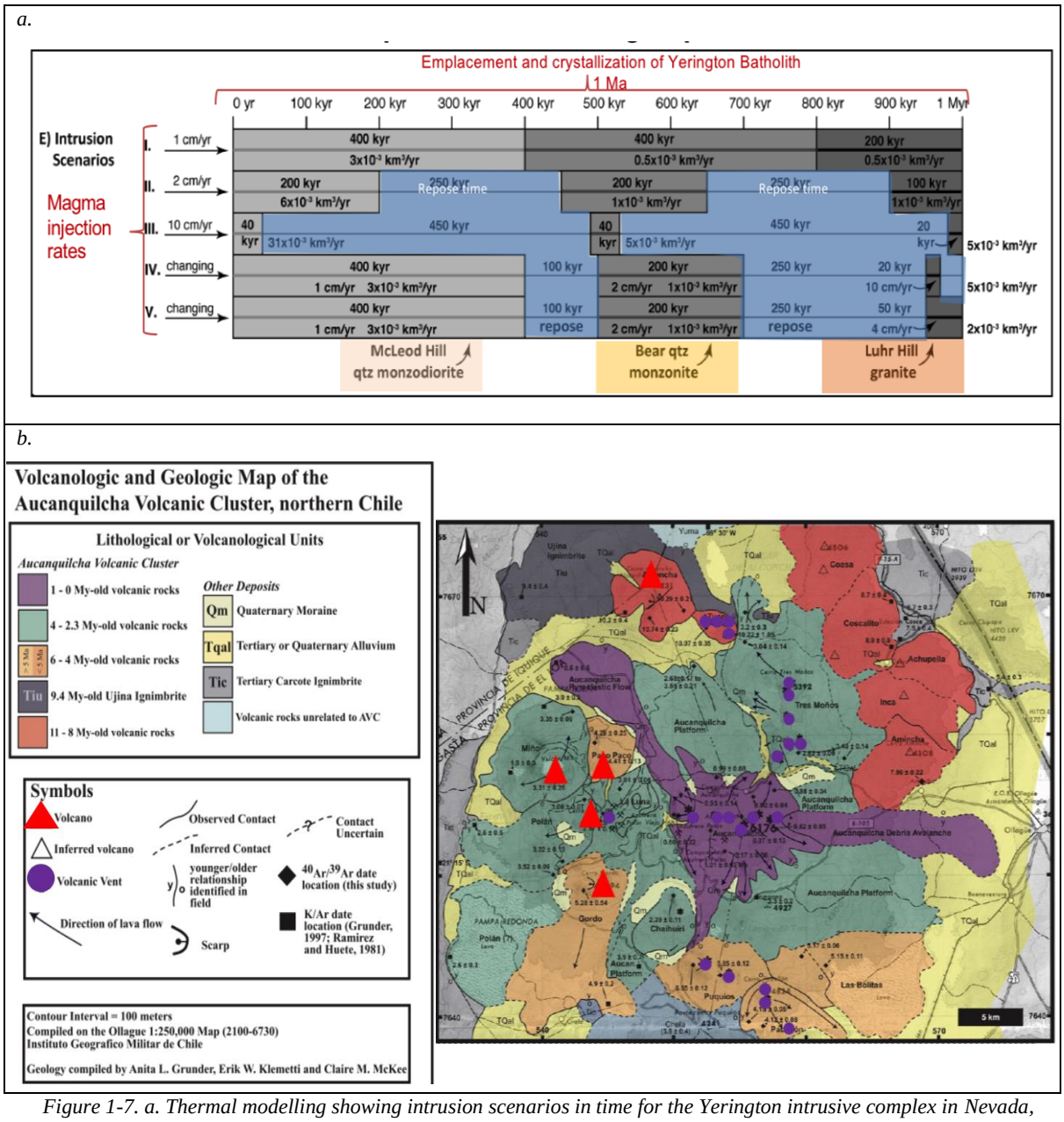


*Figure 1-7. a. Thermal modelling showing intrusion scenarios in time for the Yerington intrusive complex in Nevada, USA, comprising the main mineralised intrusions, McLeod monzodiorite, Bear monzonite and Luhr Hill granite. Simulations were performed by increasing magma injection rates and inducing different repose periods, showing that PCD intrusion could take less than 100 ky (from Schöpa et al. (2017)). b. Simplified volcanological and geological map of the Aucanquilcha volcanic cluster in northern Chile showing volcanic edifices and vents fed by the same source in the last 11 My (modified from Grunder et al. (2008)).*

### 1.1.3 Distribution of volcanoes and PCDs

De Bremond d'Ars et al. (1995) studied the distribution of 479 volcanoes in 16 active plate margins. The spacing between volcanoes was independently studied for each margin by measuring the distance from each volcano to its next nearest neighbour in the curvilinear coordinates system. They firstly checked that clustering was not biasing the data by performing a fractal analysis of volcano spacing, and then they plotted the global volcano distribution using frequency histograms. The spatial distribution of volcanos in each arc is represented by a Gamma distribution. This distribution explains data that are random in space, with no apparent pattern. They conclude that volcanoes are randomly distributed in active margins and the superimposition of several independent sets of normally distributed points gives a random distribution.

With the aim of explaining how such distributions maybe produced, De Bremond d'Ars et al. (1995) did laboratory experiments of the gravitational stability of a layer of buoyant liquid under a denser fluid, where the buoyant liquid is fed at a continuous rate. For high viscosity contrasts, plumes are created irregularly by discrete instability event. Once the plumes have moved to the surface, they continue to be fed from the material below. This mechanism may be responsible for short-term periodicity of volcanic activity. They concluded that the randomness of spatial volcano distribution may be explained by the superimposition of several magmatic pulses caused by gravity instability of buoyant melt in denser lithosphere or asthenosphere. With time and rising number of instability occurrences, the cumulative distribution of plume spacing changes from periodic to random.

A shortcoming of the analysis of De Bremond d'Ars et al. (1995) is that it does not account for changes in geological conditions and tectonic regimes, thereby missing important patterns relevant to both volcanoes and PCDs. In contrast, in my study I have considered geology to be an extremely important factor that helps to discriminate areas with the potential to have mineralised bodies from areas where those bodies could have been eroded away. I use tectonic segments in the Andes, defined by Sillitoe (1974), in conjunction with other tools, such as volcanic edifice morphology, geomorphology and erosional gradients, structural information and different PCDs types in order to target areas that are more likely to have preserved mineralised porphyries and understand when at the surface, how deep I am in the geological profile.

## 1.2 The Andes

### 1.2.1 Evolution of the Andes: tectonics, climate, erosion and magmatism

The Andes are widely recognized as mountains built at a convergent plate margin (Dewey and Bird, 1970), defined by the subduction of an oceanic plate (the Nazca plate) beneath a continental margin (the South American plate). The Andean chain persists along strike over 7000 km, from near the northern tip to southern tip of South America, yet it varies markedly in elevation and crustal thickness (e.g., Isacks, 1988; Tassar and Yañez, 1996; Allmendinger et al., 1997). In order to form and sustain a large mountain chain there is a balance between growth (controlled by crustal shortening and thickening, magmatic addition and possible

delamination) and erosion (controlled by climate and tectonics). Below I summarise these major controls on factors over the last 40 My (Figure 1-8).

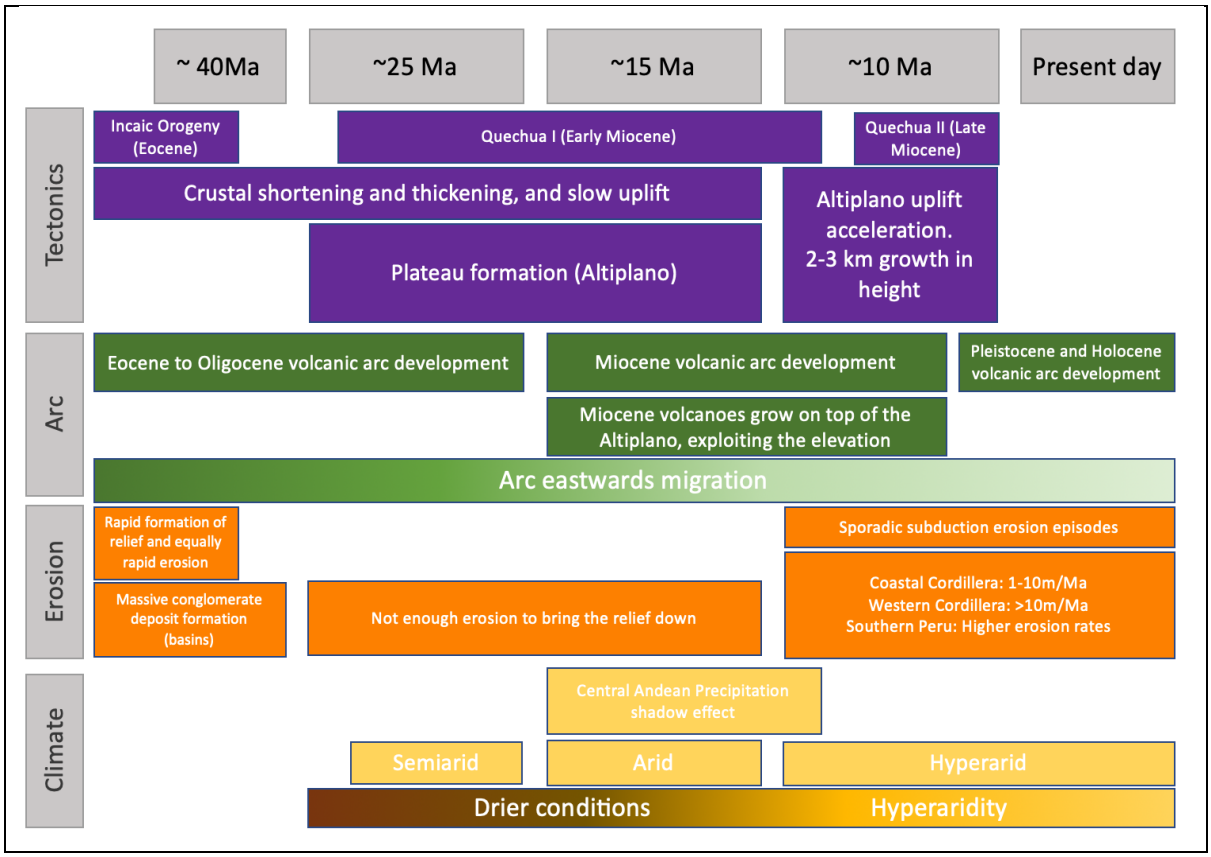


*Figure 1-8. Summary of the main tectonic, climate, erosional events, arc formation and migration in the Andes, from 40 My up to the present time.*

In this study, I focus mainly on the Central Andes, since it is the region where the highest number of volcanic edifices and PCDs are found. This region is located between 10º and 30ºS and comprise five major morphotectonic units, which from west to east are called: (1) the offshore and onshore fore-arc region, (2) the Western Cordillera (WC) which indicates the position of the present active magmatic arc, (3) the Altiplano-Puna plateau, which includes southern Peru, the Bolivian Andes and the Puna region in northern Argentina (14º-27S), (4) the Eastern Cordillera (EC) and, (5) the Sub-Andean Ranges (SA) and the Sierras Pampeanas (SP) (Figure 1-9). The EC, SA and SP are part of the belt of fold and thrust structures. These five major units are all approximately parallel to the coastline.

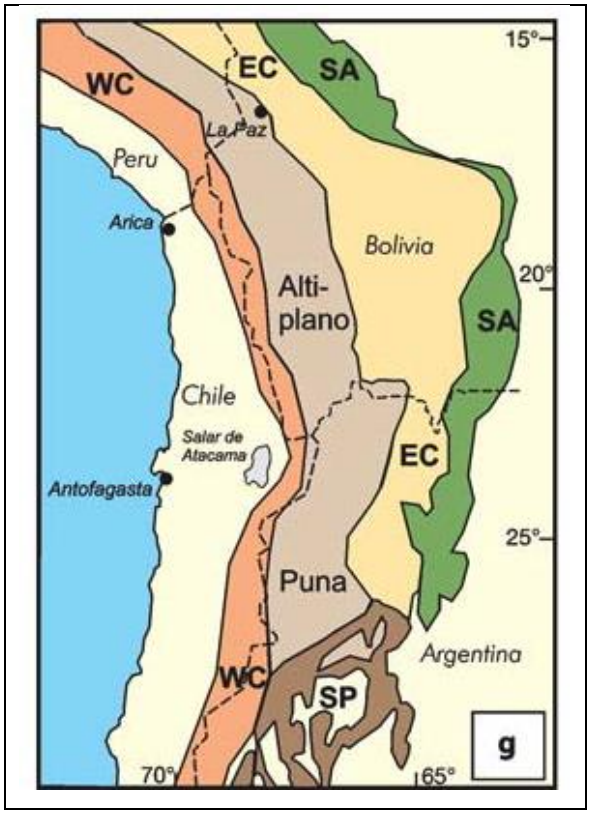


*Figure 1-9. Figure from Trumbull et al. (2006) showing the limits of the principal morphotectonic units of the central Andes, which include: Altiplano and Puna Plateaus, Western Cordillera (WC), Eastern Cordillera (EC), Subandean Ranges (SA), Sierras Pampeanas (SP).*

### 1.2.2 Magmatism

The volcanic front in the Andes migrated eastward over the past 40 My from the Precordillera to the Western Cordillera, where the current volcanic arc is now located. Post 10 Ma, the arc started to grow on top of the already developed Altiplano, exploiting the elevation that this plateau already had in place.

Figure 1-10b shows the variations in the volcanic influx between Eocene and Holocene for the southern Altiplano and the absence of evident correlation with shortening rate. Volcanic influx (red area) is constructed using the number of isotopically dated volcanoes (N=190), gathered in 3 My sliding windows, between 19° S and 22° S. To reduce bias resulting from repeatedly dated individual volcanic layers, Oncken et al. (2006) use individual volcanoes accounting only for the volcano lifetime and the associated isotopic dating error.

The relation between magmatism and deformation has been discussed for a long time. Evidence of this association are shortening and crustal thickening along with intense volcanic activity in the Central Andes during the late Paleogene to Neogene (Trumbull et al., 2006). However, there is no obvious correlation between magmatism and shortening rate (Figure 1-10b). Magmatism shows distinct pulses in the late

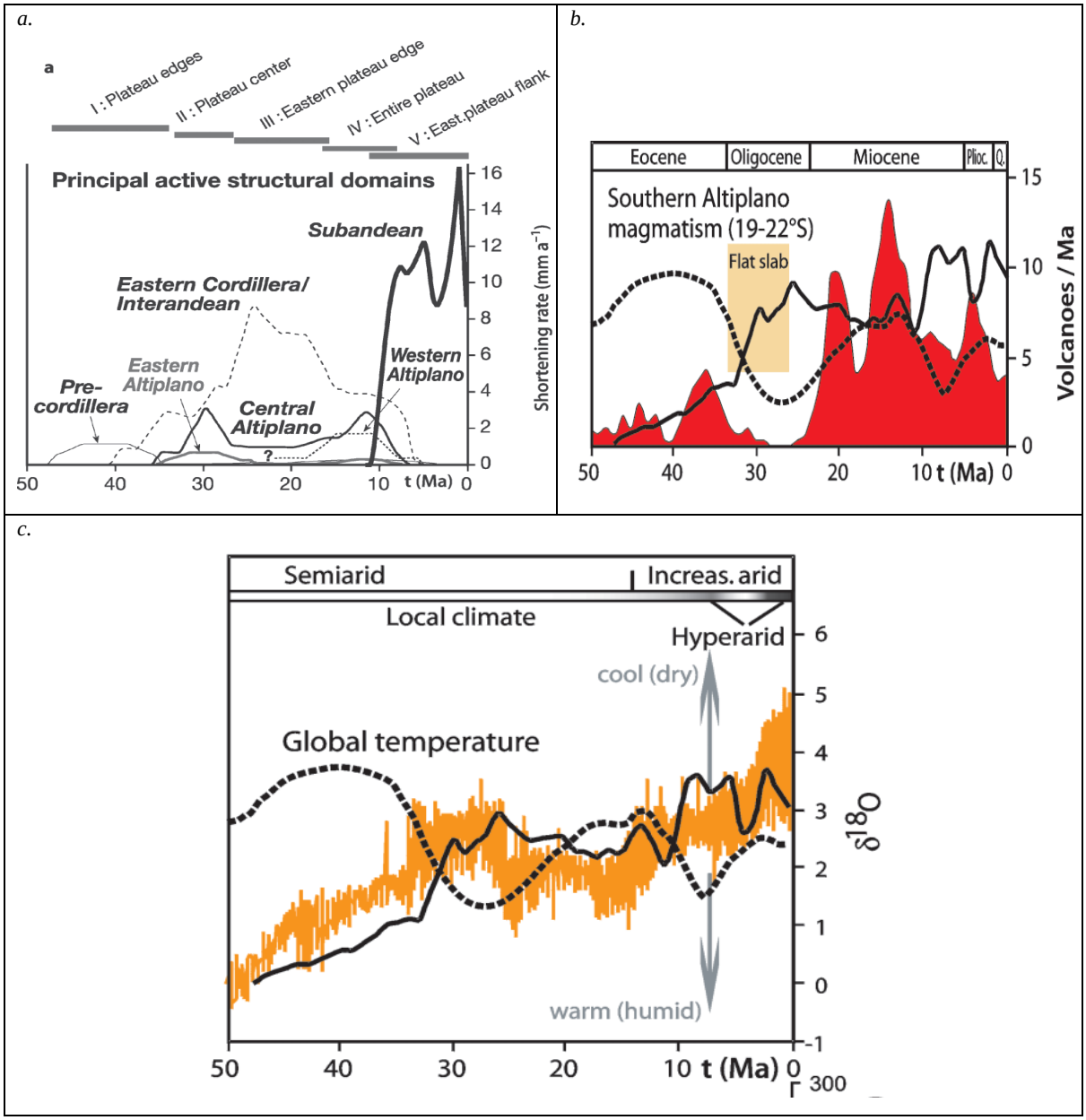


*Figure 1-10. Figures from Oncken et al. (2006) showing: a. Average shortening rates of the main active structural domains and phases of deformation in the Central Andes over the last 50 My. b. Number of isotopically dated volcanoes in red, gathered within a 3 My sliding windows, between 19° S and 22° S, superposed is the average shortening rates (black solid line), based on summing minimum and maximum shortening rates from Figure 1.10a., rollback fluctuation (black dotted line), and flat slab subduction proposed period (orange box; from Mahlburg Kay et al., (1999)). c. Shows the global climate tendency of $\delta^{18}O$ data (Zachos et al., 2001) superposed with average shortening rate (black solid line) and slab rollback fluctuation (black dotted line); in the box at the top, local climate evolution in northern Chile (Alpers and Brimhall, 1988; Gaupp et al., 1999; Hartley and Chong, 2002).*

Eocene, early and middle Miocene and finally the Pliocene, and is a well-established feature between 33–26 Ma. There is significant spatial expansion into the back-arc after 26 Ma. After plateau formation, beginning at about 10 Ma, both shortening rate and volcanic output in the Central Volcanic Zone (CVZ; **Error! Reference source not found.**), increase and reach their highest levels. During this time, the area

suffered from an exceptional number of large-volume ignimbrite eruptions, which originated in the Altiplano-Puna volcanic complex (Trumbull et al., 2006). However, magmatism on the surface may be slow to react to fluctuations in subduction and magmatic processes at depth (Oncken et al., 2006).

Changes at depth in the CVZ may have occurred for many reasons such as flat slab subduction and delamination of thickened crust. Oncken et al. (2006) conclude that crustal shortening rates only change when flat slab subduction improves plate coupling over an expanded area in a cooler and physically stronger environment. Temporal magmatic gaps between 5–12 My could be explained by sub-horizontal subduction events (Haschke et al. 2002b). Numerical modelling of the Central Andes by Sobolev et al. (2006) also suggests a non-temporal correlation between magmatism and upper plate shortening. They relate this anti-correlation to delamination events that may have started around 25 Ma, following earlier lithospheric thickening. Franz et al. (2006) explain delamination of the roots of overthickened crust into the mantle as one of the potential mechanisms for continental crust destruction at active margins (e.g., Kay and Kay 1993; Meissner and Mooney 1998). This mechanism is determined by changes in density and therefore restricted to mafic rocks that acquire sufficiently high density (by basalt-eclogite transition) to sink into the upper mantle. Kay et al. (1994) suggests that delamination took place under the ultra-thick Central Andean Plateau during the late Pliocene based on the distribution and chemical composition of back-arc basalts, seismic evidence of low-velocity reduction of S-waves in the upper mantle, and from high elevation in the Central Andean Plateau with only modest tectonic shortening (Franz et al., 2006).

### 1.2.3 Tectonics

The timing of the uplift of the Andes is controversial. It is widely accepted that the Andes is the result of a combination of crustal shortening and thickening, magmatic addition and possibly, eustatic rebound from delamination. However, researchers argue over the relative contribution of these components.

There are the two main schools of thought in terms of the evolution of the Andes. According to one theory, The Altiplano experienced a rapid surface uplift of ~2.5 km during the late Miocene (11-6 My ago) due to large-scale mantle delamination of the continental lithosphere (Farías et al., 2005; Garzione et al., 2006; Ghosh et al., 2006; Molnar and Garzione, 2007; Garzione et al., 2008; Hoke and Garzione, 2008). The other model suggests slow and constant uplift of the Altiplano region from the late Eocene onwards, attributed to the oblique subduction of the Nazca plate causing crustal shortening and thickening as a response (Victor et al., 2004; Barke and Lamb, 2006; Hartley et al., 2007; Barnes and Ehlers, 2009; Juez-Larré et al., 2010; Evenstar et al., 2015b; Lamb, 2016). It is feasible that both models are correct, starting with a slow steady uplift from Eocene onwards, that has been punctuated by rapidly Miocene uplift pulses.

Tectonic plate convergence rates, speed and angle of convergence have influenced the uplift of the Andes and this is also a topic of controversy. Jordan et al. (2001) proposed that a change in convergence dynamics indirectly triggered the change in orogenic style, through its effect on rheology. Sobolev et al. (2006) suggest that considerable modifications in the subduction rate, which in turn led to equally significant changes in the convergence rate, do not increase shortening in the overriding plate, while Oncken et al. (2006) propose that the speed of the South American plate, drifting obliquely with western direction, relates well to the

shortening rate in the Central Andes. However, there is no association with the convergence rate between the Nazca and South American Plates. In the last 30 My, the South American Plate, which has been drifting to the west over the Nazca Plate, has increased from a rate of ~2 cm $yr^{-1}$to 3 cm $yr^{-1}$ (Silver et al. 1998). The Nazca plate on the other hand, is subducting with the opposite direction (east) at a rate of about 5 cm $yr^{-1}$. Despite the opposing theories and models of plate convergence, there seems to be consensus that a strong increase in convergence rate occurred in the Late Oligocene, followed by a slowdown during Late Miocene time (Somoza, 1998).

### *1.2.3.1 Uplift during Eocene to Oligocene*

There is abundant evidence that the uplift of the Andes initiated at least 40 My, with the Incaic orogeny (Figure 1-8). Evidence of uplift during Eocene to Oligocene includes: (1) filling of thick conglomerates in Andean basins, such as the ones in the Chilean Precordillera and Longitudinal Valley (Evenstar et al., 2017, Horton, 2018); (2) exhumation rates from thermochronology (i.e., Dahlström et al., 2017) and (3) crustal shortening reconstruction using cross sections and 2D maps (i.e., Hoke et al., 2008) and 3-dimensional analysis (i.e., Hindle et al., 2005).

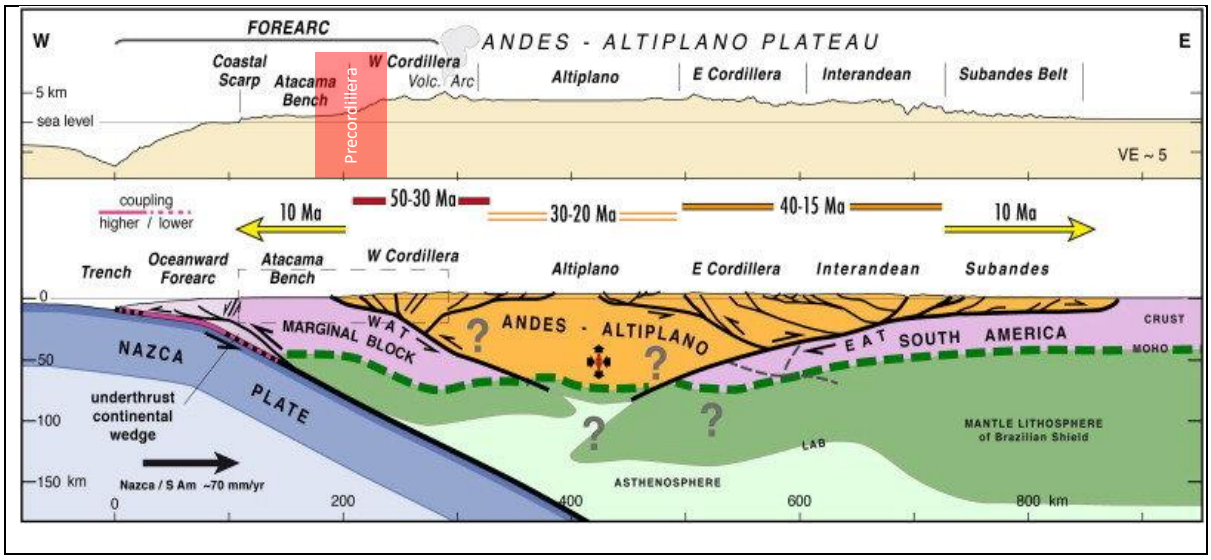


*Figure 1-11. Large-scale 2D structure of the Andes (from Armijo et al., 2015). The black arrow indicates westwards Nazca plate direction and speed rate. At the top, a topographic profile with vertical exaggeration of ~5 is shown. Horizontal coloured bars (red, orange and yellow) represent the age (My) of main deformation periods for the different geomorphologic domains in the Andes (Sempere et al. (1990); Maksaev and Zentilli (1999); McQuarrie et al. (2005); Oncken et al. (2006); Barnes and Ehlers (2009); Charrier et al. (2013)). Yellow arrows represent areas where deformation has propagated in the last 10 My. Grey question marks are placed where uncertainty is considerable. Red box shows the approximate location for the Precordillera region.*

Figure 1-11 is a cross section of the Andean orogen showing the areas affected by the shortening and the associated timing. The beginning of the uplift event had small shortening rates with significant oblique slip in the west, starting earlier in the western Cordillera (46 Ma) and then migrating to the east (40 Ma). The next episode in the Andes (36–30 Ma) was the shortening of the Eastern Cordillera, which was the only

morphotectonic unit affected during the period. During the Oligocene-Miocene, several strong uplift pulses contributed to the build-up of the Andes. The first stage, from 29-20 Ma, affected the entire Altiplano plateau from its western flank, the west Cordillera, across the central plateau (Altiplano), to the Eastern Cordillera.

### *1.2.3.2 Uplift during Oligocene to present day*

Clumped isotope palaeothermometry, palaeobotany and fluvial incision rates indicate that the second phase of uplift occurred between 19 and 8 My (Figure 1-11). The Oligocene compressive pattern continued during the Quechua I and II orogenies. Evidence of this compressive pattern are the continuous and rising deformation in the Puna region and the contrasting speed in different regions of the Altiplano plateau: the motion started and increased on the east flank while decreasing on the rest of the plateau (Oncken et al., 2006). Figure 1-10a shows average shortening rates for the main geomorphologic domains in the Southern Altiplano and the stages of principal deformation. Karátson et al. (2010) state that since 10 My ago (Late Miocene), the Altiplano has gained an additional 2-3km in altitude and as a consequence substantial valley incision occurred in the western flank of the Altiplano (Wörner et al., 2000; Thouret et al., 2007; Ehlers and Poulsen, 2009; Schildgen et al., 2007, 2009a, b, 2010). The process that accelerated the uplift of the Altiplano was the constant shortening focussed mainly on the Eastern Cordillera. Figure 1-12 shows a model for the Central Andes developed by Sobolev et al. (2006), for the period between 35 My to the present day. The model shows that starting around 10 My ago, high elevations were generated by tectonic shortening in what was the back-arc at the time (orange curve) and that these high topographic features eventually formed the Altiplano plateau (4 km high) in the last 5-10 My. The formation of the plateau is the result of the compensation for crustal thickness in depth and superficial smoothing at the surface (Figure 1-13) (Sobolev et al., 2006).

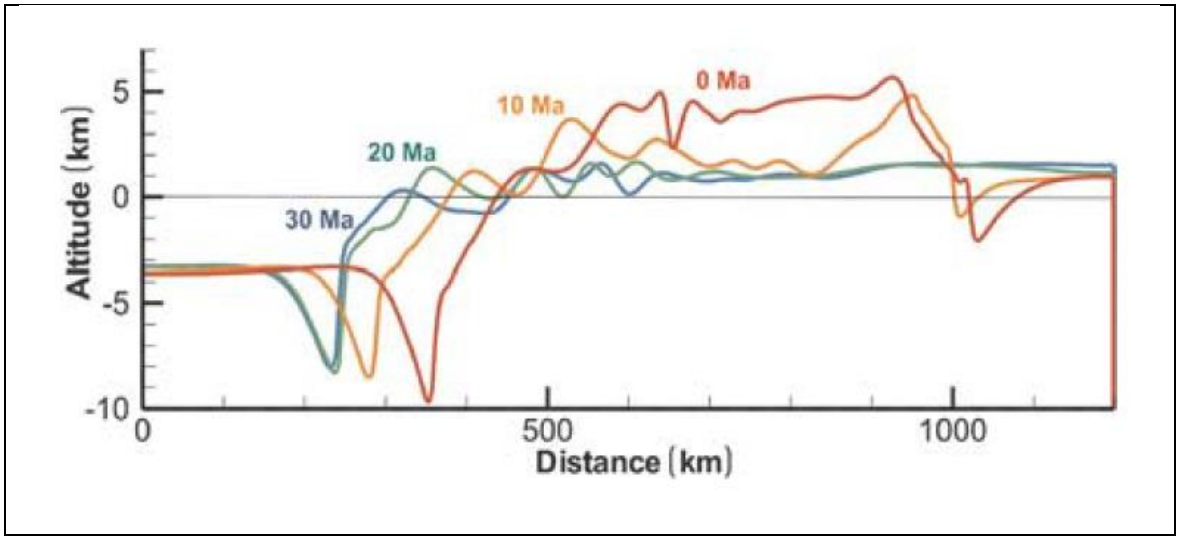


*Figure 1-12. Figure from Sobolev et al. (2006) showing the model of surface topography evolution of the Central Andes in the last 30 My. Each profile represents the changes in the Andes topography every 10 My.*

In contrast, Perkins et al. (2016) explain that a 1.5 km uplift in the last 11 My can be explained by the formation of the Altiplano-Puna Magma Body (APMB). Evenstar et al. (2020) support this hypothesis, suggesting uplift in the forearc for the same period of time (11-0 My). Lamb and Davis (2003) suggest that the climate in the Andes may had an invaluable role regulating the uplift of the Andes, and the stress in the subduction plate interface could have been increased by the change in the climate for arid to hyperarid. The associated uplift rates and topographic elevation variations in the Altiplano plateau are also controversial and estimates from different authors (Evenstar et al., 2020; Oncken et at., 2006; Perkins et al., 2016; Sobolev et al. (2006); etc) vary between 4-1.5 km high.

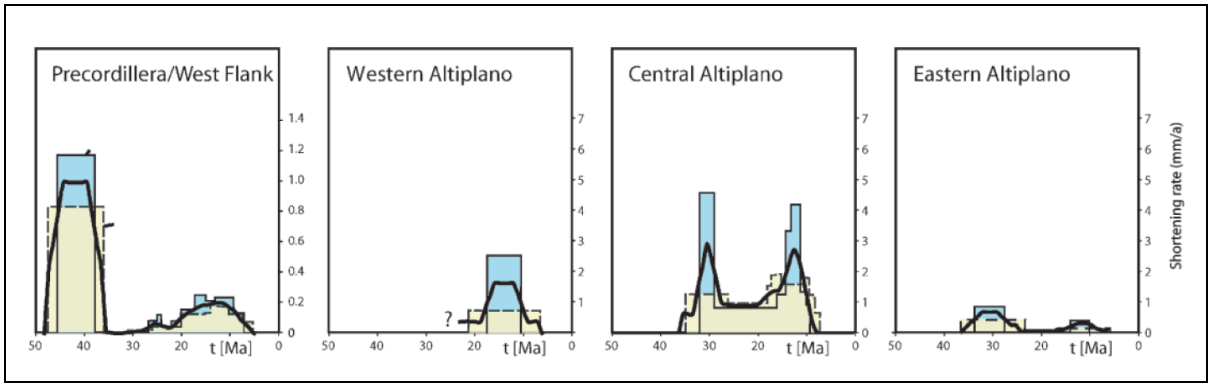


*Figure 1-13. Figure from Oncken et al. (2006) showing the cumulative shortening rates (mm/a) in the last 50 My, for four active structural domains (Precordillera, Western Altiplano, Central and Eastern Altiplano) in the Central Andes, the bold line indicates average shortening rate.*

### *1.2.3.3 The Bolivian Orocline*

There are several explanations for the formation of the Bolivian orocline, which is located at the Chile-Peru border (18°S) and its origins still remains poorly understood. The curvature in the Andes, between Chile and Peru is known as the Bolivian Orocline. Isacks (1988) and Allmendinger et al. (1997) proposed that the orocline formed due the accumulative shortening of the Andes, which was enhanced towards the Arica bend. Isacks (1988) proposed that the development of the bend started and was amplified during the formation of the Andean orogen instead of happening due to later tectonic events. Kley et al. (1999) demonstrated that the bend could have been formed by the combination of differential shortening and rotation of faulted blocks. Riller and Oncken (2003) and Kley et al. (1999) suggest that the origin of the Bolivian bend was a mix of shortening, parallel to the Andean mountain chain, and strike-slip motion that was responsible for the growth of the Central Andean Plateau. Yáñez and Cembrano (2004) developed a model showing that the bend at the Chile-Peru border could be achieved by changes in the interaction between the overriding and subducting plates, Nazca and South American respectively, along the orogen. Arriagada et al. (2008) after creating 2-D map reconstructions of the Central Andes, theorised that the Bolivian orocline formed due to differential shortening mainly occurring in the Eastern Cordillera, and that has been in place since the Eocene to Oligocene period. Hu et al. (2016) ran geodynamic models on the South American plate subducting under the Nazca plate in the last 100 My. In these simulations, they gradually include plate motion, the age of the

seafloor and strategically selected tectonic features. They take into consideration the history of central Andean deformation, as well as trench profiles following Arriagada et al. (2008) geological restorations. Hu et al. (2016) reconstruct trench profiles showing the evolution of the Bolivian orocline Figure 1-14.

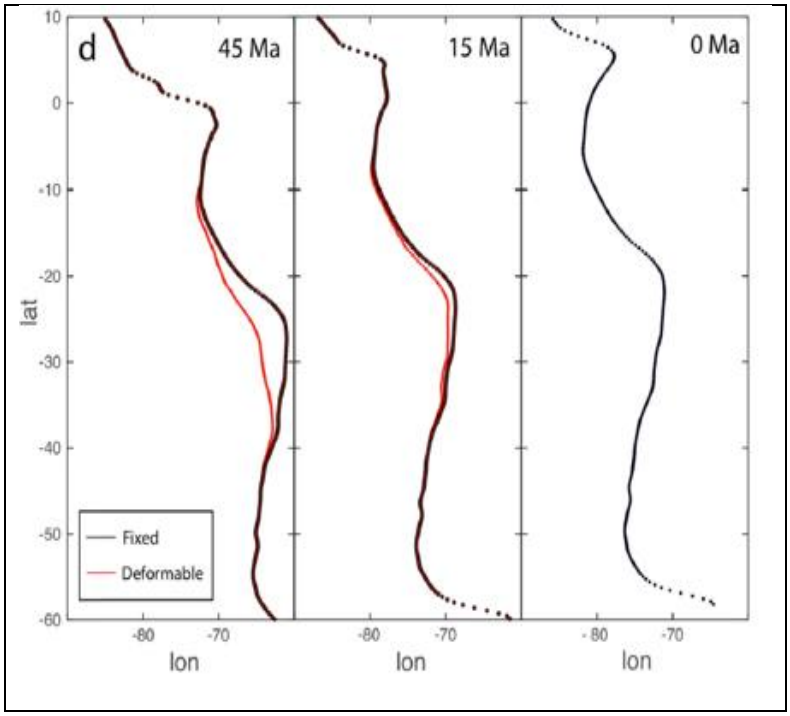


*Figure 1-14. Figure from Hu et al. (2016) showing the variation in the trench profile for the last 45 My. The red lines show the active and deformable trench contour for each episode (Arriagada et al., 2008), and the black lines indicate the current trench geometry for comparison.*

### *1.2.3.4 Precordillera region*

I am particularly interested in the Precordillera, since it is where the majority of PCDs are found in the Andes. The region has been highlighted with a red square in Figure 1-11, between the Atacama bench and the Western Cordillera.

Oncken et al. (2006) compiled and reconstructed different periods of deformation in the Andes. Figure 1-11 shows a large-scale 2D cross-section interpretation at 21°S, across the southern region of the Andes. Oncken et al. (2006) established that this region had a particular evolution. The Eocene Incaic orogeny is characterised by low shortening magnitudes and major oblique motion to the west (Reutter et al., 1996; Müller et al., 2002; Haschke and Guenther, 2003; Horton, 2005). Oncken et al. (2006) proposed that the Incaic orogeny started first in the west, around 46 My, and then migrated to the east (40 My). In an early stage, during the Incaic event, significant shortening only occurred in the Precordillera/Western Cordillera and along the Eastern Cordillera (46–37 My) (Figure 1-11; Figure 1-13). Later, between 36–30 My, the Eastern Cordillera was the only remaining region suffering from shortening. During the final phase of the Andean shortening, two new shortening episodes affected the west and east of the Central Andes. The first,

between 29-20 My caused deformation of the entire Altiplano plateau and propagated to the Eastern Cordillera, and the second, between 19-8 My, affected the Puna region (Oncken et al., 2006). In summary, the area of interest to this thesis, the Precordillera, experienced one intense shortening event at the beginning of the Incaic orogeny and later, two additional although smaller shortening episodes (Figure 1-13).

#### *1.2.3.5 Tectonic Segments*

The Andean orogen consists of a series of tectonic segments separated by transverse boundaries that reflect discontinuities of the underlying subduction zone. At these boundaries, the characteristics of belts of magmatic rocks and the type, age and size of ore deposits may change (Sillitoe, 1974). The 17 tectonic segments in the Andes delimited by Sillitoe (1974) show a clear correlation with seismic studies (Gajardo and Lomnitz, 1960, Stauder et al., 1973, Kelleher et al., 1973). The tectonic blocks correlate with metallogeny, shown by the fact that metallogenic belts crossing tectonic boundaries tend either to end or change in their characteristics, including: second-order variations in their metal contents; changes in their widths; and changes in the ages, types and sizes of ore deposits.

#### *1.2.3.6 Sediment control on subduction plate speeds*

The speed of tectonic plates depends on the balance between: i) speed variations of the subducting plate and the reaction of the mantle to the subducting slab, ii) bending lithosphere, and finally, iii) the interface between the subducting and overriding plates (Behr et al., 2018). Behr et al. (2018) propose that there is a direct correlation between the down-going slab speed and the amount of sediments trapped between plates, which may work as a lubricant influencing the convergence speed between tectonic plates. Convergence deacceleration between plates will occur if the viscosity in the deeper parts of the plate interface is considerably higher than the viscosity in the asthenosphere, and one way to generate this type of viscosity contrast is if sediments between plates were scarce. Lamb and Davis (2003) suggest that primarily erosion and sedimentation, and secondly climate are the main geological processes controlling the subduction dynamics and the formation of the Andean orogen. In the Central Andes, climate plays a key role constraining the sediment mass flux that reaches the plate boundary and Hoffmann-Rothe et al. (2006) show how this correlation is evident for different regions in the Andes (Figure 1-15a). In the case of sediment starvation, high shear stress in the plate interface are the ideal conditions for building an orogen up like the Andes. On the other hand, if sediments are available in enough quantities, they will end up lubricating the plate interface, which in turn will reduce its viscosity. The plate boundary will now become less viscose than the asthenospheric mantle, and as a consequence it will allow considerably faster plate convergence speeds (Behr et al., 2018). The viscosity contrast between oceanic–continental plates is of paramount importance, since it controls the convergence speed between them (Behr et al., 2018). When there is an overthickened continental plate, such as the South American plate, an orogeny increases the length of the viscous plate boundary, providing further resistance and consequently reducing the subduction velocity (Figure 1-16a). However, rising elevation in a thick continental plate will automatically create an excess of sediment supply

into the trench, causing the opposite effect than before by lubricating the plate and accelerating subduction (Behr et al., 2018).

*a.*

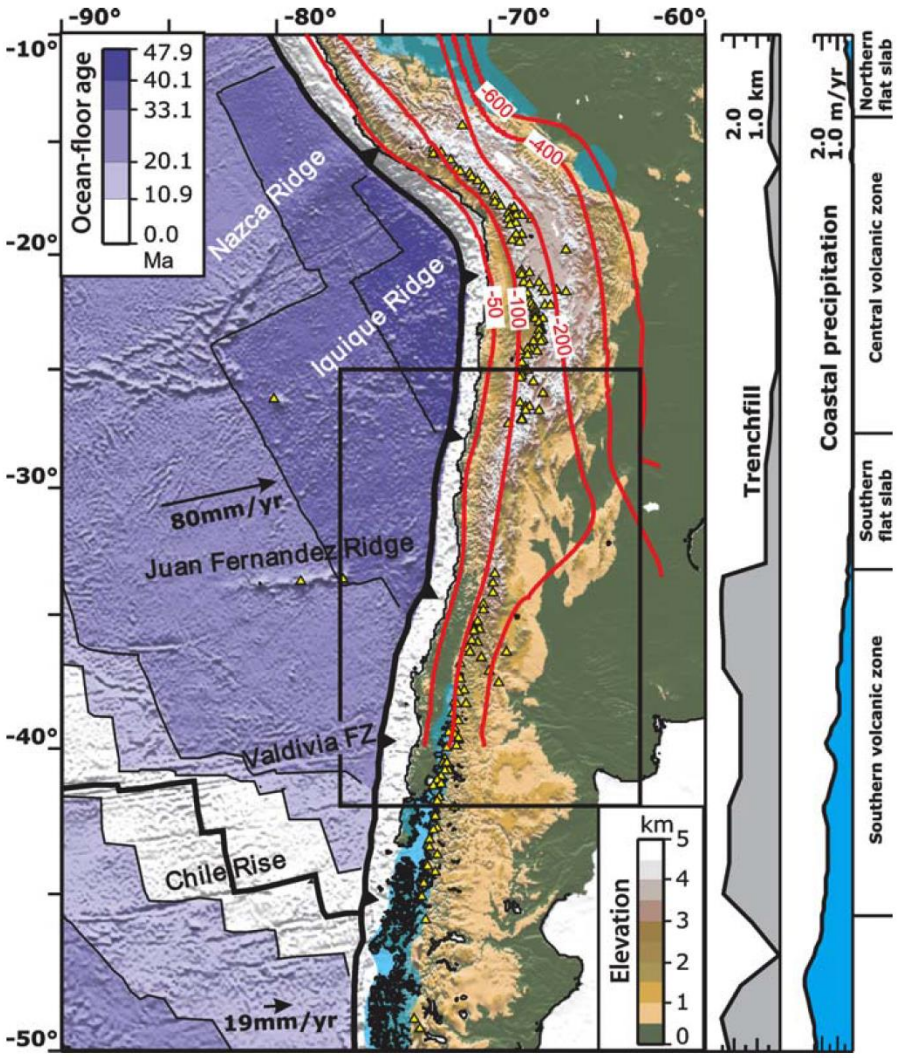


*b.*

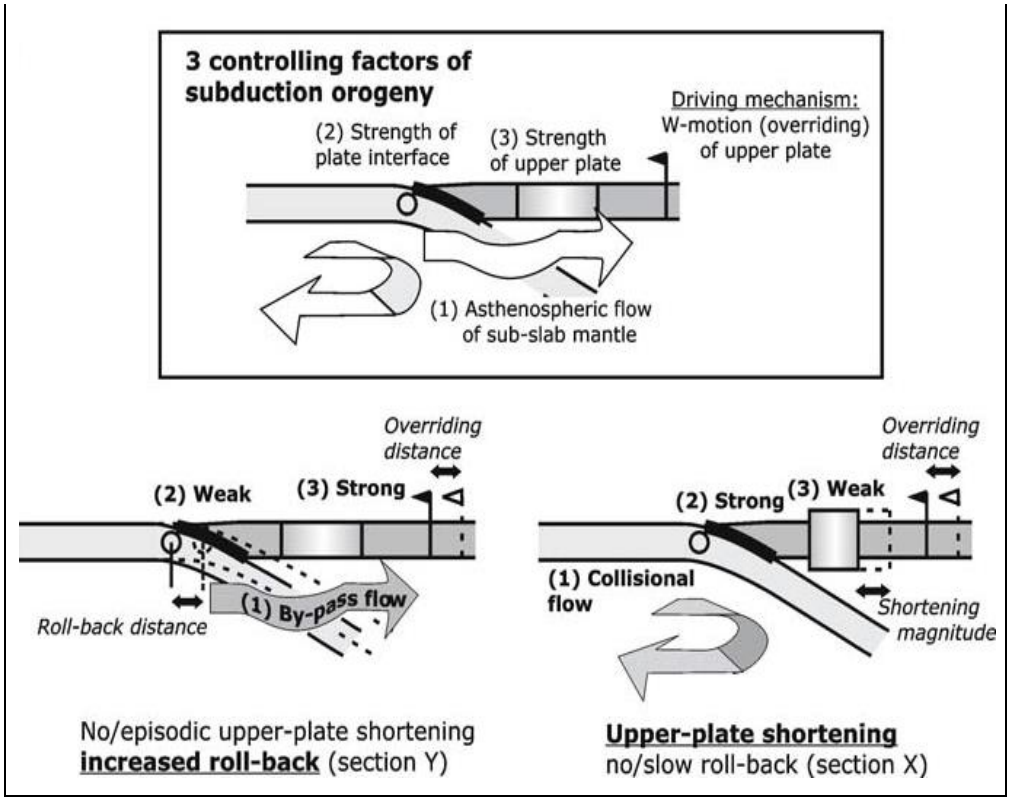


*Figure 1-15. a. Figure from Vietor and Echtler (2006) showing a shaded topographic image of the subduction zone in the Andes. Yellow triangles indicate the location of Holocene volcanoes (Smithsonian Institution, Global Volcanism Program). Red contour lines indicate the depth to the Wadati Benioff zone in km, from Creager et al. (1995). On the right panel, the grey area shows the latitudinal trench infill thickness variation (Hoffmann-Rothe et al. 2006) and the blue area indicates the annual precipitation along the coast (New et al., 2002). b. Figure from Vietor and Echtler (2006) showing the main three factors that influence if, and how much, the overriding of the upper plate leads to upper plate shortening or slab rollback. Cartoons at the bottom panel present two scenarios that could occur between plates: positive (right) and negative (left) feedback.*

According to the model of Lamb and Davis (2003), shear stresses along the plate boundary is controlled by the sediment mass flux into the trench. Variations in sediment quantities, can also affect the subduction geometry as variations in the trench fill thickness will influence the slab dip angle and resistance to overriding. Oncken et al. (2006) agree that there is a complicated correlation between sediment supply into the trench, plate coupling ("the degree to which the overriding plate is "stuck" to the subducting plate", (Hackney et al. 2006, p.365)), slab rollback, and the deformation of the upper plate. Vietor and Echtler (2006) suggest there are three components that influence and define the relation between the rate of overriding and shortening of the upper plate: flow conditions of the mantle under the subducting plate, and the strengths of the plate boundary and upper plate. Depending on the balance and magnitude of these three components, rollback of the slab or shortening of the upper plate will be favoured (Figure 1-15b). Slab rollback occurs when the upper plate is strong and the plate interface is weak, impeding shortening of the upper plate and transforming the overriding into roll-back of the slab (negative feedback; Vietor and Echtler, 2006). Sobolev et al. (2006) and Vietor and Echtler (2006) suggest that slab rollback is minimized with greater frictional strength of the plate interface. The ideal environment for the Andean orogeny is actually

quite the opposite: a strong plate boundary, a weak upper plate and limited mantle flow under the slab allow upper plate overriding, as well as deformation and shortening of the upper plate (positive feedback).

I can now take into consideration changes in sediment accumulation in the trench from the Eocene up to the present day. Figure 1-16b shows that tectonic environment reactions to the variation of sediment influx to the trench are constrained to the Eocene period; for the period between 45 and 30 Ma, greater sediment input correlates well with higher retreat rate. Conditions where better lubrication between plates exist are mainly controlled by higher topography, which depends on deformation episodes (Incaic shortening stage) and higher erosional sediment supply from the Precordillera (Oncken et al, 2016)

During the period of slowed retreat between 30 and 20 Ma, flat slab subduction probably had an important impact on sediment accumulation along the trench. Results from Hu et al. (2016) suggest that, under conditions where no overriding plate is in place and viscosity contrast between the subducting slab and the asthenosphere, then the age of the seafloor is responsible for the subducting dip angle, since it will influence the slab's mechanical strength. Hu et al. (2016) models show that subducting slab strength dictates its buoyancy for times before 30 My ago, and the opposite trend for younger ages. The presence of a thickened continental overriding plate allows the subducting slab to become less steep, enhancing the suction motion. Individual cratonic roots may have an additional effect in dip angle reduction.

In the last 10 My, the Nazca South American plate speed has increased while the Nazca plate deaccelerated and retreated. This combination seems to have inflicted higher shortening rates in the upper plate and higher erosion rates in the slab, indicating a strengthening of the plate boundary with respect to the upper plate (Oncken et al., 2016).

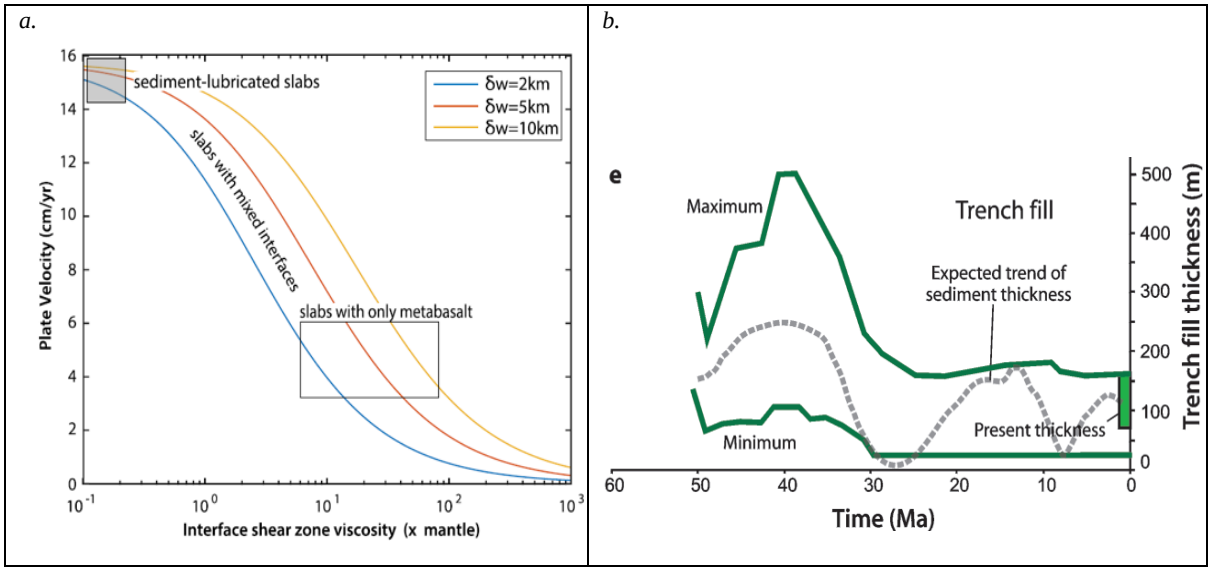


*Figure 1-16. a. Figure from Behr et al. (2018) showing how much plate velocity varies when plate interface shear zone viscosity increases, for a variety (blue: 2km, orange: 5km and yellow: 10km wide) of shear zone widths (δw). Due to higher viscosity originated by dominant mafic rocks in the plate interface, the slab should subduct slower compared to slabs lubricated with sediments. b. Figure from Oncken et al. (2006) showing an estimated range of trench fill thickness (green bold line represents maximum and minimum), comprising the present-day average thickness (green box; Kudrass et al., 1998; von Huene and Ranero, 2003) and superposed is the expected trend of sediment thickness (dotted grey line), assuming that the plate interface strength has an inverse correlation with sediment supply into the trench.*

#### *1.2.3.7 Crust Destruction and Mass Wasting*

At active margins, continental crust destruction may occur for several reasons. Delamination at the base of the crust is one of the main causes in areas that suffered from shortening and extreme thickening like the Central Andes Plateau (Franz et al., 2006). Kay et al. (1994) proposed that crust destruction may have occurred in the late Pliocene in the Central Andes. However, at a continental margin of normal crustal thickness, delamination is not a feasible destruction mechanism. Instead, crust destruction is due to tectonic erosion, remobilization and transport of sediments after weathering, and chemical erosion. Some authors (Sarin et al., 1989; Hu et al., 1982) estimate that rivers may account for a total dissolved load of more than 20% of the suspended load in fluvial systems. The implication is that a substantial amount of this sediment will be discharged into the ocean and only a small percentage is retained in the continent (Glodny et al., 2006).

A second cause for continental mass destruction is the subduction of portions of the crust into the asthenosphere. This may occur when sediments with continental provenance and/ or slices of the upper plate that have been removed by tectonic erosion are deposited into the trench (Franz et al., 2006). According to Glodny et al. (2006), tectonic erosion is likely to be the most relevant process for upper plate mass loss into the mantle. Even under conditions where mass accretion exists, like in active margins, a lot of the sediment flux in the trench will probably be subducted into the mantle (von Huene and Scholl 1991).

Several authors observed that the amount of sediments feeding the trench is key in terms of erosion of the upper plate by subduction (e.g., Lallemand et al., 1994; Lamb and Davis, 2003; Clift and Vannucchi, 2004). Oncken et al. (2006) estimated that for the circum-Pacific convergent margins, an average of more than 1000 m of sediment infill thickness in the trench is needed in order to switch from subduction erosion to accretion. On the contrary, if the infill thickness is thinner than 1 km, then subduction erosion prevails (Oncken et al., 2006).

Several episodes of tectonic erosion occurred within the timeframe for this study. A major episode during the early Permian is assumed for the region north of 38°S. Additionally, Glodny et al (2006) propose a second short-term tectonic erosion event in the Late Cretaceous and Cande and Bangs (1997) suggest a third episode during the late Miocene. Hu et al.'s (2016) models show that changes in the trench profile occurred over the last 45 My (Figure 1-14). However, Glodny et al. (2006) suggest that the width of the forearc in the Andes has been stable since the Jurassic, and that the consolidated continental South American margin has not suffered from any tectonic destruction.

### 1.2.4 Climate

Balancing the effects of uplift from crustal shortening and magmatic input are the effects of erosion, which are largely controlled by changing climate (Evenstar et al., 2017) (Figure 1-10).

#### *1.2.4.1 Summary of the climate control in the Andes*

Both palaeobotanical data (Wolfe, 1978) and oxygen isotopes (Shackleton, 1975; Shackleton and Brenchley, 1984) indicate a monotonic, but not constant, cooling of the Earth in the past 50 My. The highest temperature drops occurred near the Eocene/ Oligocene boundary (≈ 36 My ; Wolfe and Hopkins, 1967; Wolfe, 1971;

Shackleton, 1975; Savin, 1977; Wolfe, 1978; Keigwin, 1980; Shackleton and Brenchley, 1984), at approximately 15 My during the Miocene epoch (Shackleton, 1975; Woodruff et al., 1981; Shackleton and Brenchley, 1984) and at around 2.5 Ma, close to the end of the Pliocene epoch, when the Northern Hemisphere was affected by continental glaciation (Shackleton, 1975; Savin, 1977; Shackleton and Brenchley, 1984). Moreover, the drop in temperature was much more significant at high latitudes than at low latitudes (Savin et al., 1975; Savin, 1977; Wolfe, 1978).

The range of latitudes and altitudes of the Andes mean this mountain chain is exposed to a great variety of climates. Montgomery et al. (2001) characterise regions according to the annual rainfall they receive. The Intertropical Convergence Zone (10°N–3°S) has >2 $m \cdot yr^{-1}$ rainfall. As the subequatorial northern Andes (3°S–15°S) is divided by high topography into two subregions, one to the west (Amazon) and another to the east (Pacific side), rainfall rates are 2 $m \cdot yr^{-}$ and 0.2 $m \cdot yr^{-1}$ respectively. Winds originating in the west are responsible for the opposite effect in southern latitudes (south 33°S). Within the subtropical belt of deserts (15°S - 33°S) precipitation rates are low on either side of the range, including the Altiplano plateau. Lenters and Cook (1995) propose that the Andean chain plays a decisive role in controlling precipitation distribution in the inner land (Lenters and Cook, 1995), particularly during austral summer (Garreaud, 2009), since if the height of the Andes is reduced, it decreases the strength of the South American Monsoon and increases the rainfall over northern Amazonia.

All these distinctive climate conditions in the Andean mountains depend on atmospheric circulation in the Southern hemisphere and Montgomery et al. (2001) suggest that they were probably responsible for the development of the orogen. However, other researchers believe that climate provinces were determined by orographic features. For example, Huston and Hartley (2003) endorse the idea that dry conditions in the Atacama are exclusively generated by the rain shadow effect of the Andes, acting as moisture barrier for air coming into the continent. Some authors such as Ehlers and Poulsen (2009) suggest that increasingly drier climates 10-15 My ago reaching hyperaridity in the Central Andes, were caused by tectonic uplift, which increased the rain shadow effect in the Andes and in turn modifying the air circulation configuration. However, according to some models, the Atacama would not have a humid climate even if the height of the Andes is lowered, since the region is constantly receiving cool, dry air from the Pacific (Lenters and Cook, 1995; Sepulchre et al., 2008; Ehlers and Poulsen, 2009; Garreaud et al., 2009). These results are most important for understanding the relation between the uplift in the Andes and the beginning of hyperarid conditions in the Atacama region during Miocene times (e.g., Garreaud et al., 2010).

Undoubtedly, the Andean mountains alter atmospheric circulation due to its massive length and height, and as result in notable climate variations affecting certain regions and consequences of different magnitude occur in different scales.

#### *1.2.4.2 Summary of the climate in the western Andes*

The timing of the onset of hyperaridity and its causes on the western side of the Andes are controversial (Hartley and May, 1998, 2000; Hartley and Rice, 2005; Hartley et al., 2007; Hartley and Evenstar, 2010) The switch to hyperaridity has been suggested as 23 My (Urrego et al., 2005; Kober et al., 2007), 15 My

(Alpers and Brimhall, 1988; Mortimer et al., 1974), 10 My (Evenstar et al., 2017; Rech et al., 2019) or 3 My (Hartley et al., 2005). Current evidence from paleosols across the region suggests a background semi-arid climate until 23 My, an arid climate until 10 My and then hyperaridity from 10 My to the present day (Rech et al., 2019). Superimposed on this background are minor (1-2 My) fluctuations as the climate cyclically moved into relatively more humid (but still arid) climates at ~35-23 My, ~18-13 My, 12-11 My, 8-7 My and 5-3 My (Evenstar et al., 2017). Hyperaridity has characterised post-Pliocene climate, with short and smaller episodes of more humid conditions than in the past (Jordan et al., 2014). A summary of climate changes is shown in Figure 1-17.

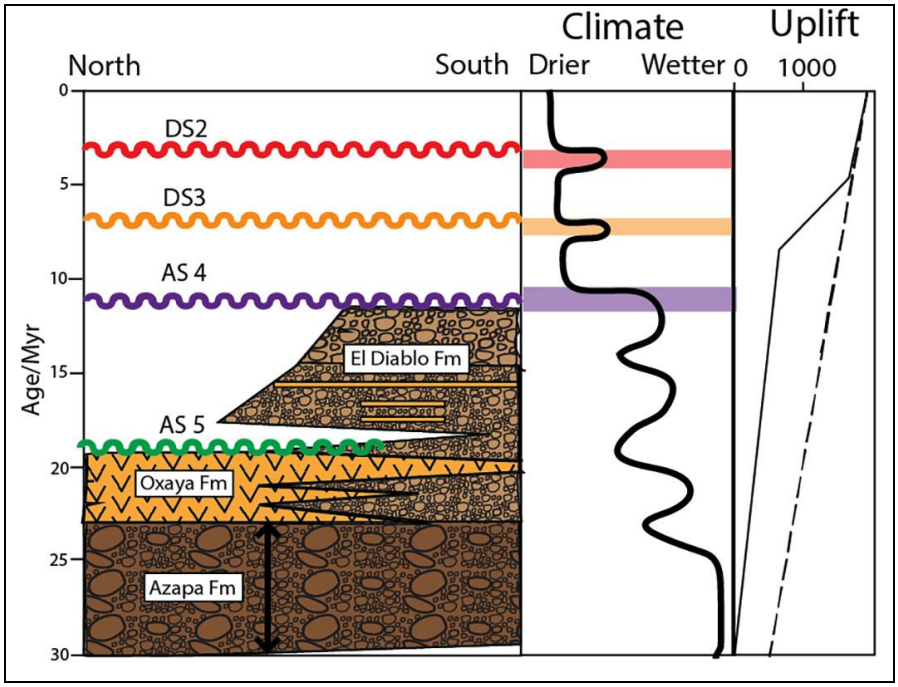


*Figure 1-17. Figure from Evenstar et al. (2020) presents a simple sedimentary basin overview of the Longitudinal Valley showing the principal geomorphic surfaces (AS5, AS4, DS3 and DS2). On the right panel, the climatic variations and pulses for the last 30 My are also shown for Longitudinal Valley (Jordan et al., 2014; Evenstar et al., 2017). On the rightest panel, two possible uplift events: one in the Late Miocene uplift (black solid line) and another during the Early Miocene (dashed line).*

### *1.2.4.3 Summary of the climate in the eastern Andes*

Karátson et al. (2012) suggest that arid conditions decline from the Atacama in the west to the East Cordillera in the east, and the uplift of the Andes has caused humid atmospheric conditions coming from the Amazon basin and the Atlantic Ocean to accumulate eastwards. During the Pleistocene and Holocene cold and more humid conditions affected the Western Cordillera and the Altiplano. These conditions caused glaciations at altitudes >4200–4700 m (Clayton and Clapperton, 1997), and also allowed the development of a series of large paleolakes (e.g., Placzek et al., 2006, 2011). Finally, the climate has remained mainly the same since the mid-Miocene (Horton ,1999, Hoke and Garzione, 2008 and Karátson et al., 2012).

### 1.2.5 Erosion

Topographic studies by Montgomery et al. (2001) indicate that the first-order control on the morphology of the Andean mountains are the hemisphere-scale variations in the climate. Erosion gradients depend on the atmospheric conditions and air flow in the Southern Hemisphere, since they strongly regulate precipitation along the latitude. Since all erosional processes (fluvial, glacial, and tectonic) dominate in certain climatic conditions, they can be estimated using cross-range asymmetry, width, hypsometry, and maximum elevation. Erosion is not uniform in the Andes, since it depends on large-scale climatic regimes, and because climate also influences the evolution of the orogen. Tectonics and erosional processes can interact and generate feedbacks between climate, erosion and tectonics (Montgomery et al., 2001) which ultimately influence processes occurring in the shallow crustal (Willett, 1999), or even deeper into the mantle.

*a.*

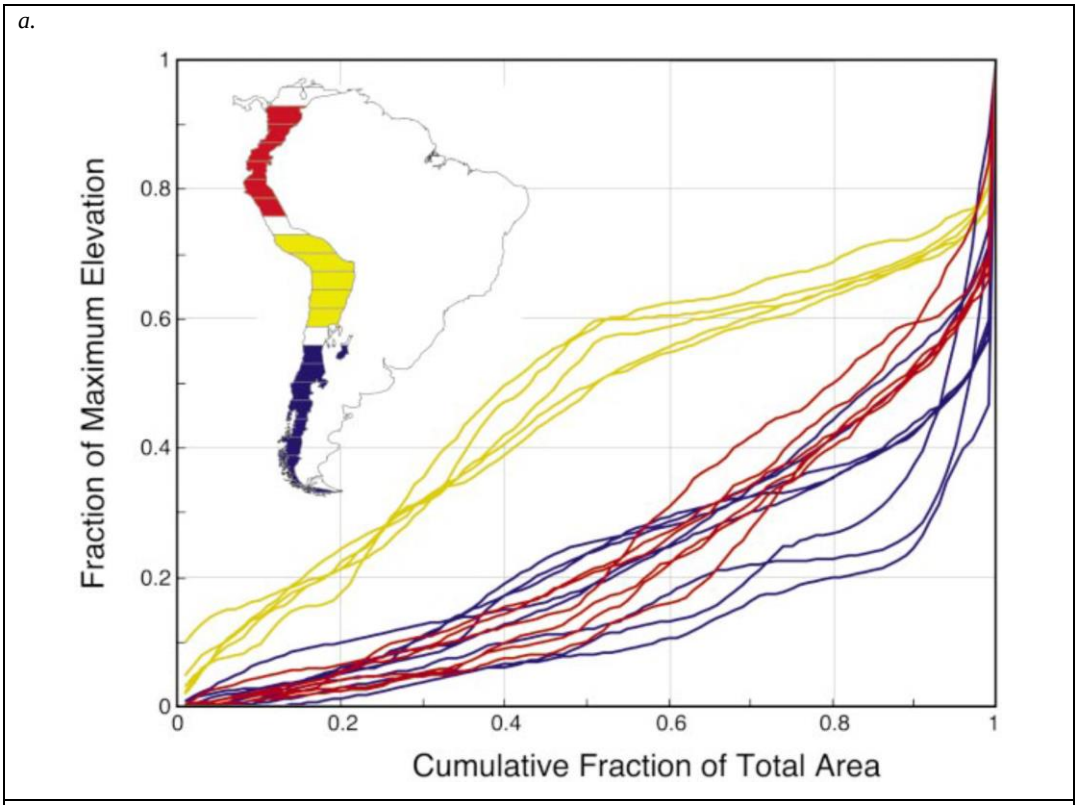


*b.*

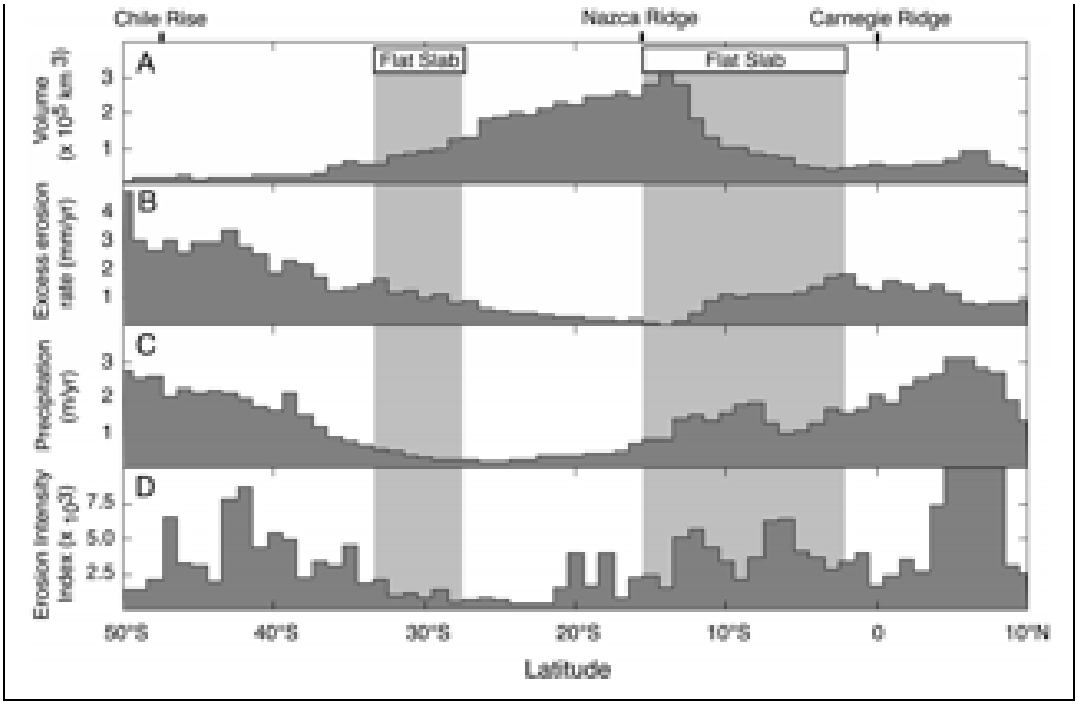


*Figure 1-18. Figures from Montgomery et al. (2001). a. It shows three environments that would create three distinctive normalized hypsometric curves along the Andes; curve colour identifies the location of each environment: northern (red), central (yellow), and southern (blue) Andes. b. 'A: Volume of Andes above sea level calculated from 1º latitude bins. B: Excess erosion rate, relative to largest 1º bin, is required to explain volume difference under uniform tectonic convergence. Latitudinal variation in erosion rates under constant tectonic convergence by calculating missing mass above sea level in each 1º latitude bin as VXSα/At, where VXS is excess volume in given bin compared to largest bin (14°–15ºS), A is bin area, t is time (taken to be 25 My.), and α=ρc/(ρm- ρc), where ρc= 2.7 g·cm-3 and ρc=3.3 g·cm-3. Note that because of the selection of strictly east-trending bins for analysis, the region between 13ºS and 17ºS, where range trends northwest rather than north, has anomalously large volume in each bin. C: Mean annual precipitation. D: Mean erosion intensity index value' (Montgomery et al. 2001, p.581).*

A few researchers (Willett et al., 1993; Brozović et al., 1997) have explored the idea that global climatic variations may be the main regulator for the large-scale morphology of the Andes. Montgomery et al. (2001) support this theory and describe three climatic archetypes affecting landscape evolution: (1) normal fluvial erosion; (2) tectonics (e.g., crustal thickening by wedge propagation; the formation of the Altiplano plateau) and (3) glaciation. Regimes with different climate should show distinctive hypsometrical signatures (Figure 1-18; Figure 4-18). In the northern Andes, fluvial erosion in a wet, tropical climate prevails above other erosion types, landscape is sculpted by dissected massive rivers and, concave-up hypsometric curves characterised them. While for the southern Andes, glacial erosion dominates erosional mechanisms by dissecting the highest elevations of the mountain range. This process creates a shoulder in the hypsometric curves. Finally, the central Andes presents a weakly incised tectonic wedge and mechanically limited plateau that indicates river incision is not as effective as tectonic uplift; the resulting hypsometric curves are nearly flat (Montgomery et al., 2001).

A direct correlation exists between hypsometry and maximum elevation (Figure 1-18; Figure 4-18). The correlation between total relief and snowline elevation supports the idea that with higher erosion rates in

glacial and periglacial environments, the relief of mountains is limited (Brozović et al., 1997). Based on this, Montgomery et al. (2001) conclude that is not possible for high topography to prevail at high latitudes and that the high Andes end at 35ºS in part because they intersect the perennial snowline at this latitude. They also suggest that variable erosion has affected the Andes: i) evidence of extreme erosion and exhumation are the igneous rocks found in the northern and southern Andes, implying that deeper levels of the crust have been exhumated, and ii) minimal exhumation and erosion is indicated by preserved sedimentary and volcanic cover of the central Andes. A good example of the latter is the Eastern Cordillera and Subandean zone of Bolivia (north of 19ºS), which have undergone 2–6 km of exhumation over the past 10 My (Benjamin et al., 1987), but only 1 km of exhumation in that time south of 19ºS (Masek et al., 1994; Gregory-Wodzicki, 2000). In conclusion, erosional gradients are strongly influenced by climatic regimes and they contribute to the latitudinal variation in mountain range width and crustal volume.

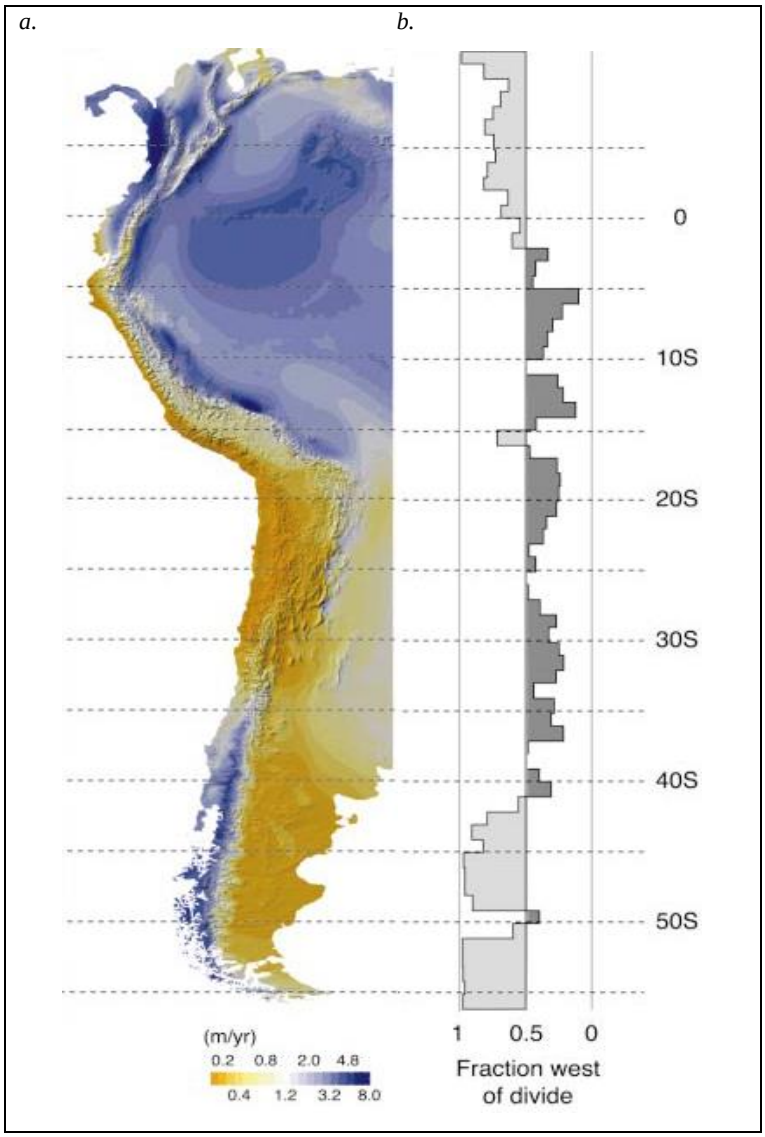


*Figure 1-19. Modified figure from Montgomery et al. (2001) showing: a. mean annual precipitation (m/yr), on top of a shaded-relief map of South America. b. cross-range asymmetry indicating which are the areas in the Andes draining to the Atlantic Ocean.*

The coincidence of low inferred erosion in the desert latitudes and the Central Andes indicates that mass accumulation is due to low rates of erosion. Pope and Willett (1998) propose that if the formation of the Altiplano plateau is the response for the physical limit of crustal thickening, then in this region of the orogen, crustal thickening has overcome erosion. It also implies that because of its location within a desertic area, tectonic shortening was possible because arid climatic conditions were predominant at this latitude (Montgomery et al., 2001). Karátson et al. (2011) compiled erosion rates from Neogene times in the Central Andes. From the Late Eocene onwards exceptional low erosion rates, between 1-10 m/My affected the Coastal Cordillera (Dunai et al., 2005; Kober et al., 2007), while erosion progressively intensifies, reaching rates up to >10 m/My (rates obtained with cosmogenic nuclides by Kober et al. (2007) and based on drainage basin analysis by Riquelme et al. (2008)). Simultaneously, a longitudinal gradient of increasing precipitation rates established along the west margin of the Andes, affecting the north of the Arica Bend area (18°S; Horton, 1999; Klein et al., 1999; Placzek et al., 2006). This region divides the low-erosion Altiplano–Puna plateau from the higher-erosion South Peruvian Cordillera (Horton, 1999) (Figure 1-19). Towards the north, fluvial erosion focused in a constrain number of large rivers, which incised some of the deepest canyons on the surface in the world during the past 10 My (Thouret et al., 2007).

The formation of different basins along the Andes also provide evidence that differential erosion rates affected the geomorphology of the Andes. Large basins were formed along northern Chile and Southern Peru, starting with cyclic formation of conglomerate and coarse sandstones deposits (e.g., Purilactis Fm, Tolar Fm, etc), in response to new uplift pulses (Figure 1-20c). These were later continuously filled in with finer sediments and volcanics, such as those from the ignimbrite flare-up of the Oxaya Formation (23-19 Ma; Van Zalinge et al., 2016a). Figure 1-20a-b show erosion and sedimentation rates and mass flux pulses in the Chilean Precordillera and Longitudinal Valley, and fore-arc sedimentation rates (Oncken et al., 2006). Maksaev and Zentilli (1999) estimated eroded volumes from the Precordillera and western Altiplano using apatite fission track data and Kober et al. (2002) using cosmogenic nuclide dating; both databases use the area of the Altiplano that has been eroded and faces the forearc in their calculations. Oncken et al. (2006) estimated the volume of fore-arc sediment (shown in Figure 1-20a-b as a yellow line) by integrating information from: Vitor et al. (2004)'s calculations on stratigraphic and thickness data from the Longitudinal Valley, González (1989)'s sediment thickness estimations obtained in the offshore Tarapacá Basin and finally, estimates on the fore-arc slope by Kudrass et al. (1998).

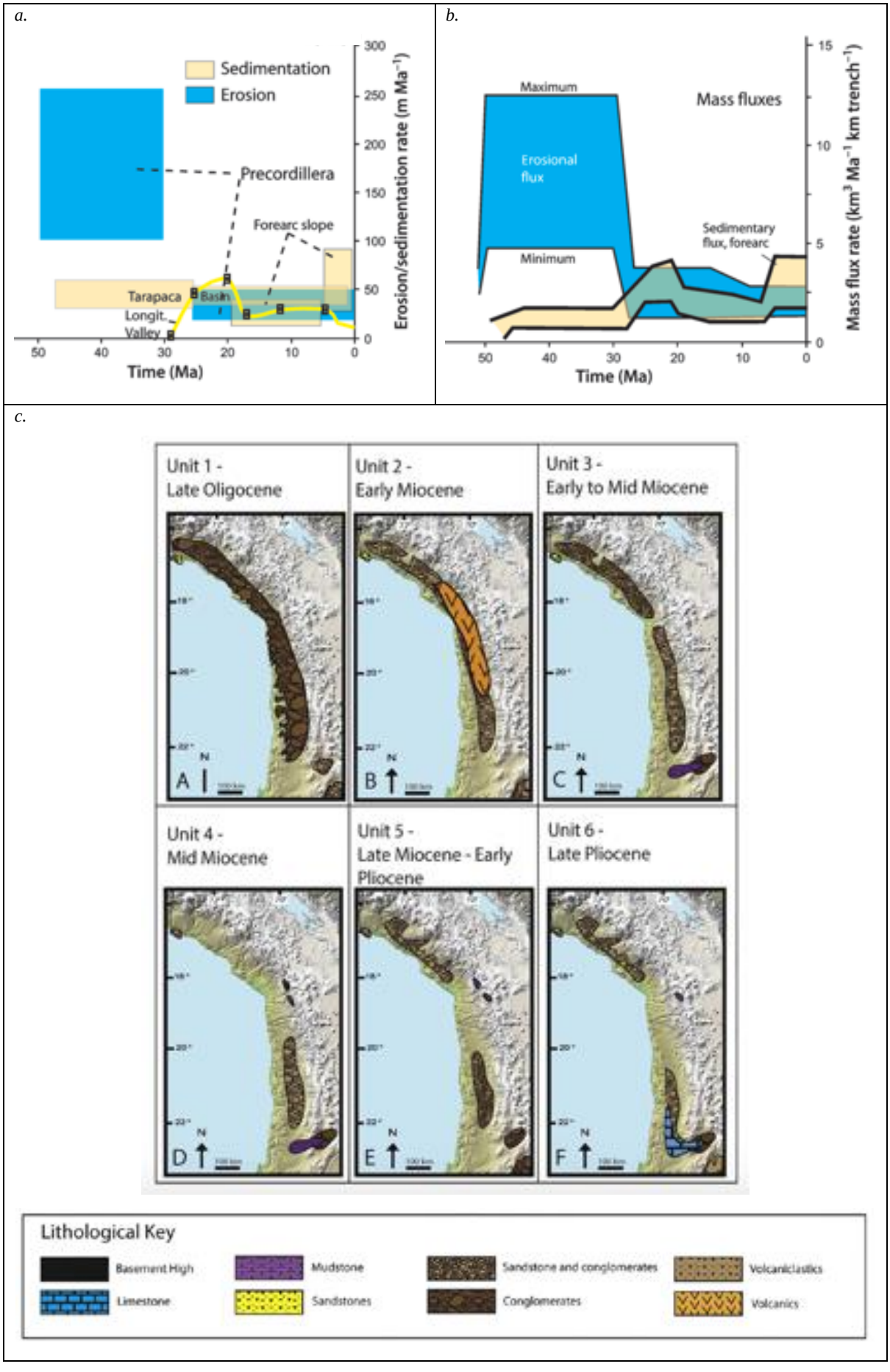
a.
Sedimentation
Erosion
Precordillera
Forearc slope
Tarapaca
Basin
Longit. Valley
Time (Ma)
Erosion/sedimentation rate (m Ma⁻¹)
b.
Maximum
Mass fluxes
Erosional flux
Minimum
Sedimentary flux, forearc
Time (Ma)
Mass flux rate (km³ Ma⁻¹ km trench⁻¹)
c.
Unit 1 - Late Oligocene
Unit 2 - Early Miocene
Unit 3 - Early to Mid Miocene
Unit 4 - Mid Miocene
Unit 5 - Late Miocene - Early Pliocene
Unit 6 - Late Pliocene
A
B
C
D
E
F
Lithological Key
Basement High
Limestone
Mudstone
Sandstones
Sandstone and conglomerates
Conglomerates
Volcaniclastics
Volcanics

*Figure 1-20. Figures a and b from Oncken et al. (2006) showing: a. The yellow solid line represents the erosion and sedimentation rates in the Chilean Precordillera and Longitudinal Valley. b. Estimated values of integrated erosion and sediments supply for the North Chilean Precordillera and fore-arc basins. c. Figure from Evenstar et al. (2017) showing regional deposition configurations from the Late Oligocene to the Late Pliocene.*

In the Central Andes, from 50 My to 30 My erosional processes were intense, removing a large amount of material from the mountain range. Figure 1-20a-b shows mass fluxes over 12 $km^3$/ My and erosion rates of over 250 m/My for this time window, during the formation and elevation of the mountain range. Regional sedimentation basins across northern Chile and Southern Peru (Figure 1-20c) provide evidence of this high erosion occurrence over time. Units dominated by conglomerates, such as Unit 1 (35 to 23 My) tend to become scarcer in time and spatially constrained, to be finally replaced by finer units such as sandstones (Evenstar et al., 2017). This indicates a diminishing of the intensity of erosional and sedimentation activity. Each uplift stage in the orogen was followed by tiny relief pulses, subsequently increasing erosion. These pulses continued but were not sufficient to strip sediments away and erode down the mountain range, since the build-up rates were much higher than erosion rates. According to Evenstar et al. (2017), intermittent humid periods of millions of years, together with arid climate conditions are enough for tectonism to modify and re-shape the geomorphology of a sector. Sedimentary basins react to variations in morphology caused by new tectonic events by creating new sedimentary units in different locations than the older units. The Altiplano region exemplifies a unique landscape that suffered from a tremendous long-term hyperaridity that in the end shows evidence of tectonism overcoming sediment deposition and accumulation (Evenstar et al., 2017). However, after 30 Ma, erosional rates diminished considerably.

I specifically want to highlight the Longitudinal Valley and Precordillera development, because it is the only region suffering from extreme erosion while still growing. Since this feature is a unique characteristic of the region, it may have important implications for PCD exposure.

Montgomery et al. (2001) suggest that changes in climatic conditions are the main control on the morphology of the Andean mountain range. However, when I focus at the regional scale or smaller, the processes controlling erosion and/ or sedimentation may vary. These processes include landslides, which are a by-product of rapid incision initiated by regional uplift (Ouimet et al., 2007) and control the environment when relief is too high, like in northern Chile, fluvial incision, which dominates where the relief is low, and aeolian processes. Margirier et al. (2015) establish that, in active mountain chains, such as the Andes, landslides are one of the most important mechanisms for long-term mass removal and therefore, aid on the geomorphologic evolution of relief. Landslides expand the valleys and accumulate sediments at the bottom. These sediment accumulations are transported once more by debris flows during more humid periods. Following, new rotational landslides occur, enlarging the amphitheatre-shaped valley (Figure 1-21). It is common to recognise several immense landslides interrupting the arid western Andean front in southern Peru and northern Chile (Margirier et al., 2015). The Lluta collapse is a good example. It is the largest, and possibly the oldest, paleolandslide documented in a continental setting (Philip and Ritz, 1999). The Chuquibamba landslide is another good example of this set of large landslides in southern Peru. Here, the Incapuquio fault plays a main role in sequestering the intermittent drainage network and favours the development of rotational

landslides (Margirier et al., 2015). Margirier et al. (2015) estimate the total volume mobilized during the Chuquibamba landslide reached 40 $km^3$, while Wörner et al. (2002) calculate 50 $km^3$ of rock was displaced by the Lluta collapse. Wet events in the arid and faulting affected Andean forearc stimulated these giant debris flows to occur (Margirier et al., 2015). Accordingly, the Lluta landslide 5-10 My coincides with a period of increased humidity at 7 My identified by Gaupp et al. (1999). Margirier et al. (2015) and Wörner et al. (2002) stress the role that coupled tectonism and climate have on constraining the generation of massive Andean landslides in the Western Cordillera and on the long-term mass transfer to the trench along the Andean front.

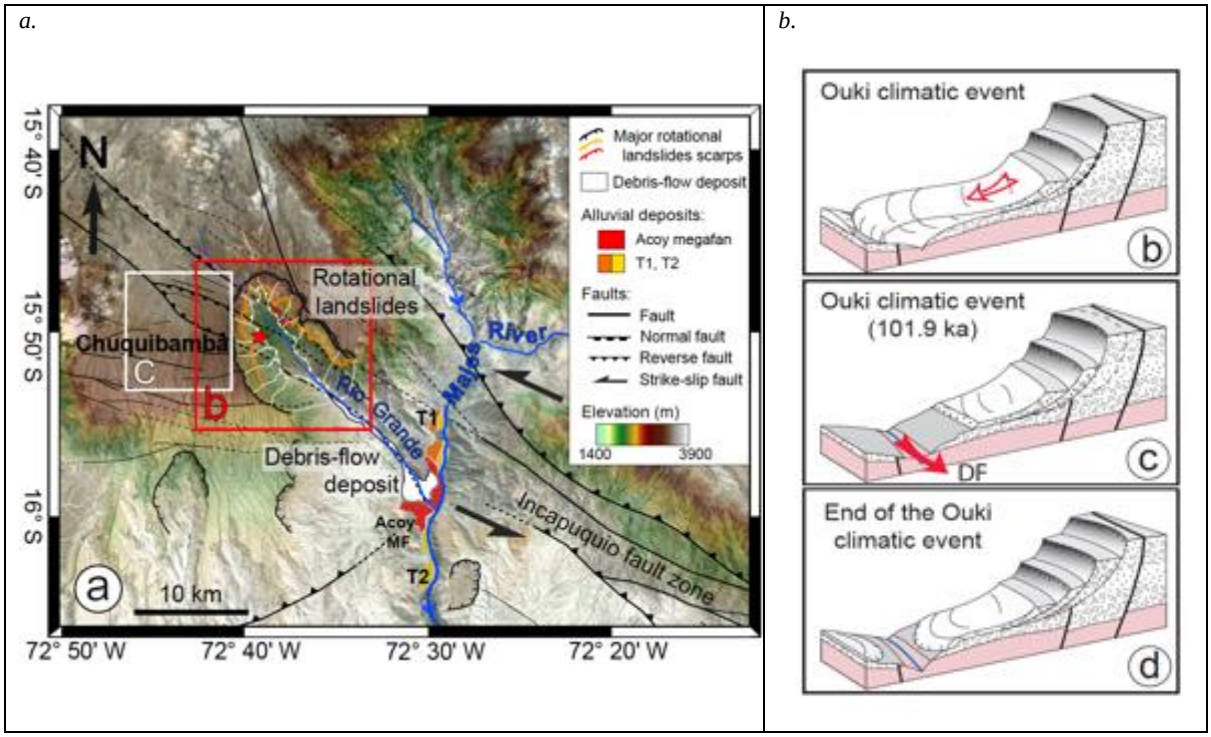


*Figure 1-21. Figures from Margirier et al. (2015). a. SRTM numerical elevation model on top of a Landsat image showing a regional view of the Chuquibamba region and the principal detachment scarps, debris-flow deposits, rotational landslides and faults. b. Cartoon showing the rotational landslide evolution triggered by the Ouki climatic event showing how landslides allow large remobilization on material.*

Local depositional processes are recognised in the Atacama Desert, where good examples of this phenomenon are shown. Located on the western margin of the Central Andes, the Atacama Desert is one of the driest and oldest deserts in the world. Evenstar et al. (2017) state that the Atacama is a unique and ancient surface called the Pacific Paleosurface (PPS). The PPS's age is estimated based on the end of the sedimentation process and abandonment of the surface, which according to some studies occurred between 14-10 My and was generated together by the uplift of the Andes and the onset of hyperaridity in the region. Evenstar et al. (2017), after the extensive study of the PPS using cosmogenic surface exposure ages, conclude that the surface is not a single paleosurface; they proposed the PPS to be a mosaic of smaller surfaces that were formed by aggradational and degradational processes over the last 19 My or more. The PPS should be

considered as a whole with each component paleosurface formation reflecting on the regional climate and tectonic activity in the area.

## 1.2.6 Surface evolution of volcano edifices

### *1.2.6.1 Stratovolcanoes morphometric model*

Karátson et al. (2010) developed a morphometric model of erosion patterns for the stratovolcanoes of the Altiplano–Puna, suggesting a climate control on erosion rates. They studied 33 stratovolcanoes, (circular andesitic stratocones), with ages spanning 14 My to the present, and located in the arid to hyperarid Central Andean Volcanic Zone (CVZ). They demonstrated that by using volcano morphometry (height in metres, from edifice base to top after erosion, and circularity) it is possible to calculate values for the degree of denudation (volume loss) by comparing reconstructed volumes of progressively eroded volcanoes against their volume, as shown in Figure 1-22 and Figure 1-23 respectively.

There is a clear inverse correlation between the reduction in edifice height and volume loss by erosion (Figure 1-22). However, this reduction in the edifice height does not mean that a linear function of erosion age exists, it rather follows specific patterns through different erosion stages.

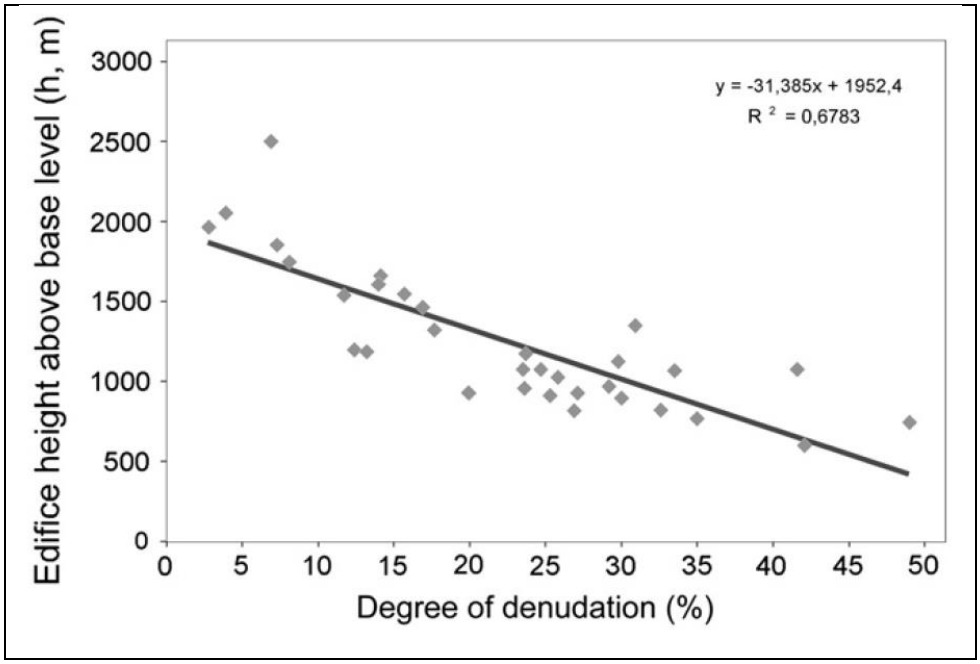


*Figure 1-22. Figure from Karátson et al., (2011) showing the negative correlation between edifice height and degree of denudation.*

The shape of a volcano in map view can be quantified with the circularity, the ratio of the area of a shape to the area of the circle with the same perimeter (Karátson et al., 2010). The more compact a shape is, the closer circularity is to unity, the value for a perfect circle (Karátson et al., 2010). Figure 1-23a establishes that mean circularity values generally decrease with the degree of denudation (which roughly correlates with time).

However, the correlation between the mean circularity and the degree of denudation is moderate ($r^2$=0.58, p=0.0000), which may be partly explained by variations in the circularity of the horizontal sections through volcanoes as a function of height above the baselevel (Figure 1-23b). According to Karátson et al. (2010) edifice sections close to or at the summit have high circularity, whereas at the mid-flanks, circularity will rapidly decrease (Figure 1-23b). Valleys on mid-flanks (i.e., ancient fluvial valleys, sometimes overprinted by glaciation) dissect and degrade the volcano, resulting in a lower circularity. Lastly, at the base, circularity values will increase greatly. At lower flanks and the apron, the energy to form streams decreases (due to smaller topographic gradient and limited discharge) inhibiting valley incision and propagation. Sedimentation also contributes to an increase circularity at the base again. In addition, these changes of circularity of the stratovolcanoes reflects longer-term erosional dissection, indicating that active or dormant volcanoes exhibit high circularity values (0.8–1) while old and mostly degraded edifices have low circularity (0.3), reflecting the increasing role of dissection.

It is also possible to obtain erosion rates from radiometric age constraints. Radiometric data also allows one to estimate volume loss for a defined period of time and infer long-term landscape evolution patterns for a specific area.

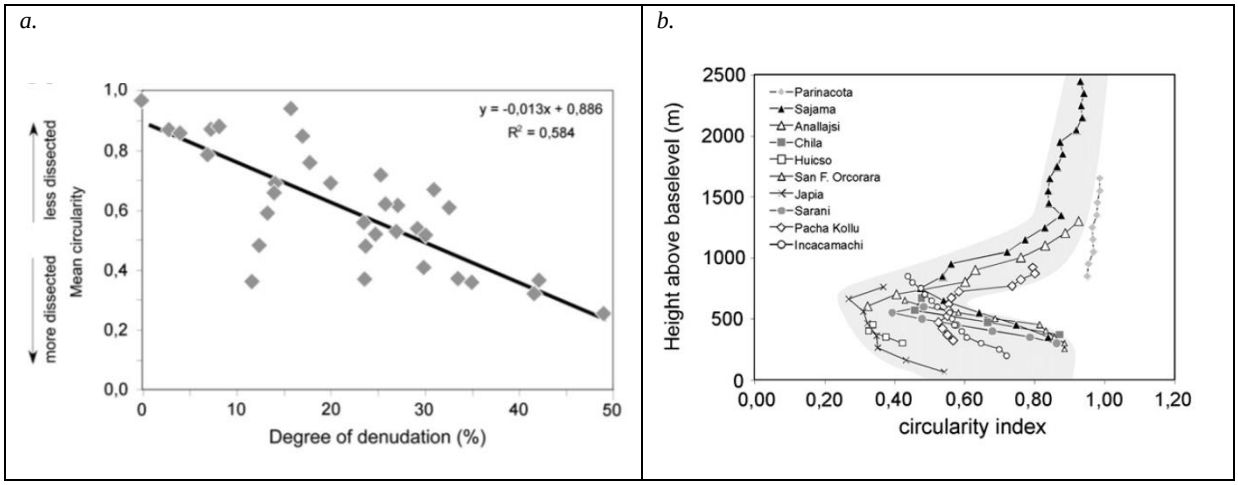


*Figure 1-23. Figures from Karátson et al. (2011). a. Mean circularity vs. degree of denudation for Central Andean stratovolcanoes. b. Contour line for Central Andean stratovolcanoes based on the mean circularity.*

### *1.2.6.2 Evolution model for the degradation for Central Andean volcanoes*

Karátson et al. (2010) established correlations and trends in the erosion model for stratovolcanoes in the Central Andes (Figure 1-24). Firstly, precipitation and erosion rates are strongly associated, and this correlation existed for a long-time span (>10Ma). Ehlers and Poulsen (2009) propose that surface uplift increased the rain shadow effect in the Andes, causing climatic conditions to evolve from arid to hyperarid in the Central Andes in the last 10-15 My and remained hyperarid until the present, exposing the region to a long-term arid climate. Consequently, low erosion rates dominate the region since 10-15 My ago. Volume loss for stratovolcanoes in the Central Andes is 22% on average and up to 50% as a maximum. It means that more than 50% of the original volume has been preserved even for the Miocene edifices (Karátson et al.,

2012). The assumptions of Karátson et al. (2010) imply that all selected volcanoes in their study, had similar cone shape, independent of the final volume they achieved during their growing period. Larger volume cones may start as a small cone, with gradual increases in height, which in turn will greatly increase the areal extent of the volcano periphery.

Secondly, during volcanic edifice formation, construction generally exceeds erosion up to the final stage. Typical long-term erosion rates for the different regions studied are: 10 to 20 m/Ma for the Altiplano–Puna Plateau, 7–9 m/Ma typify the hyperarid Puna plateau, and 13–22 m/Ma are for volcanoes in the more humid South Peru. On the contrary, young (Late Quaternary) volcanoes present significantly higher short-term erosion rates between 112 to 66 m/Ma, implying that younger volcanoes erode quicker because of their unconsolidated cover and steeper slopes. It is important to consider however, that surface denudation slows down to approximately one tenth of this after a few My (Karátson et al., 2012).

Thirdly, edifice erosion patterns depend on their geographical location and the climate affecting the region. Pre-Quaternary volcanoes in arid conditions show fossil glacial U-shaped valleys overprinting older valleys, while South Peruvian volcanoes display much deeper glacial valleys that were only preserved due to drier climatic conditions. Karátson et al. (2010) also indicate that since climate is the major factor controlling erosion, erosion rates estimated for stratovolcanoes in their study could also apply to other volcano types.

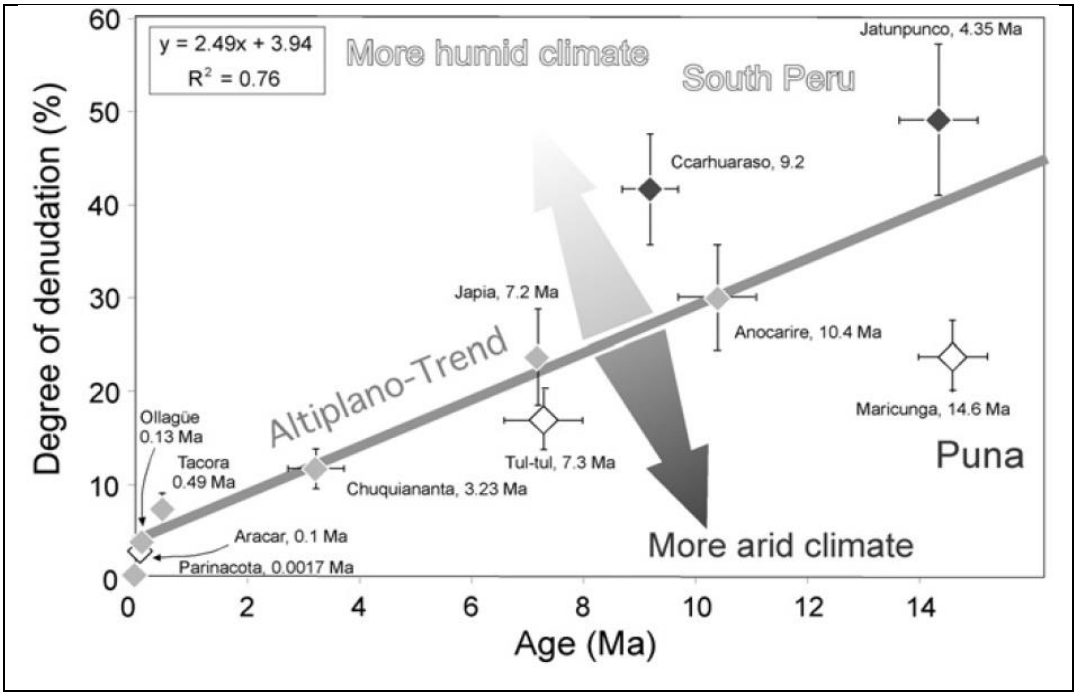


*Figure 1-24. Figure from Karátson et al. (2011) showing degree of denudation (%) against the age of Central Andean stratovolcanoes and the climatic conditions in place, as well as their location within the orogen.*

### 1.2.7 Porphyry deposits in the Andes

The combination of sediment-starved sections in northern Chile with changes in stress regimes in the Andes and the ingestion of water rich sediments into the crust may explain the abundance of PCDs in the Andes.

It is widely thought (e.g., Tosdal and Richards, 2001) that there are variations in stress regime of the crust that are particularly favourable for copper-rich porphyry and gold high-sulfidation epithermal deposit formation. In economic geology literature, contractional settings have been widely accepted as adequate conditions for porphyry ore type formation. A good example is the Andes, where enriched copper porphyries formed in a region that experienced crustal thickening, surface uplift, and rapid exhumation due to a compressional stress regime. Several authors (i.e., Takada, 1994; Sillitoe, 1998) coincide that compression in the crust allows and help large mid- to upper-crustal magma chambers development (Takada, 1994). These chambers are the places in the crust where efficient fractionation and magmatic fluid generation and release occur, particularly during periods of rapid uplift and erosional unroofing (Sillitoe, 1998). However, different authors (Simakin and Talbot, 2001; Tosdal and Richards, 2001; Richards, 2003, 2005; Gow and Walshe, 2005) suggest that a compressional regime is evidently not as auspicious as a tensional or shear stress regime for vertical magma flow, because it might postpone magma ascent until higher degrees of partial melting are achieved. It seems that the ideal forming conditions for PCDs would be a large-scale compressional stress regime, such as the subduction margin in America, that locally experience relaxation by being exposed to tensional or shear stresses. For example, both the Bingham (USA) and Bajo de la Alumbrera (Argentina) deposits apparently fit this tectonic niche (Presnell, 1997; Sasso and Clark, 1998; Halter et al., 2004; Sillitoe, 2008). In the sediment-starved sections of the Andes where tectonic erosion may have been an important mechanism, the combination of some conditions (i.e., variations in the composition of plate interface fragments (Peacock, 1996); low fluid pressures in the pores of the rock; lack of lubrication in the plate boundary (Peacock, 1996; von Huene and Scholl, 1991)) would have encouraged higher shear stresses (Lamb and Davis, 2003). On the contrary, in parts of the trench where layered turbidite sequences are present, they would act as a dry lubricant along the plate interface, by evening the upper regions of the slab out. However, this theory has been challenged by the fact that the sediment-starved margin, where PCDs are located in northern Chile, is not receiving dry sediments, it is actually quite the opposite (von Huene and Ranero, 2003).

#### *1.2.7.1 PCDs exhumation*

The presence of PCDs at the surface is dependent on the balance between the intensity and direction of erosion, depositional processes and faulting after their intrusion (Kesler and Wilkinson, 2006; Wilkinson and Kesler, 2007; Braxton et al., 2012). Erosion is especially rapid in compressive arcs because of enhanced uplift rates; for example, an uplift rate of 0.7 km/ My is documented in the vicinity of the 2.6 My (Pollard et al., 2005) Grasberg PCD (Weiland and Cloos, 1996). The generally younger ages of gold-rich porphyry deposits in western Pacific island arcs compared to those in the central Andean Cordillera mainly reflect more rapid unroofing and eventual erosion in tropical regions relative to arid environments (Sillitoe, 1997).

Yanites and Kesler (2015) found that PCDs located in territories with elevated rainfall rates, are younger and are sparsely distributed, which is also consistent with fast exhumation rates. This pattern indicates that climate is playing a significant role in eroding and shaping landscapes and exhuming mineralised intrusions around the world. Sillitoe (2010) relates PCDs and volcanoes as part of the same system, in this case erosional processes will aid in the unroofing of PCDs but also are responsible for the severe degradation of volcanic edifices, sometimes even entirely removing eruptive units located in the surrounding of the deposits (Sillitoe, 2010). However, Sillitoe (2010) also suggests that volcanic landforms could be preserved and are obviously even better preserved in the shallower high-sulfidation epithermal environment right above PCDs.

### *1.2.7.2 PCDs types and relation to depth of formation*

The dominant metals in PCD-type deposits tend to vary with depth of formation. Gold-rich porphyry deposits are mainly fine grained and present as high-fineness (>800 ppm) native metal (Sillitoe, 2000). Many gold-rich porphyry deposits are deficient in molybdenum (<20 ppm, e.g., Barr et al., 1976; Sillitoe and Gappe, 1984), whereas others possess recoverable amounts (>100 ppm) and fall within Cox and Singer's (1988) porphyry Cu-Au-Mo category. Molybdenum shows a distinct tendency to concentrate as halos to the molybdenum-poor, cooper- gold core zones of many deposits (Sillitoe, 2000).

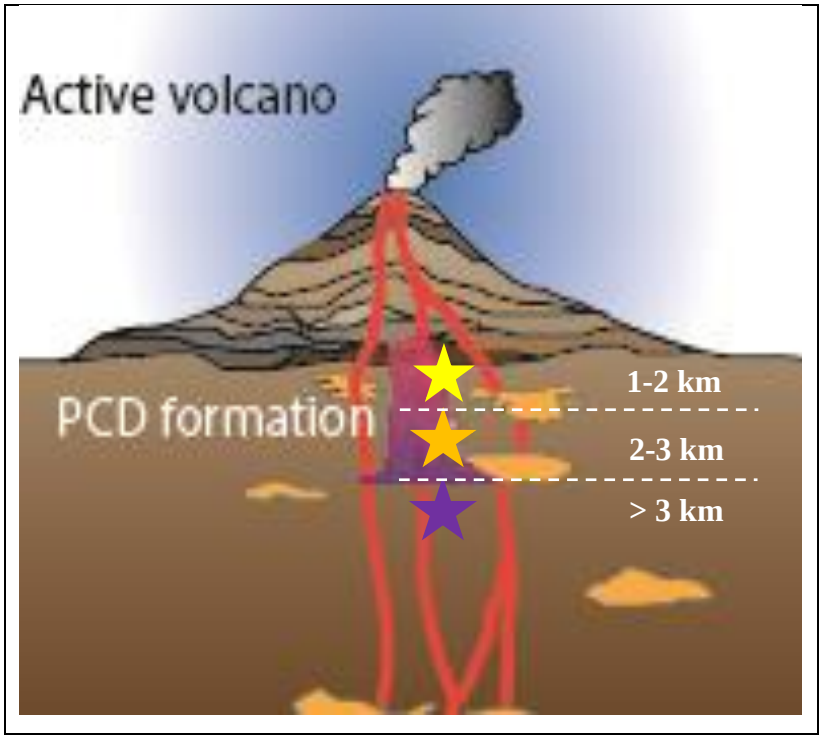


*Figure 1-25. Cartoon showing the connectivity between a volcanic edifice and porphyries. Depending on the depth of intrusion and cooling, these mineralised bodies will experience diverse pressure and temperature ranges. In consequence, different types of mineralization may occur. Gold- rich porphyries (yellow star) form between 1-2 km depth, Cu- rich PCDs (orange star) between 2-3km depth, while porphyries with Cu and Mo mineralization (purple star) occur in deeper parts of the crust, over 3 km depth.*

The extent of fluid phase separation (brine-vapour) depends on fluid pressure, resulting in the fractionation of ore-forming constituents. Additionally, both density of fluids and temperature may also cause variations in metal solubility and deposition of certain ore minerals (Murakami et al., 2010). With higher fluid pressure in a fairly deep porphyry deposit, the separation into different phases is less extreme and a dense vapour or a single-phase fluid will prevail. Higher temperatures allow these fluids to carry all types of metals in high concentrations. If the fluid cools, but the pressure remains high, then the fluid transforms into liquid state, (vapor to liquid contraction; Heinrich et al. 2004). Fluids in these conditions are the ones to precipitate Cu–Fe–sulphides and molybdenite (Hezarkhani et al. 1999; Klemm et al. 2007). However, they are still able to maintain abundant gold concentrations in solution, which depends on both fluid density and sulphur concentration. Therefore, Cu-Mo-rich porphyries, which form at greater depth (Figure 1-25), are expected to contain lower amounts of gold, compared to the Au/Cu ratio in their primary magmatic-hydrothermal fluid. Murakami et al. (2010) affirms that in the case of deep porphyries, the portion of gold that is lost in deep environment is available for the formation of separate gold deposits at lower temperature, typically kilometres higher up in the system. Figure 1-25 shows the connection between PCDs and volcanoes and different PCD types (Au-rich, Cu-rich and Cu-Mo- rich porphyries) that form depending on the depth of intrusion.

Gold-rich porphyry deposits are commonly emplaced at shallow (l-2 km) crustal levels (Cox and Singer, 1988) (Figure 1-25) and, hence, are likely to be associated closely with coeval volcanic stocks (Sillitoe, 2000). The volcanic rocks are typically andesitic to dacitic or trachyandesitic to latitic in composition and, where volcanic landforms are partially preserved, they constitute stratovolcanoes (Sillitoe, 2000).

## 1.3 Summary

The evidence that volcanoes and porphyries are related and are part of the same system (Figure 1-25) but at different depth is abundant. They both share similar features and, in some cases, mineralised deposits still have remaining portions of stratovolcanoes preserved on top. For instance, Marte deposit, an Au- rich porphyry in northern Chile and Grasberg in Indonesia, are good examples of deposits in which parts of the original stratovolcano depositional slopes are still preserved (Sillitoe and Bonham, 1984).

Volcanoes are just the surface expression of extensive magmatic systems below ground; therefore, it is logical they share similar shapes and dimensions, lithologies, and even mineralization and alteration assemblages and patterns. Firstly, volcanoes display a roughly circular zone consisting of different volcanic and volcaniclastic lithofacies (Figure 1-1; Figure 1-2). These facies are heavily altered in concentric patterns of fumaroles around central domes in volcanoes, and similar concentric alteration patterns occur in PCDs around the central intrusion. Secondly, alteration assemblages such as pyrite-rich advanced argillic alteration is not only found in PCDs, but also in deep cores (600-1200m) in stratovolcanoes, typically drilled for geothermal energy (Sillitoe and Bonham, 1984). Lithocaps with advanced argillic alteration found at the top of PCDs would be the equivalent to fumaroles in the shallow levels of volcanoes, both formed by the interaction between ground water and volatiles from degassing deep magma bodies.

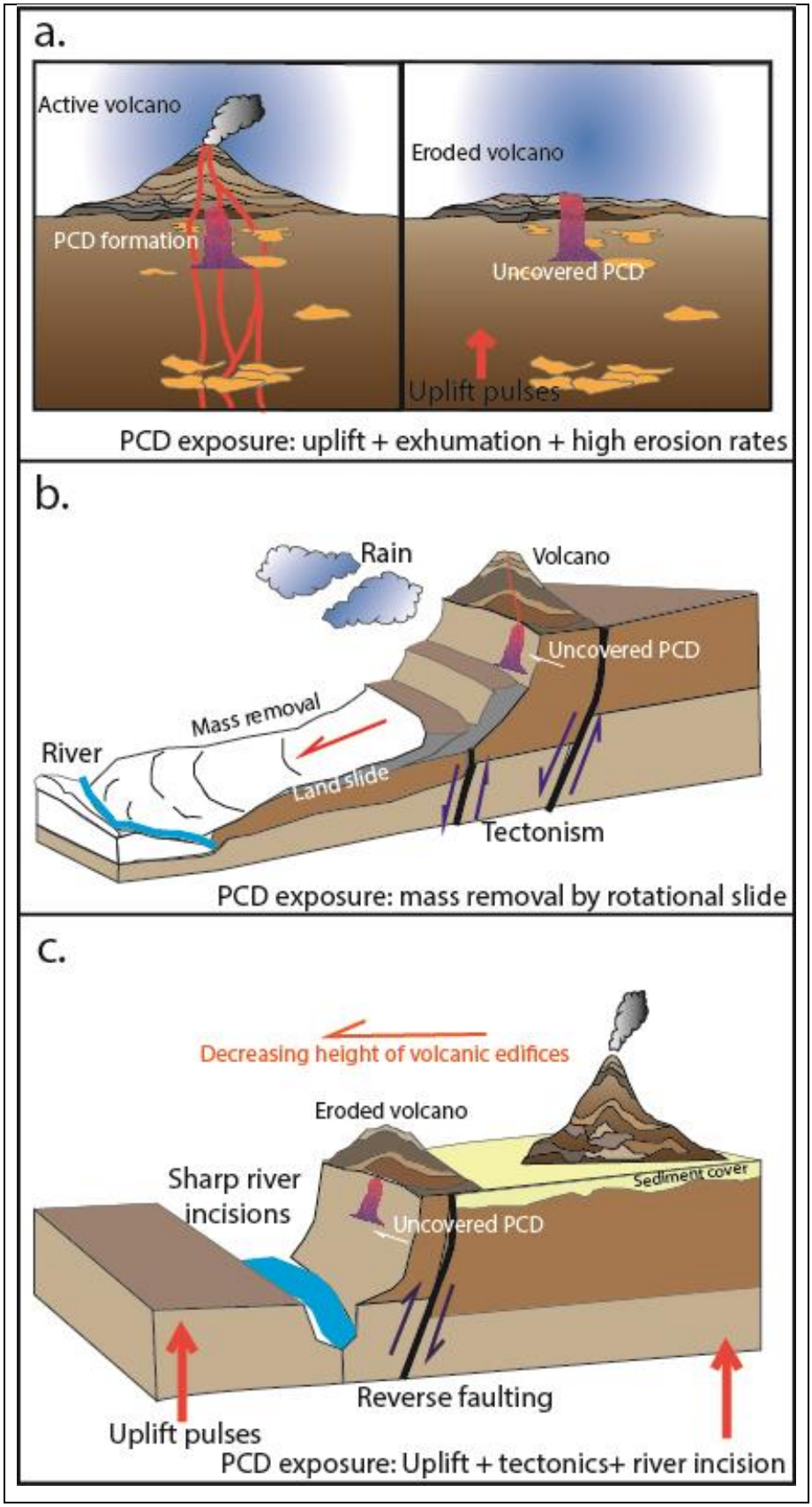


*Figure 1-26. Cartoons showing the different causes for erosion and PCD exposure in the Andes. a. On the left, an active stratovolcano and PCD formation underneath the volcanic edifice. On the right panel, uncovered PCD due to interaction between uplift pulses,*

*exhumation and high erosion rates. b. Formation of rotational landslides that removes a massive amount of sediments exposing a PCD. The formation of the landslide occurs because of the interaction between faulting and high precipitation rates during wet seasons. c. Uplift pulses increases the energy in active fluvial systems, which in return create deeper incisions and valleys, assisting on the exposure of porphyries, but also on the drop on volcanic edifices' height.*

Thirdly, large accumulations of native sulphur are common near the vents of andesitic stratovolcanoes, along with abundant pyrite deposits beneath the surface (Sillitoe, 1973), the same mineralization found in PCDs. Moreover, the presence of sulphur and base metals in gas emissions from modern volcanoes indicates metal-enriched magmas below the surface, implying another correlation between PCDs and volcanoes.

The magmatic processes that allow mineralised porphyries to form are, of course, important. However, in this thesis I focused more on the processes that allow the exhumation and uncovering of these intrusive bodies.

Figure 1-26 presents the three primordial stages necessary for the discovery of a PCD: generation of the mineralised porphyry, preservation and exhumation. Figure 1-26 shows three scenarios, in which different factors such as tectonics, climate and erosion play major roles on the exposure of PCD. Scenario I (Figure 1-26a) shows how after the intrusion of the mineralised porphyry and the end of the magmatic activity (left panel), the interaction between uplift pulses and high erosional rates affects and erode the volcanic pile, exposing the PCD on the surface (right panel). In scenario II (Figure 1-26b) the combined action between climate (high precipitation rates) and tectonics (local faulting) allows the formation of a rotational landslide, which is responsible for an enormous mass removal. Later, on humid seasons, fluvial erosion removes the sediments from the valleys, allowing the landslide to occur again, if the conditions are adequate. On the last scenario (Figure 1-26c), is the interaction between tectonics (uplift pulses) and climate (high precipitation rates in short periods of time and fluvial erosion) that allow PCDs to be exposed, particularly if they are buried by a thick cover. If PCDs were covered by volcanoes, active fluvial systems would be responsible of decreasing the height of the volcanic edifices that are located close to rivers. Furthermore, if the area was also affected by uplift pulses, fluvial systems will create sharp incisions and deeper valleys into gentle surfaces (Evenstar et al., 2020), facilitating the exposure of PCDs. In this thesis, Chapter 4 reflects on the importance of the combination of climate, tectonics, erosion and timing in the Andes, and which are the more adequate conditions that allow PCDs to be closer to the surface or nearly exposed.

# 2 Chapter 2: Database creation and basic analysis

This chapter explains how the **Andean Volcano and eruption database** (**AVEDB**), the Ignimbrites and Intrusive database (IIDB) and Porphyry Copper Deposits (PCDsDB) were created, providing details on the sources of data (books, papers, journals), how certain variables were calculated, and how the data were unified and cleaned. It also provides basic information on the number of records in various categories, which are presented later as histograms. Finally, maps created in ArcGIS show the spatial distribution of the data.

The AVEDB is found in Microsoft Excel format in Appendix I.
The IIDB is found in Microsoft Excel format in Appendix II.

## 2.1 Dataset of volcanoes and eruptions

### 2.1.1 Database compilation

The following is a detailed description of the process of extraction of the information and the cleaning process for each parameter.

#### *2.1.1.1 Appendix I: Volcanoes and eruptions*

The AVEDB is a compilation of volcanic centres and eruptions along the South American Andes. The design of the dataset is explained in Appendix I. Records were extracted from diverse sources with a total of **5477 records**. Each source and the data input are summarised in Table 2-1 with some further details in the text below.

*Table 2-1: Summary of sources of data on volcanoes and eruptions included in AVEDB.*

| Institution origin | Code in AVEDB | Data inputs | Extraction date | Register type | Author and year | Paper name/ DB name |
|---|---|---|---|---|---|---|
| i. VOGRIPA | LaMEVE DB | 187 | 03.2016 | Volcanic edifices and eruptions | Crosweller et al. (2012) | Global database on large magnitude explosive volcanic eruptions (LaMEVE) |
| ii. Smithsonian Global Volcanism Program (SGVP) | Volcanoes of the World (VOTW)-Holocene | 1140 | 03.2017 | Volcanic edifices | SGVP | Volcanoes of the World (VOTW) Database Information-Holocene |
| | Volcanoes of the World 4.6.6.-Pleistocene | 122 | 03.2017 | Volcanic edifices and eruptions | SGVP | Global Volcanism Program - Volcanoes of the World 4.6.6. Basic List of Pleistocene Volcanoes |
| | SGVP and NOAA NGDC | 40 | | Volcanic edifices and eruptions | SGVP and NOAA's NGDC | Smithsonian Global Volcanism Program and NOAA's National Geophysical Data Centre |
| iii. Volcanoes of the Andes book | Trumbull et al. (2006). The time-space distribution of Cenozoic arc volcanism | 1289 | | Volcanic edifices and eruptions | Trumbull RB, Riller U, Oncken O, Scheuber E, Munier K, Hongn F., 2006 | The time-space distribution of Cenozoic arc volcanism in the Central Andes: a new data compilation and some tectonic implications. |
| | | 156 | | Intrusive bodies | Trumbull RB, Riller U, | The time-space distribution of Cenozoic arc volcanism in the |

| | | | | | | |
|---|---|---|---|---|---|---|
| | | | | | Oncken O, Scheuber E, Munier K, Hongn F., 2006 | Central Andes: a new data compilation and some tectonic implications. |
| iv. Sernageomin (Servicio Nacional Geológico y Minero de Chile) | Mapa Geológico de Chile 1M, No 7, (2004) | 47 | | Volcanic edifices | Sernageomin (2004) | Mapa Geológico de Chile: versión digital. Publicación Geológica digital No. 7, 2004 CD-ROM, versión 1.0, Base Geológica escala 1:1.000.000. |
| | Ranking de los 90 volcanes activos de Chile | 59 | 06.2017 | Volcanic edifices | Sernageomin - OVDAS, 2015 | Ranking de los 90 volcanes activos de Chile. |
| v. BHP | BHP ArcGIS database | 111 | 06.2017 | Volcanic edifices | BHP Exploration ArcGIS dataset (2017) | Not published |
| vi. Instituto Nacional Geográfico (ING) | Volcanes Activos de la República Argentina-ING | 45 | 06.2017 | Volcanic edifices | Instituto Geográfico Nacional ING | Volcanes Activos de la República Argentina- Instituto Geográfico Nacional ING. |
| vii. Volcanoes of the Andes book | De Silva et al. (1991). Volcanoes of the Central Andes. | 1105 | | Volcanic edifices | De Silva SL, Francis PW. (1991) | Book: Volcanoes of the Central Andes. |
| viii. Elsevier | Karátson et al. (2011). Erosion rates and erosion patterns of Neogene to Quaternary stratovolcanoes. | 15 Complemented existing fields. | | Volcanic edifices | D. Karátson, T. Telbisz, G. Wörner (2011) | Erosion rates and erosion patterns of Neogene to Quaternary stratovolcanoes in the Western Cordillera of the Central Andes: An SRTM DEM based analysis |
| ix. Geological Society of London Special Publication | Mamani et al. (2010). Geochemical variations in Central Andean orocline. | 651 | | Volcanic edifices and eruptions | Mamani et al. (2010) | Geochemical variations in igneous rocks of the Central Andean orocline (13°S to 18°S): Tracing crustal thickening and magma generation through time and space. |
| x. University of California Press | Volcanoes of the World, third edition | Complemented existing fields. | | Volcanic edifices | Siebert, L., Simkin, T. and Kimberly, P. (2010) | Book: Volcanoes of the World, third edition. |
| xi. Terra Nova, Blackwell Science Ltd | Haschke et al. (2002) | 657 | | Volcanic edifices and eruptions | M. R. Haschke, E. Scheuber, A. Günther and K.-J. Reutter (2002) | Evolutionary cycles during the Andean orogeny: repeated slab breakoff and flat subduction? |
| | | 461 | | Ignimbrites and intrusive units | M. R. Haschke, E. Scheuber, A. Günther and K.-J. Reutter (2002) | Evolutionary cycles during the Andean orogeny: repeated slab breakoff and flat subduction? |
| xii. Journal of Volcanology and Geothermal Research | Singer et al. (2009) | 9 | | Volcanic edifices | A.R. Goss, S.M. Kay, C. Mpodozis and B.S. Singer (2009) | The Incapillo Caldera and Dome Complex (~28° S, Central Andes): A stranded magma chamber over a dying arc |
| xiii. Brandmeier PhD dissertation, Universität Göttingen, Germany | Brandmeier et al. (2014). A remote sensing and geospatial statistical approach of ignimbrites | 1672 | | Ignimbrites | M Brandmeier (2014) | A remote sensing and geospatial statistical approach to understanding distribution and evolution of ignimbrites in the Central Andes with a focus on Southern Peru. |
| xiv. Tectonophysics Journal | Guzmán et al. (2014). Spatial–temporal distribution of | 83 | | Ignimbrites | Guzmán et al. (2014) | Spatial–temporal distribution of explosive volcanism in the 25–28°S segment of the Andean Central Volcanic Zone. |

| | | | | | | |
|---|---|---|---|---|---|---|
| | explosive volcanism | | | | | |

i. VOGRIPA: records are from the *LaMEVE database* developed as part of *VOGRIPA* (Crosweller et al., 2012), which can be accessed online at www.bgs.ac.uk/vogripa. LaMEVE is a compilation of data from the Smithsonian Institution's Global Volcanism Program and the Geological Survey of Japan, as well as published literature. The LaMEVE database (DB) is limited to magnitude 4 and greater eruption records from present time, back to the Quaternary period. The dataset is being continually updated. For this study, an extraction was made only for the South American region, in March 2017.

ii. Global Volcanism Program (SGVP) (Global Volcanism Program, 2013), from which, three DB were obtained in March 2017, filtering for records located only in the Andes region. All three sets bring similar information: volcano names and ID (IAVCEI number), location (latitude, longitude, elevation, country and region), eruption details (last known eruption in years and epochs, evidence of the eruption and volcano type), dominant chemistry rock and tectonic settings where volcanoes are situated.

- *Volcanoes of the World (VOTW) - Holocene*: 1140 Holocene volcanoes. The information can be found at https://volcano.si.edu/list_volcano_holocene.cfm.
- *Volcanoes of the World 4.6.6. - Pleistocene Volcanoes*: 122 records (https://volcano.si.edu/list_volcano_pleistocene.cfm).
- *SGVP and NOAA NGDC:* 40 records. The access link to the site is www./volcano.si.edu.

Volcanoes active in the past approximately 10,000 years are on the Holocene list and are not duplicated in the Pleistocene one. Also, it is necessary to consider that SGVP does not provide eruption histories for Pleistocene volcanoes.

iii. The book Volcanoes of the Andes includes a compilation of the Cenozoic volcanism of the South-Central Andes (Trumbull et al., 2006), contributing a total of 1289 volcanoes and eruptions and 156 intrusive records. It contains age (Ma), dating method and the associated error, sample location and rock type information for volcanic edifices and related dykes, stocks and ignimbrites (14° S - 28° S latitude; 64°W - 74°W longitude). The compilation focusses on after 40My, although includes data from 65 My up to Holocene times (Trumbull et al., 2006).

iv. Sernageomin (Chilean National Geological Service) is the source of *Mapa Geológico de Chile 1M, No 7, 2004*. It provides 47 records of calderas and volcanic centres distributed along the Chilean Andes. Unfortunately, the data do not include ages for theses volcanic structures, only their respective location. The format of the information is a digital version of the Chile Geological map, 1 million scale, downloaded from the Sernageomin site (www.ipgp.fr/dechabal/Geol-millon.pdf).

Also listed under Sernageomin are data from an official publication provided by OVDAS, the Chilean volcanic vigilance centre (http://sitiohistorico.sernageomin.cl/archivos/Ranking-de-Volcanes). It includes the volcano names, location and volcano type of the 90 active volcanoes in Chile (90 volcanes activos de Chile, 2015).

v. The volcanic edifices in the *BHP database* (BHP, 2017 extraction) were identified by BHP staff as volcanic structures using satellite images and were drawn in ArcGIS software. There may be duplication with other sources. Because these records only contain spatial information and no age information, I do not anticipate any issues with duplication affecting any analysis, since our study focus on the changes of erosional patterns in time and the records will be automatically filtered out.

vi. The Argentinian National Geographic Institute**,** ING (Instituto Geográfico Nacional) has also published a list of 45 active volcanoes in the country (Volcanes Activos de Argentina, 2017), (http://www.ign.gob.ar/descargas/geografia/volcanes_activos.pdf). This condensed set provides official and alternative volcano name, exact location and in some cases, features sizes (crater). Last recorded eruptions are given, although not all the records have exact or even eruption ages data. Besides, the dating methods for the ages are not provided.

vii. *Volcanoes of the Central Andes* (De Silva et al., 1991) is a compilation of 1105 volcanoes recognized by the study of multi-spectral Landsat images supported by air conventional photography and field work. This set provides standard information such as volcano principal and alternative name, exact location of the centre of the volcanic edifice (latitude, longitude and elevation), volcano type and volcanic activity status. In addition, it provides volcanic edifice measurements such edifice height, cone and deposit diameter, as well as the crater diameter. Also, the flow length, deposit volume and erosion status of the edifices were measured and calculated.

viii. A publication by *Karátson (2011)*, where erosion patterns and rates were studied in stratovolcanoes in the Central Volcanic Zone (CVZ), was used to complement empty volcano parameters. The registers were classified into three main categories: Potentially active volcanoes (44 records), Minor eruptive centres (18 records) and Large silicic systems (11 records).

ix. The compilation created by *Mamani et al. (2010)* accounts for 651 registers. It comprises the location and details of the sample (sample ID and brief description, latitude, longitude, elevation, country region), eruption details (eruption age in Ma, its associated error, evidence of the eruption), dominant chemistry rock and volcanic arc name where the sample was collected. Finally, a short bibliographic reference from where the sample information was extracted, was also incorporated.

x. The book *Volcanoes of the World, third edition* (Siebert et al., 2010) was used to fill empty records for volcanoes already in the dataset, such as volcano type.

xi. The publication *Haschke et al. (2002)* accounts for 1118 ages in My (dating method and material dated, error) for intrusive and volcanic rocks, location of the sample and rock composition. From the total 1118 records, 657 were included in the AVEDB as volcanic eruptions and 461 registers were included in the IIDB (Appendix II) as intrusive rocks. Sedimentary and metamorphic rocks in this DB were not included.

xii. The paper *Singer et al. (2009)* brings 9 records to the AVEDB, from the Incapillo Caldera and Dome complex located in Argentina.

#### *2.1.1.2 Appendix II: Ignimbrite and intrusive Database (IIDB)*

The Ignimbrites and Intrusive database (IIDB) are a compilation of ignimbrites and intrusive samples along the South American Andes extracted from diverse sources with a total of **2373 records**, and it is included as Appendix II. Each source and the data input are summarised in Table 2-1 with some further details in the text below.

The main source of data for the ignimbrite compilation is *Brandmeier et al. (2014)*, which includes 201 mapped ignimbrite sheets and caldera structures, including unit ages, area covered, estimated volume, petrography, related faults and references. The IIDB compilation includes a total of 1672 ignimbrite samples, which in some cases several samples were taken from the same unit (e.g., Aguas Calientes complex). Only the following fields were extracted: sample name and coordinates, rock type,
classified by composition; eruptive centre name; country and area where the sample was recollected; dating method and material analysed; age and its correspondent error (Ma), as well as the age class; and finally, the references where the literature compiled age was extracted.

The second source of ignimbrite data is *Guzmán et al. (2014)* accounts for 83 records. In this work, all known pyroclastic deposits, between the 25°–28°S were mapped, summing a total of 85 units. For each unit the following data were extracted: location, areal extent, composition, age, degree of welding, crystal and pumice content, and, the type, name and location of the eruptive centre source. Additional information can be obtained from *Guzmán et al. (2014)* such as brief descriptions of the collapse calderas and of pyroclastic deposits, but it has not been included in the IIDB.

The third source for the IIDB is *Haschke et al. (2002).* It accounts for 83 ignimbrite samples and 430 intrusive records.

And finally, *Trumbull et al. (2006)* includes a total 156 intrusive samples.

### 2.1.2 Database design

The 63 data fields remain the same for the AVEDB as well as for the IIDB, and they are described in detail in Appendix I. In the next chapter, Chapter 3, a statistical analysis of the most relevant data is performed. For that reason, in this section of the thesis, I only explain the most relevant columns on the AVEDB that will be used later in the analysis. For more detail on the rest of the variables, see Appendix I.

- *Volcano height (m)* is the vertical difference between the peak of the edifice and the volcano base. For heights extracted from the book *Volcanoes of the Central Andes*, the error is about +- 150m (De Silva et al., 1991). When I determined heights using the Google Earth profile tool, the edifice base was identified as the maximum break in the slope (Figure 2-1).

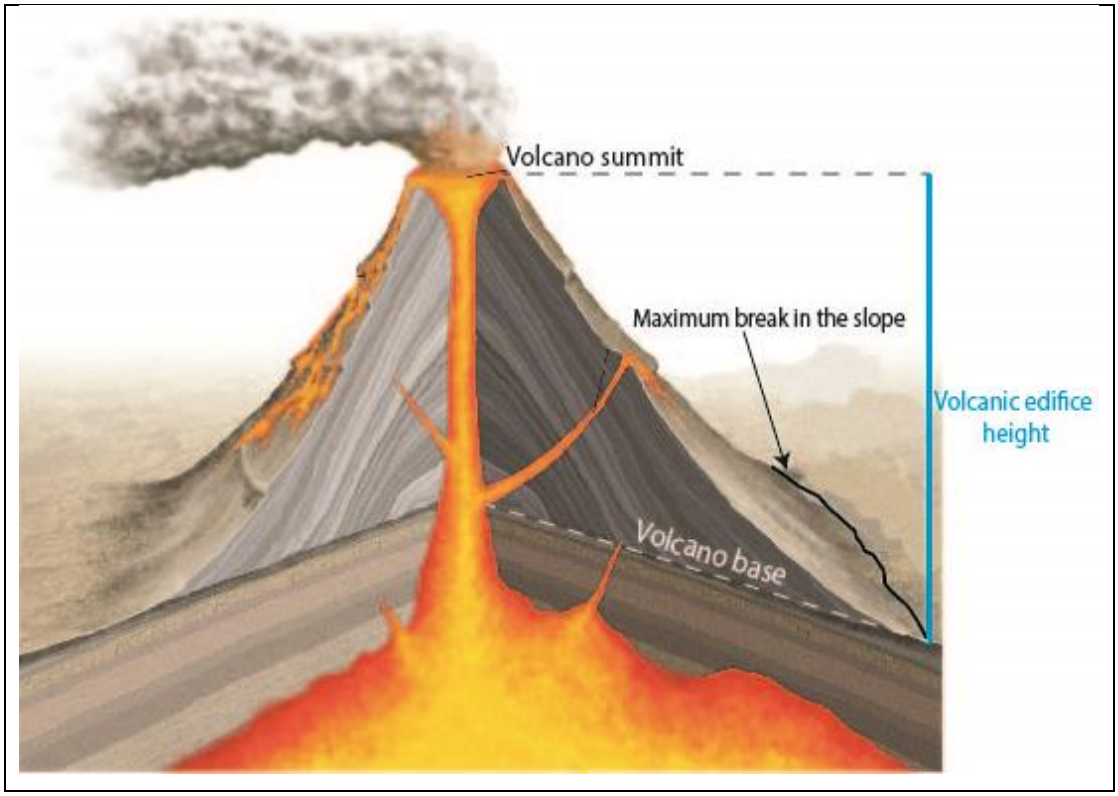


*Figure 2-1. Modified volcano diagram (Oxford University Press, 2021) showing how volcanic edifice height was measured when constructing the AEVDB. Volcano height is calculated firstly, by identifying the maximum break in the slope of the edifice (base of the edifice). Secondly, estimating the altitude at the base and at the summit of the edifice, using a DEM (digital elevation model). Finally, using the following formula:*

***Volcano height= altitude*** $_{summit}$ ***- altitude*** $_{base}$

- *Volcano type*

  Volcano edifices and its deposits were classified using the categories described in Table 2-2 and shown in Figure 7-3. A histogram showing the distribution of the data can be found in Figure 7-3.

  A unification was needed since the different sources have different names for the same type o volcano (i.e., Stratovolcano = Composite volcano = Volcanic complex = Complex Composite Volcano or Lava dome = Dome).

*Table 2-2: Volcano type classification.*

| Volcano type | Database | Description |
|---|---|---|
| Breached Cone | AVEDB | Stratovolcano with broad amphitheatre or valleys cutting from the summit through flanks. |
| Caldera | IIDB | Volcanic crater (its diameter has several times the vent dimension) generated by the collapse of the central portion of a volcano or by explosions during eruptions. |
| Dome | AVEDB | Extrusive lava dome. |
| Fissure vent | AVEDB | Linear volcanic vent through which lava erupts, usually without any major explosive activity. (Pfeiffer, 2004) |
| Ignimbrite Shield | IIDB | Low shield often cut by radial valleys and topped by domes. |
| Intrusive units (stocks, dykes, porphyry) | IIDB | Intrusive bodies are not volcanoes but are included in the IIDB. |
| Lava flow | AVEDB | Lava flow without an obvious source. |
| Maar | AVEDB | Circular volcanic crater produced by a phreatomagmatic eruption, often filled with a shallow water body. |
| Monogenetic centre | AVEDB | Group of small volcanoes, each of which erupts only once. |
| Pyroclastic deposit | AVEDB | Deposit of ash and magma fragments from an explosive eruption. |
| Scoria cone | AVEDB | Simple scoria cone formed around the vent, consisting of loose pyroclastic debris after an explosive eruption. |
| Shield Volcano | AVEDB | Constructed from basaltic low viscosity lava flows, they have a broad profile due to the cumulative built up of flows over time, erupting from vents or fissures on the surface of the volcano. |
| Stratovolcano | AVEDB | Simple composite volcano, most common type in the Andes. |
| Central volcano and domes | AVEDB | Focal point for volcanic activity and normally is the largest edifices within the system. They are generally at the centre of a volcano cluster. They could be a proper volcano edifice or a dome. |
| Volcanic Centre | AVEDB | Also called “volcanic field”, they are characterised by many cinder cones or other volcanic features that have not been independently recognised as separate volcanoes. They could be scattered over a large area, if many short-lived volcanoes are built rather than a major volcano with frequent eruptions. |
| Subglacial | AVEDB | Volcanic edifice constructed in whole or in part by eruption beneath ice. Although eruptions may start subglacially initially, many subglacial volcanoes culminate subaerially, having melted their way completely through the overlying ice. (Smellie, 2014) |

- *Climate*

  Table 2-3 shows a classification of modern climate, from Tropical to Hyperarid, according to a defined range of precipitation (Figure 7-17b). Annual precipitation rate was obtained CHELSA dataset.

*Table 2-3: Climate classification following a determined Annual precipitation rate.*

| Climate | Annual Precipitation rate (mm) |
|---|---|
| Tropical | >2000 |
| Subtropical | 2000-600 |
| Semiarid | 300-600 |
| Arid | 100-300 |

| | |
|---|---|
| Hyperarid | <100 |

- *Age (Ma)* represents the number of millions of years since a volcanic eruption happened. These values are also available in a different unit, years, in the field *Age (A)*.

- *Error (Ma)* is the estimated age error, in millions of years. These values are also available in a different unit, years, in the field *Error source (A)*.

- *Period by arc*

  When age was not provided by any of the sources, a period estimation was made using the volcano/ sample location within magmatic arcs created using ArcGIS in this study (Figure 2-2). These belts were constructed using metallogenic belts created by different authors (e.g., Sillitoe, 1974; Mpodozis and Cornejo, 2012), known ages of volcanic and plutonic rocks, in addition to PCDs ages. Once a period was assigned to the data point, those values were transformed into an age in My. Figure 7-9 compares the number of registers with ages from literature against ages assigned by the location within magmatic arcs.

- *Age by arc (Ma)*

  After a volcano/sample was given a period age according to the arc where it is located, an age in My was assigned, using Table 7-6. Empty cells were filled in with data from *Age (Ma)*. This field is the most complete compilation of ages within the AVEDB.

*a.*

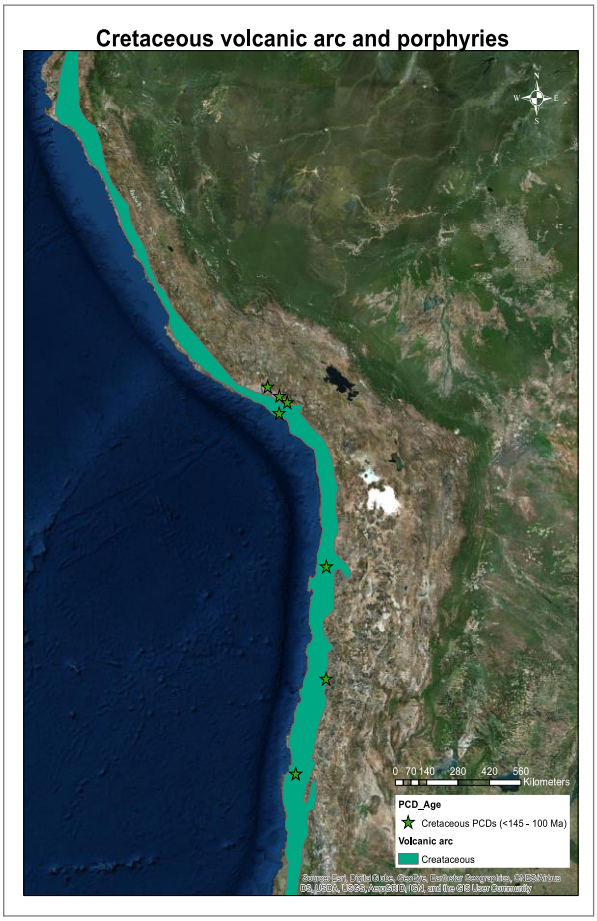
Cretaceous volcanic arc and porphyries
0 70 140 280 420 560
Kilometers
PCD_Age
Cretaceous PCDs (<145 - 100 Ma)
Volcanic arc
Creataceous

*b.*

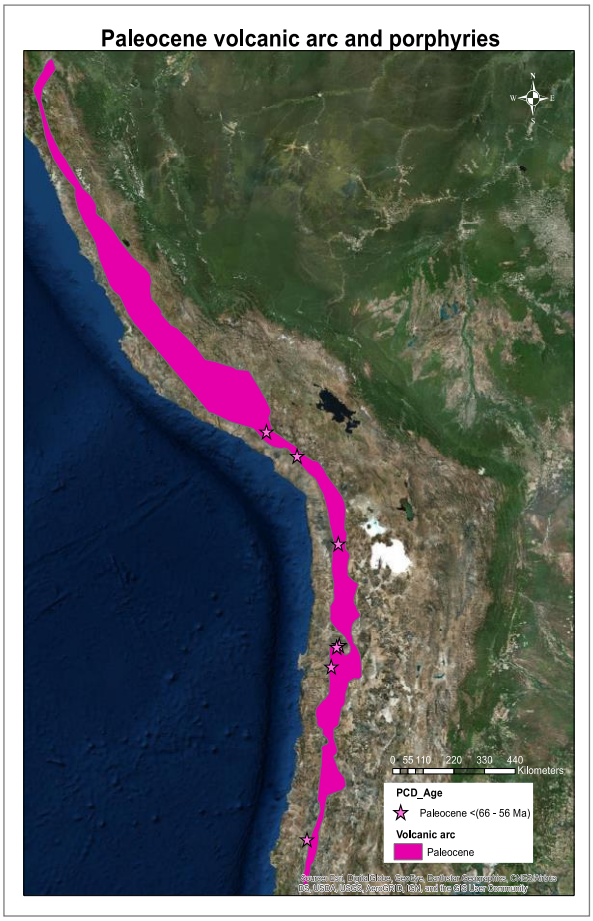
Paleocene volcanic arc and porphyries
0 55 110 220 330 440
Kilometers
PCD_Age
Paleocene <(66 - 56 Ma)
Volcanic arc
Paleocene

*c.*

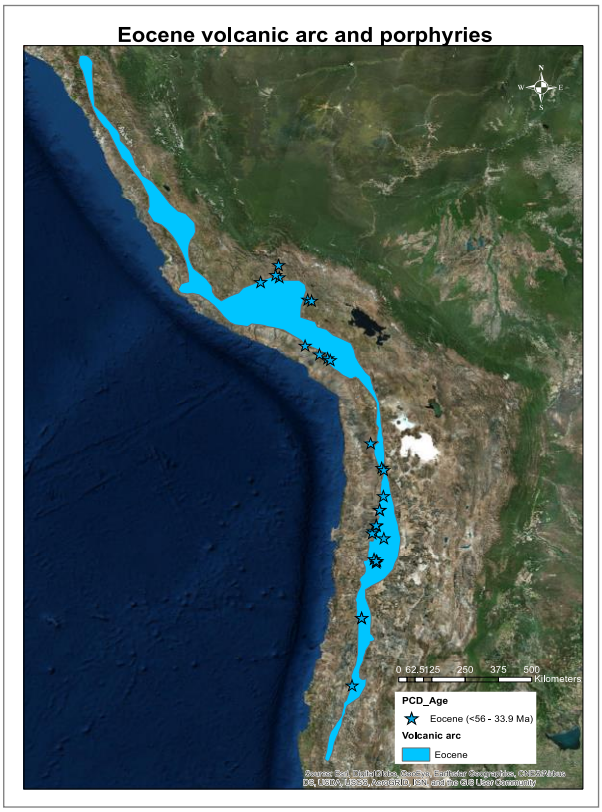
Eocene volcanic arc and porphyries
0 62.5125 250 375 500
Kilometers
PCD_Age
Eocene (<56 - 33.9 Ma)
Volcanic arc
Eocene

*d.*


Oligocene volcanic arc and porphyries
0 70 140 280 420 560
Kilometers
PCD_Age
Oligocene (<33.9 - 23 Ma);
Volcanic arc
Oligocene

*e.*

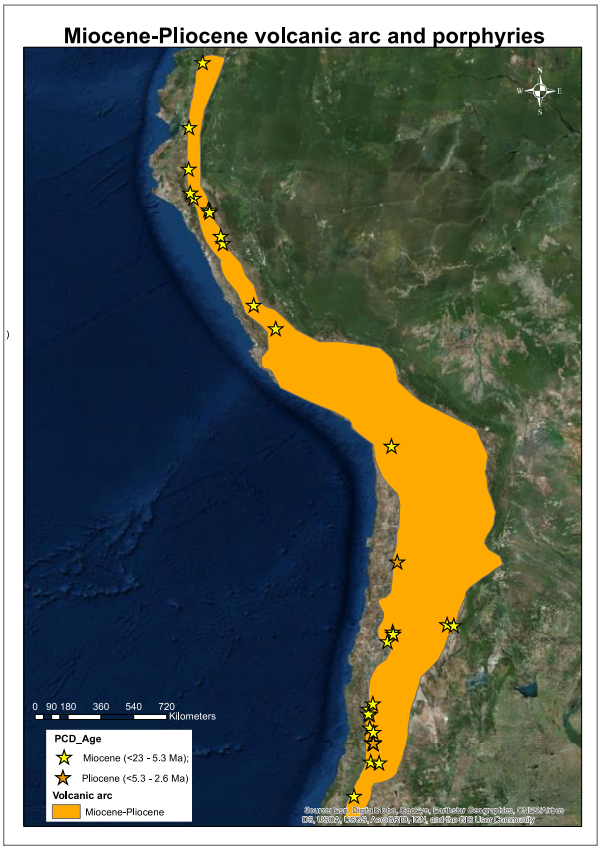


*Figure 2-2. Magmatic (volcanic and plutonic) arcs from Cretaceous to Pliocene time. a. Cretaceous magmatic arc with Cretaceous PCDs on top (green stars). b. Palaeocene magmatic arc with Palaeocene PCDs on top (pink stars). c. Eocene magmatic arc with Eocene PCDs on top (blue stars). d. Oligocene magmatic arc with Oligocene PCDs on top (purple stars). e. Miocene-Pliocene magmatic arc with Miocene PCDs (yellow stars) and Pliocene PCDs (orange stars) on top.*

## 2.2 Appendix III: Dataset of Porphyry Copper Deposits (PCDsDB)

This dataset is the result of an extraction of the Cu Atlas BHP dataset. It includes a total of 593 PCDs, skarns and epithermal deposits, with Au, Mo and Cu as commodities, located in America. It also includes a geological summary report, and references for the information for all of the deposits. Sources are mainly internal reports and by SNL Mine Economics (market intelligence company which compiles high quality mining dataset).

The PCDs dataset and the explanation for its design can be found in Appendix III.

## 2.3 Dataset combination of volcanoes, eruptions and PCDs and AVEDB subsets

### 2.3.1 Appendix IV: Dataset of volcanoes, eruptions and PCDs

This dataset is the result of the combination between the AVEDB, IIDB and PCDs datasets and can be found in Appendix IV. It is used in Chapter 4 in the erosional patterns' assessment. It contains: 1239 volcanoes, these are the edifices that have height values in the AVEDB, from which 116 have age information; 507 PCDs and epithermal deposits, from which 143 have ages; finally, 18 dated ignimbrite deposits extracted from the IIDB, that resulted from eruptions from active volcanoes.

This set of data keep the same format as the AVEDB and IIDB, but categories in the field *Unit filter* changed slightly due to the aim of the analysis in Chapter 4. Categories are: *Volcano-arc* (for edifices with ages assigned according to their spatial location), *Volcano-dated* (for edifices with dated ages), *Ignimbrite-dated* (for dated ignimbrite deposits). Finally, these data are combined with porphyries from the PCDsDB. When adding PCDs into the volcano set, I assigned 0 m as height, while elevation values, when not given by the source, correspond to the elevation extracted from a DEM raster image used in ArcGIS.

### 2.3.2 Appendix V: AVEDB subsets

These datasets are the result of filtering and eliminating duplicated values in the AVEDB, and can be found in Appendix V. It is used for a statical analysis of volcanic edifice parameters in Chapter 3. As the AVEDB includes both volcanic edifices and all the registered eruptions per each volcano, it may be possible to find duplication in the volcanic parameters within the dataset, bringing additional bias into the data. Therefore, for statistical analyses I have filtered the AVEDB for volcano parameters and created subsets of the AVEDB, so there is only one volcano dimension parameter value per volcanic edifice. In summary, I created 4 subsets from the AVEDB that contain has 1239 volcanoes with height values, 1139 volcanic edifices with volcano volume records, 1162 volcanoes with cone diameter information and 1162 edifices with crater diameters.

# 3 Chapter 3: Descriptive Statistical Analysis of the AVEDB

## 3.1 Introduction

In this chapter I study the statistics volcanoes and eruption parameters of the **AVEDB** in order to summarize, organize, and make sense of the data. The statistical data analysis helps to understand the distribution of the data, and how biases and correlations in the records could impact future analysis. I have focused the analysis on the parameters that define the dimension of a volcanic edifice, such as cone and crater diameter and volcano volume, but in particular the height of the edifices. Edifice height is extensively studied in this chapter by comparing height changes in time, the correlation height has with cone diameter and finally, edifices height in relation to volcano types. Edifice's height in the absence of erosion depends on magma buoyancy, magma density and magma chamber depth (Castruccio et al., 2017). Castruccio et al. (2017) proposed that the volume and length of the largest eruption reflects the maximum height a volcanic edifice can reach. A volcano will grow in height until the magmatic system is not able to produce enough pressure gradient, which permits the magma to ascend though the volcanic vent up to the surface. Cone diameter is another dimension of volcanic edifices that I am interested in, and because edifice height and diameter tend to be well correlated, when volcanoes are heavily eroded, the diameter gives an indirect indication of the original height of a volcanic edifice before erosion. Karátson et al. (2010) established that some of the youngest volcanic edifices in the Central Andes could reach heights up to 2.5 km (measured from the local base), and all Quaternary volcanoes included in their study, have large height-diameter (H/D) ratios (0.10-0.15), consistent with ratios of active volcanoes around the world (Wood, 1978; Grosse et al., 2009). On the contrary, most volcanoes included in Karátson et al. (2010) study show much smaller H/D ratios (the average is 0.08), consistent with their older ages and associated erosional degradation processes.

Castruccio et al., 2017 also suggests that the basal radius, maximum volcano height and maximum volume are regulated by the depth and size of the magma chamber, in turn, these parameters will influence the lifetime of the volcano. Eruption decline could be caused by the increase in vent elevation as the volcano grows. Therefore, the dimension of volcanoes can be considered as an indicator of the characteristics of the plumbing system in depth.

Additionally, in Chapter 4, I extend the study of volcano height by assessing the changes in this parameter depending on climate, location in the Andes and time, to finally use it as a proxy of erosional patterns in South America.

## 3.2 Methodology

I start by plotting in a bar chart the number of registers per category. Then, I perform a descriptive statistical analysis for every parameter within the dataset. I have calculated basic statistics such as measures of central tendency (mean, median, mode), dispersion (standard deviation) and distribution (kurtosis, skewness) for the whole population and also for subpopulations such as different volcano types. Categories within the AVEDB have been classified as follow:

- Volcanoes parameters: Height, Cone Diameter, Crater Diameter, Volcano volume, Volcano Size;
- Eruption parameters: Deposit diameter, Deposit area, Flow length, Eruption magnitude and Bulk and Bulk DRE volume;
- Tectonic parameters: Crust thickness and Volcanic zone;
- Geomorphological features: Geomorphology, Denudation Rate, Climate and Slope.

In order to compare populations, I statically analyse these parameters using histograms, box whiskers, density and scatter plots. When using histograms, I fit the data into normal probability distribution. Normal distributions are critical in statistics and are usually utilised in different branches of sciences to characterise random variables whose distributions are unknown (Casella and Berger, 2001). Their significance is because under certain conditions, the average of numerous samples of a variable defined as random, with known mean and variance is itself a random variable. The distribution of this random variable converges to a normal distribution when the number of samples rises. For this reason, I have fitted our data to a Gaussian distribution and measured skewness and kurtosis. Skewness is a measure of the symmetry of a distribution, while kurtosis is a measure of the combined sizes of the two tails, quantifying the amount of probability in the tails.

When using box whisker plots, I calculate and show outliers if they exist. An outlier is a value that lies abnormally far away from the rest of the data and can be challenging because they can disturb the results of the analysis. Two different types of outliers are considered, outliers, represented in the whisker plot as a circle and extreme outliers, represented by an asterisk. For the outlier calculations I use the following equations:

*Equation 3-1*

**Lower outlier = $25^{th}$ percentile – 1.5 * interquartile range ($25^{th}$ percentile-$75^{th}$ percentile)**

**Upper outlier = $75^{th}$ percentile + 1.5 * interquartile range ($25^{th}$ percentile-$75^{th}$ percentile)**

*Equation 3-2*

**Lower extreme outlier = $25^{th}$ percentile – 3 * interquartile range ($25^{th}$ percentile-$75^{th}$ percentile)**

**Upper extreme outlier = $75^{th}$ percentile + 3 * interquartile range ($25^{th}$ percentile-$75^{th}$ percentile)**

Next, I perform a multiple linear correlation analysis using the SPSS statistics (IBM) software, where I build a model that correlates volcanoes parameters. Because *Volcano height* is an important factor in our study and I use it later in the following chapters, I have decided to use it as the dependent variable, leaving *Volcano volume*, *Cone* and *Crater diameter* as the independent ones. Following, I compare our results to Castruccio et al. (2017) conclusions. For the calculation of the correlation matrix and I do a stepwise multiple linear regression analysis. A regression analysis is a mathematical method that sorts out which variable influences the others and to what degree. In a regression analysis, there is a dependent variable which is the factor to understand and predict. And there are also the independent variables, which are the elements that have an impact on the dependent variable. In order to conduct a regression analysis, the data are plotted in a scatter plot, where the dependent variable is on the y-axis. Then the line that best fits the data, the regression line, is the best representation of the correlation among the independent and dependent variables. In this analysis, I use the *SPSS statistics* (IBM) software, which, for instance can output:

*Equation 3-3*

**Volcano height (m) = a + b * Independent variable + error**

where ***a*** is the intersection with Y axis and ***b*** represent the regression line slope.

A regression line for a natural system always has an error associated because, independent variables cannot completely predict dependent variables. The regression line is an estimation based on the existing data. Therefore, the error indicates how certain the model can be about the formula. The larger the error value, the less confident the regression line will be.

For my analysis *SPSS statistics* software builds a model with independent variables that only includes statistically significant contributors to the multiple regression equation. However, I did not perform a simple regression analysis, but a stepwise multiple regression analysis instead. The *Stepwise* module determines the independent variables with the largest Pearson correlation with the dependent variable. The regression analysis is done multiple steps. It will eliminate the variable with the weakest correlation, step by step. At the end of the analysis, the remaining variables are the ones explaining the distribution best. There are certain requirements that it is necessary to comply with: the residuals of the data need to be normally distributed and no correlation exists whatsoever between the independent variables, which is called collinearity (University of Leeds, n.d.). Before calculating the multiple linear correlation analysis, it is necessary to remove extreme outliers if present in the data, which are calculated in Equation 3-1and Equation 3-2.

## 3.3 Initial analysis: Understanding raw data.

### 3.3.1 Valid, missing and non-valid values

Figure 3-1 shows valid, missing and non-valid values for each field in the AVEDB. Non-valid value refers to registers that will not have a category assigned in a field, i.e., Volcano volume will provide the volume only if the register belongs to a volcanic edifice and not to an eruption. It is easy to recognise that tectonics

and geomorphology are the most complete parameters, while volcano and eruption parameters are the ones showing the highest numbers of missing values. Despite the fact I expected a non-complete set of values, numbers show I should be very cautious when making statistical analysis.

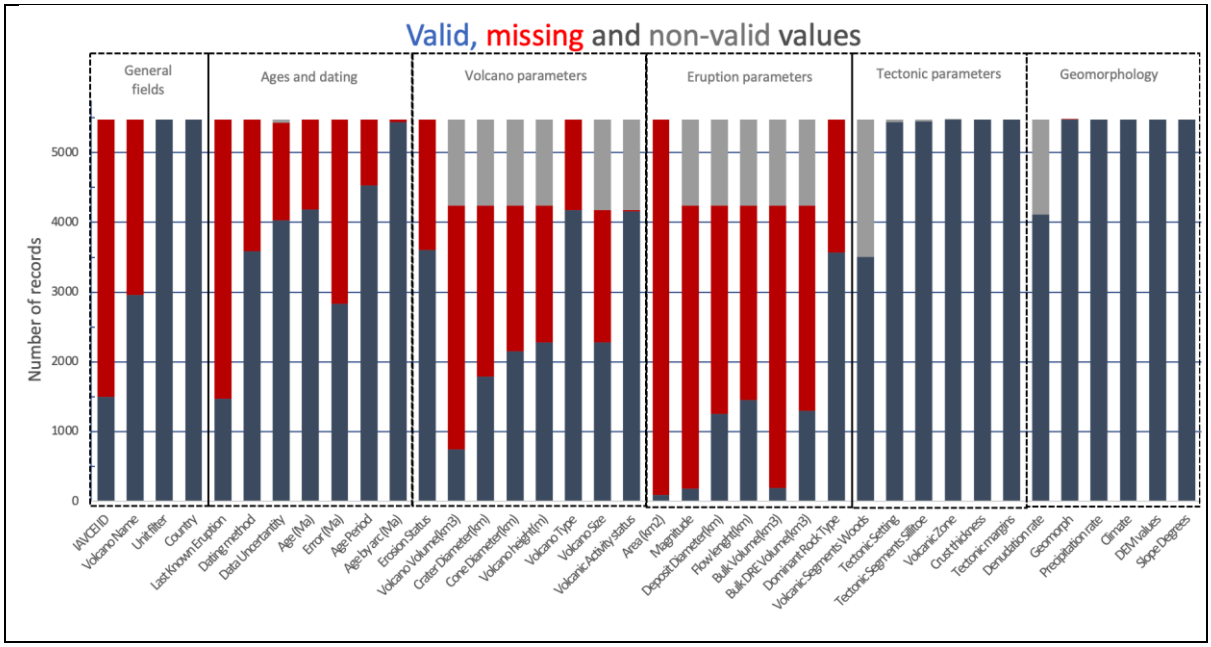


*Figure 3-1. Bar plot showing valid, missing and non-valid values for the Volcano and Eruption dataset, classified into the main parameters.*

## 3.4 Results for Volcanic edifices

Below, I statically analyse volcano and eruption dimension parameters within the AVEDB using histograms, box whiskers and scatter plots.

Note that certain volcano types could be thought as part of the same volcanic activity and could be grouped. For example, *Stratovolcanoes* and *Breached cones*, since the latter represent the remaining stratovolcano edifice left after an explosive eruption. The same applies to *Ignimbrite Shield* and *Calderas:* they are part of the same volcanic process, when an ignimbrite shield is formed the remaining feature is a caldera. Also, *Ignimbrite Shield* and *Lava Flow* categories are not proper volcanic edifices; they are more likely to be volcanic deposits without a spatial defined source. However, when it was not possible to identify a volcanic edifice, height values for these features provided by the source authors (e.g., Da Silva, 1991) represent the best approximation to a volcanic edifice available.

As the AVEDB includes both volcanic edifices and all the registered eruptions per each volcano, it may be possible to find repeated rows for the same edifice. For example, Llaima volcano, a stratovolcano located in Chile, contain 62 rows in the AVEDB. This generates duplication in the dataset, for example the cone diameter is repeated several times. Therefore, for statistical analyses I have filtered the AVEDB for volcano parameters and created subsets of the AVEDB (Appendix V in Section 2.3.2), so there is only one volcano dimension parameter value per volcanic edifice. In summary, the AVEDB has 1239 volcanoes with height

values, 1139 volcanic edifices with volcano volume records, 1162 volcanoes with cone diameter information and 1162 edifices with crater diameters.

Figure 3-2 shows that *Stratovolcanoes* dominate the whole AVEDB distribution for all volcano dimension parameters, as they account for over 80% of the values, followed by *Domes* and *Calderas*.

When classifying histograms and distribution curves by volcano type, the majority of the curves are unimodal, asymmetrical and systematically skewed to lower values. The main exception for most of the volcano dimension parameters are *Stratovolcanoes*, which show values closer to a normal distribution.

I also use box whisker plots, which are useful particularly to compare volcano dimension and eruption parameters. Since there is systematic difference for the volcano types, I decided to present distributions using this category and ordering them from higher to smaller values. It becomes evident that *Stratovolcanoes* (+*Breached cones*) and *Calderas* (+ *Ignimbrite Shields*) show consistently the highest values and the biggest values variations.

I also use scatter plots to show the differences between volcano sizes and identify and highlight the biggest edifices.

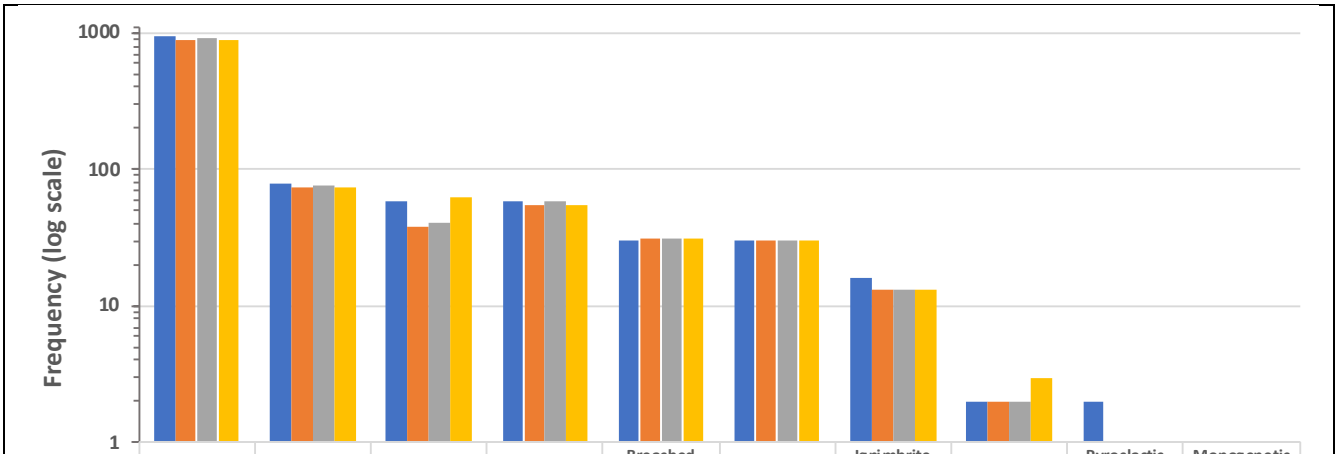


| | Stratovolcano | Dome | Caldera | Scoria cone | Breached Cone | Lava flow | Ignimbrite Shield | Maar | Pyroclastic deposit | Monogenetic centre |
|---|---|---|---|---|---|---|---|---|---|---|
| Volc Height | 958 | 80 | 59 | 58 | 30 | 30 | 16 | 2 | 2 | 1 |
| Volc Volume | 896 | 74 | 38 | 55 | 31 | 30 | 13 | 2 | 0 | 0 |
| Cone Diam | 917 | 75 | 40 | 58 | 31 | 30 | 13 | 2 | 0 | 1 |
| Crater Diam | 894 | 73 | 62 | 55 | 31 | 30 | 13 | 3 | 0 | 1 |

*Figure 3-2. Bar plot showing number of values for the Volcano dimension categories classified by Volcano type.*

## 3.4.1 Descriptive analysis for volcano parameters

### *3.4.1.1 Volcano height (m)*

Height of volcanic edifices are considered to be one of the most important parameters in this study, since it is an indirect measure of volcanic activity and erosion patterns that will be studied in Chapter 5.

I start applying EDA (Exploratory data analysis) methodology in order to understand the volcanic height distribution. I focused firstly on volcanoes types and in the following section, in height distribution in time. The AVEDB accounts for 1239 volcanoes height values.

Table 3-1 displays descriptive statistics for all volcanic edifice heights. The maximum height found in the AVEDB is 2913 m, which corresponds with a stratovolcano named *El Misti,* located in Peru. Whereas the shortest volcano, a scoria cone type, has 75m height. The mean and median are 848m and 750m respectively, with a standard deviation of 508 m and mode of 200 m. I can easily observe that a mode of 200m it is not really representative of the whole population, especially when I classify the data by volcano type.

Figure 3-3a shows a box whisker plot for heights, which complements the histograms.

For the whole-dataset (Table 3-1), 0.94 skewness value for heights indicates that the distribution is asymmetric and moderately shifted to lower values. Most volcano types show that type of asymmetric distribution, except for *Stratovolcanoes* exposing a slightly skewed to high height values distribution. Kurtosis, on the other hand, with a value of 0.71 for the whole height population, reveals a reasonably leptokurtic curve (Figure 3-3b).

*Table 3-1. Descriptive statistics for volcanic edifice height (m).*

| Descriptive Statistics: Edifice Height (m) | |
|---|---|
| Count | 1239 |
| Minimum | 75 |
| Maximum | 2913 |
| Mean | 848.45 |
| Standard Error | 14.46 |
| Median | 750 |
| Mode | 200 |
| Standard Deviation | 508.99 |
| Kurtosis | 0.71 |
| Skewness | 0.94 |

*a.*

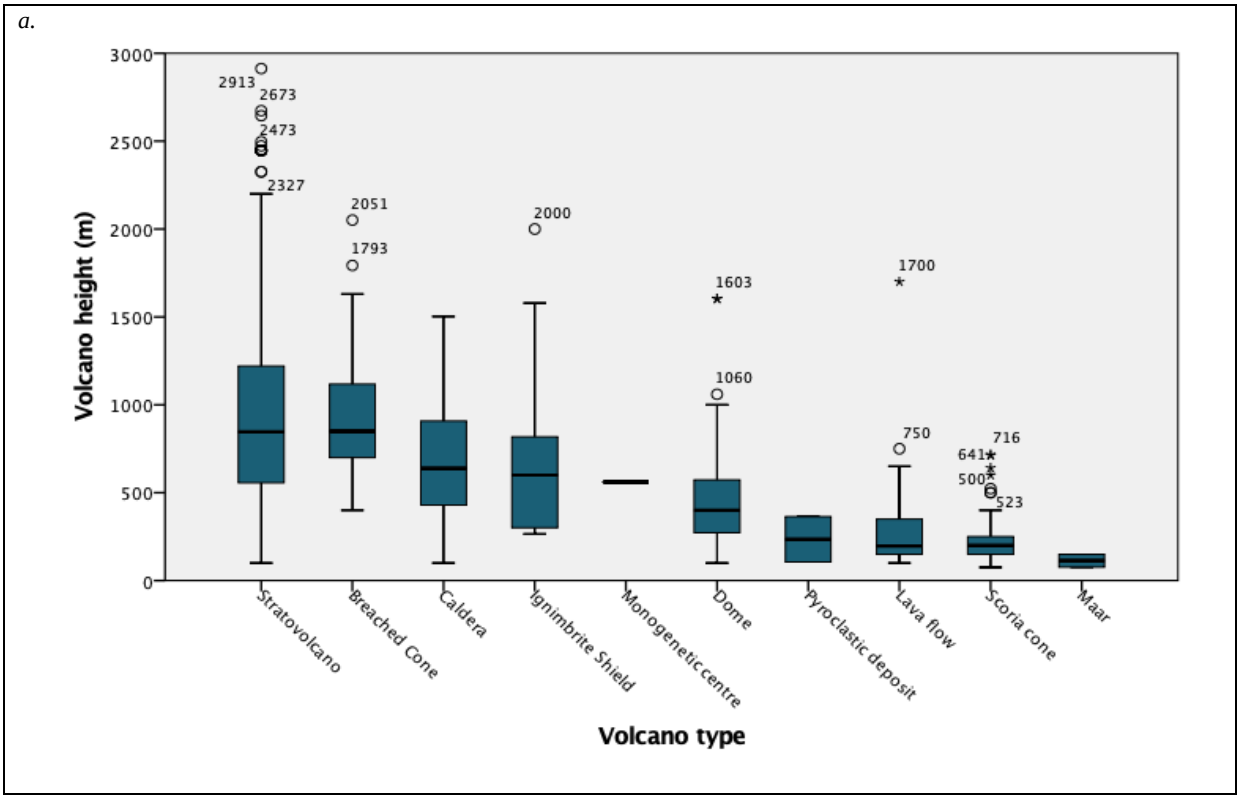

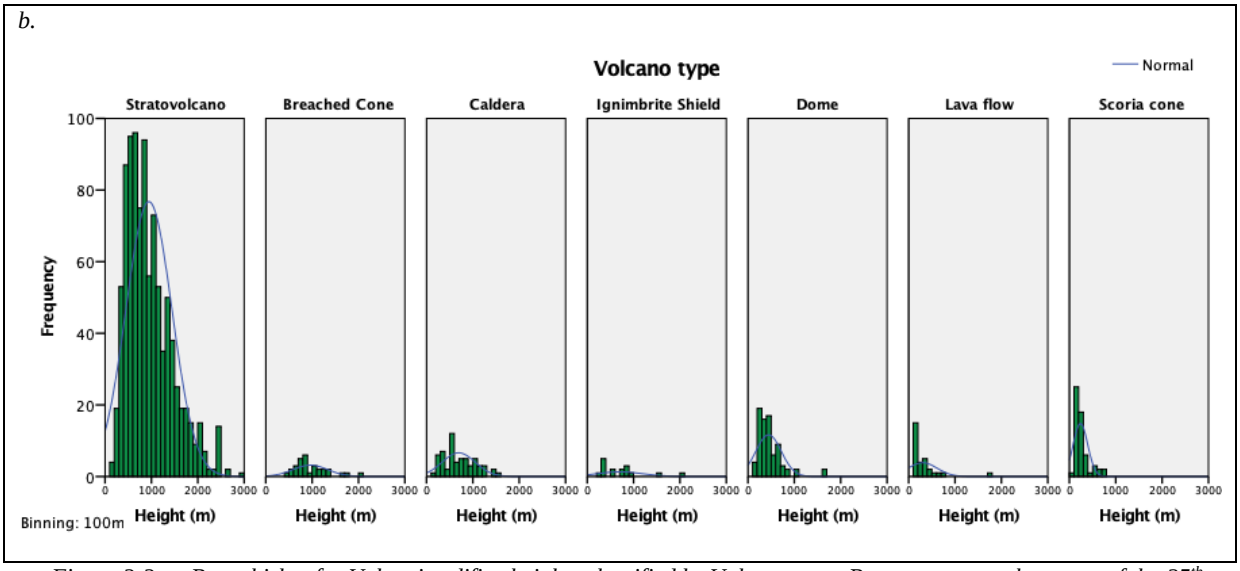


*Figure 3-3. a. Box whisker for Volcanic edifice heights classified by Volcano type. Boxes represent the range of the 25th and 75th percentiles with the dividing line being the median. Whiskers represent the minimum and maximum values. Circles outside the boxes represent outliers and asterisks are extreme outliers (values more than three times the height of the boxes. b. Histograms and normal distribution curves for volcanic edifices classified by Volcano type.*

### *3.4.1.2 Volcano height in time*

Figure 3-4a shows how edifices height varies in time, I can see similar heights, between 500m to 1200m, from Cretaceous to Miocene. Although, there is a slight drop in the height mean during Palaeocene, in general the height mean maintains around 750m. From Pliocene, the tendency seems to change into a steady increase in volcanoes heights. Variability in height spreads considerably during the Pliocene and Pleistocene, between 200m to 1700m to narrow again between 1000m to 2000m during the Holocene.

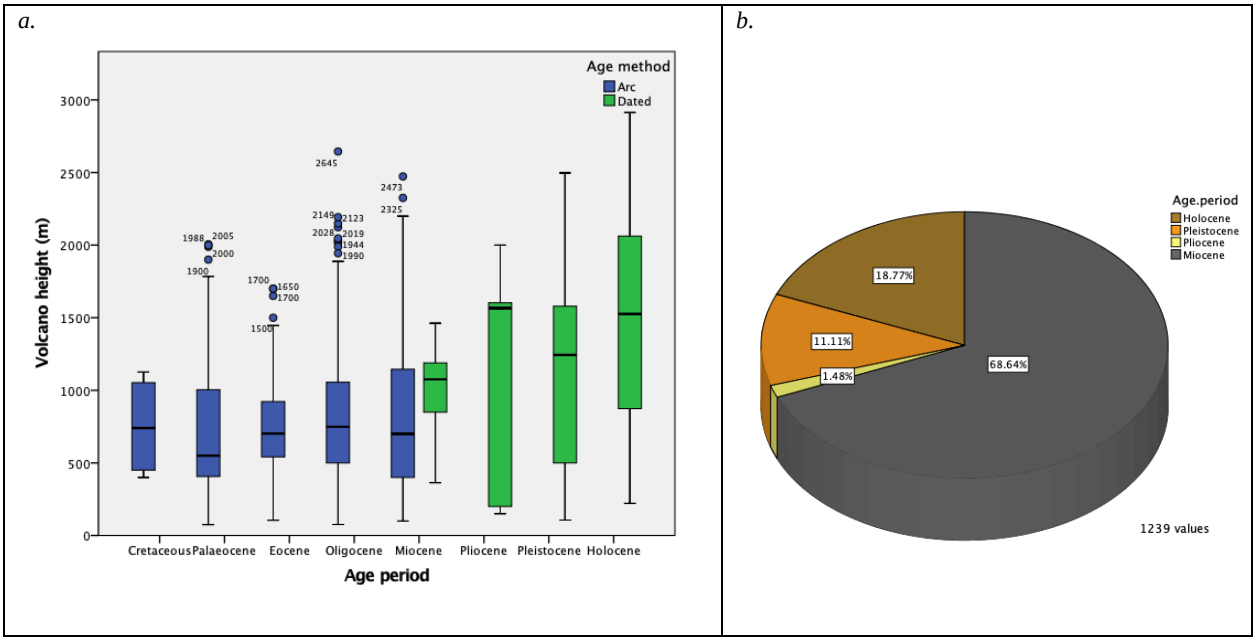


*Figure 3-4. a. Box plot showing the variation in volcanic edifices height (m) through time from Cretaceous to present time. Note the differentiation on dated records and records with ages assigned according to their location. Boxes represent the*

*range of the 25th and 75th percentiles with the dividing line being the median. Whiskers represent the minimum and maximum values. Circles outside the boxes represent outliers. b. Pie chart showing the percentages of values classified by epochs from Miocene to Holocene time.*

Figure 3-4b shows the distribution of the data in different time epochs. Most volcanic edifices with height data belong to Miocene times (282 registers), followed by Holocene (75) and Pleistocene (46) and last by Pliocene (6). However, from the Miocene registers, less than 3% have been dated (7 registers; Figure 3-5b); the rest of the ages have been assigned according to the location of those edifices (Section **Error! Reference source not found.**; **Error! Reference source not found.**). One might expect the majority of the volcanic edifices in the AVEDB with height data to be Holocene in age because the youngest volcanoes have not had time to be completely eroded and therefore, they will show higher frequencies. However, there are significantly more Miocene edifices than Holocene edifices with height data (Figure 3-4b). Whereas the Holocene represents only last 11.7 thousand years, which is much shorter than the earlier epochs considered, the Miocene represents 17.7 million years, and so while there could be many older edifices misattributed to the Miocene due to lack of age data. It is also possible, that younger edifices have been assigned Miocene ages as well. However, this is less likely since the more reliable sources feeding the AVEDB contain the most recent eruptions and volcanoes, Holocene and Pleistocene (Section 2.1.1.1 and 2.1.1.1ii). In terms of how reliable assigned ages for edifices are, I can confidently say that from the 282 Miocene registers, only 7 have been dated, 9 registers belong to the Miocene ignimbrite flare-up that occurred in the CVZ (Cerro Aguas Calientes, Cerro Bonete, Cerro Coranzuli, Cerro Mulas Muertas, La Pacana Caldera and Nevado Queva) and the others 266 could simply belong to other epochs and the only way to prove it would be dating those volcanoes. In the same way I could move registers away to other periods of time, I can bring data from older periods into Miocene times. Twenty registers with Palaeocene and Oligocene assigned ages, were detected to be part of the Miocene flare-up in the CVZ (Nevado Curahuara, Frailes ignimbrite, Cerro Kari ignimbrita Caldera, Cerro Kapina, Cerro del Carcanal, Cerro Panizo, Cerro Vilama, Cerro Piedras Grandes, Cerro Puripica Chico, Cerro Puripica Grande, Sierra de Chaxas, Sierra de Chaxas Ignimbrite, Cerro Purico Complex, Cerro Wheelwright Caldera, Pampa Galeras Caldera, Huaylillas ignimbrite, Moroccocala Ignimbrite plateau, Cerro Pastos Grandes). Because the aim of this study is focusing on other periods of time and not particularly in the Miocene flare-up, I am still comfortable with these inconsistencies and I think that the considerations above are robust enough to carry on with our study in volcanoes dimensions.

Figure 3-5 shows volcanoes heights distribution categorised by time epochs. Holocene time is the epoch with the highest quantity of values compared to others, followed by Pleistocene. While Holocene edifices tend to have the highest frequencies for tallest edifices, showing a distribution skewed to the right in a density plot, Miocene volcanoes in general terms are limited to heights of 1500 m, representing the lowest frequencies. Finally, Miocene edifices seem to show two different populations, with similar frequencies but pretty dissimilar height values, 0-1200 m height and 2000 m height.

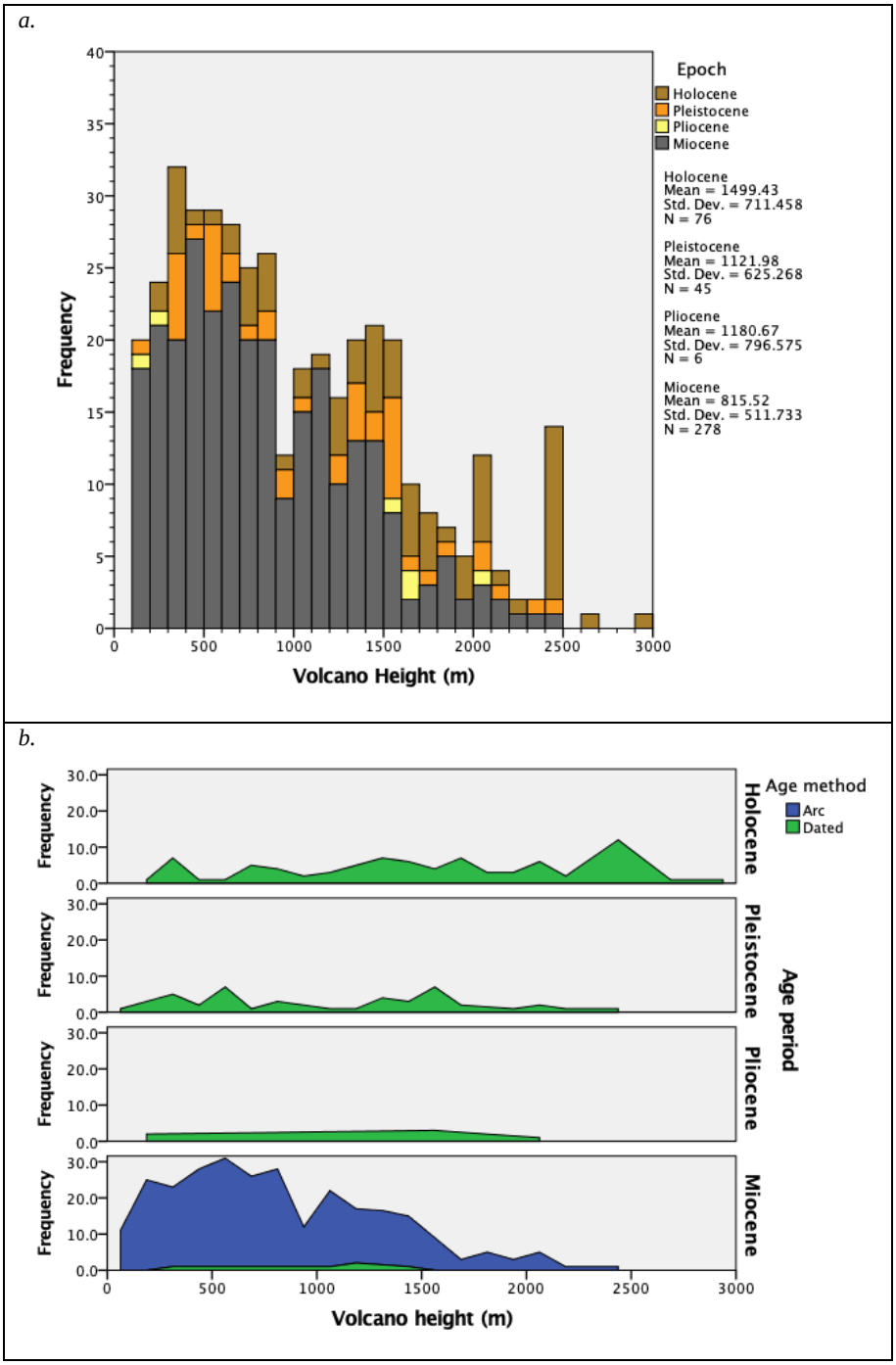


*Figure 3-5. a. Histogram of volcanoes heights showing the number of records for different epochs. b. Kernel density plots of volcanoes heights showing the distribution of the values in different epochs for dated non-dated records.*

### *3.4.1.3 Cone Diameter (km)*

Cone diameter can be used in combination with height to understand how much of an edifice is left after erosional processes have occurred. It can be also used as an indirect way of estimating the original height of an edifice and denudation rates. Karátson et al. (2010) concluded that Quaternary volcanoes have large

height/diameter (H/D) ratios of 0.10–0.15, while much smaller H/D values (average 0.08) correspond to older edifices affected by erosional degradation. Cone diameter will not be affected by erosion as much as height, on the contrary, if something, some flanks of the edifice may elongate and extend because of material deposition.

In this study cone diameter accounts for 1167 volcanoes with diameter calculations, with a maximum diameter of 65 km and a minimum of 1 km, and mode of 5 km of diameter. Mean and median are both approximately 7 km, with a standard deviation of 5.58 km (Table 3-2).

There are two main populations, the first group are *Ignimbrite Shields* and *Calderas* with values up to 65 km and the second group with cone diameters up to 25 km. Figure 3-6b.c.d show positive asymmetrical and leptokurtic distribution for all volcano types and a long tail into big diameters for *Ignimbrite Shields* and *Calderas*.

*Table 3-2. Descriptive statistics for Cone Diameter (km).*

| Descriptive Statistics: Cone Diameter (km) | |
|---|---|
| Count | 1167 |
| Minimum | 1 |
| Maximum | 65 |
| Mean | 7.72 |
| Standard Error | 0.16 |
| Median | 7 |
| Mode | 5 |
| Standard Deviation | 5.58 |
| Kurtosis | 33.77 |
| Skewness | 4.32 |

*a.*

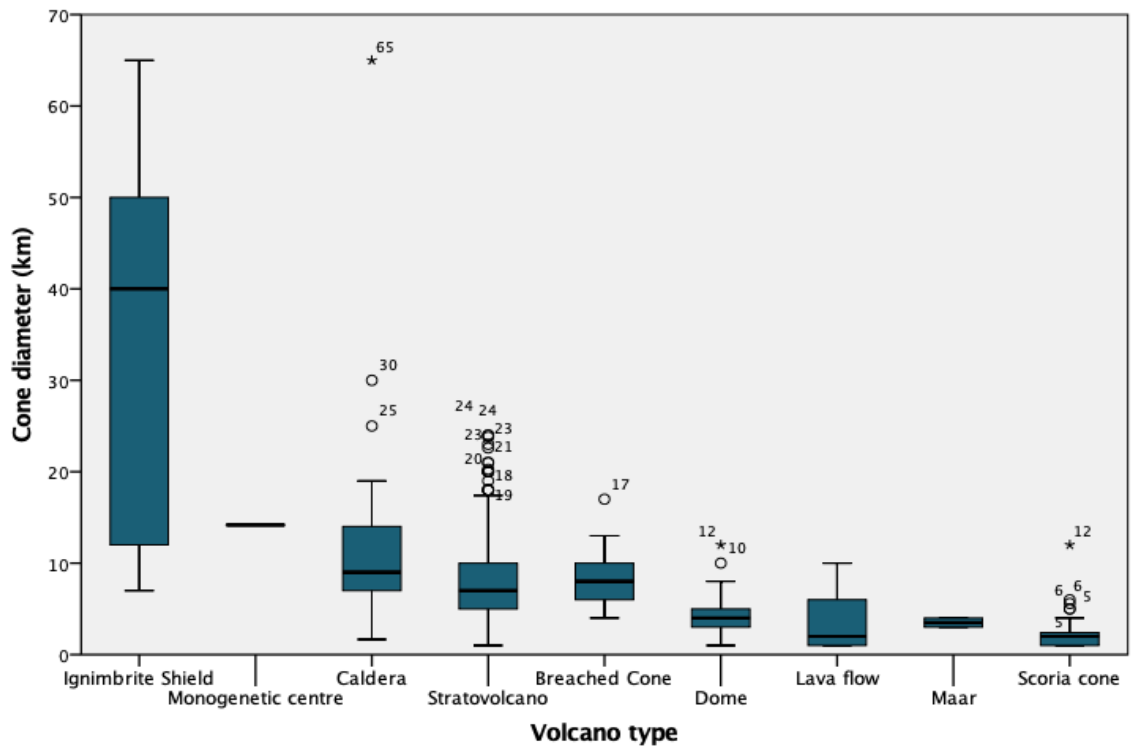


*b.*

*c.*

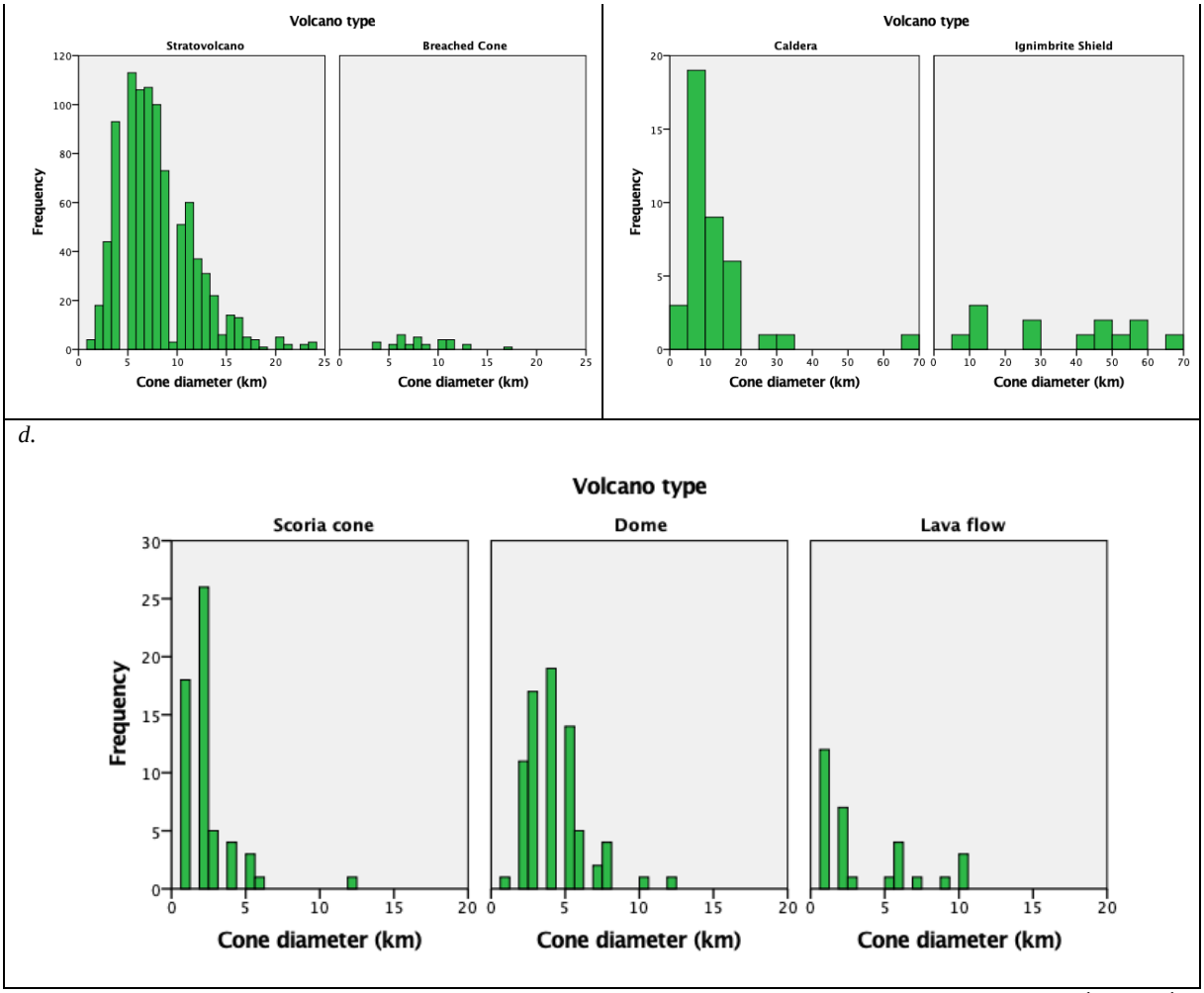


*Figure 3-6. a. Box whisker for Cone diameter classified by Volcano type. Boxes represent the range of the 25th and 75th percentiles with the dividing line being the median. Whiskers represent the minimum and maximum values. Circles outside the boxes represent outliers and asterisks are extreme outliers (values more than three times the height of the boxes. b.c. d. Histograms for Cone diameter classified by Volcano type, which were plotted in separated charts because of diameter scale differences.*

Following Karátson et al. (2011), I consider Height versus Diameter (H/D) ratios and I plot them in a whisker graph (Figure 3-7). Our results coincide with Karátson et al. (2011), Quaternary edifices have an average ratio of 0.12, whereas Miocene to Cretaceous volcanoes there is a clear decrease in H/D ratio from 0.11 to 0.7. Despite Pliocene and Cretaceous values seem to fit well in the overall H/D ratio trend, they count with a small number of datapoints, 3 and 4 respectively. Since they may not represent those periods accurately, they should be considered cautiously.

I also need to be careful with outliers. Table 3-3 show outliers' details, where I can recognise that they do not seem to correspond with the H/D expected values. A simple explanation for these 8 eight volcanic edifices is that height and cone diameter measurements are not reliable. These edifices are far from being perfect cones, in some cases they have suffered so much degradation that it is even hard to recognise the edifice at all. Some of these edifices seem to be old and other such as Romeral and Chacana have been

affected by an extremely humid climate, heavily eroding the flanks of the edifices and dissecting them into smaller portions by the presence of quebradas and water discharge paths.

Outliers are not considered in further analyses presented.

*Table 3-3. H/D ratio outliers and age estimation.*

| H/D ratio outliers | | | | |
|---|---|---|---|---|
| **Volcano name** | **Country** | **H/D ratio** | **Volcano type** | **Age estimation** |
| Cerro Jaquela | Peru | 0.85 | Stratovolcano | Eocene arc |
| Cerro Bencasa | Peru | 0.79 | Stratovolcano | Oligocene arc |
| Cerro Huacho | Chile | 0.75 | Lava flow | Oligocene arc |
| Cerro Huagra | Peru | 0.64 | Stratovolcano | Eocene arc |
| Romeral | Colombia | 0.47 | Stratovolcano | Holocene<br>Dating method |
| Romeral | Colombia | 0.47 | Stratovolcano | Pleistocene<br>Dating method |
| Cerro Santa Catalina | Bolivia | 0.46 | Stratovolcano | Oligocene arc |
| Chacana | Ecuador | 0.45 | Caldera | Holocene<br>Dating method |
| Chacana | Ecuador | 0.45 | Caldera | Pleistocene<br>Dating method |
| Cerro Laguna Verde | Chile | 0.40 | Stratovolcano | Miocene arc |

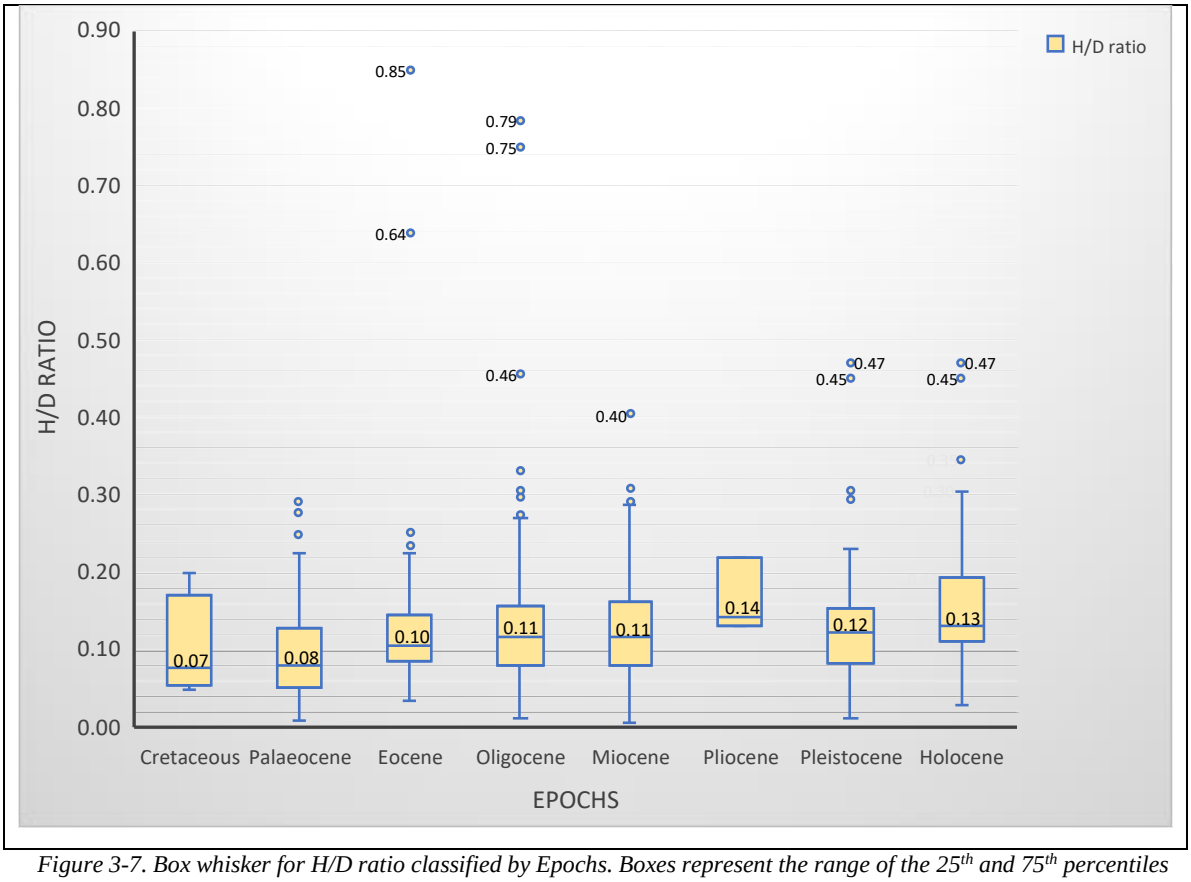


*Figure 3-7. Box whisker for H/D ratio classified by Epochs. Boxes represent the range of the 25$^{th}$ and 75$^{th}$ percentiles with the dividing line being the median. Whiskers represent the minimum and maximum values. Circles outside the boxes represent outliers.*

#### *3.4.1.4 Volcano volume ($km^3$)*

Volcano volume depends on the amount of volcanism (number and volume of each eruption responsible for the edifice growth) and erosion by wind, water, material creeping, etc, but also different eruption activity (e.g., some energetic eruptions can cause destruction of the volcanic edifice). I do not perform volume calculations in this study.

The database contains 1139 edifices with volume estimations, of which 78% are stratovolcanoes. Table 3-4 describes basic statistics for this parameter. Maximum volume is 6200 $km^3$, which belongs to La Pacana Caldera, whereas the minimum is 0.03 $km^3$ from Cerro Porunita.

The mean (36 $km^3$) is over three times greater than the median (11 $km^3$) due to one specific outlier shifting the mean into higher values. Precisely, a massive 6200 $km^3$ caldera called La Pacana Caldera, located in Northern Chile. The inclusion if this value has only an important effect on the overall statistics, therefore I have decided to remove the outlier from the analysis and recalculate the basic statistics. In the second column of Table 3-4, I see that the maximum volcano volume is 1700 $km^3$, which correspond to Cerro Galín volcano, located in Argentina. As expected, dispersion values, such as standard deviation, skewness and kurtosis drop considerably.

*Table 3-4. Descriptive statistics for Volcano volume ($km^3$).*

| **Descriptive Statistics: Volcano Volume ($km^3$)** | | |
|---|---|---|
| | Statistic with outliers | Statistic without outliers |
| Count | 1139 | 1138 |
| Minimum | 0.03 | 0.03 |
| Maximum | 6200 | 1700 |
| Mean | 36.27 | 30.85 |
| Standard Error | 5.98 | 2.55 |
| Median | 11 | 11 |
| Mode | 1 | 1 |
| Standard Deviation | 201.98 | 85.96 |
| Kurtosis | 768.77 | 173.48 |
| Skewness | 25.87 | 11.33 |

The distribution of volcano volumes for the whole dataset and for each volcano type are all asymmetrical and strongly skewed to low values (Figure 3-8 a, d, e). It becomes particularly necessary to plot *Calderas* (Figure 3-8c) and *Ignimbrite shields* (Figure 3-8d) in a different chart, since the scale needed is much bigger (0-6200 $km^3$). Excluding these, *Stratovolcanoes* have the largest volumes, up to 700 $km^3$, and a mean of 27.44 $km^3$ (Figure 3-8b).

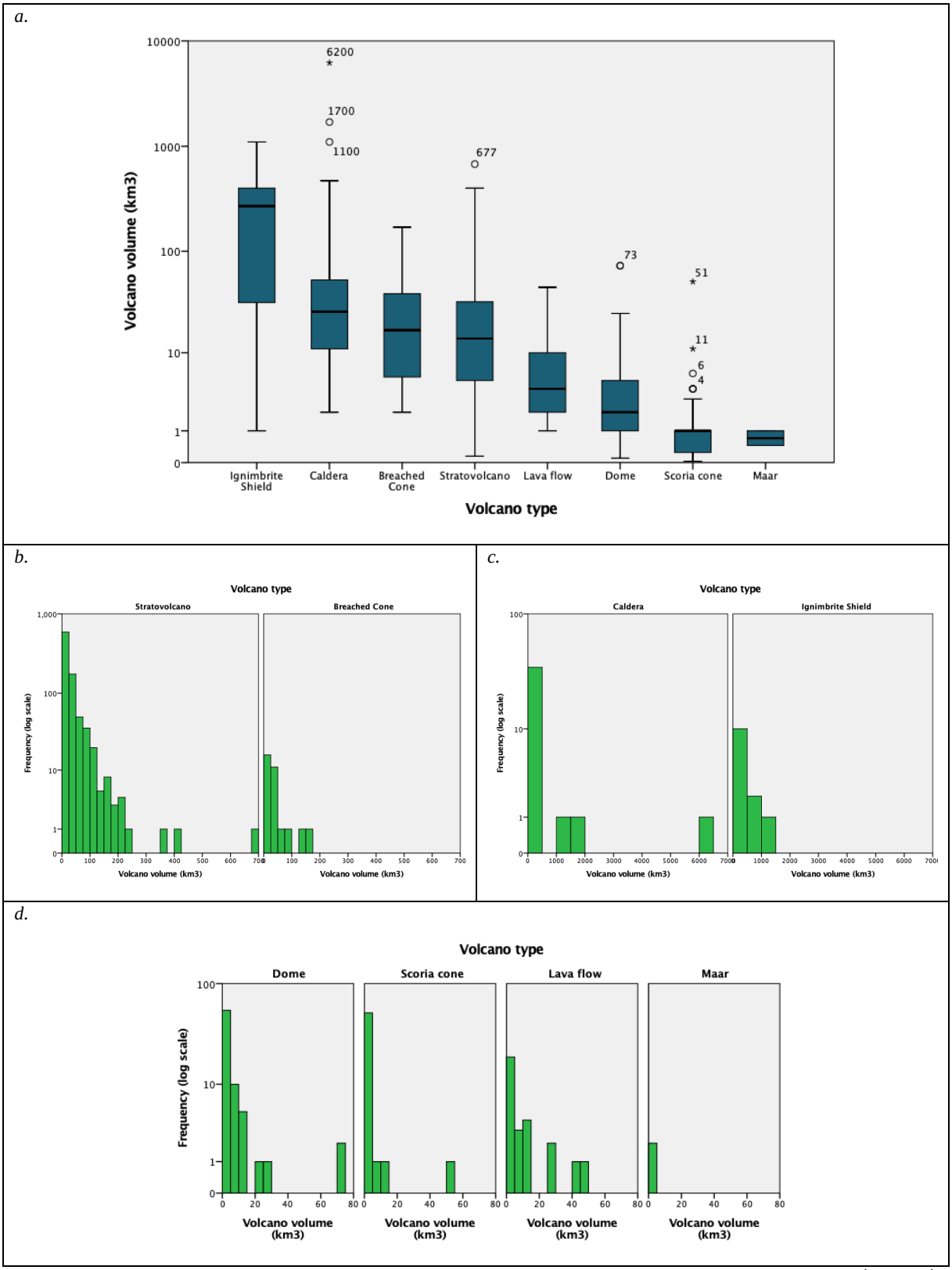


*Figure 3-8. a. Box whisker for Volcano volume classified by Volcano type. Boxes represent the range of the 25$^{th}$ and 75$^{th}$ percentiles with the dividing line being the median. Whiskers represent the minimum and maximum values. Circles outside the boxes represent outliers and asterisks are extreme outliers (values more than three times the height of the boxes. b. c. d. Histograms for Volcano volume classified by Volcano type, note Y axis (Frequency) in log scale and they were plotted in separated charts because of volume scale differences.*

### *3.4.1.5 Crater Diameter (km)*

There are 1162 volcanoes with crater diameter values, with a maximum of 47.5 km and a minimum of 0 km, indicating the edifice has no crater. In this case, I do not consider 0 values for the statistical analysis, which represent around 72% of the total data. Even though it is useful to know that an edifice has no crater, here, I am trying to comprehend crater diameter trends. Table 3-5 show the statistic variation when considering or removing 0 values. The maximum crater diameter value of 47.5 km for La Pacana Caldera is an outlier; this is the same volcanic structure that is the major outlier in Volcano volume parameter.

*Table 3-5. Descriptive statistics for Crater Diameter (km).*

| **Descriptive Statistics: Crater diameter (km)** | |
|---|---|
| | Statistic non-accounting for 0 values |
| Count | 317 |
| Minimum | 0.1 |
| Maximum | 47.5 |
| Mean | 2.99 |
| Standard Error | 0.32 |
| Median | 1 |
| Mode | 0.25 |
| Standard Deviation | 5.70 |
| Kurtosis | 32.49 |
| Skewness | 20.11 |

The statistical analysis shows there are two main populations, the first one with smaller crater values (0-10km) and higher frequencies, respond to the combination of 5 volcano types (Figure 3-9c). The high frequency in smaller diameters is responsible of the high values in skewness.
*Calderas*, *Ignimbrite shields* and *Stratovolcanoes* (Figure 3-9b) belong to the second population, which show bigger crater values and lower frequencies.

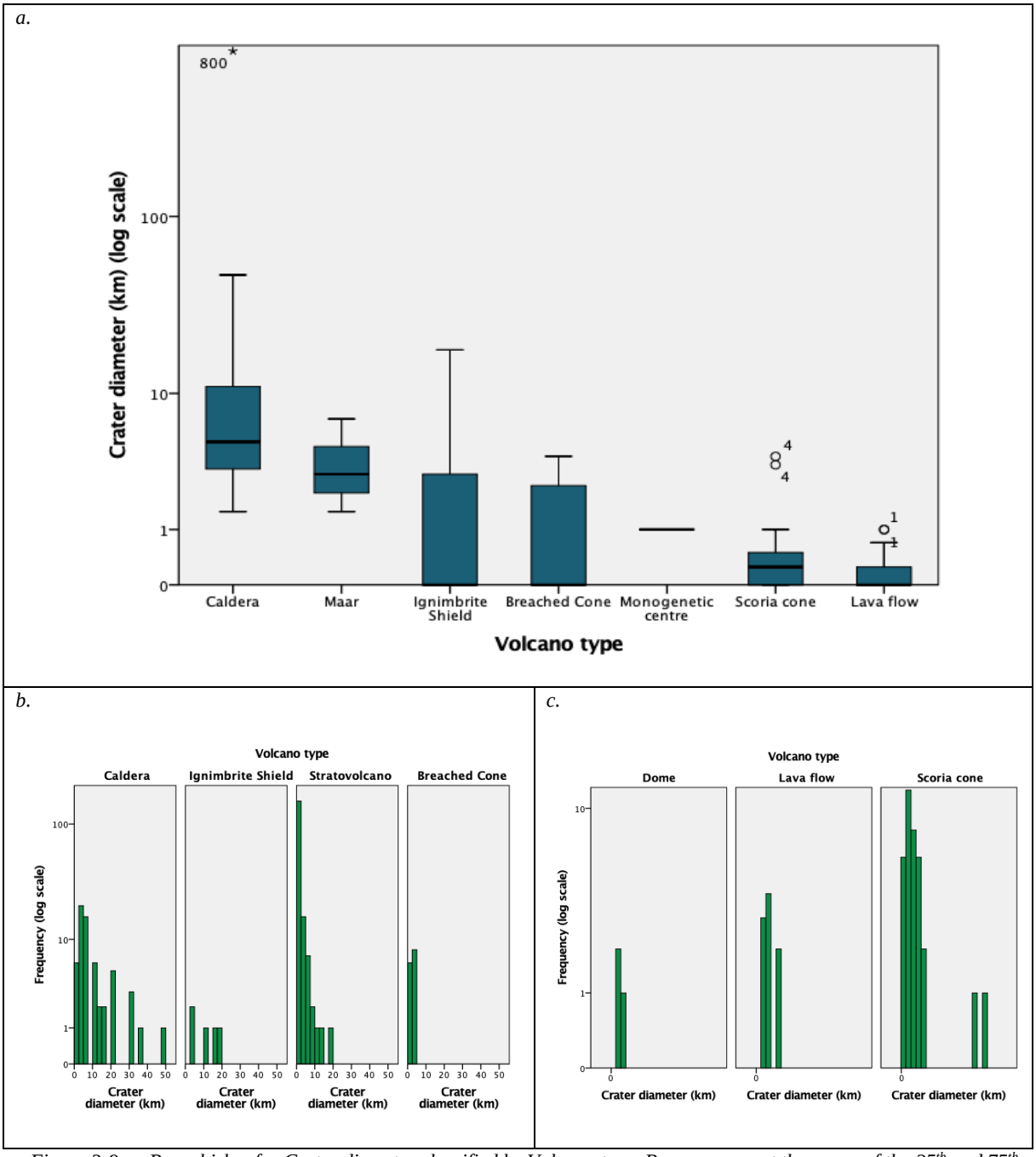


*Figure 3-9. a. Box whisker for Crater diameter classified by Volcano type. Boxes represent the range of the 25th and 75th percentiles with the dividing line being the median. Whiskers represent the minimum and maximum values. Circles outside the boxes represent outliers Note Y axis in log scale. b. c. Histograms for Crater diameter classified by Volcano type, note Y axis (Frequency) in 10 based log scale.*

### *3.4.1.6 Volcano Size*

I classify volcanoes by size (7.1.1.2 Volcanoes parameters) according to Castruccio et al. (2017) proposition. Next, I plot Volcano height against Volcano volume (Figure 3-10a) and Cone diameter (Figure 3-10b) to

explore relationships between these parameters and categorise the scatter plots according to volcano types. Then, I establish the minimum requirements to distinguish larger from small volcanic edifices from Castruccio et al. (2017). And finally, I highlight the name of the volcanoes with the proper characteristics to be considered related to basaltic systems.

In my analysis, *Stratovolcano* is the only volcano type returning large edifices. However, if I want to be strict when using Castruccio et al. (2017) classification, edifices need to have heights over 2000m, cone diameters larger than 24 km and volumes greater than 100km$^3$. Only *Nevado Coropuña* meets these criteria. If I am slightly more flexible on the size classification and consider volcanoes that are close to cone diameter limit (24km), although they comply with minimum heights and volumes. In this case, the edifices number will expand to 6: *Socompa*, *Nevado Chachani*, *Nevado Ampato*, *Nevado Coropuña*, *Llaima* and *Nevado de Sajama*.

Castruccio et al. (2017) modelled arc volcanoes as essentially a pile of lavas losing volume over time and which are erupted from a single point source. Their model can be applied to simple cones with only one source and an uniform and levelled base; however, it unexpectedly fits with many other volcanoes types suggesting that this simple correlation is valid not only for the piling lava flows originated from the same vent, but probably also for different flow types (pyroclastic, density currents, lahars) that also characterise a significant portion of the entire volume of most volcanoes (Castruccio et al., 2017). If that is the case, I could consider the Huaylillas ignimbrite, which is the only ignimbrite deposit that complies with the previous classification.

According to Castruccio et al. (2017), large stratovolcanoes correspond to systems fed by deep overpressured magma chambers that connect with shallower magma storages sporadically during eruptions. Magmatic volatile exsolution, which is one of the essential steps in the formation of porphyry Cu deposit generation, is an inevitable result of the shallow-level crystallization and cooling of hydrous arc magmas (Whitney, 1975; Burnham, 1979; Eichelberger, 1995; Castruccio et al., 2017). However, it is important that the process does not catastrophically vent the volatiles essential for hydrothermal ore formation. Explosive vesiculation and eruption most commonly occur in viscous felsic magmas because gas bubbles cannot separate quickly enough from the melt; thus, Plinian and ignimbrite- forming eruptions are typically generated from high silica dacitic and rhyolitic magmas. While intermediate-composition magmas, such as andesites and lower silica dacites, are able to degas more readily because they tend to ascent more slowly and undergo decompression-induced crystallization, with outgassing of volatiles through magma and the volcanic edifice to vent as fumaroles or to condense into ground water. In this study, Huaylillas ignimbrite is the only ignimbrite deposit to comply with Castruccio requirements of large edifices. Huaylillas ignimbrite is a good example for non-ideal environment for PCD formation, because of the catastrophic release of volatiles into the atmosphere during the eruption.

*a.*

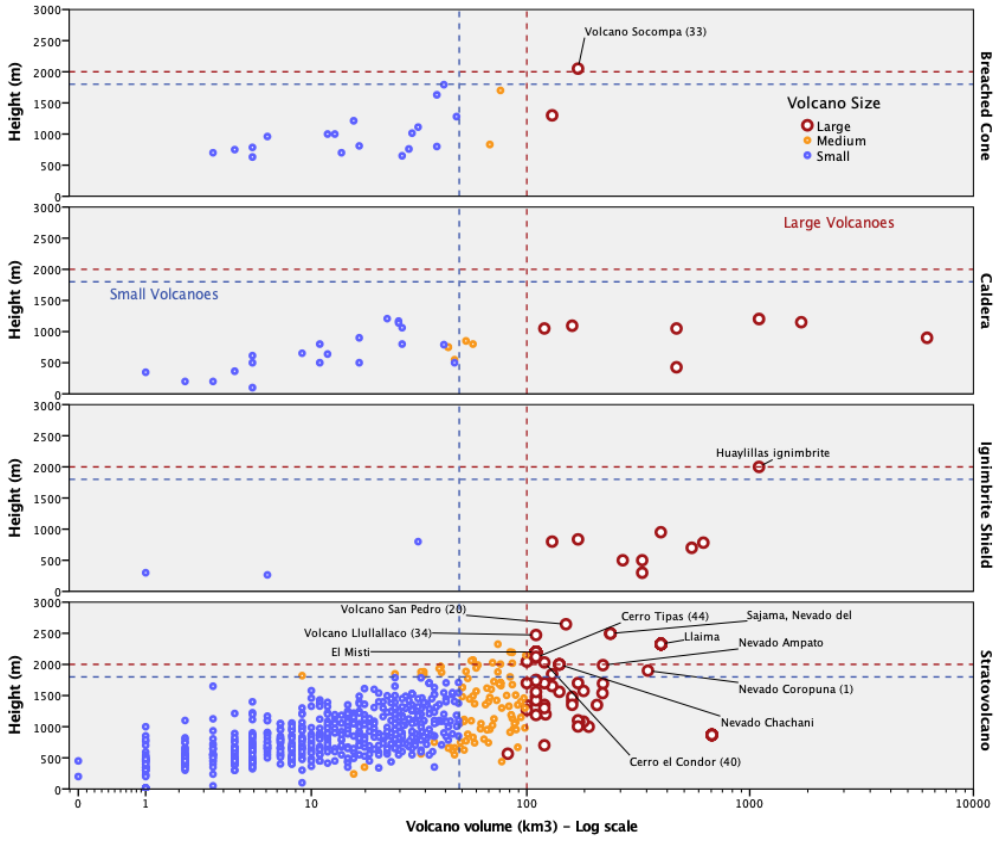
Volcano Socompa (33)
Volcano Size
Large
Medium
Small
Breached Cone
Large Volcanoes
Small Volcanoes
Caldera
Huaylillas ignimbrite
Ignimbrite Shield
Volcano San Pedro (20)
Volcano Llullallaco (34)
El Misti
Cerro Tipas (44)
Sajama, Nevado del
Llaima
Nevado Ampato
Nevado Coropuna (1)
Nevado Chachani
Cerro el Condor (40)
Stratovolcano
Height (m)
Volcano type
Volcano volume (km3) – Log scale

*b.*

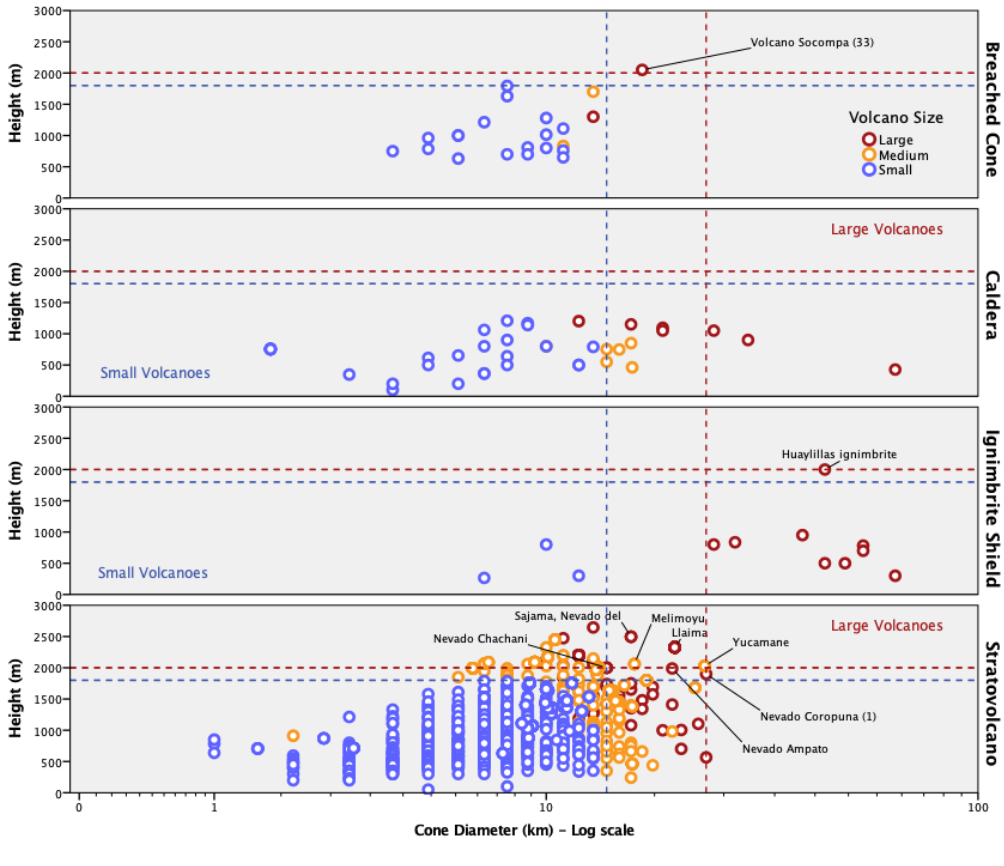
Volcano Socompa (33)
Volcano Size
Large
Medium
Small
Breached Cone
Large Volcanoes
Small Volcanoes
Caldera
Huaylillas ignimbrite
Ignimbrite Shield
Sajama, Nevado del
Melimoyu
Llaima
Yucamane
Nevado Chachani
Nevado Coropuna (1)
Nevado Ampato
Stratovolcano
Height (m)
Volcano type
Cone Diameter (km) – Log scale

*Figure 3-10. Scatter plots showing differences in volcano types for Edifice height (m) against a. Volcano volume (log scale) and b. Cone diameter (log scale). Markers are coloured by volcano size. Vertical lines represent the limit to be considered a large volcanic edifice in terms of Volume limit (50 and 100km$^3$) and Cone diameter (14 and 24km), and horizontal ones show Height limits (1800 and 2000m).*

### *3.4.1.7 Volcano parameters correlations*

To assess how volcano parameters, relate and influence each other I calculate a correlation matrix and do a stepwise multiple linear regression analysis using *SPSS statistics* (IBM) software. For this analysis, I am particularly interested in *Edifice height*, and I have chosen this parameter as the dependent variable and *Volcano volume*, *Cone* and *Crater diameter* as the independent ones ( Equation *3-3*). The nature of the method required that the analysis was restricted to the set of 1115 volcanoes, because valid values for all four of these variables need to exist.

Before starting the analysis, I remove extreme outliers, which are calculated in Equation 3-2. There are no extreme lower outliers for any of the volcano parameters and no extreme upper outliers at all for volcano height. Table 3-6 shows for each variable, which is the value to be considered an outlier. After extracting outliers, 1058 records remain. Those are the records that will be used in the multiple correlation matrix. Table 3-7 presents the mean and standard deviation for each variable and number of samples used for the correlation analysis.

*Table 3-6. Percentiles and the minimum value to be an upper outlier for the Volcano parameters considered for the multiple correlation analysis.*

**Percentiles and outliers for volcano parameters**

| | Maximum value | Percentiles | | | Minimum value to be considered as an extreme upper outlier |
|---|---|---|---|---|---|
| | | 25 | 50 | 75 | |
| **Volcano height (m)** | 2645 | 450 | 712 | 1077 | 2958* |
| **Volcano Volume (km$^3$)** | 6200 | 4 | 11 | 29 | 104 |
| **Cone Diameter (km)** | 65 | 4 | 7 | 9 | 24 |
| **Crater Diameter (km)** | 47.5 | 0.25 | 0.75 | 2.00 | 7.25 |

* The maximum value for volcano height is inferior to the value to be considered an outlier.

*Table 3-7. Descriptive statistics for the Volcano parameters values considered for the multiple correlation analysis.*

**Descriptive Statistics for volcano parameters**

| | Mean | Std. Deviation | Number or records |
|---|---|---|---|
| **Volcano height (m)** | 771 | 433 | 1058 |
| **Volcano Volume (km3)** | 17.8 | 20.6 | 1058 |
| **Cone Diameter (km)** | 6.82 | 3.35 | 1058 |
| **Crater Diameter (km)** | 0.28 | 0.85 | 1058 |

Table 3-8 and Figure 3-11 show a multiple correlation matrix that interrelates the dependent variable (*Volcano height*) against the independent ones. On the one hand, volcanic edifice height is correlated with volcano volume (yellow box) and in decreasing order, with cone diameter. However, it shows a negative

correlation with crater diameter (orange box). On the other hand, volcano volume is highly correlated with cone diameter.

*Table 3-8. Correlation matrix showing the relationship between variables.*

**Multiple correlations for volcano parameters**

| | | Volcano height (m) | Volcano Volume ($km^3$) | Cone Diameter (km) | Crater Diameter (km) |
|---|---|---|---|---|---|
| **Pearson Correlation** | **Volcano height (m)** | 1 | 0.65 | 0.49 | -.027 |
| | **Volcano Volume (km3)** | 0.65 | 1 | 0.78 | 0.03 |
| | **Cone Diameter (km)** | 0.49 | 0.78 | 1 | 0.07 |
| | **Crater Diameter (km)** | -.027 | 0.03 | 0.07 | 1 |

** The first column relates Volcano height (m), the dependent variable, with the other independent variables. The following columns correlate the independent variables between them.*

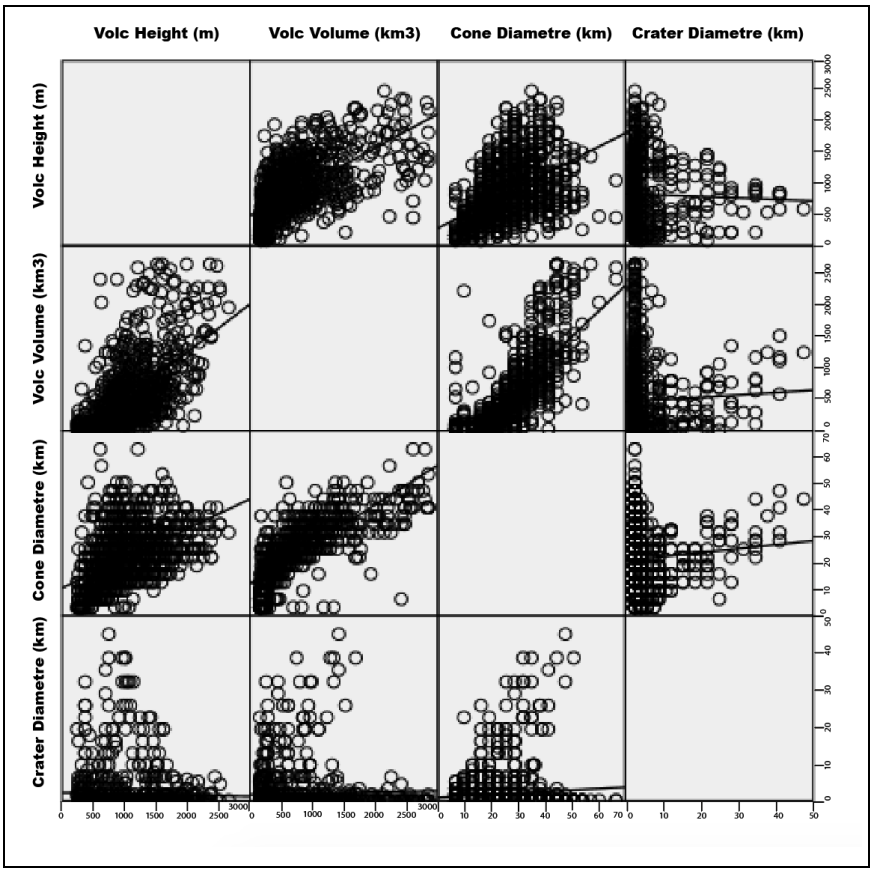


*Figure 3-11. Correlation matrix showing Height(m) as the dependent variable, against Volcano volume($km^3$), Crater (km) and Cone diameter (km) for the valid 1058 records in the AVEDB. Black lines are linear regression lines that fit the whole population (all volcano types included).*

At this stage in the analysis, it becomes crucial to reconcile volcanic edifice dimensions with the type of edifice, since interpretations could change depending on the volcano type. The strongest positive correlation

between height and volcano volume derives from Stratovolcanoes (Figure 3-12a), although the tendency can be documented in other volcano types as well, such as calderas and domes (Figure 3-12b). The same occurs for cone diameter. However, volcano height and crater diameter are inversely related. There are two reasons for this tendency. Firstly, more than 80% of the volcanoes in the database do not have a crater, meaning that a 0km value was assigned for these records. Therefore, crater diameter is a parameter that is biased to low values. Secondly, Calderas and Ignimbrite shields are responsible for increasing the inverse correlation values (Figure 3-12b). There is also a strong positive correlation between volcano volume and cone diameter, with the trend dominated by stratovolcanoes and calderas.

*a.*

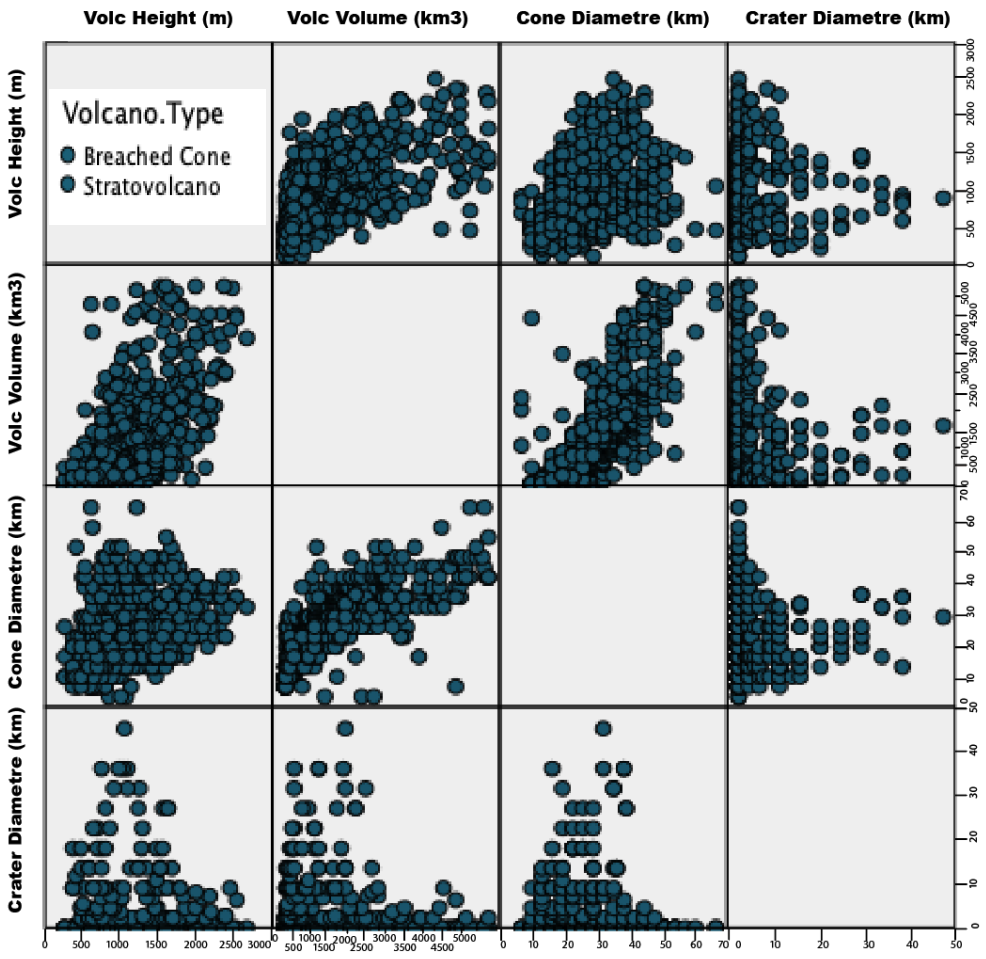


*b.*

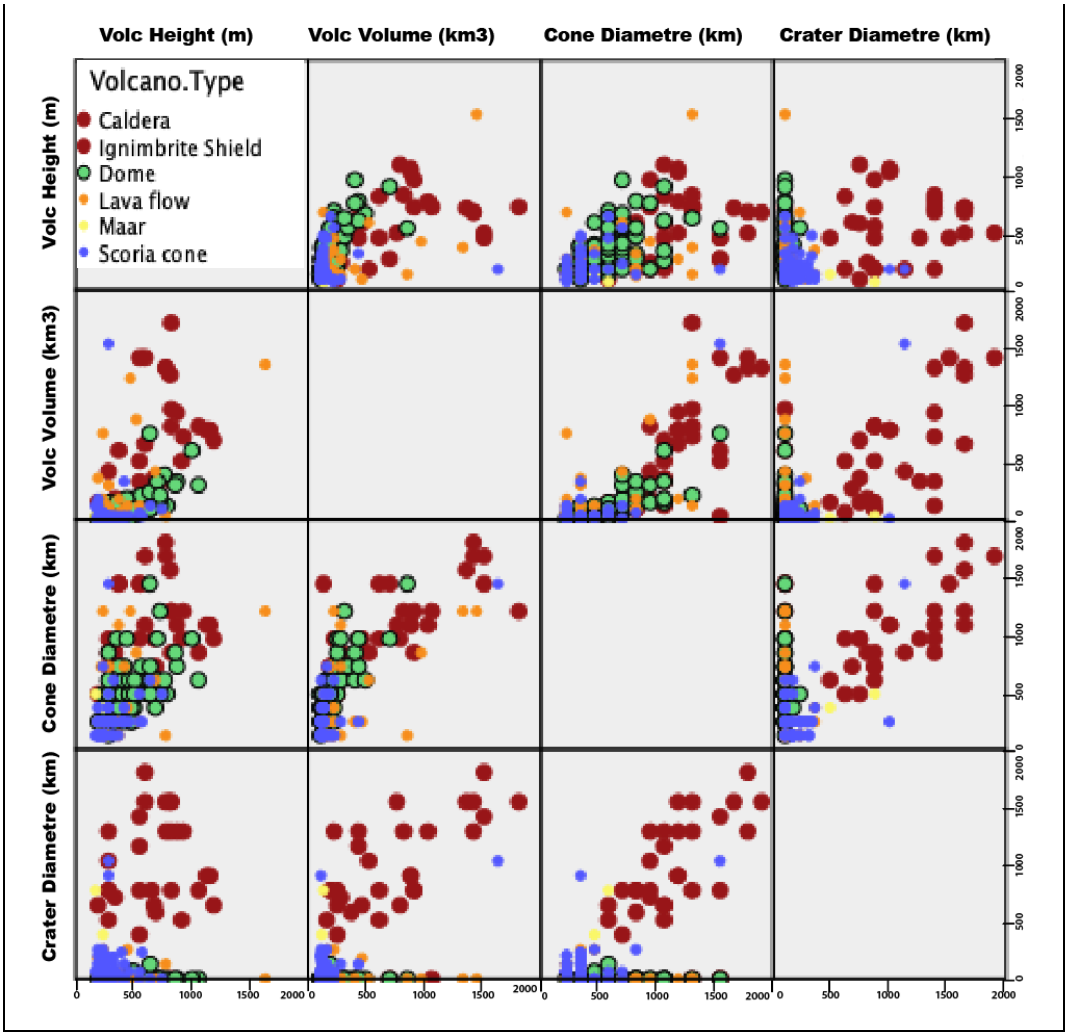


*Figure 3-12. a. Correlation matrix showing Height(m) as the dependent variable, against Volcano volume (km$^3$), Crater (km) and Cone diameter(km). Coloured markers stand for different volcano types and the line represents a linear regression line for the whole population. a. shows stratovolcanoes and breached cones, which have been plotted together because they show the same trend and are part of the same volcanic system. b. Same as plot a, but grouped for the rest of the volcano types and its deposits.*

Table 3-9 compares the results of three correlations models, which includes the independent variables one by one as soon as the analysis progresses (Model 1 to Model 3). The coefficient of correlation *R* is the degree of relationship between dependent and independent variables, it may vary between -1 and 1, indicating compared variables are perfect opposites or that the two variables are moving in unison respectively. A value close or equal to 0 would mean no correlation whatsoever. Here, I can see that because edifice height is related to cone diameter, I get a good, although not perfect, correlation and it will not change significantly when adding the rest of the variables.

R-squared measures how strong the relationship between the correlation model and the dependent variable is, in a 0 – 100% scale. Correlation models in Table 3-9 show that the biggest correlation between volcano height and the independent variables occurs with volcano volume. Also, around 42.8% of volcano height variation ($R^2$ for Model 1) can be accounted for the volume of the volcano. Only 0.3% variation can be

explained by crater ($R^2$ for Model 2) and another 0.01% ($R^2$ for Model 3) by cone diameter. In summary, crater and cone diameters could have been left out of the models, since they do not significantly affect the prediction of volcano height.

Cone diameter is highly correlated to volcano volume, as shown in Table 3-8, which indicates correlation between the independent variables: cone diameter is a function of volcano volume. This means that there are signs of collinearity here, and if I decide to be more rigorous in the analysis and adjust the settings in SPSS, cone diameter will be removed from the model. I decided to show the results with 3-independ variables, Model 3, because there are no significant differences showing only 2 models and also allowed me to explain the collinearity issue.

*Table 3-9. Multiple correlation models with the volcano height (m) as the dependent variable, where each model will progressively include an independent variable.*

**Correlation summary models for volcano height as the dependent variable**

| Model | R | $R^2$ |
|---|---|---|
| 1 | 0.655 | .428 |
| 2 | .0657 | .431 |
| 3 | .0657 | .432 |

Model 1. Predictors: Volcano Volume ($km^3$); Model 2: Predictors: Volcano Volume ($km^3$) and Crater diameter (km); Model 3. Predictors: Volcano Volume ($km^3$), Crater diameter (km) and Cone diameter (km);

Table 3-10 quantifies the relation between variables, showing the linear regression equation coefficients (Equation 3-3) for the dependent variables. The linear regression equation is expressed as follows:

**Volcano height (m) = a + b * Independent variable + error**

The names for the equation coefficients are firstly, ***a***, which is the intercept with Y axis equivalent in the equation. This is an important value, since it establishes the minimum edifice height necessary so the correlation with the independent variables exists. Secondly, ***b***, which stands for the *95.0% Confidence Interval*. It represents the confidence within the model when calculating the interception with Y axis (***a***). This means the model could predict, with 95% confidence, the minimum height a volcano will be between 506 m and 560 m in order to find correlation with the independent variables. Next, I focus in the *Standardized beta coefficients*, which help us to understand the impact the independent variables have as a predictor of the dependent variable. It varies between -1 and 1, indicating that variables are perfect opposites (-1), or that variables present a perfect positive correlation (1). In Model 2, the *Standardized beta coefficient* is statically significant only for Volcano volume. On the contrary, Crater diameter shows a weak negative correlation with Height. In practical terms, it means that the higher the volcano edifice is, the bigger the volcano volume will tend to be, although Crater diameter would tend to be smaller in case of an eruption.

Beside the linear regression equation coefficients, in Table 3-10, it is most relevant to look at *Sig* values. ***Sig*** stands for the *correlation coefficient*, also known as *p-value*. It determines whether a correlation between variables exists and if it is significant. The correlation coefficient *Sig* needs to be smaller than 0.05 in order to be considered statically significant. A value of .000 means the figure is too small for three decimal place representation. For this analysis, Volcano volume and Crater Diameter are the only parameters that shows a significant correlation with height (Sig<0.05; Table 3-10). For this reason, I decide that Model 2 it is the most appropriate to use (green boxes). While Model 3 showed signs of no statistical significance (orange box), which I already knew from Table 3-9.

*Table 3-10. Multiple correlation models, where each model will progressively include an independent variable.*

| **Volcano height (m) = a + b * Independent variable + Std. error** | | | | | | | |
|---|---|---|---|---|---|---|---|
| Model | | Unstandardized coefficients | | Standardized Coefficients | Sig. | 95.0% Confidence Interval **b** | |
| | | **a** | Std. Error | | | Lower Bound | Upper Bound |
| 1 | Volcano volume ($km^3$) | 526 | 13.3 | | .000 | 500 | 552 |
| 2 | Volcano volume ($km^3$) | 533 | 0.4 | 0.656 | .000 | 506 | 560 |
| | Crater diameter (km) | | 11.7 | -0.052 | .027 | | |
| 3 | Volcano volume ($km^3$) | 559 | 0.7 | 0.692 | .000 | 508 | 610 |
| | Crater diameter (km) | | 11 | -0.049 | .034 | | |
| | Cone diameter (km) | | 4.8 | -0.045 | .238 | | |

**a.** Intersection with Y axis; **b.** 95.0% Confidence Interval; **Sig.** Correlation coefficient.

## 3.5 Results for Volcanism

### 3.5.1 Descriptive analysis for eruption parameters

Descriptive statistics for eruption parameters can be seen in Table 3-11. While *Deposit diameter*, *Bulk DRE volume* and *Flow length* account for the highest number of values, between 1200 to 1500, the rest of the parameters sum less than 200.

*Table 3-11. Descriptive statistics for eruption parameters.*

| Descriptive Statistics: Eruption parameters | | | | | | |
|---|---|---|---|---|---|---|
| | Deposit Diameter (km) | Magnitude | Bulk Volume ($km^3$) | Bulk DRE Volume ($km^3$) | Flow Length (km) | Deposit Area ($km^2$) |
| Count | 1272 | 188 | 197 | 1304 | 1471 | 169 |
| Minimum | 1 | 3.70 | 0 | 0 | 0 | 0.02 |
| Maximum | 213* | 8.20** | 801** | 630** | 95*** | 5200**** |
| Mean | 11.65 | 5.03 | 18.04 | 1.24 | 4.59 | 244.97 |
| Standard Error | 0.46 | 0.06 | 5.41 | 0.53 | 0.18 | 48.76 |
| Median | 9 | 4.95 | 1 | 0 | 0 | 129.90 |
| Mode | 9 | 4.80 | 0 | 0 | 0 | 213 |
| Standard Deviation | 16.47 | 0.78 | 75.98 | 19.08 | 6.94 | 633.82 |
| Kurtosis | 121.68 | 1.51 | 65.23 | 912.73 | 19.58 | 45.87 |
| Skewness | 10.35 | 0.84 | 7.46 | 28.52 | 2.52 | 6.47 |

** Payun Matru caldera; ** Cerro Galán caldera; *** Planchón - Peteroa stratovolcano; **** Nevado del Ruiz stratovolcano.*

Minimum and maximum records show that the value variability is immense. There are two calderas in Argentina responsible for the highest values of Bulk, Bulk DRE volumes and Magnitude and the biggest deposit diameter, called *Cerro Galán* (** Table 3-11) and *Payun Matru* (* Table 3-11) respectively.

*Planchón - Peteroa*, is a stratovolcano also located in Argentina, with a flow length of 95km (*** Table 3-11). Finally, *Nevado del Ruiz* in Colombia, a stratovolcano with the biggest deposit area within this dataset (**** Table 3-11).

Mean and median, in general, show no appreciable differences, except for Bulk volume and Deposit area, the reason for this are extreme positive outliers. The same tendency that can also be seen in the std deviation. Histograms are shown in Figure 3-13. Normal distribution curves have similar characteristics for Deposit diameter, Bulk volume, Bulk DRE Volume, Flow length and Deposit area, showing unimodal, asymmetrical, positively skewed, leptokurtic curves. The main difference between them is that Deposit Diameter and Flow length display higher frequency for lower values. Oppositely, Magnitude distribution is the one more similar to a normal distribution, slightly skewed to higher eruption magnitudes.

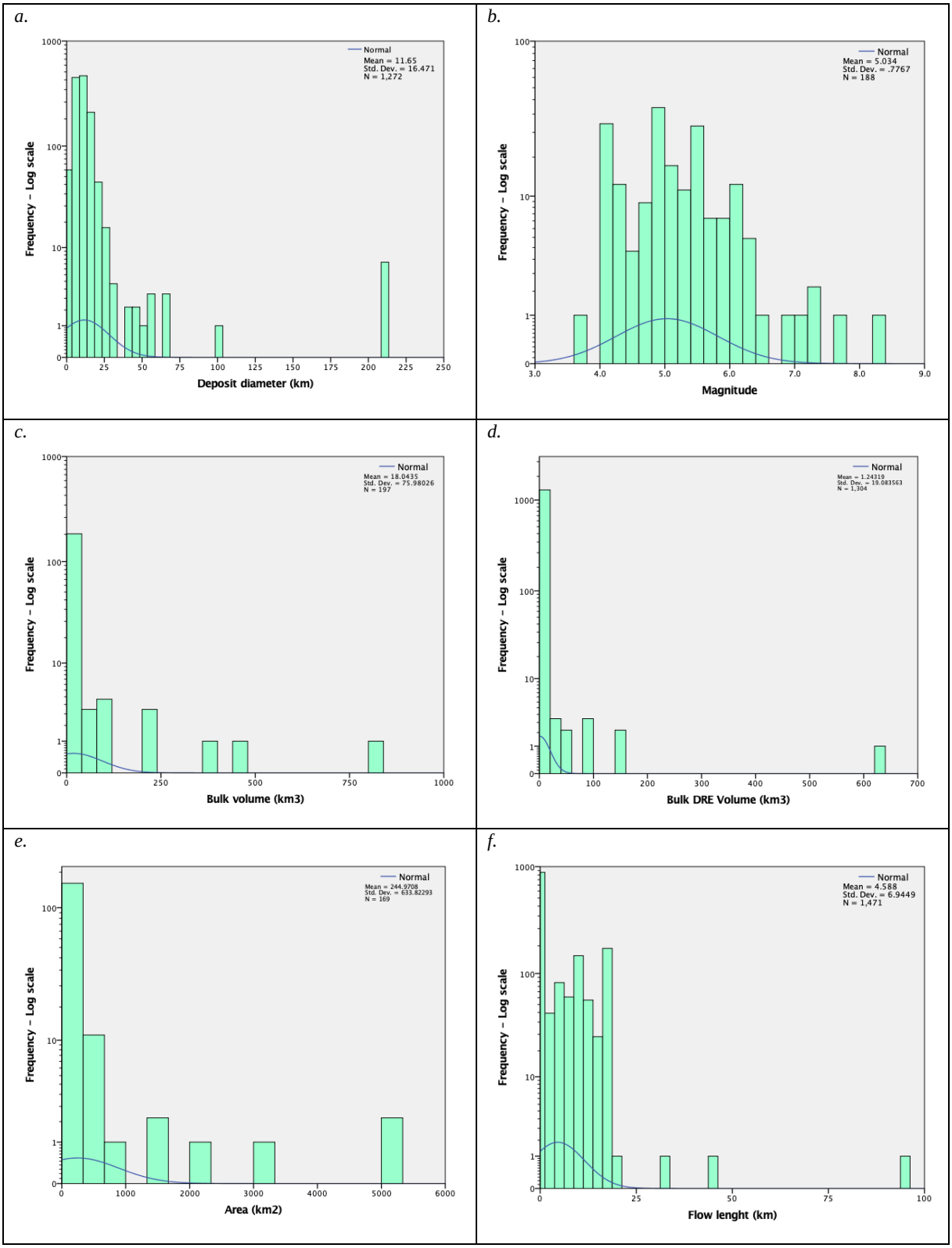


*Figure 3-13. a. Frequency distribution for Eruption parameters, showing histograms (note Frequencies in Log scale) and bell curves. a and f. histograms showing high frequencies in low values and unimodal, asymmetrical and strongly positively skewed bell curves for Deposit diameter and Flow length. b. Magnitude histogram and bell curve, showing a normal distribution. c, d and e. Unimodal, asymmetrical and strongly positively skewed bell curves and histograms for Bulk volume, Bulk DRE volume and Deposit area.*

Figure 3-14 presents Eruption parameters classified by volcano type. *Calderas* and its deposit (*Ignimbrite shields*) exhibit the biggest deposit diameters and areas, eruption magnitudes and bulk volumes, whereas *Stratovolcanoes* lead flow lengths values. In terms of magnitude, unfortunately the box whisker plot seems not to be very conclusive.

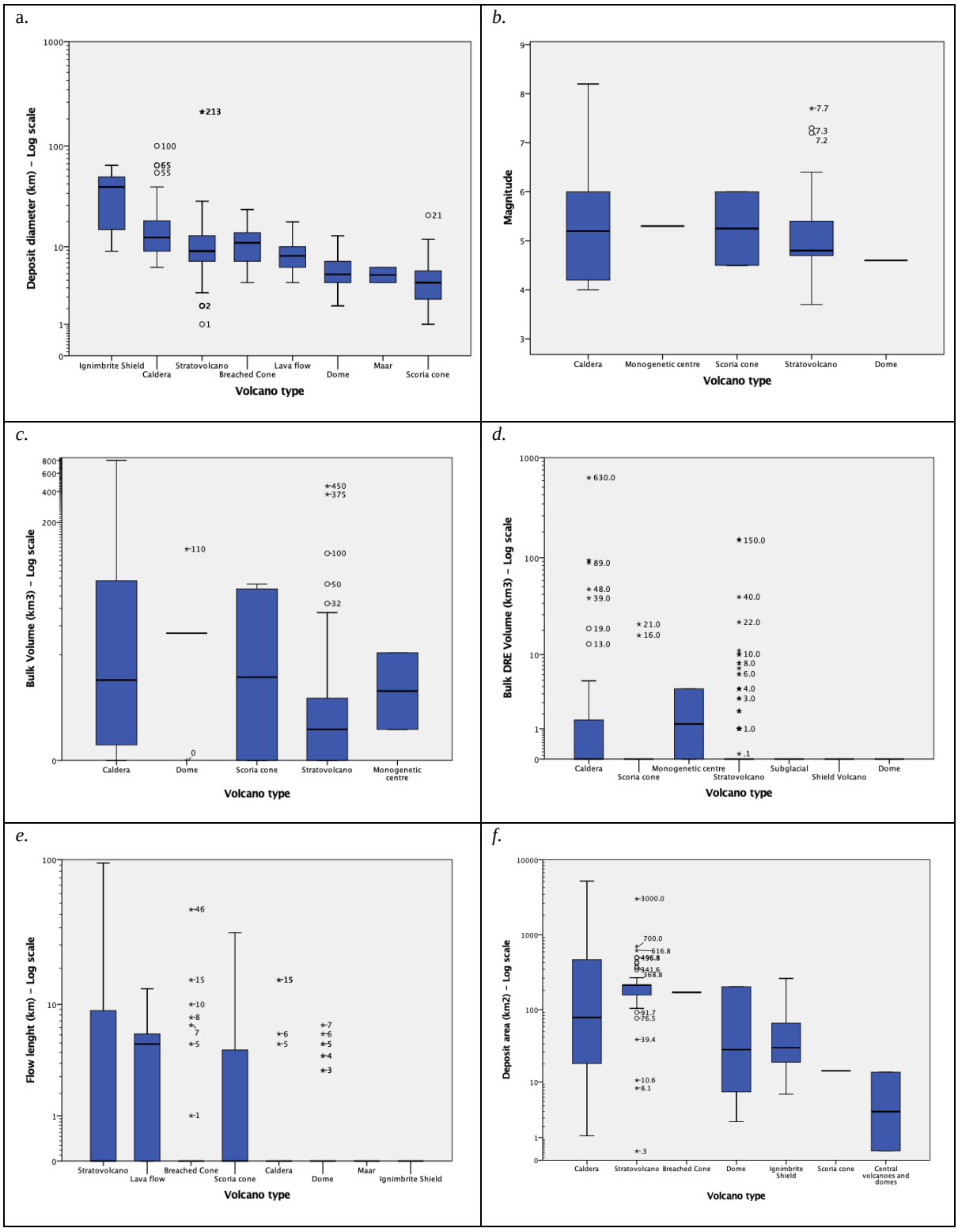

*Figure 3-14. Box whisker for Eruption parameters classified by Volcano type. Boxes represent the range of the 25$^{th}$ and 75$^{th}$ percentiles with the dividing line being the median. Whiskers represent the minimum and maximum values. Circles outside the boxes represent outliers and asterisks are extreme outliers (values more than three times the height of the boxes). Note Y axis (Frequency) in log scale.*

## 3.6 Results for Tectonics and Morphotectonic provinces

For all tectonic environments and morphotectonic provinces, *Stratovolcanoes* (and *Breached cones*) lead the whole AVEDB distribution, accounting for almost 50% of the records, followed by *Domes* (14%). In this section of the study, I use mainly histograms in order to see the frequency distribution of the data and compare between the subcategories. Secondly, I use box whisker plots presenting the data by decreasing values.

### 3.6.1 Descriptive analysis for Tectonic parameters

I use Tectonic parameters established in Chapter 02: Database creation and basic analysis, to study the frequency distribution of different volcano types in different location of the Andes.

#### *3.6.1.1 Crust thickness*

For this category, the same trend remains for all volcano types, with *Stratovolcanoes (*and *Breached cones)* leading distributions. The main distinction is considerable higher frequencies for volcanic edifices placed in continental crust over 25 km thick (Figure 3-15a).

#### *3.6.1.2 Volcanic zone*

Central Volcanic zone (CVZ) has the highest edifice frequencies, where again with *Stratovolcanoes* lead the numbers. A small change respect the previous plots is that *Pyroclastic deposits* are slightly more abundant than *Domes* for the area. Another interesting fact is that despite having *Calderas* in all regions, *Ignimbrite shields* can only be found in the CVZ and Peruvian flat slab region (Figure 3-15b).

*a.*

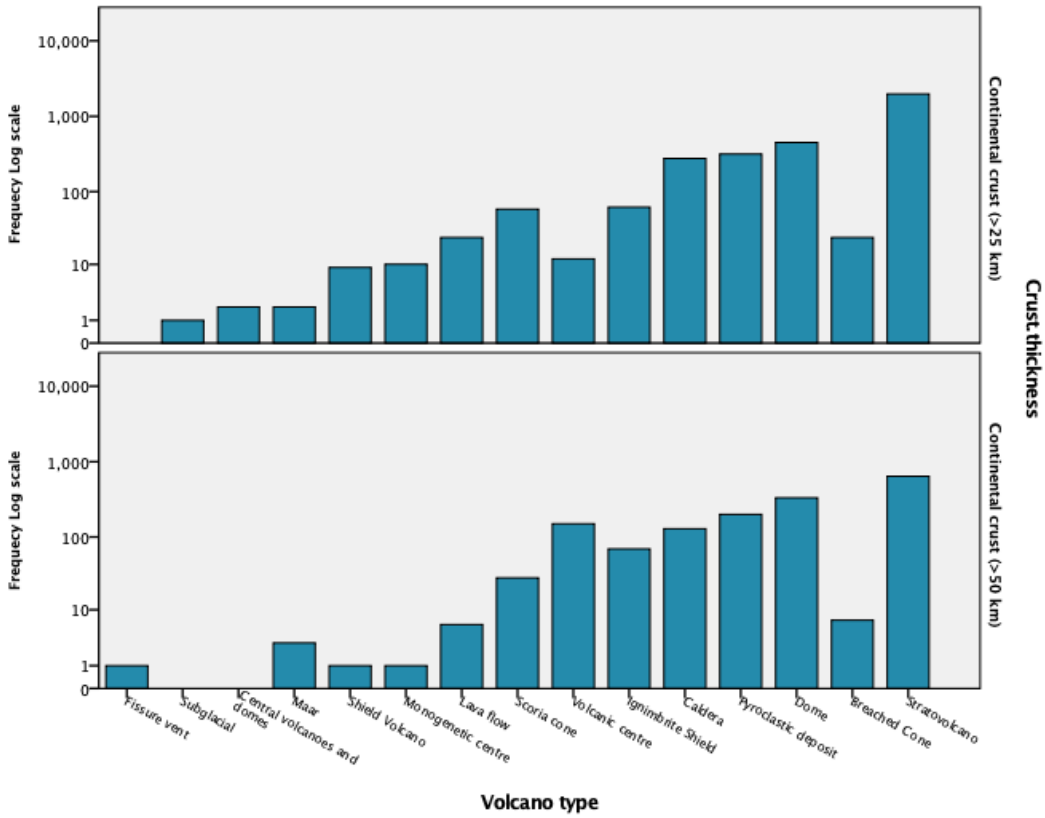
Frequecy Log scale
10,000
1,000
100
10
1
0
Continental crust (>25 km)
Continental crust (>50 km)
Crust thickness
Fissure vent
Subglacial
Central volcanoes and domes
Maar
Shield Volcano
Monogenetic centre
Lava flow
Scoria cone
Volcanic centre
Ignimbrite Shield
Caldera
Pyroclastic deposit
Dome
Breached Cone
Stratovolcano
Volcano type

*b.*

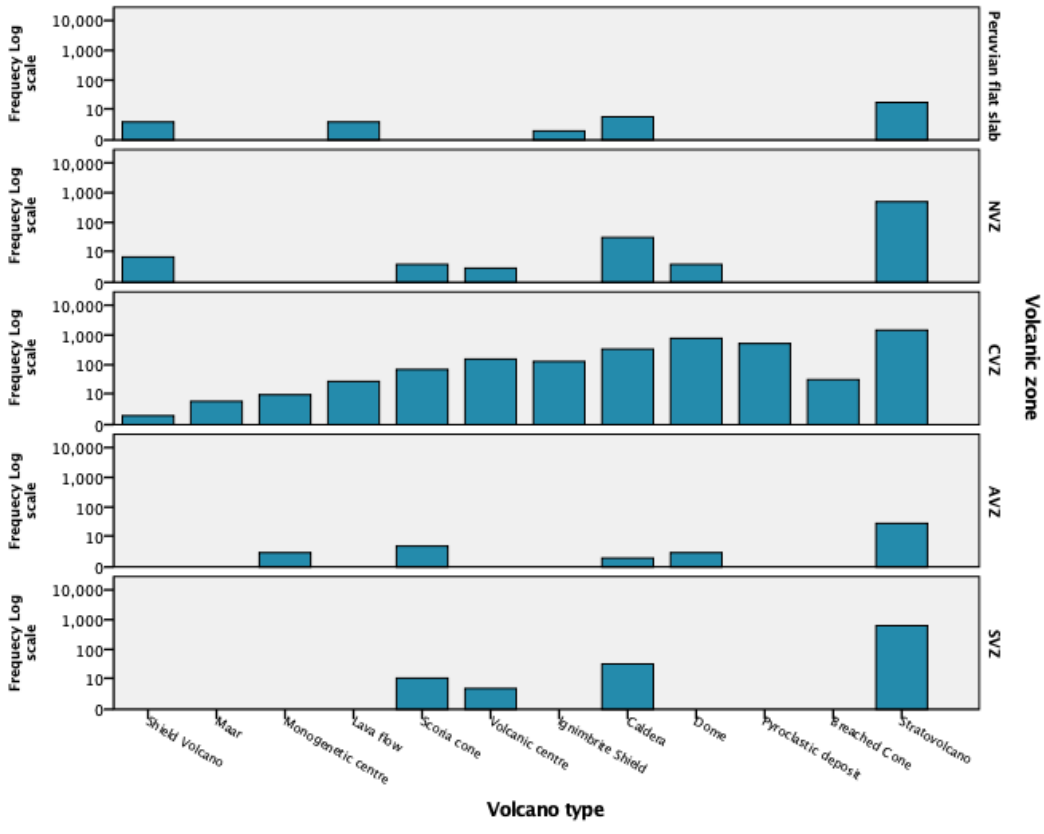
Frequecy Log scale
10,000
1,000
100
10
0
Peruvian flat slab
NVZ
CVZ
AVZ
SVZ
Volcanic zone
Shield Volcano
Maar
Monogenetic centre
Lava flow
Scoria cone
Volcanic centre
Ignimbrite Shield
Caldera
Dome
Pyroclastic deposit
Breached Cone
Stratovolcano
Volcano type

*Figure 3-15. Histograms of volcanic edifices classified by a. Location within areas with differential continental crust thickness. b. Volcanic zones in the Andes. Note Frequency in log scale.*

### *3.6.1.3 Tectonic margins*

*Stratovolcanoes* are the more abundant volcano type in all tectonic environments of the Andes, followed by *Domes*, *Pyroclastic deposits*, *Calderas* and its deposits *(Ignimbrite shield*). As expected, the area classified as *Volcanic arc*, yields the highest number of records, associated with *Retroarc* and *Intra-arc basins.*

If I now consider less abundant types of volcanoes, *Shield volcanoes* are only present in *Volcanic arc* provinces and *Foreland basin. Maars* and *Monogenetic cones* are located in *Volcanic arc* provinces and *Foreland and Retroarc basin*, the latter also can be found in *Accretionary prisms. Scoria cones* on the other hand are in all tectonic environments except for *Rifts* (Figure 3-16).

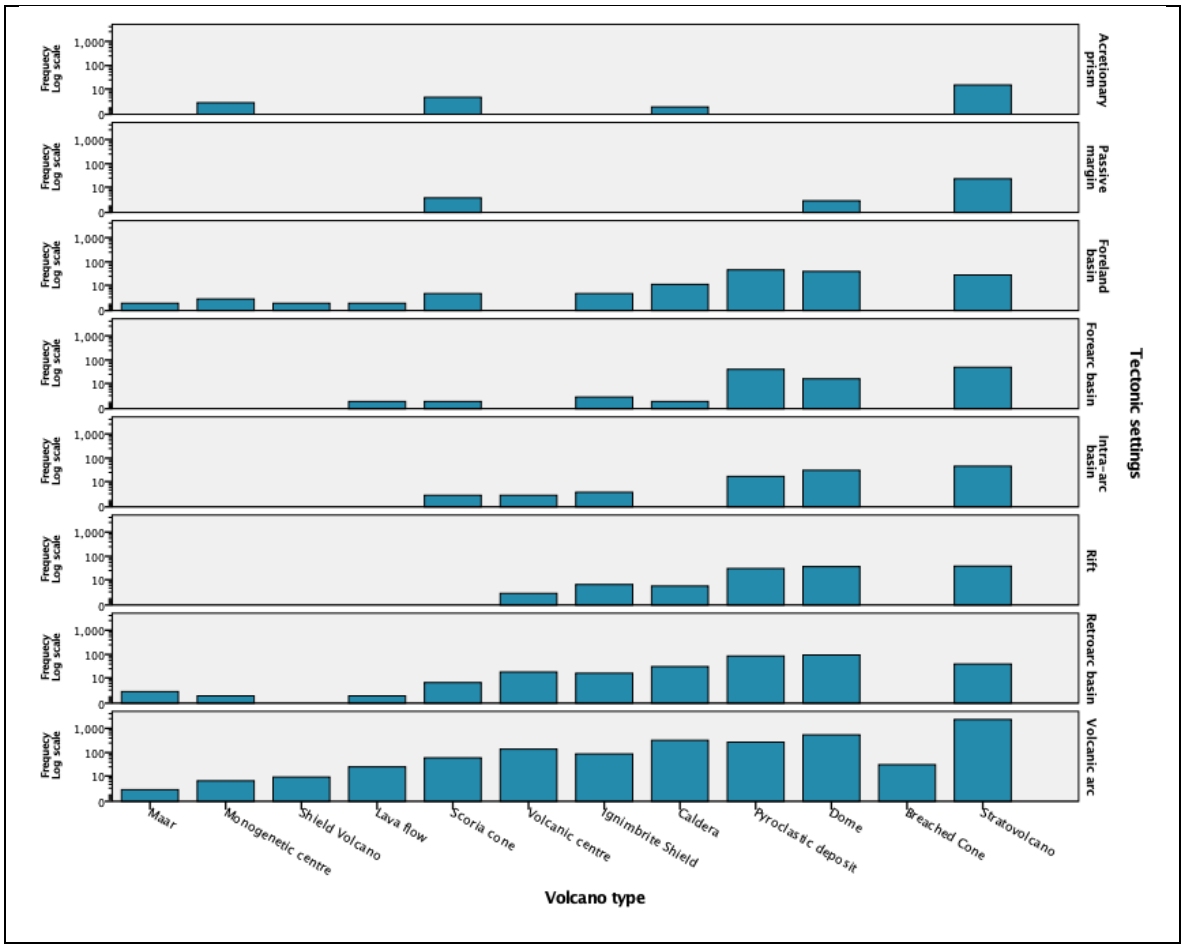


*Figure 3-16. Bar plots of volcanic edifices classified by location within different tectonic settings in the Andes. Note Frequency (y left axis) in log scale.*

## 3.6.2 Morphotectonic provinces

### *3.6.2.1 Geomorphology*

Figure 3-17 shows that the highest numbers of volcanic edifices are in Central Cordillera followed by Eastern Cordillera, conversely to the Intermediate Depression and Western Patagonia Cordillera. Again, Stratovolcanoes and Domes are the larger edifice populations present in all different geomorphological settings. Comparably, Pyroclastic deposits and Calderas are present in most of the Andes's regions, except for Western Patagonia Cordillera and Intermediate Depression respectively. Precordillera and Central Depression are regions that yield similar edifices frequencies and distributions, with two main differences, Volcanic centres are not be found in the Precordillera and in addition, Ignimbrite shields are present in larger numbers.

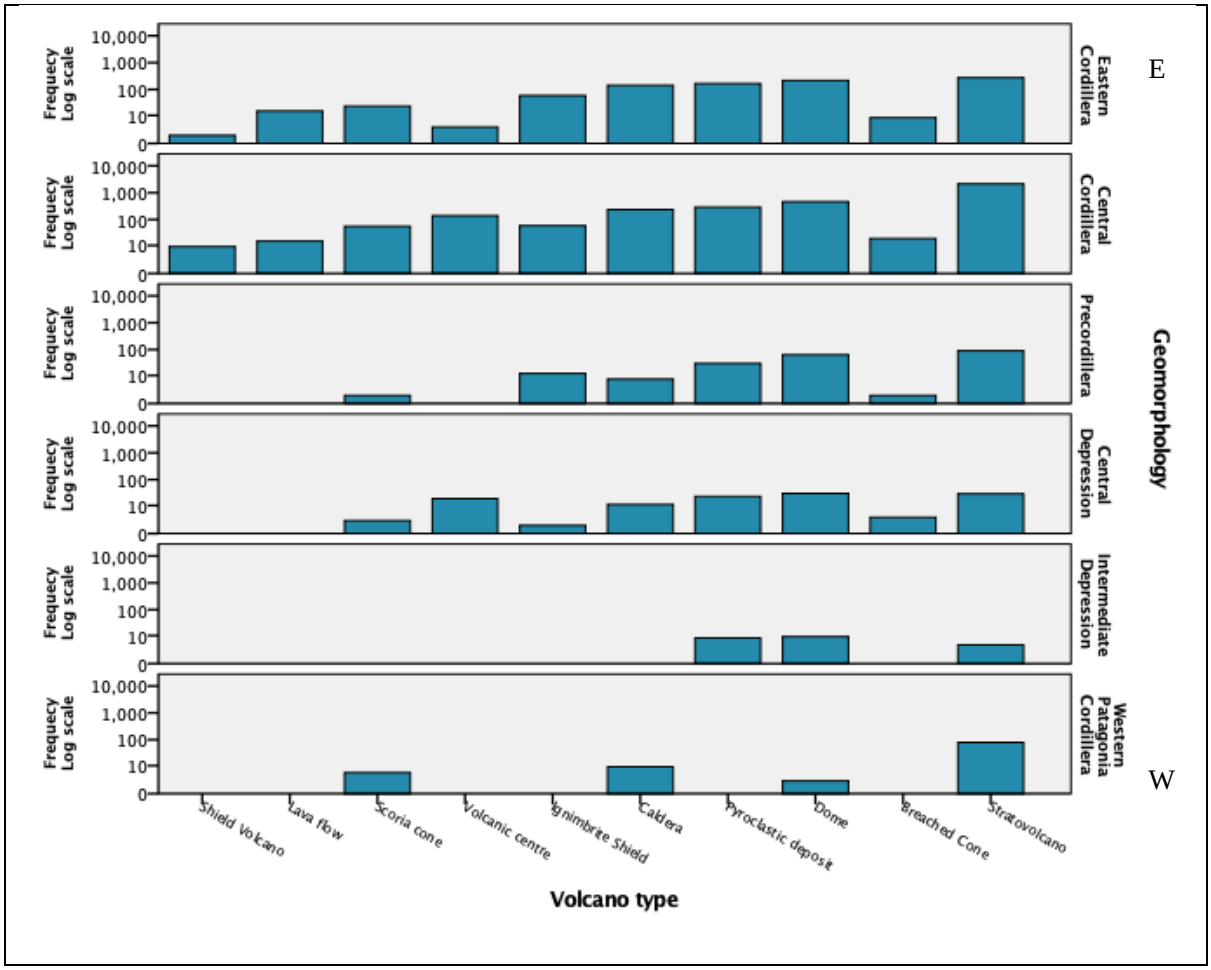


*Figure 3-17. Bar plots of volcanic edifices classified by location within different morphotectonic provinces in the Andes. Note Frequency (y left axis) in log scale.*

### *3.6.2.2 Denudation Rate*

Denudation rates impact the conservation of volcanic edifices: the frequency of volcanic cones drops dramatically in areas with high denudation rates (Figure 3-18). In this study, denudation rates were extracted

from Karátson et al. (2010) and because erosion rates have not changed much since the Miocene, they are considered to be modern rates. Where denudation rates are 66- 112 m/Ma, the few edifices that remain are *Stratovolcanoes. Breached volcanoes*, which represent the remnant edifices of stratovolcanoes after explosive eruption or collapse, are not found in areas with denudation rates >20 m/Ma. The frequencies of other volcano types decrease more gradually with increasing denudation rate.

The areas with the lowest denudation rates (0-10 m/Ma), along the coast in Northern Chile and Southern Peru, are anomalous: they have low cone numbers. This is because this region represents one of the oldest arcs in the Andes (**Error! Reference source not found.**a), the Cretaceous volcanic arc, and there has been enough time to erode away the edifices despite the low denudation rates.

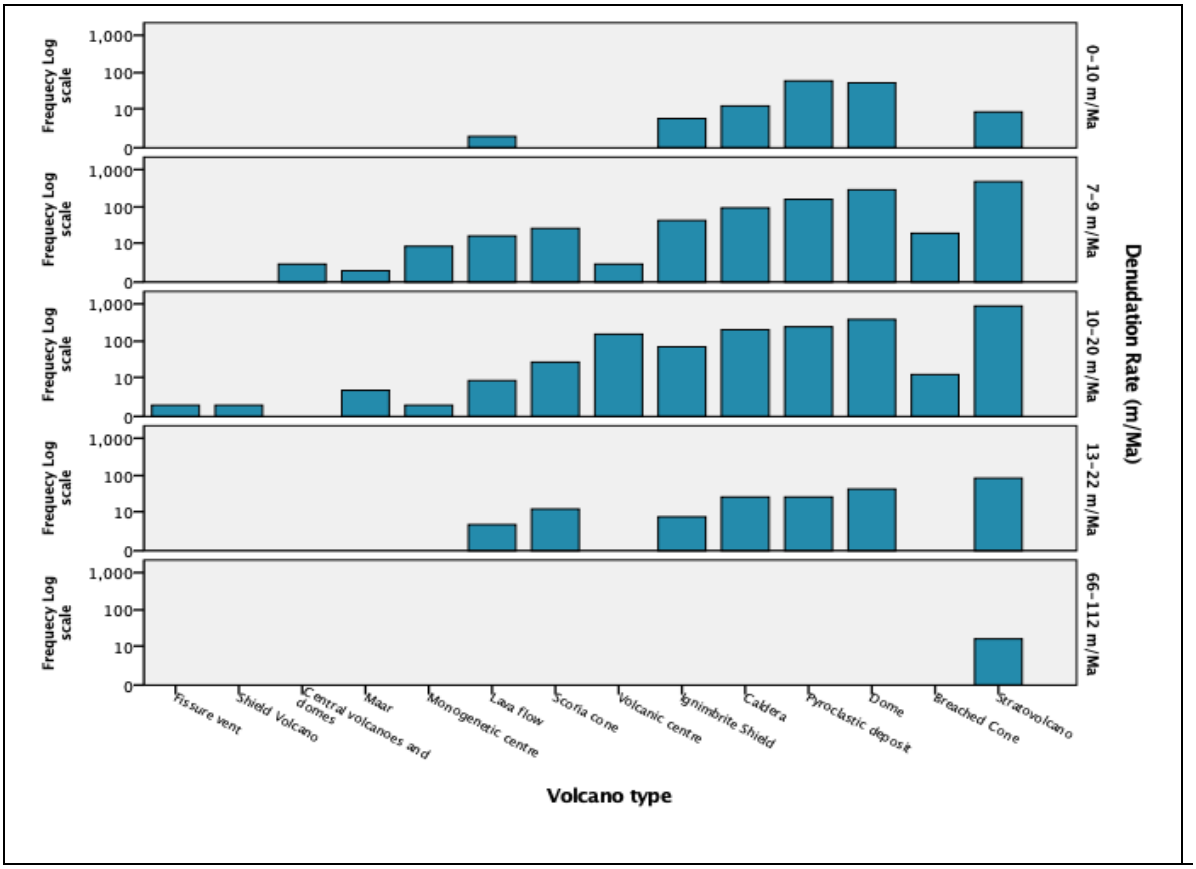


*Figure 3-18. Bar plots of volcanic edifices classified by location within regions with differential denudation rates. Ranges from Denudation rate to match Karátson et al. (2011). Note Frequency (y left axis) log scale.*

### *3.6.2.3 Climate*

Even though I am comparing volcanic edifices in climates that may have changed significantly from million years ago, this parameter can still be used as an indicator of erosion processes. Actually, volcanoes in areas that have wetter climates today show a consistent decrease in frequency and volcano type. On the contrary, cones in more arid places show the opposite trend. *Stratovolcanoes and Breached cones* remain stable in number despite the change on precipitation. *Domes*, *Pyroclastics* and *Calderas* show similar frequencies for Subtropical to Arid climates, and interestingly show the opposite behaviour for Tropical and Hyperarid, frequencies decrease from Domes to Calderas in the latest climate (Figure 3-19).

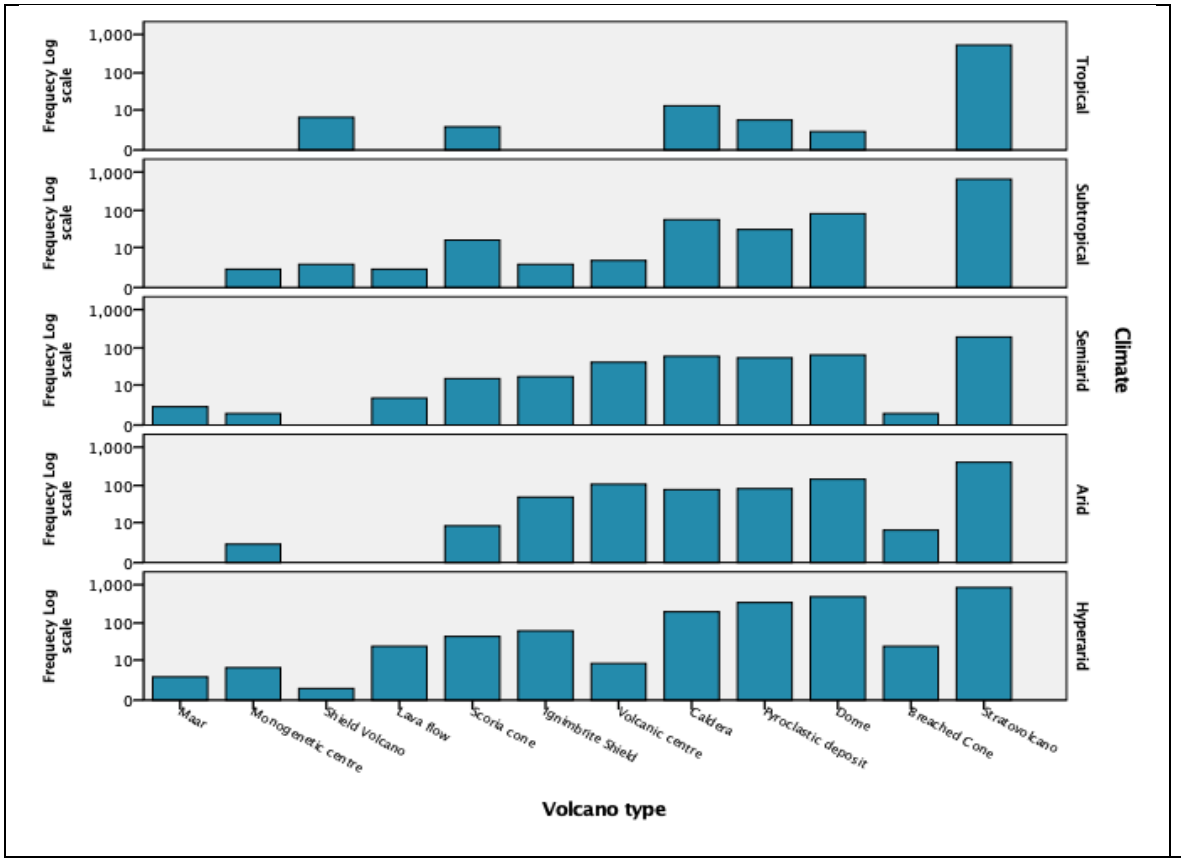


*Figure 3-19. Bar plots of volcanic edifices classified by present climate. Note Frequency (y left axis) in log scale.*

### *3.6.2.4 Slope*

Figure 3-20a shows the variations in slope of edifices for all volcanic edifice types. This parameter will depend on the erosion rate of the edifice and the volcano activity, but in general, steeper slopes indicate more active systems where there is not enough time for degradational processes (i.e., erosion due to precipitation, material creeping, etc) to dominate (overgrowth of the edifice), with the exception of edifice collapses, which will increase slopes. Moreover, the type of volcano and the composition of the magma are also a strong control for slopes; for instance, *Stratovolcanoes* tend to have a higher height - cone diameter ratios (and so steeper) than *Shield volcanoes* (Figure 3-20b).

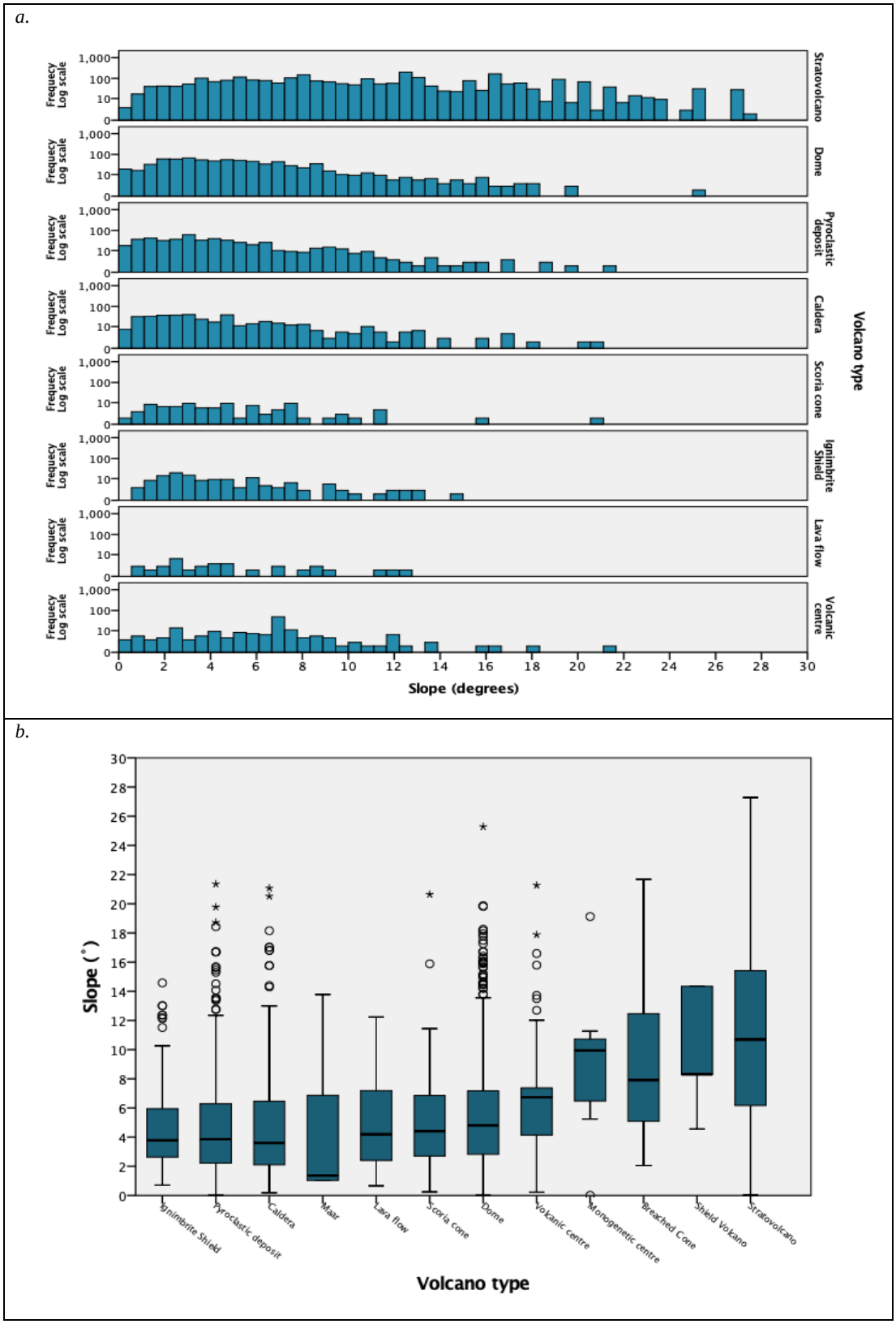


*Figure 3-20. a. Histogram of volcanic edifices showing slope degree values. b. Box whisker for Slope degrees classified by Volcano type. Boxes represent the range of the 25th and 75th percentiles with the dividing line being the median. Whiskers represent the minimum and maximum values. Circles outside the boxes represent outliers and asterisks are extreme outliers (values more than three times the height of the boxes).*

## 3.7 Conclusions

From the statistical analysis of the volcanic edifices dimensions and eruption parameters I can conclude:

- *Stratovolcanoes (+Breached cones)* not only dominate the whole-dataset distribution, but they also show consistently the biggest values in the Andes for volcano parameters, such as edifice height, volcano volume, cone and crater diameters. *Stratovolcanoes* are followed in numbers by *Domes* and C*alderas (Ignimbrite shields).*
- C*alderas (Ignimbrite shields)* account for the biggest outliers in the AVEDB.
- In most parameters there is systematic difference for the volcano types.
- Particularly for certain edifices, volcano type and the composition of the magma have a strong control on volcanic edifices slope. Moreover, the relation H/D will directly define the steepness of the slope.
- The relation H/D is a useful parameter to indirectly determine the age and degradation of volcanic edifices. H/D ratios between 0.10-0.07 represent Miocene to Palaeocene edifices, while values between 0.14-0.11 correspond to Quaternary volcanoes, possibly active. Our results coincide accurately with Wood (1978) and Grosse et al. (2009) for Quaternary volcanoes and with Karátson et al. (2010) for older volcanic edifices.
- In this study, all modern volcanoes that were classified as large, are stratovolcanoes, and they have the potential to generate PCDs if conditions beneath them persist for a sufficient amount of time. Large edifices are the only volcanoes with the capability to intermittently connect with deeper magma sources, events that allow magmatic volatile exsolution in shallow levels of the crust, which is a fundamental stage in the formation of PCDs. Therefore, when exploring for PCDs, a high potential place to look are the eroded and remaining edifices of inactive stratovolcanoes.

  On the contrary, no economic deposit could be generated if a catastrophic release of volatiles into the atmosphere occurs, which are vital for ore precipitation during the hydrothermal event. In terms of exploration, areas where ignimbrites are abundant and were erupted during an interesting PCD forming period of time, should be immediately abandoned.
- The height of a volcanic edifice is relatively highly correlated with volcano volume, has a weak positive correlation with the cone diameter and a weak negative correlation with the crater diameter. These correlations between volcanic dimension parameters suggest that the higher the volcano edifice is, the bigger the volcano volume and consequently the cone diameter. However, in case of an eruption, a different process may take place changing from a building-up event into a destructive episode, generating a crater.
- Volcanism parameters in the Andes show the most common magnitude for eruptions in the database is 4. For the rest of the parameters, outliers in the AVEDB generate big shifts in the dispersion parameters. The main responsible for these variations are stratovolcanoes and calderas.
- Volcanoes are unevenly distributed in the Andes, the concentrate in the Eastern and Central Cordillera, and additionally to these two regions, the only area where all volcano types are represented is the CVZ.
- Volcanic edifices in the Andes are affected by a variety of climates, which have remained similar since Miocene times, influencing the way they erode.

# 4 Chapter 4: Assessing erosional patterns in the Andes

## 4.1 Scope of this study

PCDs are intricate systems, characterised by the innumerable veinlet systems carrying copper and iron sulphides, precipitated from hydrothermal solutions, and are responsible for almost 75% of the world copper production, (Sillitoe, 2010). The majority of PCDs form at depths around 2 km and are useful for constraining depth and time events that occurred within the crust (McInnes et al., 2005; Sillitoe, 2010). Whether a porphyry copper deposit is exposed at the surface depends on to the magnitude of erosion, sedimentation rates and faulting since the moment they were emplaced (Kesler and Wilkinson, 2006; Wilkinson and Kesler, 2007; Braxton et al., 2012). According to Yanites and Kesler (2015) the number of PCDs in a region should evidence host rocks' cumulative history of exhumation. While exhumation reduces the amount of covering deposits, the units underneath rise towards the surface, and the period of time that an intrusion remained in the crust varies depending on the exhumation history of a region. The most auspicious conditions for PCD formation are rapid exhumation and short crystallisation and cooling periods at shallow crustal depths (~2 km), therefore not many deposits are to be found when these levels are exposed at the surface.

**Uplift** is a vector opposite to gravity that uses the geoid (sea level corrected for eustatic changes) as reference, as well as the Earth's surface; the objects that move are either particular rocks or, the Earth's surface. In terms of the processes that relate elevation and climate change (Birchfield and Weertman, 1983; Ruddiman and Kutzbach, 1989), what matters most is the uplift of the Earth's surface relative to sea level, which is the change in mean elevation. **Exhumation** has been defined as the uplift of rocks using the local Earth surface as a reference, which is measured using geochronology and petrological geobarometers and geothermometers. Exhumation represents the thickness of rock removed from the Earth's surface (Clark and Jager, 1969; England and Molnar,1990) by erosional processes:

***surface uplift = uplift of rock – exhumation***

In terms of volcanism, I discovered eruption records in the Andes decrease dramatically in time and after a couple of thousands of years volcanic deposits tend to be disappear extremely fast from the geological records, independently of the volume of material ejected during the eruption or the frequency of these events. I count with less than 70% of the total data for each magnitude eruption in the last 2.5 Ma. Incompleteness of the dataset has proven that the eruption database is not useful for comparing with another geological systems such as PCDs, therefore I decided to focus on volcanoes rather than eruptions. There are significant advantages of using edifices geometry; firstly, edifices last longer than individual eruption deposits and secondly, height (and shape) of edifices reflect erosion rates and durations which can be exploited to assess regional erosion rate and timings.

The main goal of the chapter is to assess how climate, location and timing relate to the dimensions and abundance of volcanic edifices, considering factors like the incomplete sampling of volcanoes, decreasing preservation with age, and lack of exposure of volcanic edifices due to sediment cover. This allows us to define areas of intensive erosion, that can be used as an exploration tool to determine regions with high probability of finding PCDs close to the surface. I also consider different elements that may have a strong influence on exposure of the intrusive bodies such as uplift, exhumation and erosion to understand the geological processes that underlie PCD emergence spatial patterns.

The major questions that this study addresses are:

- Can I use volcanic edifices as an indirect tool to find regions with sufficient erosion and uplift to bring PCDs to surface?
- Which are the areas in the Andes that have the potential to conserve PCD deposits close to the surface?
- How do climate and location impact the exposure of PCDs and conservation of volcanic edifices?
- How can I use erosional and depositional processes to identify PCD emergence patterns in the Andes?
- What are the implications for mineral exploration?

In this chapter, I analyse each magmatic arc, including volcanoes and porphyries of the same age in order to identify any spatial and temporal relationships. I assess the data looking for a correlation between volcanic edifice properties against Cretaceous to Miocene PCDs, and younger magmatic belts were not required for the comparison. When I drew the magmatic belts (Section **Error! Reference source not found.**; Figure 2-2), I knew that younger volcanoes with dated ages occur within them. I would also expect to find belts overlapping and superimposition of younger eruptions occurring on top of older ones. Moreover, in general terms I would expect to find younger edifices to the east and older ones to the west, since the volcanic arc is shifting eastwards in the Andes.

My hypothesis considers that porphyry deposits represent the shallower portions of the magmatic system under a volcano. Different erosion rates will expose different parts of the volcanic- magmatic system. Within this chapter I explore where in the Andes erosion rates are favourable for the exposure of PCDs and I test where in the magmatic arc PCD are most proximal to the surface. I evaluate differential erosion in the Andes using volcanic edifice geometries height (of the volcanic edifice measured from the bottom centre to the summit) extracting only volcanoes with height values form the AVEDB and economic deposits from the PCDsDB (Appendix IV: *Descriptive_Stats_Height1239+BHPPCDsEpith*). Using this new subset, I examine the temporal and spatial constraints on the edifice heights for defined geological time periods (Cretaceous-Holocene). The final aim of this chapter is defining and identify prospective areas of possible undiscovered economic deposits.

## 4.2 Methodology

In this chapter I build on the descriptive statistical analysis of height of volcanoes in Chapter 03: Descriptive Statistical Analysis, and study how edifice height variation varies spatially (latitude, longitude and elevation) depending on factors such climate, tectonics and timing and then, I compare volcanoes results against PCDs spatial location. The outcomes in this study result from the understanding of what were the main processes and events that shaped the Andes and exposed mineralised PCDs, which was only possible because of the combination of the following factors:

- Local tectonic events: such as exhumation of intrusive bodies, rotational blocks, landslides.
- Regional tectonic episodes: main tectonic orogeny events, crustal shortening and thickening, followed by differential uplift of certain tectonic blocks; Altiplano plateau formation; Precordillera tectonic evolution; arc formation and migration; tectonic erosion.
- Climate: precipitation rates (extracted from CHELSA raster image) for different regions in South America; precipitation shadow effect; aridification of northern Chile and southern Peru.
- Geomorphology concepts: basin formation; paleosurfaces formation and conservation; river incision due uplift episodes; differential erosion rates;

In this chapter I use the previous results with the aim to complement Chapter 03: Descriptive Statistical Analysis, by bringing more detail into the study and comparing results against the spatial location of the edifices (latitude, longitude and elevation). From the AVEDB only a total of 1239 registers have height information that I use in this study, I add the PCDs dataset and plot them into scatter plots. When adding PCDs into the volcano dataset, I assigned those registers 0 m as height. When elevation values, where not given by the source, I assigned an elevation value extracted from a DEM raster image using ArcGIS. I want to observe the distribution in the Andes of eroded volcanoes but also, I want to compare them against other parts of the same system. In order to demonstrate how climate may impact in the height of volcanic edifices and exposure of copper deposits I plot the records during relevant time periods in terms of copper fertility, which are Palaeocene, Eocene, Oligocene and Miocene. In this analysis I distinguish between different types of mineralization within PCDs, because they develop at different depths (Murakami et al., 2010; Hezarkhani et al. 1999; Klemm et al. 2007; Sillitoe, 2000; Cox and Singer, 1988) and I can use that knowledge to identify different levels of erosion and exposure. So, I visualise in GIS maps the spatial location of edifices and PCDs for specific time periods in order to find patterns where PCDs could be close to the surface. Next, I evaluate the influence of changing climate conditions in the Andes in volcanic edifice height using scatter plots. I use histograms, bar and scatter plots to compare how volcanic edifices varies within different epochs and for different volcano types for different regions within the Andes. When I compare the volcanic edifice height by regions, I need to know if there is a significant difference between these areas. For that reason, I performed an *ANOVA* and *Tukey test* using the statistical software *SPSS Statistics*. I also study the frequency of volcanoes and PCDs by regions following the morphotectonic provinces. Finally, I compare my result against Montgomery et al. (2001). He suggests that there is a clear relation between hypsometry and elevation, therefore is not possible for high topography to persist at high latitudes, consequently the high

Andes end at 35ºS in part because, at this latitude, they intersect the perennial snowline. For comparison, I plot the volcanic edifices and PCDs on top of Montgomery et al. (2001) erosion versus latitude scatter plots.

## 4.3 Spatial distribution of volcanoes and PCDs depending on time epochs

In the Andes, economic deposits are clustered along specific metallogenic belts formed in pulses during periods of intense magmatic activity (Rosenbaum et al., 2005). Clark et al. (1976) and Sillitoe (1981, 1988) showed that porphyry deposits in the Andes occur within several linear belts of coeval Cenozoic magmatism, corresponding to the position of the magmatic arc, from the Cretaceous up to the Miocene. García et al. (2017) indicate each metallogenic belt formed gradually from west towards the east. The Palaeocene to early Eocene metallogenic belt formed between 62 to 51 My. It is located in the western margin of the Andes; it has between 30 to 50 km wide and contains mainly Cu and Mo rich porphyry deposits. Towards the west, the middle Eocene to early Oligocene belt (43-31 My) is characterised by gold rich skarns and Cu rich porphyries with Mo as a secondary commodity. This belt shows width fluctuations between southern Peru (130 km) and northern Chile (30-50 km) (Sillitoe, 1988; Perelló et al., 2003; Sillitoe and Perelló, 2005; Maksaev et al., 2007). These middle Eocene to early Oligocene major sized deposits are mainly located in Chile and are related with rich supergene blankets and exotic Cu deposits (Münchmeyer, 1996; Sillitoe, 2005). The youngest belt, Miocene to early Pliocene (20-4 My), is found in the eastern region of the Andes, it is the widest of the three belts, up to 400 km. It extends along Peru, Bolivia, Chile and Argentina, and comprises a wide range of deposit types (Cu-Au-(Ag) and Cu-Mo porphyry deposits, skarn deposits, enargite carbonate replacements, high-sulfidation Au-Ag epithermal deposits and red-bed copper deposits (Sillitoe and Perelló, 2005).

### 4.3.1 Cretaceous volcanoes and PCDs

Cretaceous and Palaeocene arcs are the most ancient ones of interest in my PCD and AVEDB datasets because they contain the oldest economic deposits in the Andes. The only volcanoes that are designated as Cretaceous are not radiometrically dated: their ages have been assigned according to their location within the magmatic arc. The four Cretaceous volcanoes are all heavily eroded and are located along the most western region of the Andes, in the Intermediate depression and Central Cordillera (Figure 4-1). Therefore, all analysis of Cretaceous volcanoes should be taken with caution. These volcanoes have been mainly striped away from the Andes, all with heights <1050m, and with no apparent pattern to their distribution in the Andes. My dataset shows that volcanoes located close to the current coastline (Intermediate depression and Precordillera) (Figure 4-1), are considerably more sparse and shorter in height than the central Cordillera.

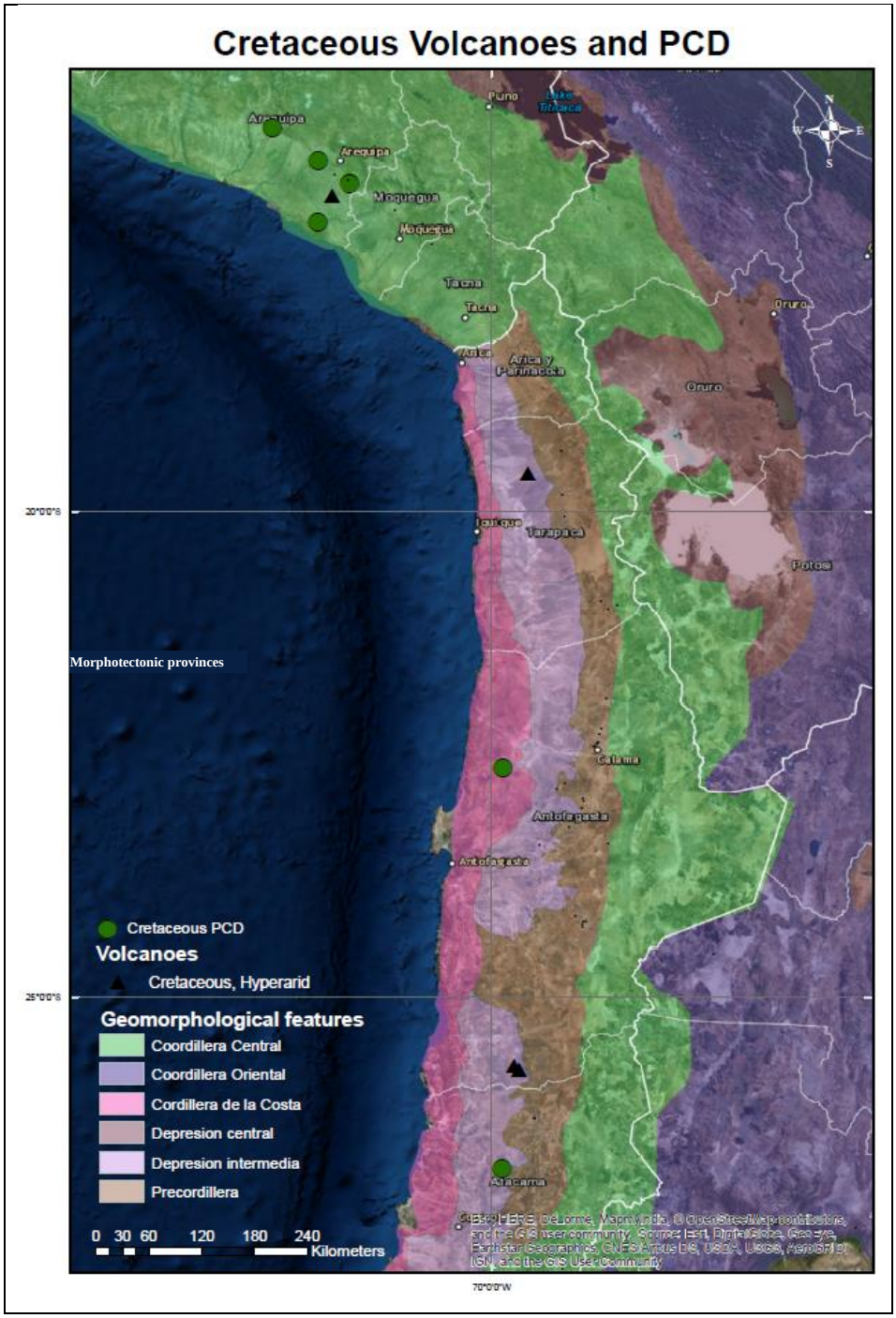


*Figure 4-1. Satellite image of northern Chile and southern Peru showing morphotectonic provinces on top, Cretaceous volcanoes (triangles) classified by climate and Cretaceous PCDs (circles).*

### 4.3.2 Palaeocene volcanoes and PCDs

Palaeocene volcanoes are only found in Precordillera and Central Cordillera, while porphyries of the same age are also found in the Intermediate depression. There is also a bigger number of volcanoes in the Central Cordillera. Figure 4-2 shows a map with volcanoes that have been colour classified by climate and PCDs (circles) plotted on top of morphotectonic provinces, flat slabs areas, ridges, and tectonic segments defined

by Sillitoe (1974). These segments are separated by transverse boundaries that reflect discontinuities on the underlying subduction zone and are based on seismic studies, distinguishable magmatic units, unique magmatic episodicity and spatial distribution, and changes in tectonic and structural regimes. Figure 4-2 shows how these tectonic segments isolate pretty well areas with PCDs from the ones only with volcanoes, showing blocks exhumated into different levels. Climate is playing an important role in the conservation and distribution of these volcanic structures and I will demonstrate later how climate starts to gain importance until it becomes a first order control on volcanoes height. Interestingly, there are no, or very few porphyries in sectors with high numbers of volcanoes, particularly in hyperarid an arid climate. Most porphyries seem to be are located preferentially: (1) in the centre of the segments defined by Sillitoe (1984), (2) in Precordillera and, (3) Mo-Cu porphyries are westwards in comparison to Cu-rich PCDs.

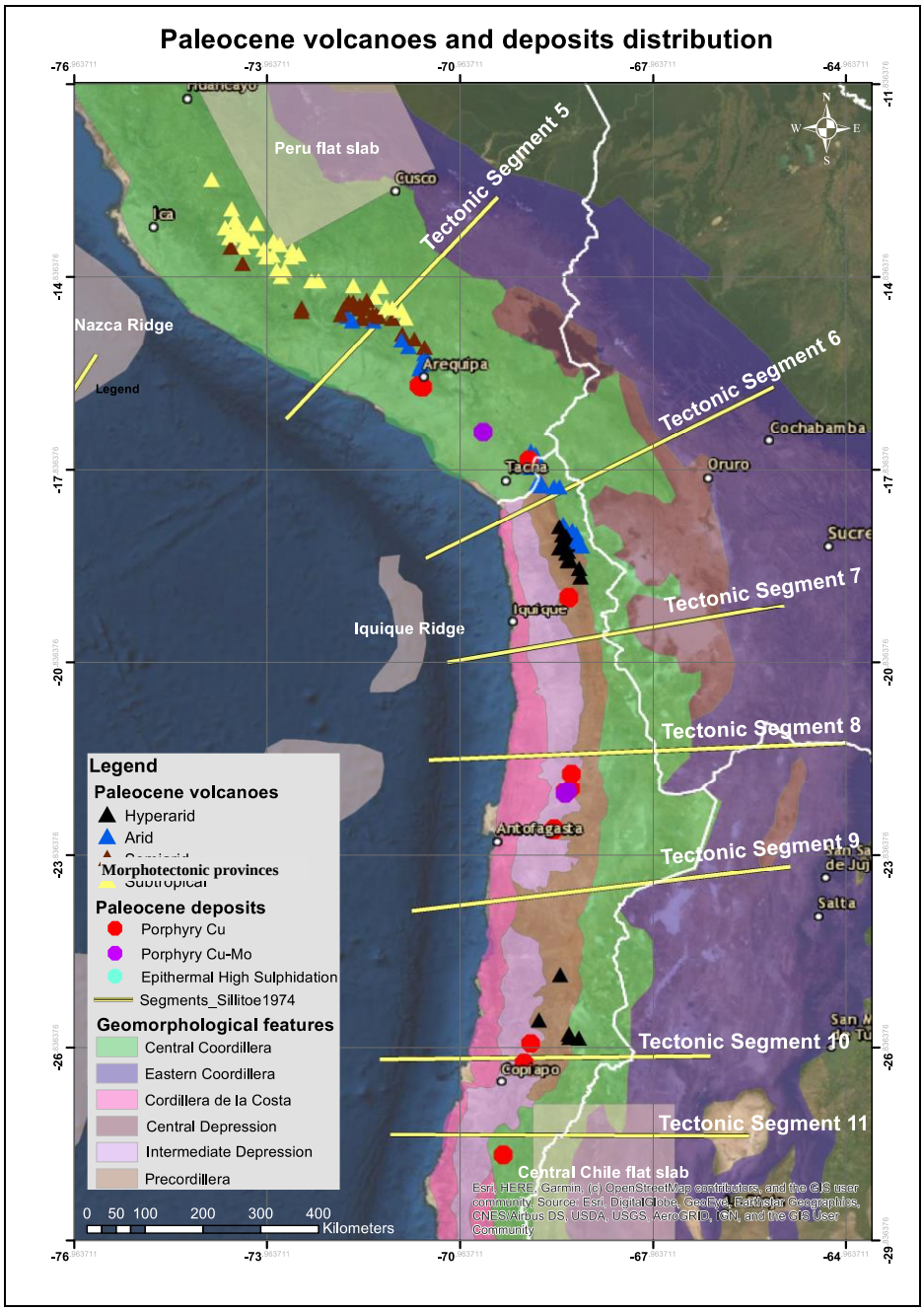

*Figure 4-2. Satellite image of northern Chile and southern Peru showing morphotectonic provinces on top, Palaeocene volcanoes classified by climate (triangles), Palaeocene PCDs (circles) and tectonic segments (yellow lines) (Sillitoe, 1984) on top.*

Figure 4-3 focuses on northern Chile and southern Peru, including the Arica inflexion. Volcanic edifices height decreases westwards particularly in tectonic segment 5 (Figure 4-3b). Only two Palaeocene Cu-porphyries have been discovered in segment 7, they sit between the remnant volcanic edifices and paleosurfaces defined by Evenstar et al. (2017). Interestingly, volcanoes in this region become smaller the closer they are to main river systems, like those close to the Camarones river in Figure 4-3a. One of the observations commonly used to infer recent uplift is the sharp incision by fluvial systems into gentle slopes covered by late Cenozoic sedimentary units. It is a basic tenet of geomorphology that the uplift of a surface with respect to the base level of the rivers, offers the fluvial system higher potential energy and steeper slopes, resulting in fast incision of the surface (Molnar and England, 1990).

In the Arequipa region of southern Peru, between segments 5 and 6, of Figure 4-3b, the story seems a bit different. Volcanic cones tend to decrease in height in a north-eastern direction, while PCDs are located along the Incapuquio fault and immediately next to the highest volcanoes in the area. This intensively faulted region has a robust geomorphic imprint on the Andean mountains (Huaman, 1985; Sébrier et al., 1985). By the use of microtectonic studies, Sébrier et al. (1985, 1988) and Schildgen et al. (2009) recognised different kinematic episodes. Sébrier et al. (1985, 1988) suggest that major compressional episodes occurred during the Tertiary and early Quaternary, and a minor normal faulting in the late Quaternary. Studies in relocated microseismicity (Grange et al., 1984) and teleseismic data (Devlin et al., 2012) has shown that the Incapuquio fault system in the Arequipa region, as well as the Lluta fault, are both is presently being affected by reverse and strike-slip faults.

Between segment 4 and 5, despite the fact I find no PCDs in the area, volcanic edifices are shorter in some sectors than in others. Clearly, river systems influence once again on the height of volcanic edifices.

*a.*

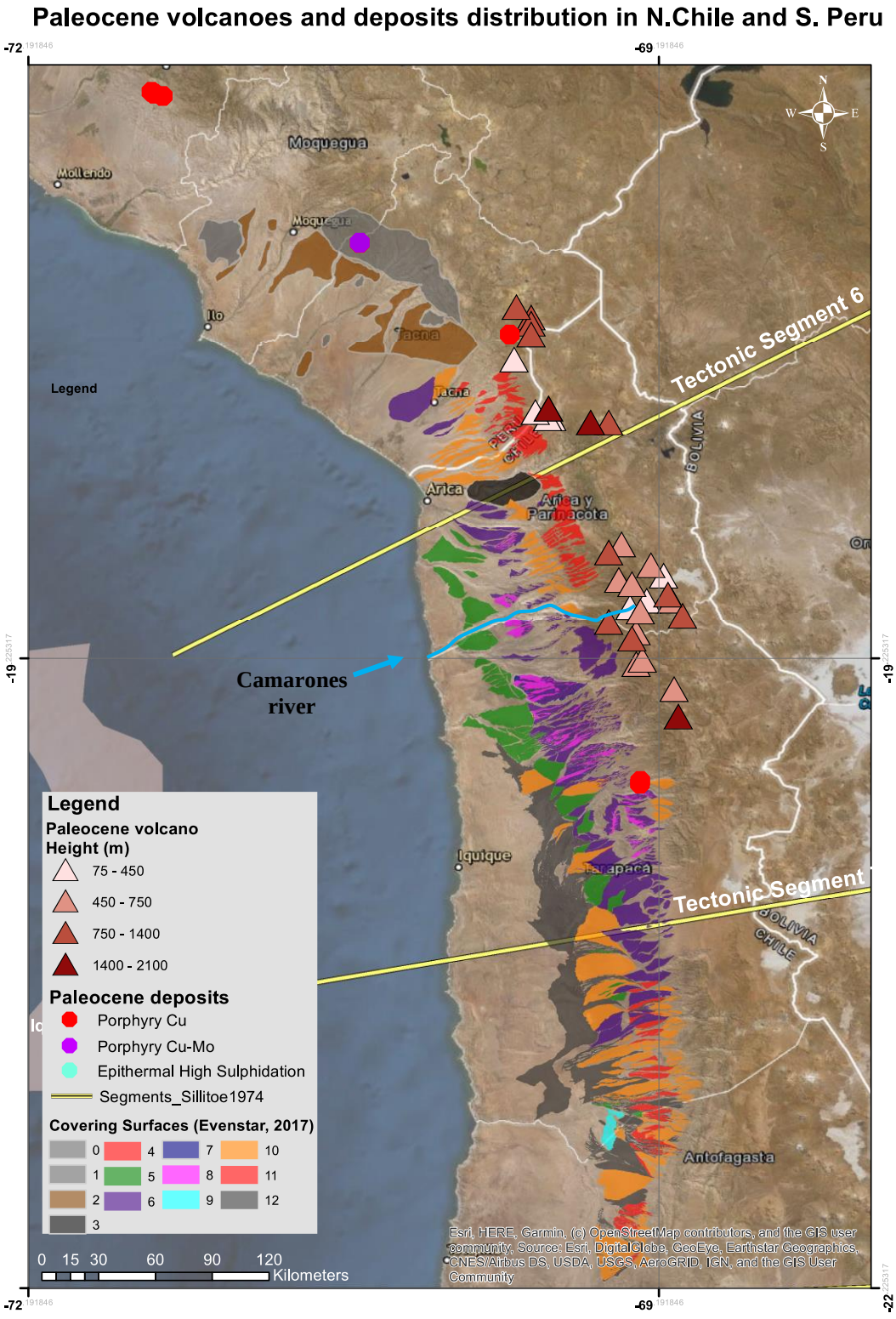
Paleocene volcanoes and deposits distribution in N.Chile and S. Peru
-72
-69
-19
-22
Moquegua
Mollendo
Ilo
Tacna
Arica
Arica y Parinacota
Iquique
Tarapaca
Antofagasta
BOLIVIA
PERU
CHILE
Tectonic Segment 6
Tectonic Segment
Camarones river
Legend
Paleocene volcano
Height (m)
75 - 450
450 - 750
750 - 1400
1400 - 2100
Paleocene deposits
Porphyry Cu
Porphyry Cu-Mo
Epithermal High Sulphidation
Segments_Sillitoe1974
Covering Surfaces (Evenstar, 2017)
0 4 7 10
1 5 8 11
2 6 9 12
3
0 15 30 60 90 120
Kilometers
N
W
E
S
Esri, HERE, Garmin, (c) OpenStreetMap contributors, and the GIS user community, Source: Esri, DigitalGlobe, GeoEye, Earthstar Geographics, CNES/Airbus DS, USDA, USGS, AeroGRID, IGN, and the GIS User Community

*b.*

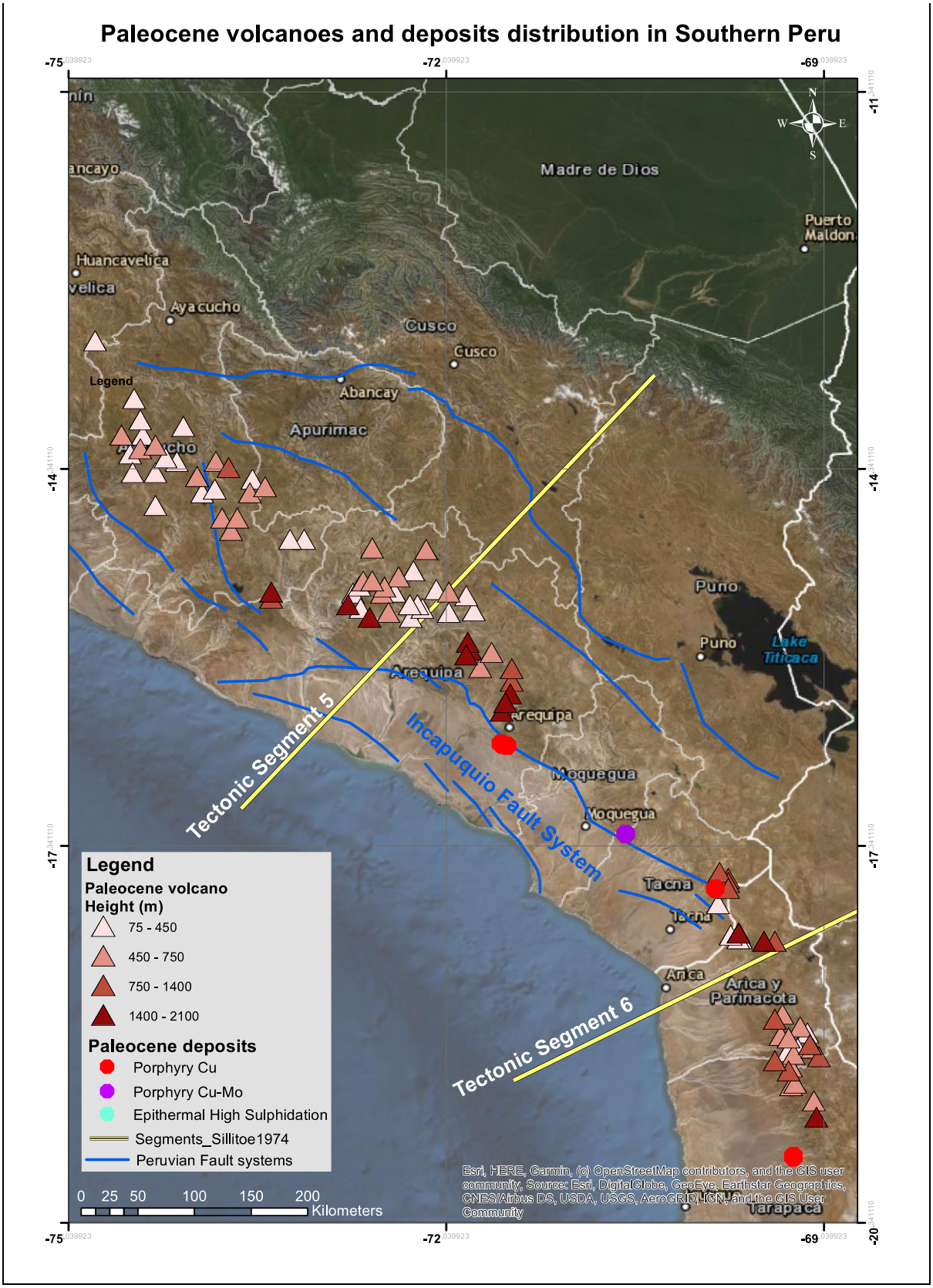


*Figure 4-3. a. Satellite image of northern Chile and the Arica inflexion showing paleosurfaces (Evenstar et al., 2017) on top, Palaeocene volcanoes classified by height (triangles), Palaeocene PCDs (circles) and tectonic segments (yellow lines) (Sillitoe, 1984) on top. b. Satellite image of southern Peru showing main faults (blue lines), Palaeocene volcanoes classified by height (triangles), Palaeocene PCDs (circles) and tectonic segments (yellow lines) (Sillitoe, 1984) on top.*

### 4.3.3 Eocene volcanoes and PCDs

Eocene edifice distribution is constrained to Central Cordillera (133 edifices) and only a few more in Precordillera and Central Depression (Figure 4-10). Spatial trend remains the same as in the Palaeocene, however the trends are clearer for this period.

In Figure 4-4 I use colour boxes to highlight patterns arising. I start in the Chilean Central Cordillera and moving westwards, I find firstly volcanic edifices, exposed to different climates and showing different level of erosion, where the highest volcanoes oscillate between 1000-1500m (Figure 4-17). Secondly, I see Cu PCDs and finally, I find Mo-Cu rich deposits. At the northern area of segment 10, there is an epithermal deposit near the remaining volcanic edifices (Figure 4-4). Sectors like this one, suggest that even though I am still able to recognise a volcanic cone, I am very close to its roots. There is a conglomeration of Eocene PCDs on the Precordillera, just as seen in the Palaeocene data.

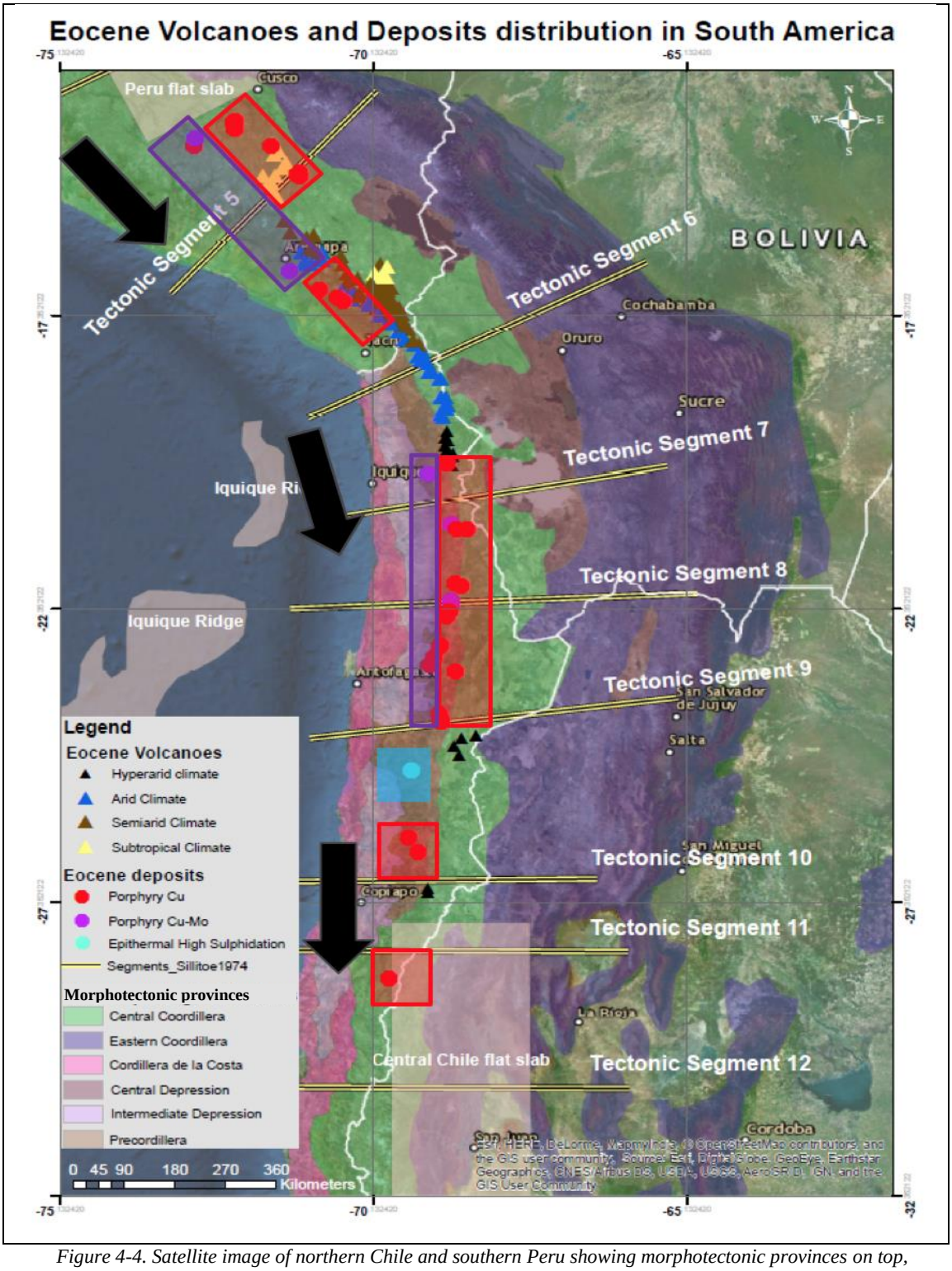


*Figure 4-4. Satellite image of northern Chile and southern Peru showing morphotectonic provinces on top, Eocene volcanoes classified by climate (triangles), Eocene PCDs (circles), epithermal deposits (circles) and tectonic segments (yellow lines) (Sillitoe, 1984) on top. Coloured boxes highlight regions with different level of exposure, where red boxes represent Cu PCDs, purple boxes show Mo-Cu rich deposits and epithermal deposit are shown inside light-blue boxes. Black arrows show increasing an erosion gradient.*

If I now start in the Peruvian Central Cordillera and move south-westwards, on segment 6 (Figure 4-5a), I can see that PCDs are again being exposed by the Incapuquio fault and there is a decreasing height gradient

for volcanic edifices further away from the fault system. Figure 4-5b shows intercalated clusters of PCDs and volcanoes with decreasing heights when closer to fluvial systems.

*a.*

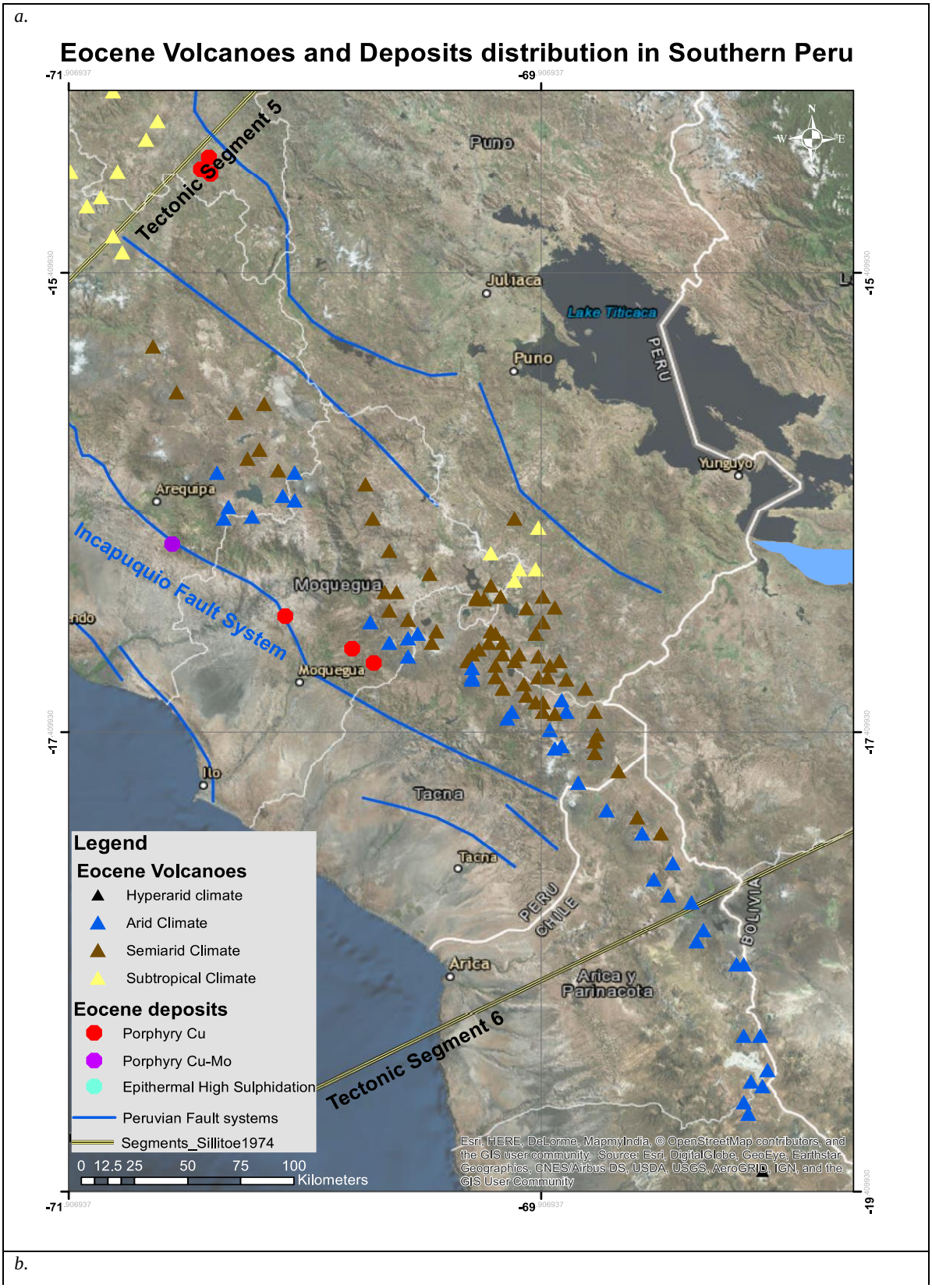


*b.*

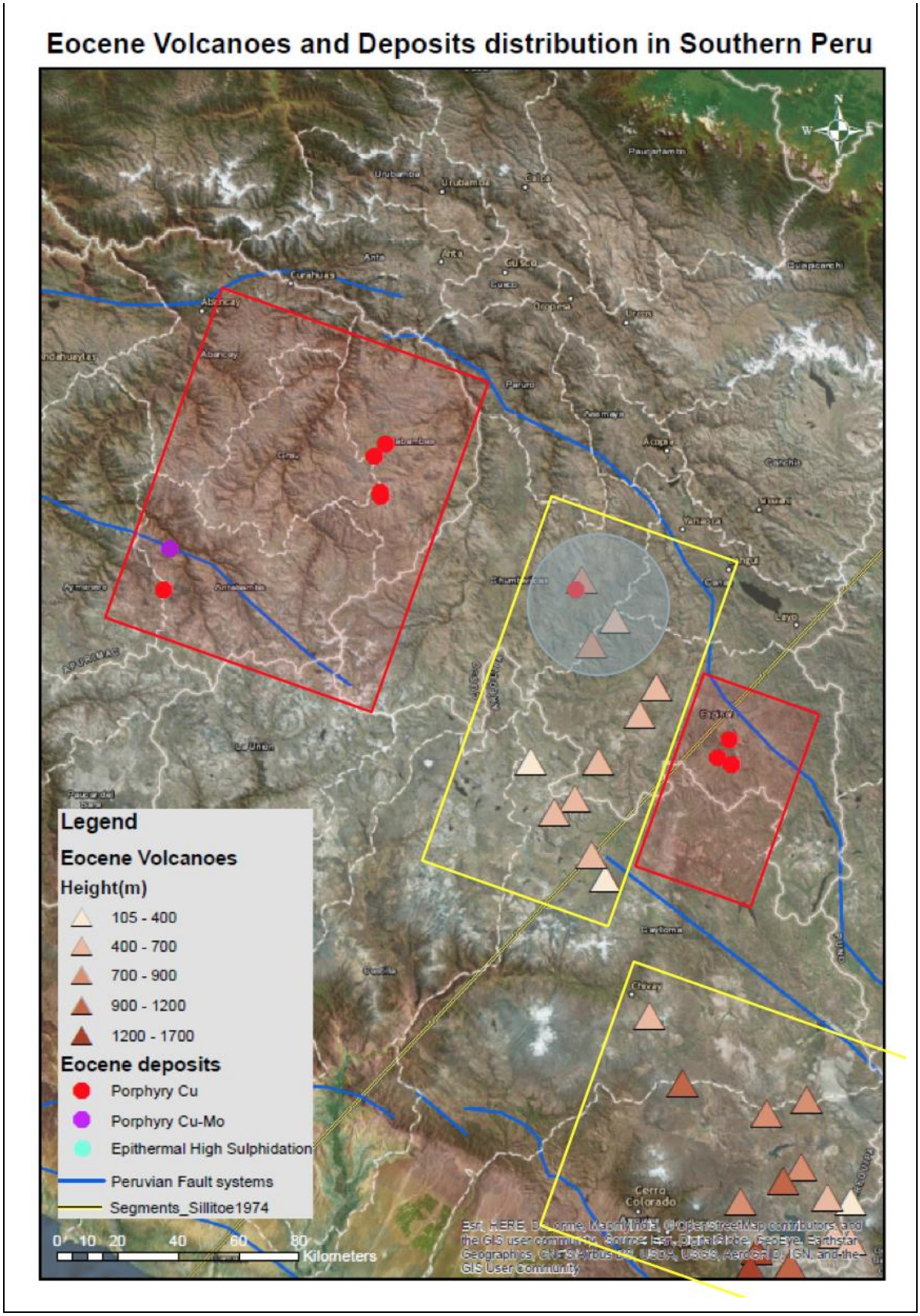


*Figure 4-5. a. Satellite image of northern Chile – southern Peru and the Arica inflexion showing Eocene volcanoes classified by climate (triangles), Eocene PCDs (circles), tectonic segments (Sillitoe, 1984) and main fault systems (blue lines), the Incapuquio fault. B. Satellite image of southern Peru, Arequipa region, showing main faults (blue lines),*

*Eocene volcanoes classified by height (triangles), Eocene PCDs (circles) and tectonic segments (Sillitoe, 1984) on top. Coloured boxes highlight regions with different level of exposure and light blue circle show the location of Constancia mine.*

### 4.3.4 Oligocene volcanoes and PCDs

Oligocene PCDs and volcanoes tend to show fewer clear patterns in space. Figure 4-6 shows volcanoes classified by modern climate, however this time their frequency seems to be immensely high. For this particular time, I should be extra cautious. Since I classified their ages according to their location, following the Oligocene volcanic arc polygon, and not a single volcano in my dataset has been dated for this period. Figure 4-6 shows that volcanoes from Oligocene are more abundant, more widely distributed and taller than their older volcanoes. They appear in Precordillera, Central Cordillera, Central depression and Eastern Cordillera, with heights < 2000 m. They follow the same trend as older volcanic edifices with rising heights and bigger numbers of conserved edifices for drier climate conditions, suggesting the climate is an important contributor to the preservation of those edifices.

The flat slab area in the CVZ is easily identifiable, due to lack of volcanic activity in the region. During Palaeocene and Eocene and now again during the Oligocene, PCDs in northern Chile are located in the Precordillera region. In addition, there is a small conglomeration of Oligocene PCDs, which are situated north to the Arequipa region and remaining volcanic edifices are found only to the southeast.

*a.*

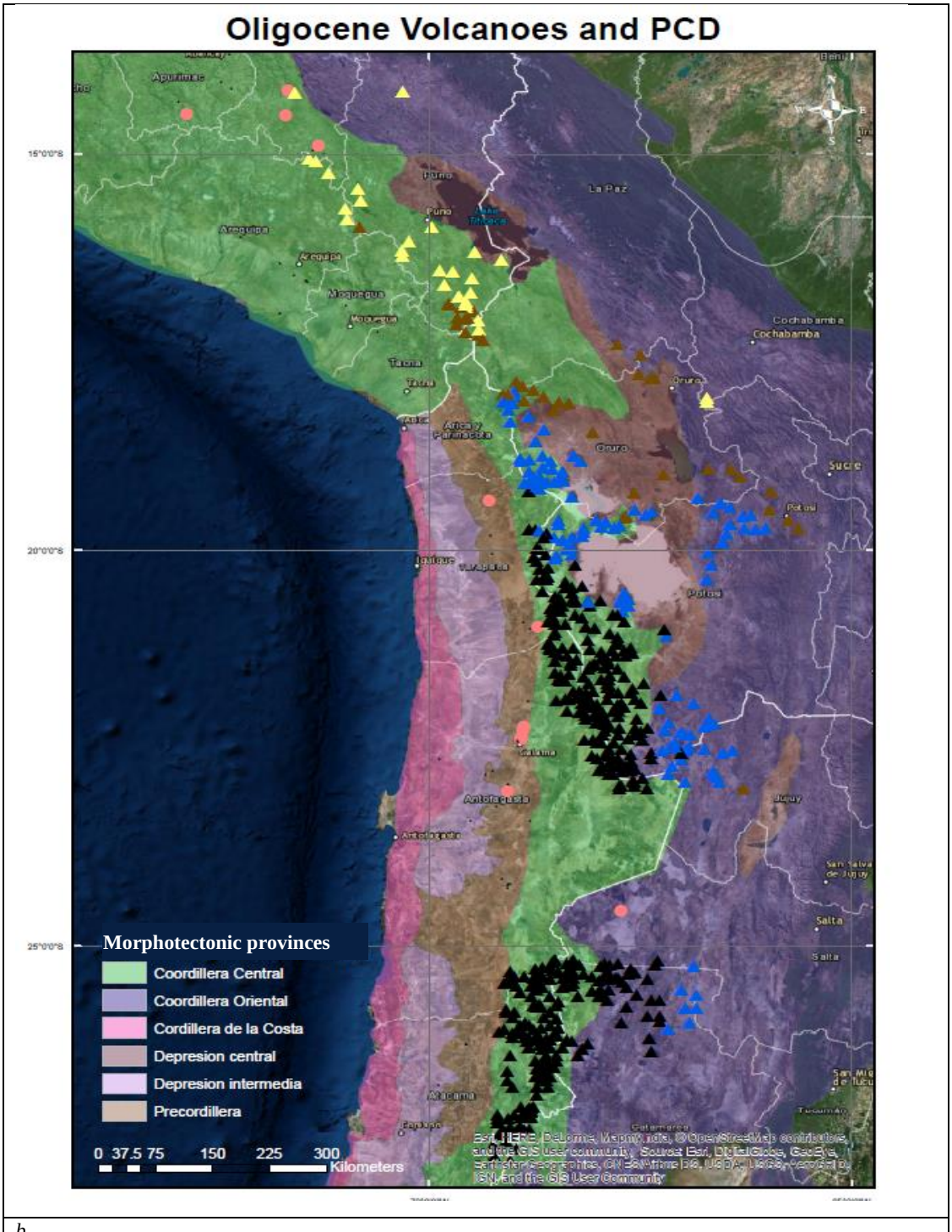
Oligocene Volcanoes and PCD
Morphotectonic provinces
Coordillera Central
Coordillera Oriental
Cordillera de la Costa
Depresion central
Depresion intermedia
Precordillera
0 37.5 75 150 225 300
Kilometers
15°0'0"S
20°0'0"S
25°0'0"S
Puno
La Paz
Arequipa
Moquegua
Tacna
Cochabamba
Oruro
Sucre
Potosi
Antofagasta
Jujuy
Salta
Atacama

*b.*

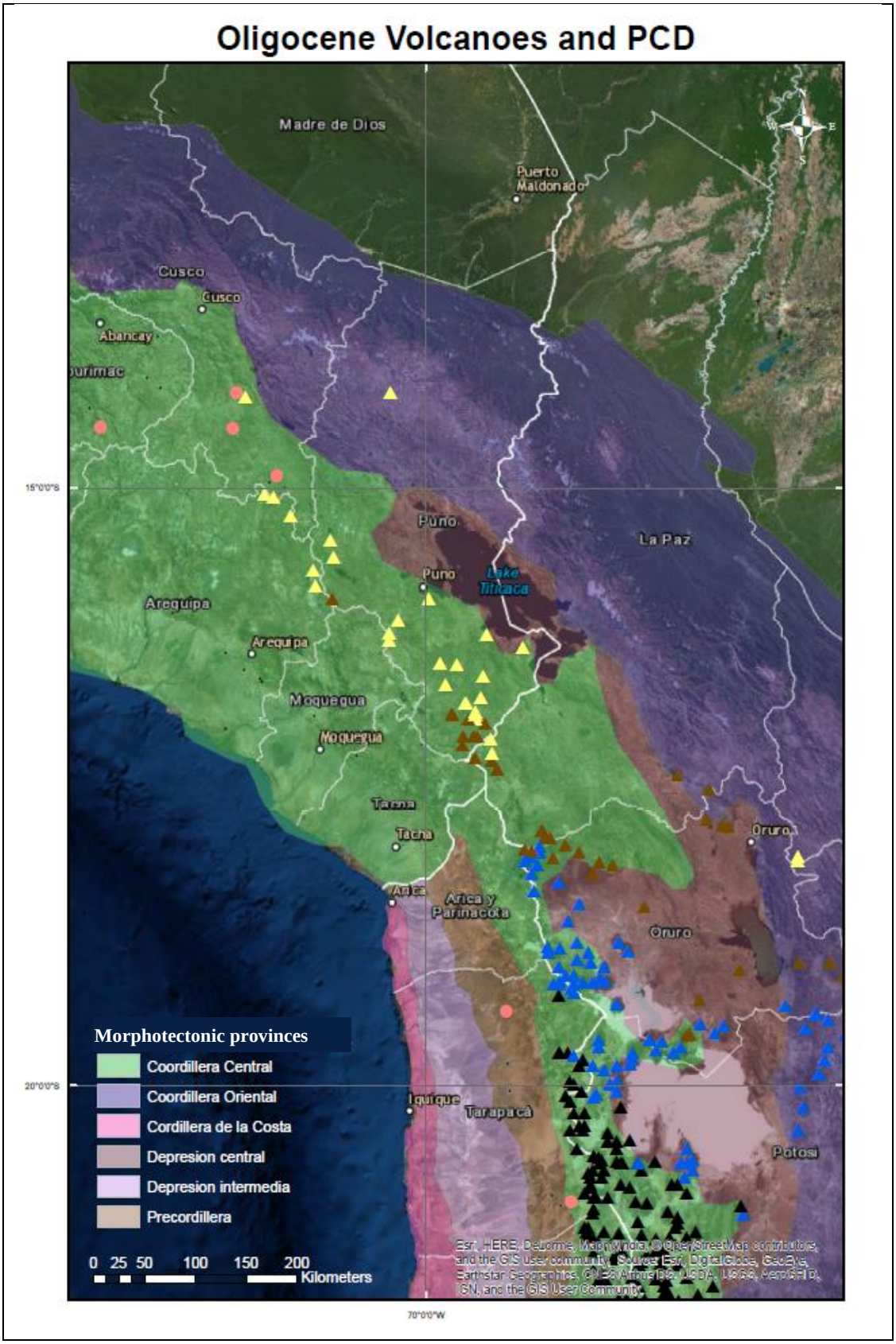


*Figure 4-6. a. Satellite image of northern Chile – southern Peru showing morphotectonic regions with Oligocene volcanoes classified by climate and Oligocene PCD on top. b. Zoom in on the map in a., southern*

*Peru and the Arica inflexion, showing Oligocene volcanoes classified by climate (triangles) and Oligocene PCDs (circles).*

### 4.3.5 Miocene volcanoes

My main interest relies on volcanic activity in a determined age range, from Cretaceous to Oligocene, since this is the time window where the biggest and richest copper deposits occurred. Additionally, I decided not to show the maps because, unlike earlier epochs, there is no clear trend in volcanic height and edifices and PCDs spatial distribution. However, these edifices are mainly located in the Central and Eastern Cordillera. As for older edifices they show shorter heights and smaller numbers for more humid climate conditions.

So far, I was able to recognise a spatial trend relating height and elevation between PCDs and volcanic edifices, where an increasing exhumation of economic deposits and deepening into the magmatic system with a southwest-westward direction exists. However, the trend tends to disappear from Miocene onwards, possibly because volcanism and magmatism were affected by the formation of the flat slab and accentuated changes in the subduction angle and in consequence a cessation in volcanism occurred.

### 4.3.6 Pleistocene and Holocene

Figure 4-7 and Figure 4-8 shows a variety of altitude, regions and climates affecting volcanic cones and a wide range of heights. Pleistocene and Holocene volcanoes show different distributions and height patterns than older volcanoes. They are exceptionally well represented for all climate conditions, particularly in the Central Cordillera, showing a wide variety of heights. Even in relatively wet environments, Holocene edifice heights (and abundance) seem not to be significantly affected by climate. Undoubtedly, exposure time in terms of erosion is quite limited, when comparing to older edifices.

In the Precordillera and Western Patagonia Cordillera, there are only a couple of Pleistocene-Holocene edifices in subtropical and tropical areas while in the Eastern Cordillera there are edifices in more arid settings (Figure 4-8a). Erosional processes are still in place, affecting these structures, which some are still active, particularly in more humid conditions like in Southern Peru, where volcanoes are more abundant (Figure 4-8b).

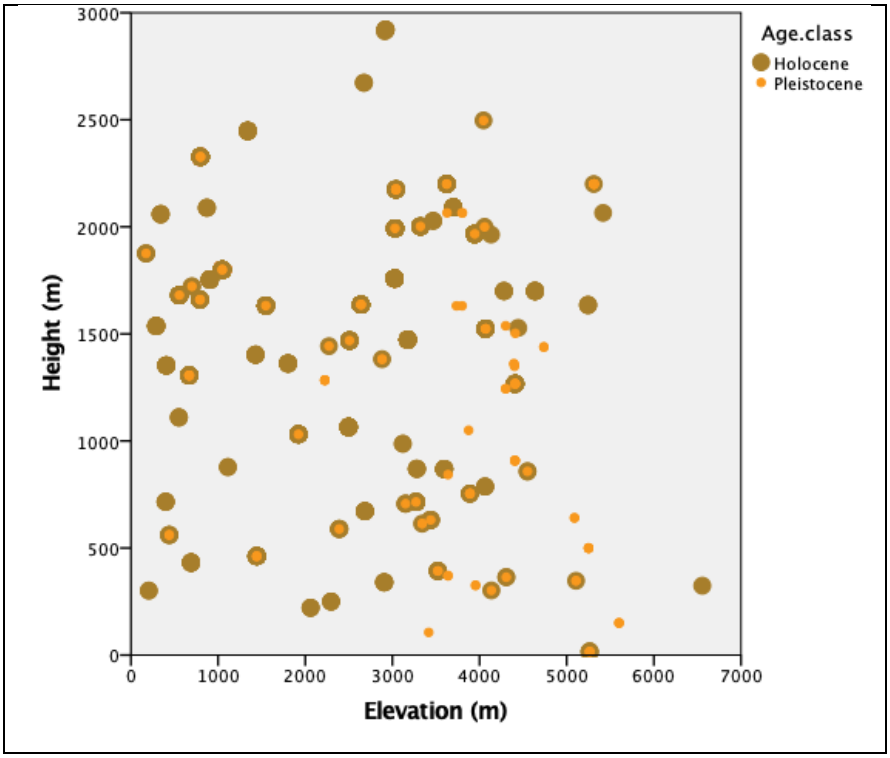


*Figure 4-7. Scatter plot for Pleistocene and Holocene volcanic edifice heights against Elevation (m).*

*a.*

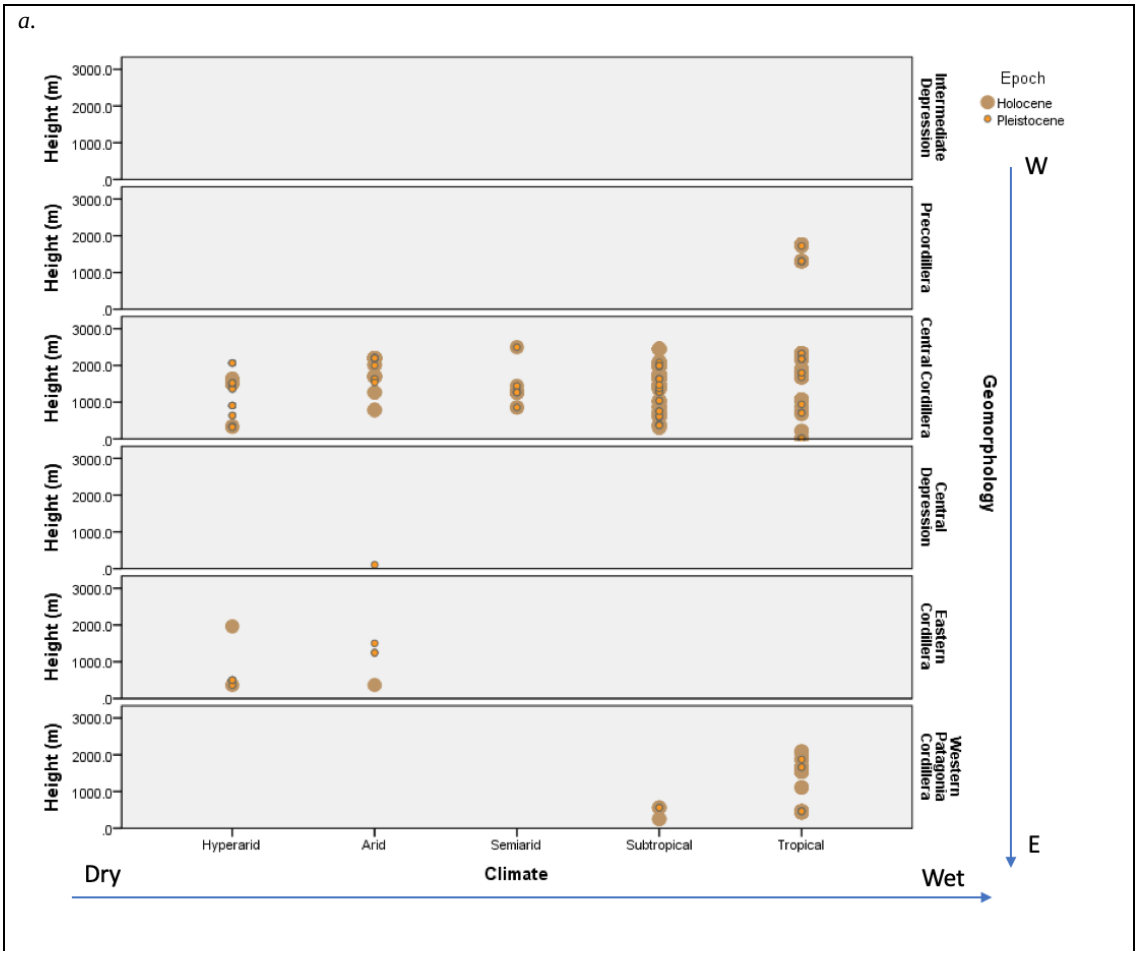

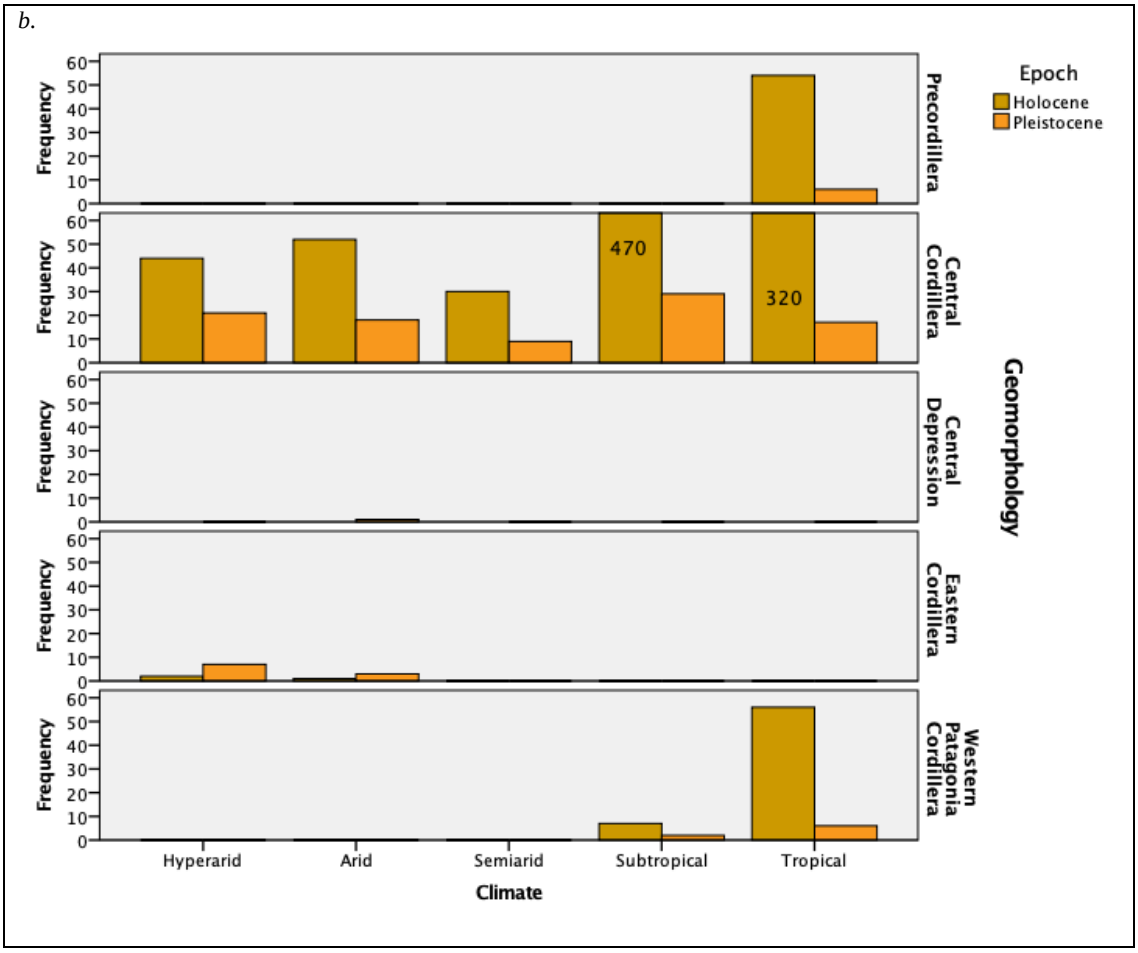


*Figure 4-8. a. Scatter plot for Pleistocene and Holocene volcanic edifice heights against climate, classified by morphotectonic provinces (right Y axis). b. Frequency bar plot of Pleistocene and Holocene volcanic edifices classified by climate and morphotectonic provinces.*

### 4.3.7 Variation in edifice height with spatial location

#### *4.3.7.1 Height variation according to location within morphotectonic provinces*

The Eastern and Central Cordillera host the highest volcanoes, while Central Depression accounts for the greatest median edifice height. The largest variations in height can be seen in Central Cordillera, the region with the most volcanic edifices, but height distributions in the Precordillera and Eastern Cordillera are similar.

Figure 4-9a shows median values for volcanic edifice heights according to the location of volcanoes within the morphotectonic provinces. From the Central Depression to Precordillera, the median height drops more than 100m. Nonetheless, the greatest drop in height and number of volcanoes occurs when moving into the Intermediate Depression. If now, I move eastwards, into the Eastern Cordillera, height median fall a bit more than 150m.

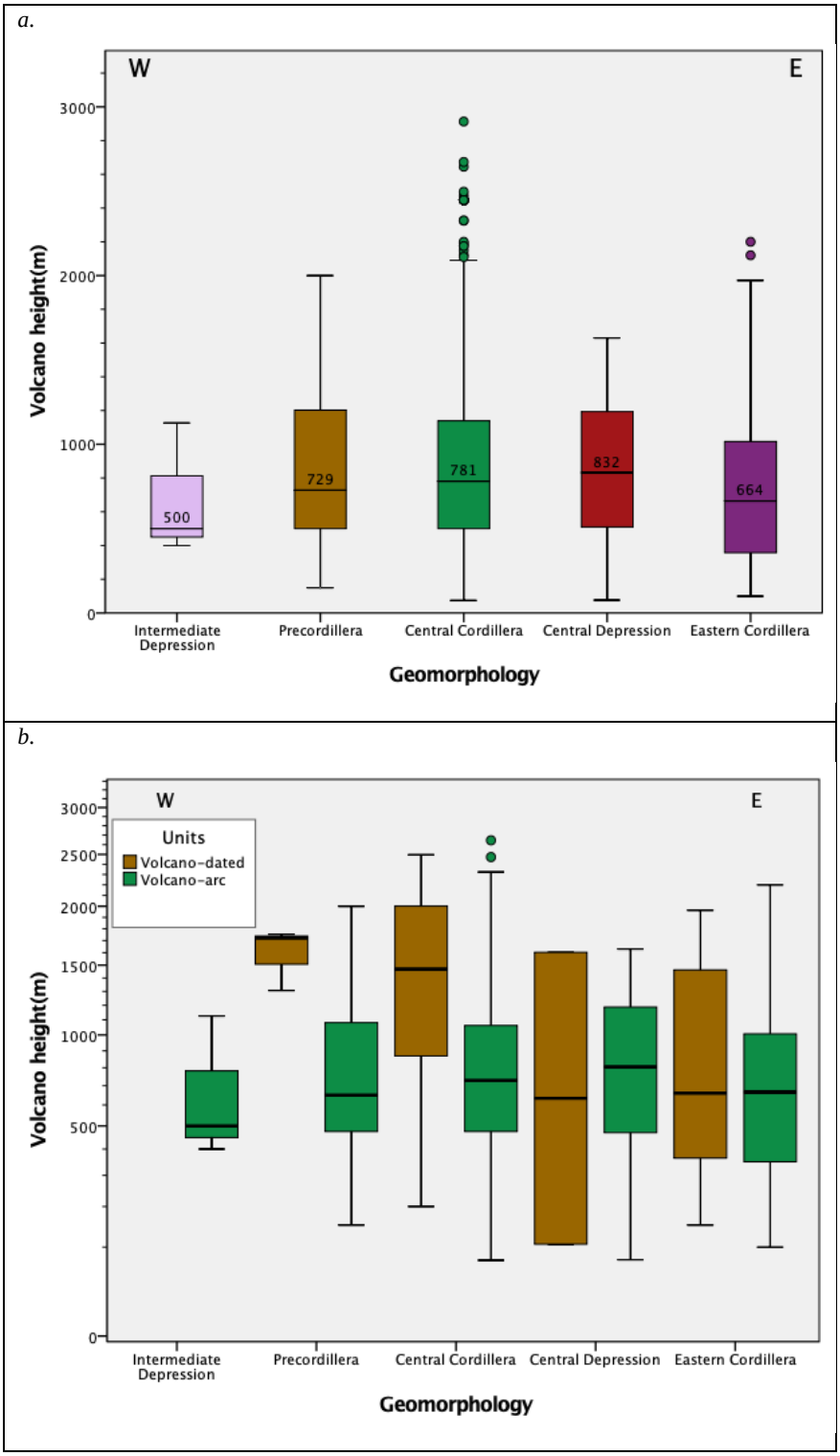


*Figure 4-9. Box whisker for Volcanic edifice heights classified by Geomorphological areas in the Andes, from west to east. Boxes represent the range of the 25$^{th}$ and 75$^{th}$ percentiles with the dividing line being the median. Whiskers represent the minimum and maximum values. Circles outside the boxes represent outliers (calculated as 25$^{th}$ and 75$^{th}$ percentile ± 1.5*interquartile range (25$^{th}$ percentile-75$^{th}$ percentile). a. The figure shows height ranges that characterise different morphotectonic regions in the Andes. b. This figure shows height ranges for different morphotectonic regions, but in*

*this case, it distinguishes between volcanoes that have been dated from the ones with an assigned age according to their location in the Andes.*

In order to define if there is any significant difference in volcanic edifice height between the different morphotectonic provinces, I perform a one-way ANOVA (analysis of variance) analysis in *SPSS statistic* software. The ANOVA analysis allow to compare the means of two or more independent (unrelated) groups and decide if they are similar to each other. In order to apply this analysis and obtain a valid result, it is required for the next six assumptions to be true: 1) the dependent variable is continuous; 2) the independent variables need to be: two or more categorical, independent groups; 3) no relationship between values in each group or between the groups themselves must exist (i.e., it is not allowed to use the same record for different groups); 4) significant outliers need to be eliminated; 5) the dependent variable should be approximately normally distributed for each category of the independent variable; 6) homogeneity of variances is required (Laerd Statistics, 2018).

For this analysis, I define *Volcano height* as the dependent variable and *Morphotectonic provinces* as the groups and then remove outliers, which are calculated following Equation 3-1and Equation 3-2.

There are 28 outliers in my database, (3 in Argentina, 1 in Bolivia, 2 in Colombia, 3 in Peru and 19 in Chile) with a range of heights between 2913m to 2110m. For the purpose of the ANOVA study, outliers are removed.

The results of the ANOVA test are shown in Table 4-12. The value that defines if there is a significant difference between the group means is *Sig* (also known as *p* value). If $p<0.05$, I reject the non-hypothesis that there is no difference between the mean of the groups (yellow box in Table 4-12). However, the ANOVA test does not tell us which groups are different from each other, it simply indicates there is a difference between at least two groups. Therefore, it is necessary to perform another analysis for multiple comparison between groups, which is called the *Tukey test.* The results are shown in Table 4-13. The first column (*(I) Morphotectonic provinces*) is the group being compared against the rest of the groups (second column). *Mean Difference (I-J)* column accounts for the mean difference between the groups that are being compared. Again, I use *p* values to detect if there is any significant difference between groups and the main ones are highlighted in yellow boxes: Central cordillera and Eastern cordillera; Eastern cordillera and Western Patagonia Cordillera.

*Table 4-12: ANOVA analysis for volcanic edifices height grouped by morphotectonic provinces.*

**Volcano height (m)**

| | Sum of Squares | df | Mean Square | F | Sig. |
|---|---|---|---|---|---|
| Between Groups | 3928093 | 5 | 785618 | 3.8 | .002 |
| Within Groups | 248157627 | 1203 | 206282 | | |
| Total | 252085721 | 1208 | | | |

*For Sig.<0.05, there is a statistically significant difference in the mean of heights between the morphotectonic provinces.*

*Table 4-13: Multiple comparisons for volcanic edifice height and Morphotectonic provinces, using the Tukey test.*

| (I) Morphotectonic provinces | (J) Morphotectonic provinces | Mean Difference (I-J) (m) | Std. Error (m) | Sig. | 95% Confidence Interval | |
|---|---|---|---|---|---|---|
| | | | | | Lower Bound (m) | Upper Bound (m) |
| Central Cordillera (1) | 2 | -1.278 | 70.910 | 1.000 | -203.68 | 201.12 |
| | 3 | 109.016* | 33.584 | .015 | 13.16 | 204.88 |
| | 4 | 154.296 | 262.663 | .992 | -595.43 | 904.02 |
| | 5 | -47.071 | 84.303 | .994 | -287.70 | 193.56 |
| | 6 | -373.971 | 144.427 | .101 | -786.21 | 38.27 |
| Central Depression (2) | 1 | 1.278 | 70.910 | 1.000 | -201.12 | 203.68 |
| | 3 | 110.294 | 75.460 | .689 | -105.09 | 325.68 |
| | 4 | 155.574 | 271.216 | .993 | -618.56 | 929.71 |
| | 5 | -45.793 | 108.043 | .998 | -354.18 | 262.60 |
| | 6 | -372.693 | 159.454 | .180 | -827.82 | 82.44 |
| Eastern Cordillera (3) | 1 | -109.016* | 33.584 | .015 | -204.88 | -13.16 |
| | 2 | -110.294 | 75.460 | .689 | -325.68 | 105.09 |
| | 4 | 45.280 | 263.927 | 1.000 | -708.05 | 798.61 |
| | 5 | -156.087 | 88.164 | .485 | -407.74 | 95.56 |
| | 6 | -482.987* | 146.714 | .013 | -901.76 | -64.22 |
| Intermediate Depression (4) | 1 | -154.296 | 262.663 | .992 | -904.02 | 595.43 |
| | 2 | -155.574 | 271.216 | .993 | -929.71 | 618.56 |
| | 3 | -45.280 | 263.927 | 1.000 | -798.61 | 708.05 |
| | 5 | -201.367 | 275.022 | .978 | -986.36 | 583.63 |
| | 6 | -528.267 | 298.980 | .488 | -1381.65 | 325.12 |
| Precordillera (5) | 1 | 47.071 | 84.303 | .994 | -193.56 | 287.70 |
| | 2 | 45.793 | 108.043 | .998 | -262.60 | 354.18 |
| | 3 | 156.087 | 88.164 | .485 | -95.56 | 407.74 |
| | 4 | 201.367 | 275.022 | .978 | -583.63 | 986.36 |
| | 6 | -326.900 | 165.844 | .360 | -800.27 | 146.47 |
| Western Patagonia Cordillera (6) | 1 | 373.971 | 144.427 | .101 | -38.27 | 786.21 |
| | 2 | 372.693 | 159.454 | .180 | -82.44 | 827.82 |
| | 3 | 482.987* | 146.714 | .013 | 64.22 | 901.76 |
| | 4 | 528.267 | 298.980 | .488 | -325.12 | 1381.65 |
| | 5 | 326.900 | 165.844 | .360 | -146.47 | 800.27 |

*For Sig.<0.05, there is a statistically significant difference in the mean of heights between the compared morphotectonic provinces.*

My dataset has only three volcanoes in the Intermediate Depression, and all are Cretaceous. Edifices located close to the current coastline, which are in the Intermediate depression and Precordillera, are considerably shorter (~300 m) in height than in other regions of the Andes. In contrast, edifices located in the Central Cordillera, show the greatest heights, elevation and frequency (Figure 4-10b).

*a.*

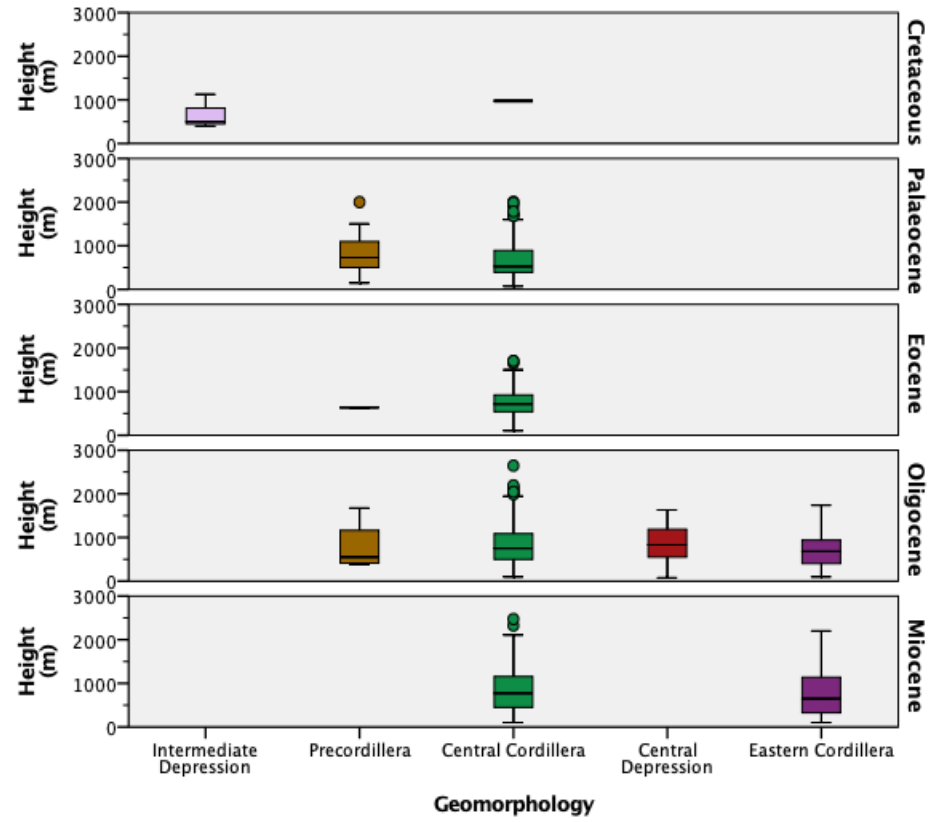
Height (m)
3000
2000
1000
0
Cretaceous
Palaeocene
Eocene
Oligocene
Miocene
Intermediate Depression
Precordillera
Central Cordillera
Central Depression
Eastern Cordillera
Geomorphology

*b.*

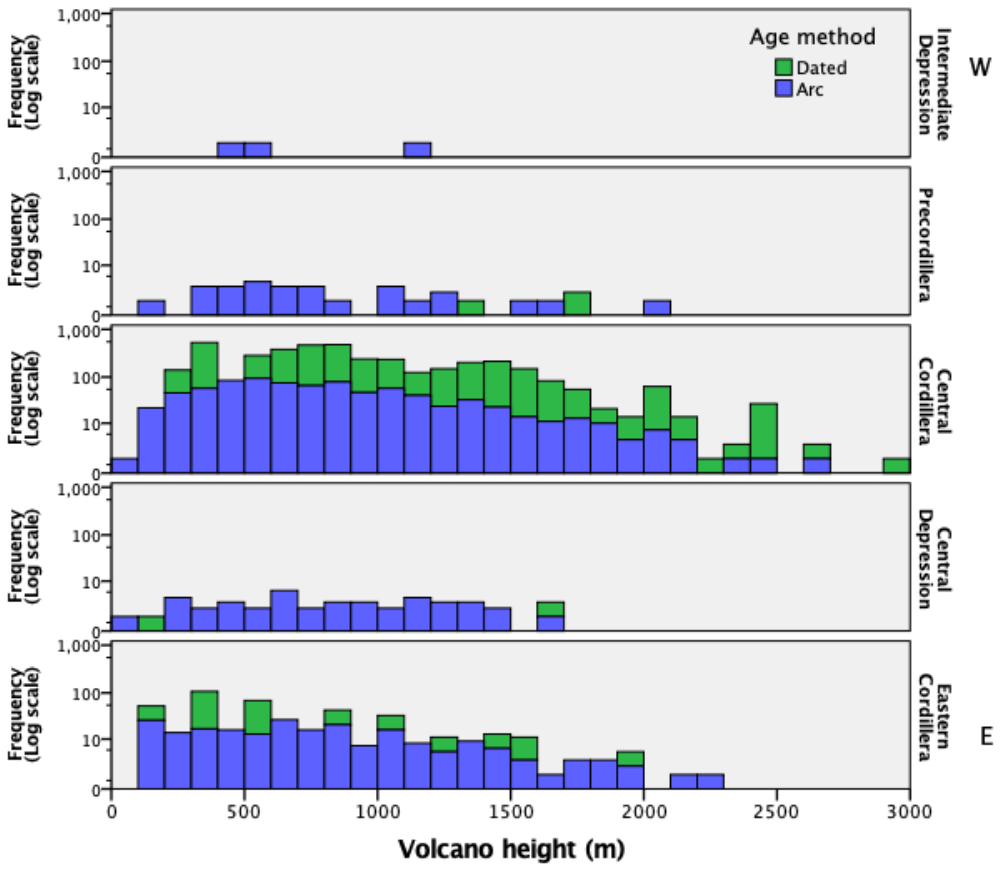
Frequency (Log scale)
1,000
100
10
0
Age method
Dated
Arc
Intermediate Depression
Precordillera
Central Cordillera
Central Depression
Eastern Cordillera
W
E
0
500
1000
1500
2000
2500
3000
Volcano height (m)

*Figure 4-10. a. Box whisker for Volcanic edifice heights classified by Epoch (right Y axis) and regions (X axis) in the Andes. Boxes represent the range of the 25th and 75th percentiles with the dividing line being the median. Whiskers represent the minimum and maximum values. Circles outside the boxes represent outliers (calculated as 25th and 75th percentile ± 1.5*interquartile range (25th percentile-75th percentile)). b. Histogram of volcanic edifice height classified by morphotectonic provinces.*

#### 4.3.7.2 *Volcano height variation according to their coordinate location: latitude, longitude and elevation*

I now compare volcanoes heights and PCDs against their location in the Andes. Figure 4-11 shows edifices height (m) against latitude and longitude, classified by dated economic deposits (PCD) and volcanoes (and its deposits) or with an assigned aged according to the arc where they are located.

On one hand Figure 4-11a, shows higher concentration of volcanoes between 28ºS to 15ºS and lower frequencies and decreasing height to the north. Edifices show a tendency of shorter heights in locations closer to the equator, which is expected due to more humid climate (Figure 4-14). Furthermore, in flat slab areas I see abundant PCDs and no volcanoes of any age.

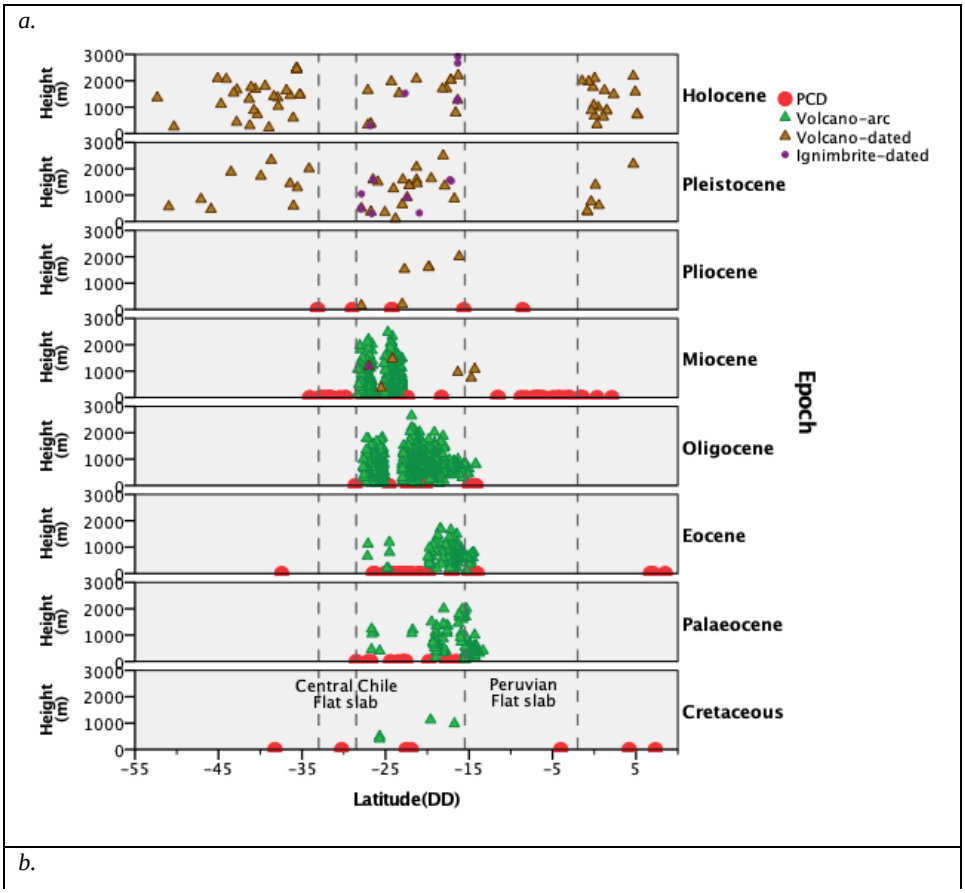

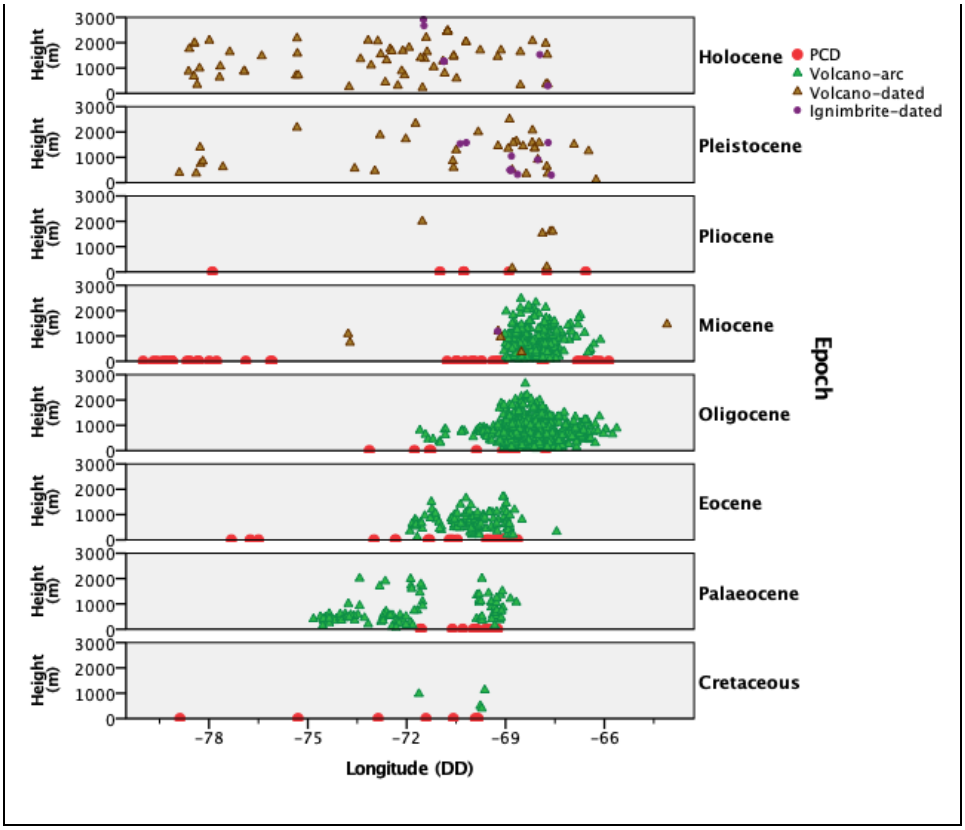


*Figure 4-11. Scatter plots of PCDs and volcanoes height values against a. Latitude (decimal degrees); b. Longitude (decimal degrees). For both plots, the data has been classified by time period, and dotted black lines represent flat slab areas (Central Chile and Peruvian) formed during Miocene times.*

Towards more extreme latitudes, pre-Holocene volcanoes are scattered and present at all altitudes, and have lower frequencies and decreasing height. Contrary to volcanic edifices, PCDs seem to concentrate closer to the Central Chile flat slab for Cretaceous and Palaeocene, expanding to the north up to Miocene times. Interestingly, for all the time epochs in the Peruvian flat slab area, the Miocene epoch (23-5 Ma) contains the biggest number of PCDs.

Holocene, Pleistocene and Pliocene edifices show the same behaviour as per latitude as in longitude (Figure 4-11b), a wide range of different elevation values (Figure 4-12) and an extensive variety of heights. Distinctively, only volcanoes younger than Miocene rise above 2000m height. Figure 4-11b clearly shows the eastern migration of the volcanic arc from Palaeocene to Miocene times.

Figure 4-12 shows edifice heights (m) and PCDs (assigned a height of 0m) against elevation above sea level classified by epochs. Elevation for volcanic edifices refers to the base of the edifices. For PCDs with no elevation values assigned by the source, elevation has been extracted from a DEM raster image.

Holocene, Pleistocene and Pliocene edifices, all have the same tendency, a wide range of elevation values and a wide height variability. Miocene and older volcanoes seem to show a trend of increasing elevation and height with time, but it could be an effect of spatial dispersion of the data and decreasing number of volcanoes the older they are.

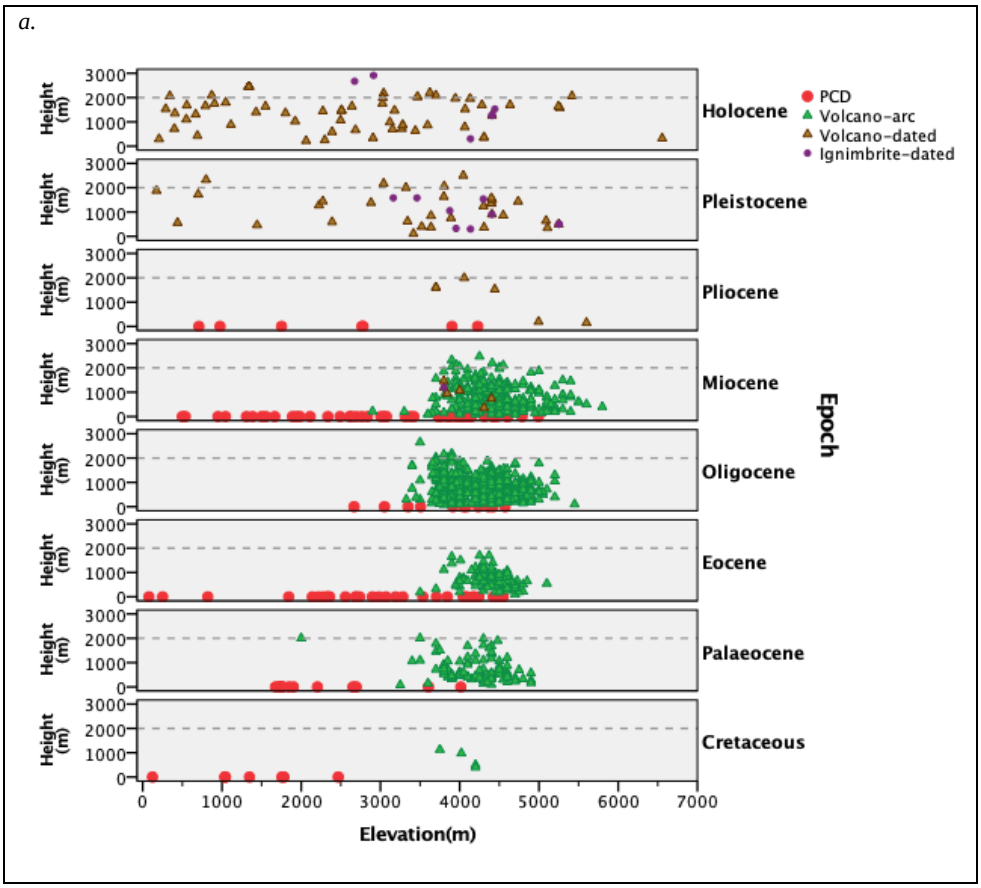


*Figure 4-12. Scatter plot for dated (brown triangle; purple circle) and non-dated (green triangle) volcanic edifice heights, dated PCDs (red circle) and elevation in metres above sea level (X axis), classified by Epoch (right Y axis). Dotted grey line marks 2000 m.a.s.l.*

#### *4.3.7.3 Volcanic edifices and PCDs trends according to their spatial location in time*

Figure 4-13 locates economic deposits and volcanic edifices registers in terms of Longitude (DD) and Elevation (m.a.s.l). Figure 4-13a distinguishes between epithermal deposits from different types of PCDs, for different time periods. It shows that the highest concentration of Mo-rich PCDs is located close to the Arica bend region. However, the distribution of economic deposit differs with epochs and regions. Main highlights are: (1) Palaeocene deposits show 2 main clusters, one in the Precordillera at around 2000m and the other cluster in the Central Cordillera, displaying increasing elevation to the east. (2) For the Eocene, Au, Cu-rich and Mo-rich porphyries are restricted to the East of the Arica bend and found in lower elevations than the ones in the Central Cordillera. In the Precordillera, the numbers of deposits drop considerably after the Eocene. While in Central Cordillera, PCDs are more scattered during all time periods, and there is a relative trend of reducing elevation eastwards. (3) During Oligocene times, in the Central Cordillera, as soon as I move further away from the Arica bend region, PCDs present the following sequence: epithermals, Cu-rich PCDs and Mo-rich PCDs. (4) Exactly opposed to what happened during the Miocene in the Central Cordillera. To the East of the Arica bend, epithermals are abundant and located in the higher altitudes, while

in the Arica bend area, Mo-rich PCDs converge. West of the Arica bend, another cluster another porphyry cluster occurs at around 80ºS.

*a.*

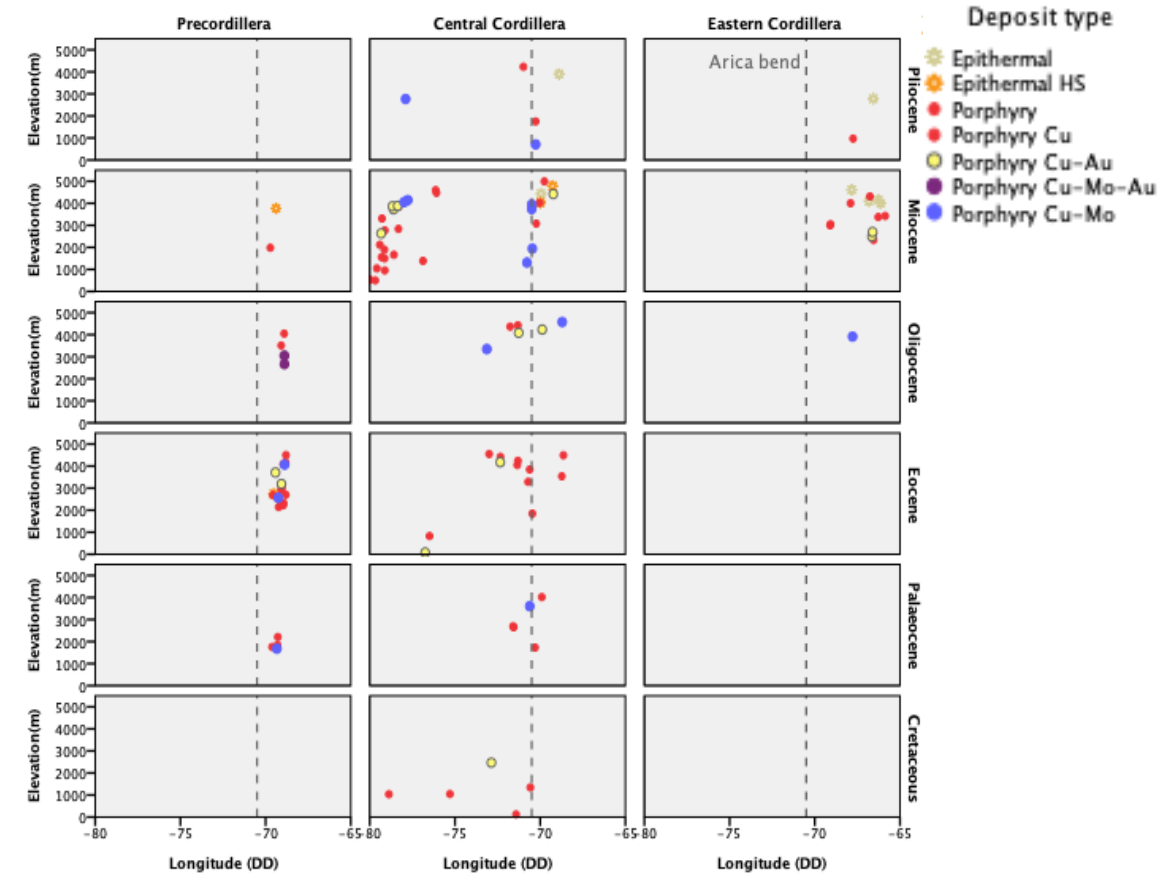


*b.*

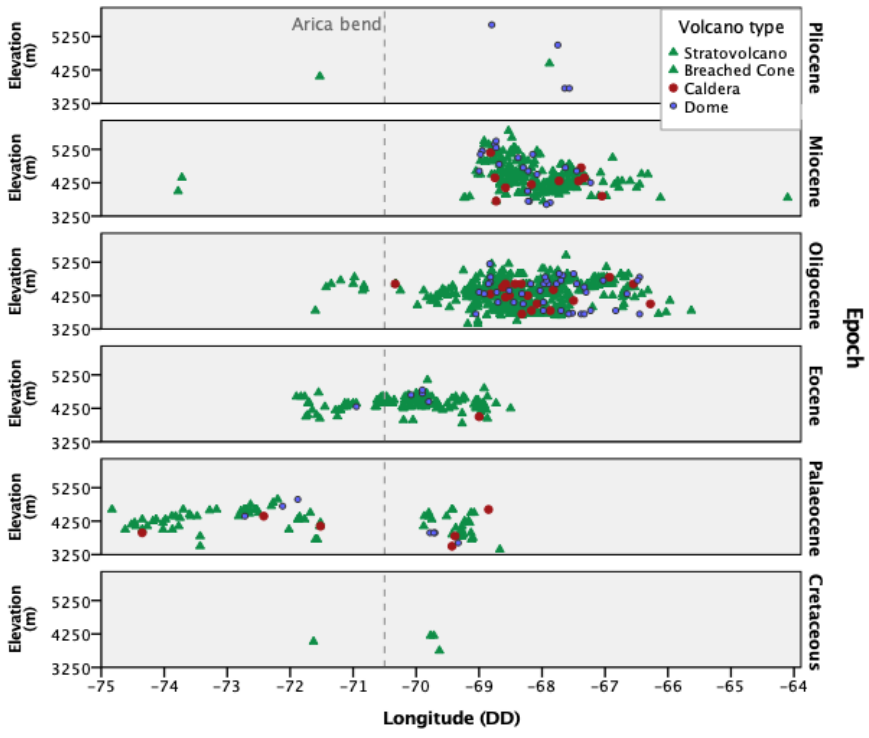

*Figure 4-13. a. Economic deposits classified by deposit type and geomorphologic regions where they are located. b. Volcanoes from Cretaceous to Pliocene time, showing elevation above current sea level against longitude. Dotted black line represent the location of the Arica inflexion*

### 4.3.8 Differential erosion related to climate

Figure 4-14a shows volcanic edifices heights (m) against annual precipitation, classified by climate affecting the region where those edifices are located. Climate is ordered by increasing humid conditions from left to right. There is a strong negative correlation between height and more humid climate (Figure 4-14a), that remains independent of time (Figure 4-14b). I can identify this correlation not only for present times but also during the Paleogene, and even before that. Additionally, if I focus on the height distribution it is possible to distinguish young Quaternary volcanoes from older ones. Such volcanoes are tall even in subtropical to tropical climate, while for the same climatic conditions, older edifices, prior to Pliocene times, have been completely eroded away (Figure 4-14b). Most of volcanic edifices in the dataset are stratovolcanoes, and in order to discard that the type of volcano is parameter that would affect the height of edifices with changing annual precipitation, I plotted them in a scatter plot that I decided not to show, due to no apparent trend in the plot.

*a.*

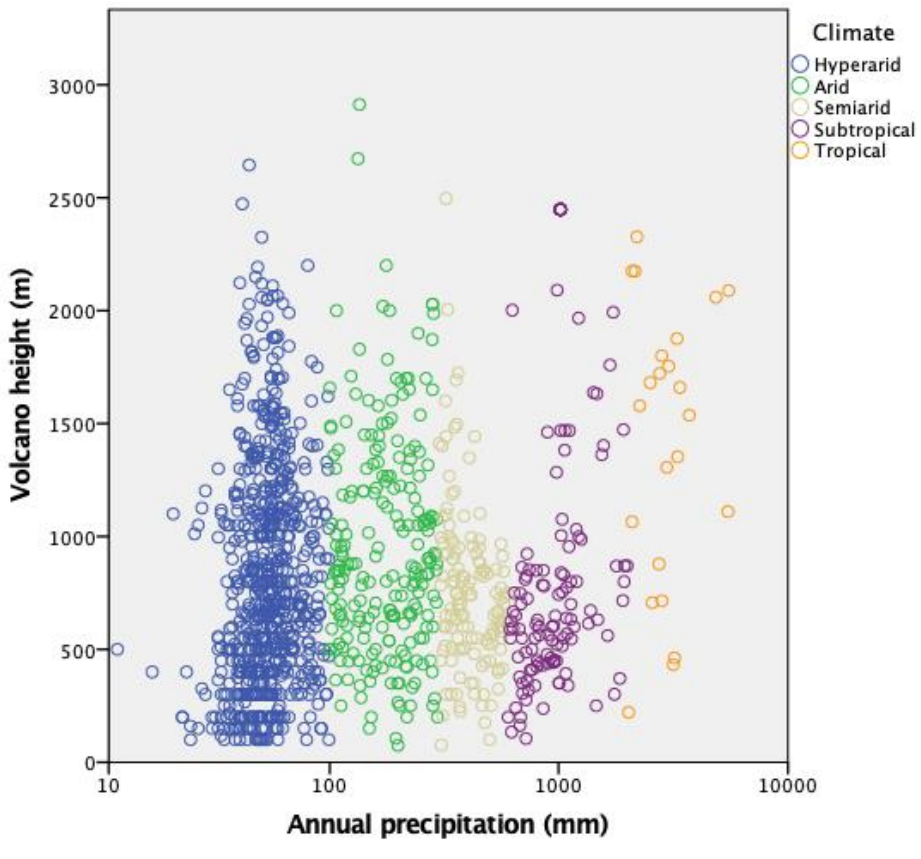


*b.*

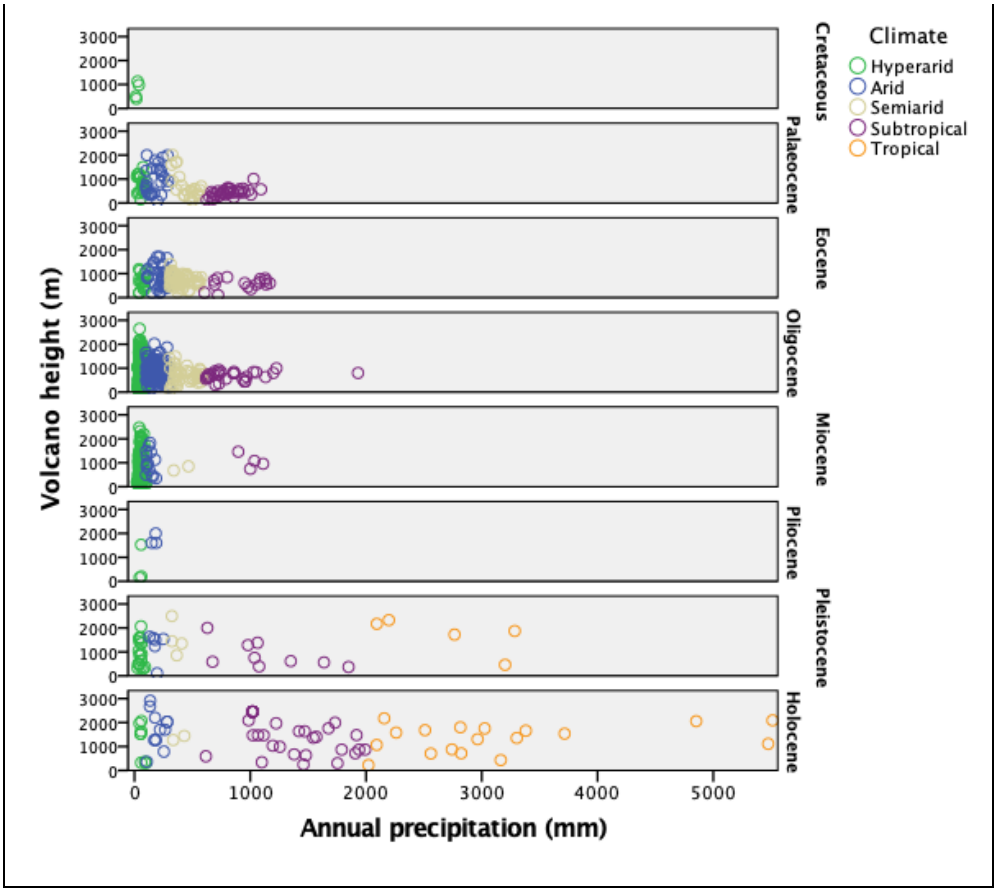


*Figure 4-14. a. Scatter plot for Volcanic edifice heights against Annual precipitation rate (mm) classified by Climate showing decreasing height with wetter climate. b. Scatter plot for Volcanic edifice heights against Annual precipitation rate (mm) for different time epochs.*

#### *4.3.8.1 PCDs and volcanic edifices frequency affected by climate, location and time*

Next, I analyse each magmatic arc, including volcanoes and porphyries of the same age in order to identify if there are any spatial and temporal relationships between them. I explore where in the magmatic belts, erosion rates are favourable for the exposure of PCDs. Depending on the erosion rates, different parts of the volcanic system will be exposed and, if I consider that porphyry deposits are part of the same magmatic system, I would expect to find PCDs located immediately under a volcano.

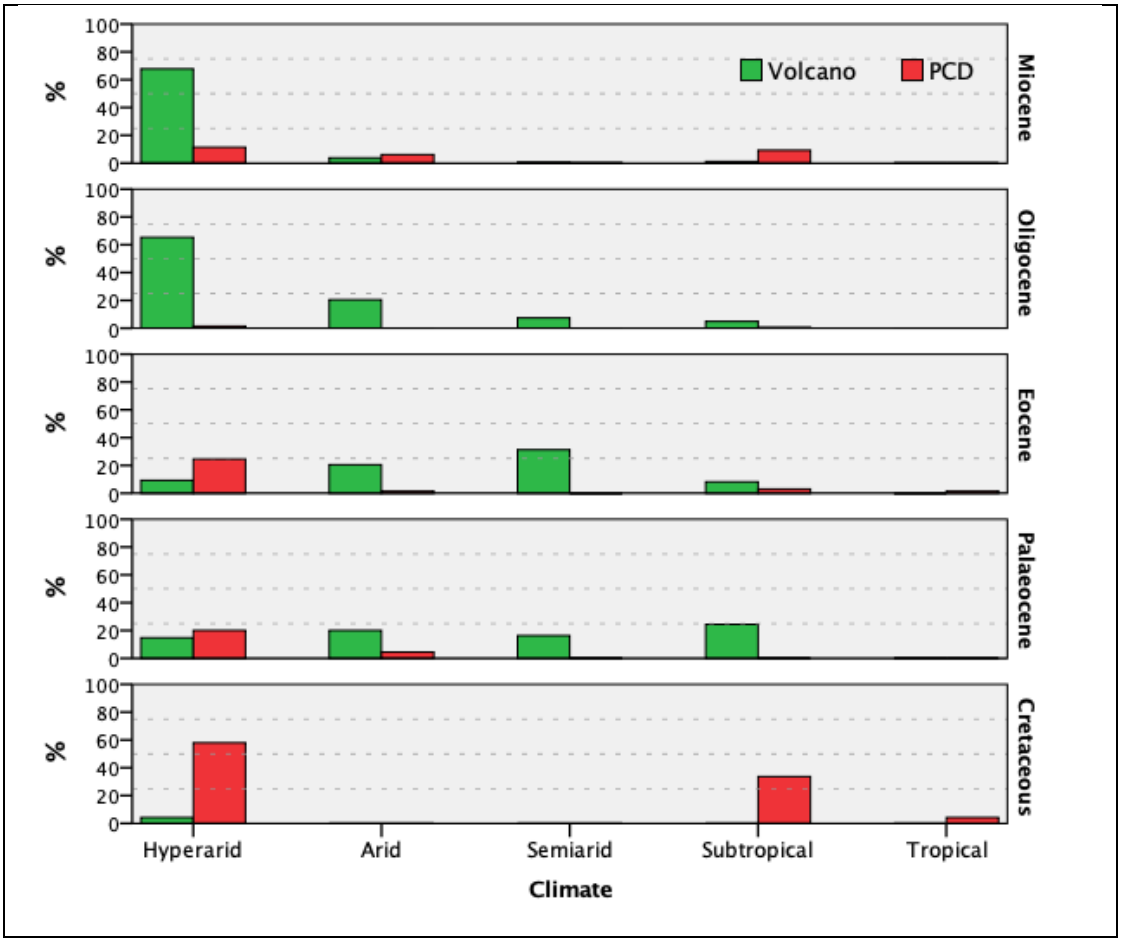


*Figure 4-15. Bar plot for volcanic edifices and PCDs against present climate (X axis) comparing units' percentages for defined time epochs. Each panel represents 100% total for the units (volcanoes + PCDs) present in that specific time period.*

Figure 4-15 compares the amount in percentage of volcanoes and PCDs against climate for specific time periods. Each panel contain a total of 100%, between volcanoes and PCDs, distributed between different climatic conditions. The Cretaceous is the epoch with the lowest number of volcanoes and the higher numbers of PCDs. Volcano quantity drops from hyperarid to subtropical conditions during Oligocene and Miocene contrary to the Palaeocene, which shows a rising number of volcanoes from hyperarid to tropical climate. In all time periods, there is a decline in the number of PCDs from hyperarid to semiarid climate, to then rise again in wetter conditions.

I want now to understand if any spatial control exists in the Andes, so I use Figure 4-15 and classify every time period by the morphotectonic regions in the Andes. Figure 4-16a shows the percentage of volcanoes and PCDs distributed in different morphotectonic provinces in the Andes, affected by different climatic conditions. I transform the sum of volcanoes and PCDs in each panel (specific time period and region in the Andes) into a 100% total in order to unravel tendencies in the data. Figure 4-16a is valuable because it allows us to compare what is the percentage of volcanoes in an area compared to the share of PCDs, while Figure 4-16b allows to see the number of those units.

In the Central Cordillera, there is a relative gradual increasing in volcano numbers from hyperarid to wetter climate in the Palaeocene and Eocene. However, volcanoes show the opposite tendency during Oligocene time, showing a drop in the number of volcanic edifices the wetter the climate. Similarly, volcanic edifices in the Eastern Cordillera decrease in number for wetter conditions, during the Oligocene and Miocene. The Intermediate depression and Precordillera account for the higher shares of PCDs from Cretaceous to Miocene compared to the volcanic edifices in those regions.

The Central Cordillera region has the greatest number of PCDs, 61, followed by Precordillera with 52 (Figure 4-16b). Particularly, for Palaeocene and Eocene, the Precordillera reports higher numbers of PCDs than other regions.

*a.*

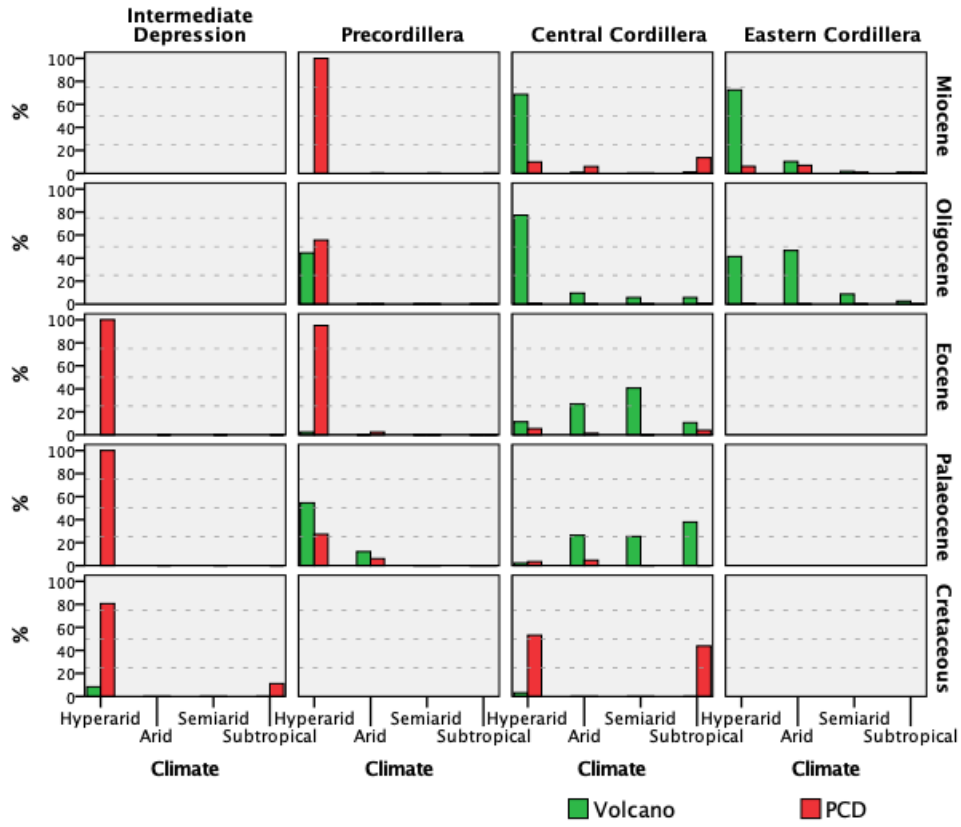


*b.*

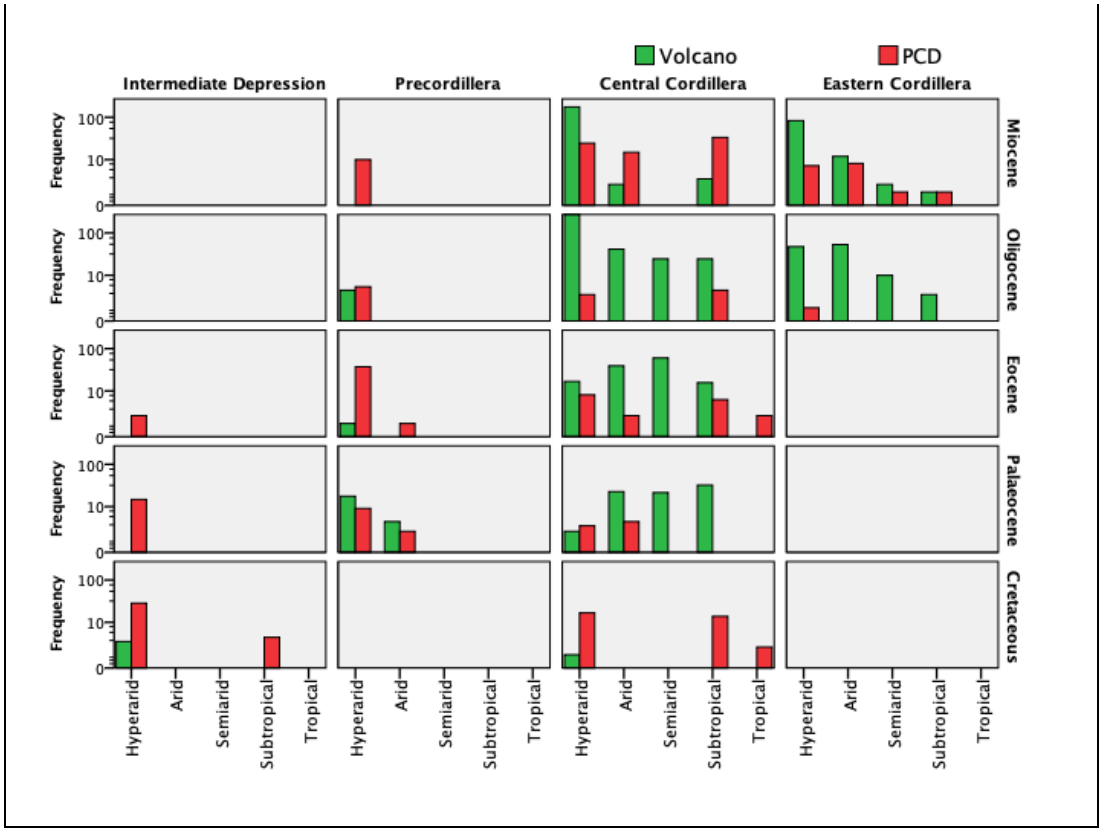


*Figure 4-16. a. Bar plot for volcanic edifices and PCDs against present climate (X axis) and Morphotectonic provinces and time epochs. a. Compares units' percentage, where each panel represents 100% total for the categories (volcanoes + PCDs) present in that specific time period. b. Bar plot showing frequency of volcanic edifices and PCDs against present climate (X axis) and Morphotectonic provinces for defined time epochs.*

## 4.4 Discussion

### 4.4.1 Spatial distribution of volcanoes and PCDs depending on time epochs

The Cretaceous arc contains the oldest volcanoes and PCD in my datasets. Cretaceous volcanoes have been almost striped away from the Andes and only 4 remain. They are the shortest edifices in the entire set, are found close to the current coastline (Intermediate depression and Precordillera) and sparsely distributed. Their frequency and spatial location suggest a combination of strong erosion rates in the west, in addition to a long period of exposure and degradation. The Andes is located at a continental margin that due to interaction and subduction between a continental and oceanic plate has undergone crustal thickening. In this environment, tectonic erosion is, probably the most relevant mechanism for continental mass loss into the mantle (Glodny et al., 2006). Several episodes of tectonic erosion occurred starting at the early Permian, possibly followed by a short-term tectonic erosion in the Late Cretaceous and another one since the late Miocene (Cande and Bangs, 1997). My results show that the Cretaceous volcanic arc, which corresponds to the western portion of the Coastal Cordillera, has suffered a significant width reduction, possibly due to tectonic erosion, and as a result the frequency of volcanoes along the arc is exceptionally low. Nevertheless,

I am not denying the fact that sediment coverage and time are immensely important factors in term of edifice exposure and conservation.

Palaeocene volcanoes are only found in Precordillera and Central Cordillera, while porphyries of the same age are also found in the Intermediate depression. This is the oldest epoch where I start to see spatial distribution patterns arising and I believe that climate and tectonic are the main factors playing a role in the conservation and distribution of these volcanic edifices. I found Palaeocene PCDs only in certain areas of the Andes (Figure 4-2), like the Precordillera, emerging mainly in the centre of the blocks defined by Sillitoe (1984), and aligning and concentrating according to different mineralization type (Mo-Cu porphyries are westwards in comparison to Cu-rich PCDs). This could be related to exhumated blocks, showing different levels of exposure, suggesting higher rates of erosion towards the centre of the blocks and closer to coastline or trench. Despite the fact I have not calculated erosion rates I can see a clear west-southern trend of increasing number of outcropping intrusive bodies (porphyries).

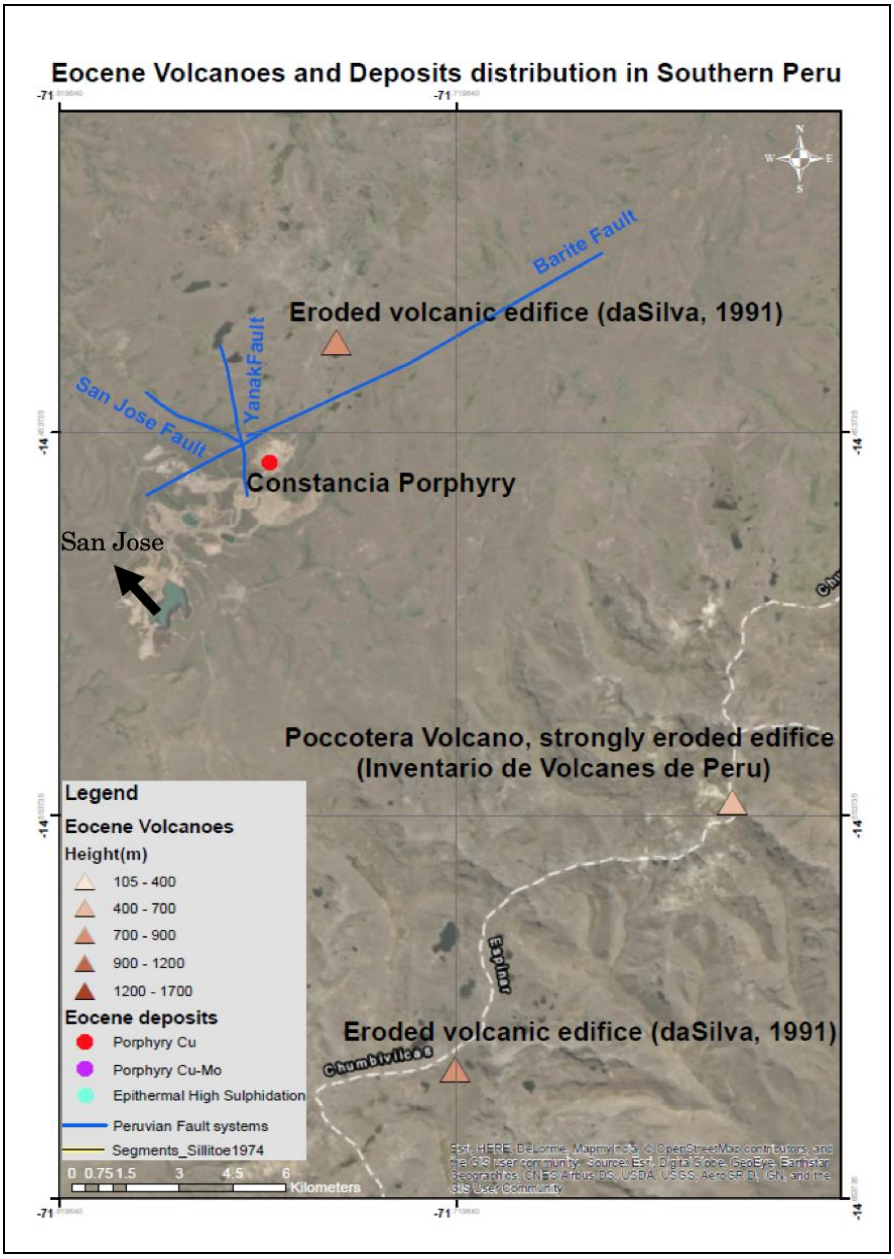

| Category | Tonnes | NSR Cut-Off | Cu (%) | Mo (g/t) | Ag (g/t) | Au (g/t) |
|---|---|---|---|---|---|---|
| Measured | 627,900,000 | ≥ $6.04 | 0.27 | 84 | 2.72 | 0.033 |
| Indicated | 253,700,000 | ≥ $6.04 | 0.21 | 61 | 2.38 | 0.034 |
| **Mea+Ind** | **881,600,000** | ≥ $6.04 | **0.25** | **77** | **2.62** | **0.033** |
| *Inferred* | *54,100,000* | ≥ $6.04 | *0.24* | *43* | *1.71* | *0.018* |

*Figure 4-17. Map of Constancia open pit mine showing three intensely eroded volcanic edifices in the surroundings and fault system affecting the deposit and information on reserves and resources (Hudbay internal report, 2017).*

Eocene volcanic edifice distribution is constrained to the Central Cordillera and only a few more in Precordillera with heights that oscillates between 1000-1500m (Figure 4-4). Whereas Eocene PCDs conglomerate on the Precordillera, just as seen in the Palaeocene data. Spatial trends remain the same as in the Palaeocene, but they become clearer for this period, showing some tectonic blocks suffered higher erosion rates, particularly westwards, displaying signs of higher exhumation rates. I see first epithermal deposits close to extremely eroded volcanic edifice remnants. From east to west, I find Cu PCDs first, and then Mo-Cu rich deposits. Sectors with epithermal deposits and volcanoes relics suggest that even though I am still able to recognise a volcanic cone, close to its roots. There is clear evidence than I am getting deeper into the magmatic system and extremely deep parts of these systems are now outcropping on the surface. In Figure 4-4 I use colour boxes to highlight this pattern. My results in terms of erosion and climate seem to match with several authors (Horton, 1999; Klein et al., 1999; Placzek et al., 2006; Benjamin et al., 1987; Masek et al., 1994; Gregory-Wodzicki, 2000). These authors suggest the existence of a north–south erosional gradient along the western Andean margin, characterised by increased precipitation rates northward of the Arica Bend region, dividing the low-erosion Altiplano–Puna plateau from the higher-erosion South Peruvian Cordillera.

Despite the similarities between time periods, I also need to consider that geology may change significantly locally. In Figure 4-5b, I highlighted in red rectangles areas with PCDs exposed and in yellow boxes regions with relatively short volcanic cones. They seem to intercalate, showing the presence of smaller blocks, probably with different rates of uplift and in consequence, different levels of erosion. Since climate in the area remained similar from Miocene times, it suggests there must be a tectonic component affecting the area locally and exposing deeper portions of the magmatic system onto the surface.

In Arequipa, southern Peru, two mineralised porphyries were recognised (Figure 4-5b): Constancia and San José. Constancia has deeper mineralization (up to 1200 m in the north-south direction and 800 m in the east-west direction (Hudbay internal report, 2017)) compared to San José, which occurs at surface.

Figure 4-6 shows the location of Constancia porphyry surrounded by 3 deeply eroded volcanic edifices and their heights in metres. It also indicates the direction of San Jose mine and the fault system, which is probably exposing this porphyry system on the surface. At the bottom of the figure, resources and reserves in tonnes for the Constancia deposit can be seen.

This is a simple, but clear example of how I could use eroded volcanic cones to constrain areas where I am more likely to find an enriched intrusive body, and also how important mapping local structures is, since they allow for these porphyries to get exposed and be in the vicinity of remaining volcanic edifices.

There are some particular regions in the Andes where erosion has been so high that volcanic edifices have been completed (or almost completely) eroded and maybe due to high exhumation rates, intrusive bodies are now outcropping. However, if a later intense sedimentation process occurred, it is possible that undiscovered porphyries lie underneath these surfaces. A good example of this is segment 7 (Figure 4-3b), where two Palaeocene Cu-porphyries have been discovered sitting between the remnant volcanic edifices and paleosurfaces defined by Evenstar et al. (2017).

In other areas of the Andes, uplift seems to be the main factor affecting the morphology of the region and actively exposing PCDs, i.e., Camarones river in northern Chile (Figure 4-3a) or between segment 4 and 5 in southern Peru (Figure 4-5b). Evidence of uplift are: (1) volcanic edifices becoming shorter close to main fluvial systems; (2) sharp incision by streams and rivers into gentle surfaces. In summary, active river systems assist the exposure of PCDs, particularly when they are hidden by thick cover, playing a strong role on the erosional processes in the region. Additionally, using those fluvial patterns and rivers abundance I can establish that a strong uplift component has affected the region. Conclusions for Evenstar et al. (2020) fit well with my results. They studied the Pacific Paleosurface (PPS) fluvial systems, which are deeply dissected (up to 1700 m.a.s.l) by five main rivers (Lluta, Azapa, Victor, Camarones and Tana) that drain to the

Pacific Ocean with a terminal base level of 0 m.a.s.l. According to Evenstar et al. (2020) the region that includes the Camarones river, has the highest rates of fluvial incision through time (ca. 200 to 100 m/Ma) and the constrains uplift of this region to a minimum of 1200 m in 11 My which supports Late Miocene uplift. From Miocene onwards, the spatial trend I have been observing between PCDs and volcanic edifices, where there is an increasing exhumation of economic deposits and deepening into the magmatic system with a southwest-westward direction, tends to disappear (Figure 4-12).

Pleistocene and Holocene volcanoes show a completely different distribution and heights compared to older volcanoes. Their distribution and preservation are remarkably good for all climate conditions, particularly in the Central Cordillera, showing a wide-ranging variety of heights.

### 4.4.2 Variation in edifice height depending on spatial location

#### *4.4.2.1 Height variation according to location within morphotectonic provinces*

According to Behr et al. (2018), in a subduction zone, the amount of sediment that ends up in the trench will control the speed and friction of the subducting slab. Certain erosion is expected to be generated in the western limit of the n plate, where, if sediment concentration is high enough and the slab sufficiently weak, the subduction process will be gentile and smooth. However, if these conditions change, with a decrease in the amount of sediment eroded on the continent, erosion rates in the interface between plates will dramatically escalate. Friction between plates will strip away portions of the continent and modify significantly the coastline and trench location. In consequence, this will end up migrating the coastline to the east by considerable distances (Hu et al., 2006). My dataset shows that Cretaceous edifices are located close to the current coastline, they have low frequencies and are rare in the Andes (Figure 4-9a). They are in

the Intermediate depression and are considerably shorter (~300 m) in height than younger edifices. There are only three Cretaceous edifices in my dataset, which is far fewer than in the other geomorphological regions of the Andes. This could suggest strong erosion in the west, probably due to subduction erosion, which would be responsible for stripping these volcanoes away. Because these are the oldest edifices in my dataset, a long-term erosion could also be the reason for these edifices showing such low numbers. Nonetheless, there has not been enough erosion to get rid of old edifices and so the lack of younger volcanoes in this region suggests there were never any young volcanoes in this region because the arc geometry has migrated to the east. However, due the low amount of data for Cretaceous time, it is extremely difficult to reach a satisfactory hypothesis.

In contrast, edifices located in the Central Cordillera, show the highest heights, elevations and frequency (Figure 4-10b). Pre-Miocene volcanoes were certainly affected by long-term erosion, while post- Miocene edifices were shaped by the combination of short-term erosion (Karátson et al., 2010), the uplift of the Altiplano region (e.g., Oncken et al., 2006) and the persistent hyperarid- arid climate since 15 My ago (e.g., Montgomery et al., 2001).

#### *4.4.2.2 Volcano height variation according to their coordinate location: latitude, longitude and elevation*

In this section, I compare volcanoes heights and PCDs against their location in the Andes, using coordinate but also their location within the morphotectonic provinces. It is worth having in mind that my dataset suffers from a strong bias in terms of Longitude. A total of 1106 of 1239 volcanoes with height data, are from a study in the Central Andes (Trumbull et al., 2006 and de Silva et al., 1991). Despite this, it is still possible to recognise the arc migration towards to the east from 40 My (Figure 4-11b).

My dataset contains over 360 dated economic deposit registers plus over 1200 volcanic edifices distributed in the Andes. I compared the relationship between these two portions of a magmatic system. Oncken et al. (2006) studied the variations in the volcanic influx for the southern Altiplano using the number of isotopically dated volcanoes. Despite the fact my dataset is different, my data show that volcanic edifices and PCDs increase in number significantly after 26 Ma. A clear correspondence with Oncken et al. (2006) results exists, where they show that magmatism is a well-established feature between the Upper Oligocene (33-26 Ma), that suffers a significant spatial expansion into the back-arc after Late Oligocene (26 Ma).

In flat slab areas, I see abundant PCDs and no volcanoes, either pre or post Miocene. It is expected not to find volcanic cones of Miocene and younger ages in flat slab areas, since volcanism and magmatism ceased during and after changes in the subduction angle (Hu et al., 2016; Yáñez et al., 2002; Espurt et al., 2009; Rosenbaum et al., 2005; Gutscher et al., 1999b). The absence of pre-Miocene volcanoes and some PCDs suggests that flat slab areas have suffered intensive erosion and exhumation, eroding older volcanic edifices and exposing porphyries on the surface.

Benjamin et al. (1987), Masek et al., (1994) and Gregory-Wodzicki (2000) suggest that outcropping intrusions at the northern and southern Andes imply deeper exhumation. My results show a high

concentration of economic deposits discovered in northern Chile and southern Peru. These deposits on the surface, located between the Peruvian and Central Chile flat slabs, are clear evidence of highly exhumated and eroded regions. The Miocene epoch in particular, show a great abundance of deposits in the Peruvian flat slab area that extends north of the equator, suggesting that specifically the region has suffered a substantial erosional process.

Some authors (e.g., Charrier et al., 2002; Farías, 2007) agree that between 33°S and 37°S, the volcanic arc basement comprises massive outcrops of Mesozoic to the Cenozoic volcano - sedimentary rocks, that was locally intruded by Mio–Pliocene plutons. This geological configuration strongly changes south of 38°S, with modern volcanoes growing directly on top of Meso–Cenozoic Patagonian Batholith. Estimations of Cenozoic regional exhumation rates in the area, show an intensification in the exhumation at 38°S, from <0,1 mm/year to the north, up to >1 mm/year to the south (Glodny et al., 2008). Moreover, Tassara and Yáñez (2003) estimated a significant drop in crustal thickness (50 km at 33°S to 35 km at 46°S), associated with a reduction in the average altitude of the main cordillera (5000 m to <2000 m). My results show that except for young volcanoes, volcanic edifices decrease in height in more extreme latitudes (>35ºS), where erosion rates are expected to be higher because glacial environment prevails (Montgomery et al. (2001)). Additionally, my data also shows that volcanoes decrease in height when I move closer to the tropics. This is also expected, since high erosional rates exist when the climate is more humid, but at least 2 orders of magnitude smaller than in latitudes over 35ºS (Figure 1-18b from Montgomery et al. (2001)).

In terms of altitude, Miocene and older volcanoes seem to show a trend of increasing elevation and height with time. Particularly for Miocene volcanoes, there are two feasible explanations: i) it could be an effect of spatial dispersion of the data and decreasing number of volcanoes the older they are; ii) another possibility is that around 15 My ago, after the development of the Altiplano, volcanoes started exploiting the elevation that this plateau already had in place, naturally growing in higher altitudes.

Young volcanoes, such as Pliocene to Holocene, are present at all latitudes and are characterised by a huge range of heights, probably representing edifices at different growing stages (i.e., the heights of young volcanoes are not dominantly related to erosion as in older volcanoes).

#### *4.4.2.3 Volcanic edifices and PCDs trends according to their spatial location in time*

Figure 4-13 locates economic deposits and volcanic edifices registers in terms of Longitude (DD) and Elevation (m.a.s.l). I plot the distribution of these eroded volcanoes in the Andes and compare them to deeper parts of the same system. My results back up my previous suggestions that the Arica bend divides the Andes from a low erosion region (Altiplano) to an intensely exhumated area (southern Peru). In fact, the highest concentration of Mo-rich PCDs is located close to the Arica bend region (Figure 4-13a). However, it seems that depending on the epoch and the region, the exhumation may have occurred differently. For the Palaeocene and the Eocene, the Precordillera region exhibits again evidence of greater exhumation rates compared to the Central Cordillera. For the Precordillera, economic porphyries are restricted to the east of the Arica bend, suggesting not only exhumation happened at a higher rate, but also erosional processes. If

this is true, I would expect to see a subsequent drop in the numbers of deposits, and it is exactly what occurs later in time. While in the Central Cordillera, PCDs are more scattered in terms of Longitude. Abundance of Mo-rich porphyries further away from the Arica bend region suggests of moving deeper into the crust. Au and Cu-rich PCDs occur closer to the Arica bend, indicating I am moving upwards in the magmatic system. This is contrary to the Miocene in the Central Cordillera, where porphyries show the following order: Mo-rich PCDs, then Cu-rich PCDs and epithermals when I move from the Arica bend region to the east. PCDs locate consistently in lower elevations compared to other regions in the Andes.

In summary, the Precordillera show signs of greater exhumation and erosion rates from Palaeocene to Oligocene times. The total number of PCDs remain high in the region, and the percentage of volcanoes lower when compared to other morphotectonic provinces.

The Arica bend region (70.5ºS) repetitively confirms an elevated number of porphyries, and the closer I get to the area the deeper into the crust I seem to move, finding more and more Mo-rich systems.

Da Silva (1989) states that at about 12-10 Ma, crustal thickening of the central Andes reached a maximum value of 70 km (Isacks, 1988), in response to tectonic shortening. This resulted in elevated geotherms which coincides with the timing of the ignimbrite flare-up in the Altiplano-Puna volcanic complex. Prior to the ignimbrite onset, volcanism had been dominantly andesitic, reflecting assimilation and fractional crystallization processes in ascending basaltic magmas (De Silva, 1989). The Altiplano-Puna complex model led us to think that if an increase in the volcanism in the CVZ occurred, then two scenarios would be recognised in my data from the Oligocene up to Miocene. The first one, would be a rise in the number of calderas and/ or the second, a reduction in the andesitic volcanism, meaning a drop in the number of stratovolcanoes. Unfortunately, there is no direct link between the Altiplano-Puna complex event and either the increase of calderas (or ignimbrites) or the drop in the number of stratovolcanoes from Oligocene to the Miocene in my data (Figure 4-13b).

### 4.4.3 Differential erosion related to climate

Karátson et al. (2010) established that volcanic edifice erosion is highly dependent on climate. They founded that precipitation and erosion is greatly correlated, and this correlation existed for a long-time span (>10Ma). Even though I have compared different parameters (height vs precipitation), my results show a similar correlation: height of volcanic edifices decreases in wetter climate.

Karátson et al. (2010) states that low erosion results, were mainly caused by the predominant and long-term arid climatic conditions, which may have been in operation since 10–15 My ago. I was able to expand this correlation back to Cretaceous times. These distinctive climatic conditions are responsible for preserving more than half of the total volume of volcanoes, even for the Miocene edifices (Karátson et al., 2012). Assuming that precipitation does not substantially affect the construction of volcanoes, and so the maximum height is reached, I suggest that a shorter edifice has been exposed to either intense humid climatic conditions

eroding the volcanic deposits away, or the edifice has been exposed to a long period of restricted erosion rates, or both. In essence, I could use volcanic cone height as a proxy for erosion rates and exposure time. Karátson et al. (2010) also suggest that because climatic conditions are the main factor affecting erosion, estimations for erosion rates in stratovolcanoes can also be applied to other volcano types. This hypothesis was tested with the AEDB and found to be correct in the Andes.

Karátson et al. (2011) suggest that during volcanic edifice formation, construction generally overcomes erosion at the final phase of edifice construction, and therefore, short-term erosion rates decrease with age. This means that modern volcanic edifices erode faster due to their unconsolidated deposits and steeper slopes, and surface denudation decelerates close to one tenth of normal rates, after a few My. My results show that Pleistocene and Holocene edifices display a diverse range of height values, from 300m up to >3000m. These younger volcanoes have not been affected by long-time exposure and they appear not to be significantly affected by climate, particularly Holocene edifices. The main reason may be that plenty of these young volcanoes might be still under construction.

#### *4.4.3.1 PCDs and volcanic edifices frequency affected by climate, location and time*

Overall, edifice heights drop with increasing humid conditions (Figure 4-14a), and this trend is seen in most time epochs. It is remarkable how frequency of volcanic edifices and PCDs varies with time and climate. It is reasonable that the number of volcanoes drops in wetter conditions and the numbers of mineralised deposits rise (Figure 4-16), since erosional processes are unroofing deeper portions of the magmatic system. However, during the Palaeocene and Eocene in Central Cordillera, the tendency seems to be the opposite (Figure 4-16a). A sensible explanation would be that volcanic activity and therefore volcanic edifices growth, developed in Central Cordillera more intensively than in other areas.

Whilst PCDs show a particular distribution, numbers grow from semiarid to tropical conditions while they reduce in quantity from hyperarid to semiarid. This leads us to believe there must be another process operating. When plotting these data in terms of location in the Andes, I see that Central Cordillera region accounts for the biggest number of PCDs for every epoch, but it is the Precordillera that contains a high proportion of PCDs relative to volcanic edifices. I believe this to be evidence that at least for the Palaeocene and Eocene, the Precordillera region exhibits greater exhumation rates compared to the Central Cordillera, exposing a bigger number of mineralised porphyries. My hypothesis fits well with exhumation data and tectonic studies of the Andes such as Allmendinger et al. (1997), Hartley et al. (2000), Garcia and Herail (2005), etc. The maximum elevation that the Precordillera has been able to reach is 4000 m (Hartley et al., 2000). Locally, this morphotectonic domain has been deformed into great wavelength anticlines and monoclines (Garcia and Herail, 2005; Van Zalinge et al., 2016a, 2016b). The Western Cordillera, located to the easternmost of the Precordillera, comprises a foreland fold and thrust belt, as well as the recent volcanic arc. Precordillera and Western Cordillera are active fault belts, with topographic highs and therefore, they are areas of active erosion. Contrary to the region now occupied by the Altiplano, between the Western Cordillera and Eastern Cordillera, which started as a backarc basin (Allmendinger et al., 1997) that since the

Late Cretaceous, it has been affected by uplift. Now, it is part of an internally drained basin infilled with Neogene to recent sedimentary and volcanic deposits (Lamb and Hoke, 1997). In summary, the Central Cordillera is an area where accumulation prevails, whereas both the Precordillera and Western Cordillera are areas of operating erosion. Finally, PCDs were preserved thanks to low erosion rates during and after Miocene times, due to climate change into hyperaridity.

Montgomery et al. (2001) suggests that a correlation exists between hypsometry and elevation, therefore is not possible for high topography to persist at high latitudes and that the high Andes finish at 35ºS in part because they intersect the perennial snowline at this latitude. For comparison, I use Montgomery et al. (2001) figure as base, plotting on top the distribution of my data. Edifice heights from my dataset correlate reasonably well with Montgomery et al. (2011) results. My findings reveal that volcanic edifices are not found in latitudes over 35ºS, probably because a rise in precipitation rates and erosion intensity are responsible of eroding volcanoes away.

*a.*

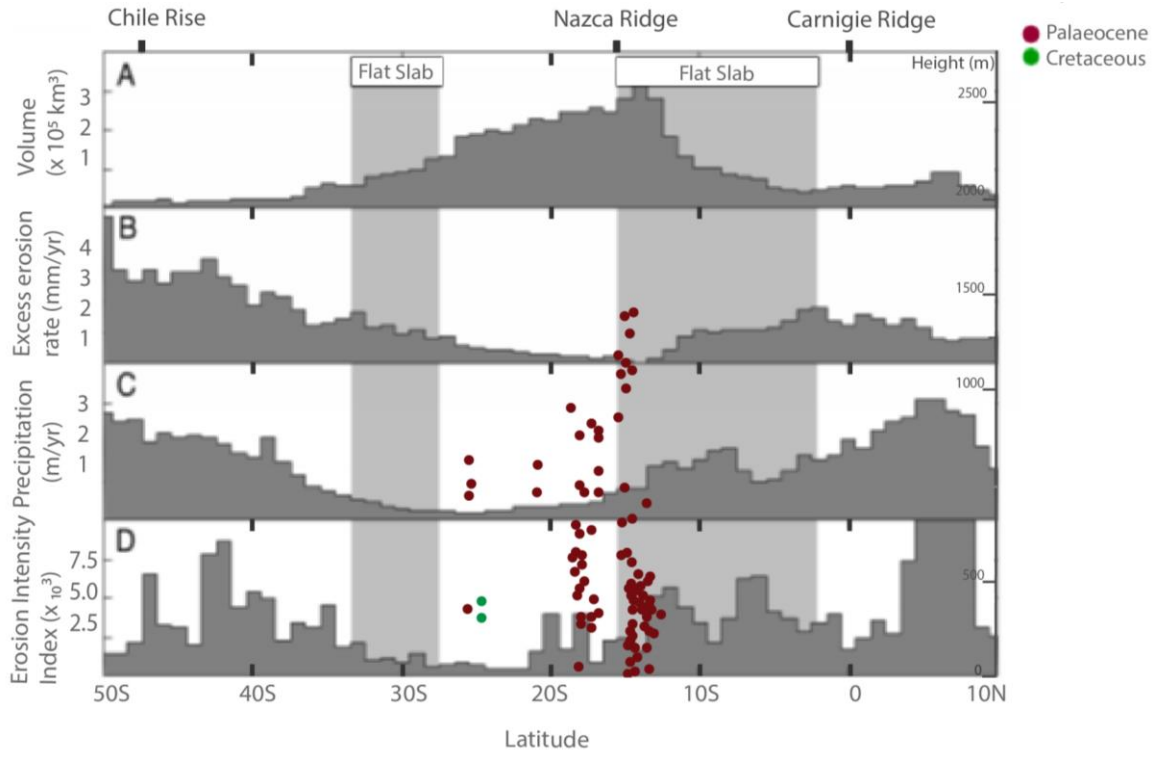


*b.*

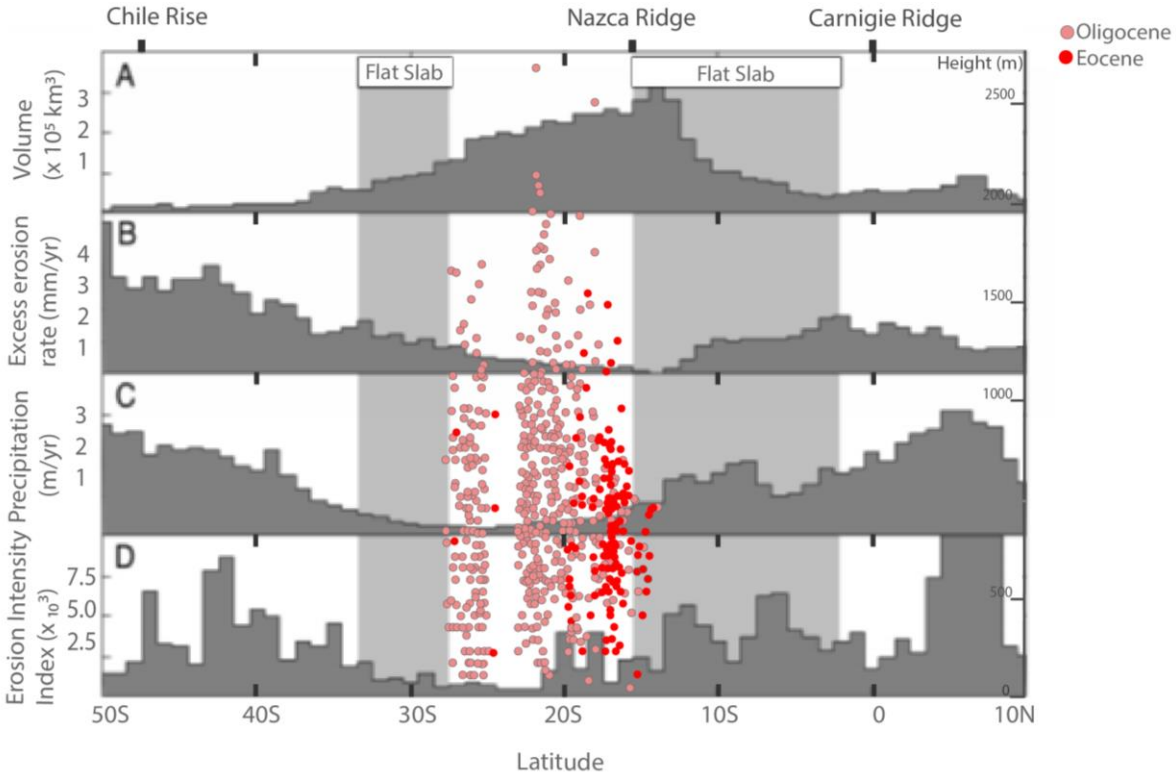


*Figure 4-18. Scatter plot for Volcanic edifice showing heights (right Y axis) against Latitude (m) (X axis), classified by Epoch (coloured dots). a. Cretaceous and Palaeocene volcanoes. b. Eocene and Oligocene volcanoes.*

*Figure in the background (grey) extracted from Montgomery et al. (2001). "A: Volume of Andes above sea level calculated from 1° latitude bins. B: Excess erosion rate, relative to largest 1° bin, is required to explain volume difference under uniform tectonic convergence. They calculated required latitudinal variation in erosion rates under constant tectonic convergence by calculating missing mass above sea level in each 1° latitude bin as VXSα/At, where VXS is excess volume in given bin compared to largest bin (14°–15°S), A is bin area, t is time (taken to be 25 My), and α=ρc/(ρm- ρc), where ρc= 2.7 g·cm-3 and ρc=3.3 g·cm-3. Note that because of selection of strictly east-trending bins for analysis, region between 13°S and 17°S, where range trends northwest rather than north, has anomalously large volume in each bin. C: Mean annual precipitation. D: Mean erosion intensity index value.", (Montgomery et al. 2001, p.581).*

*a.*

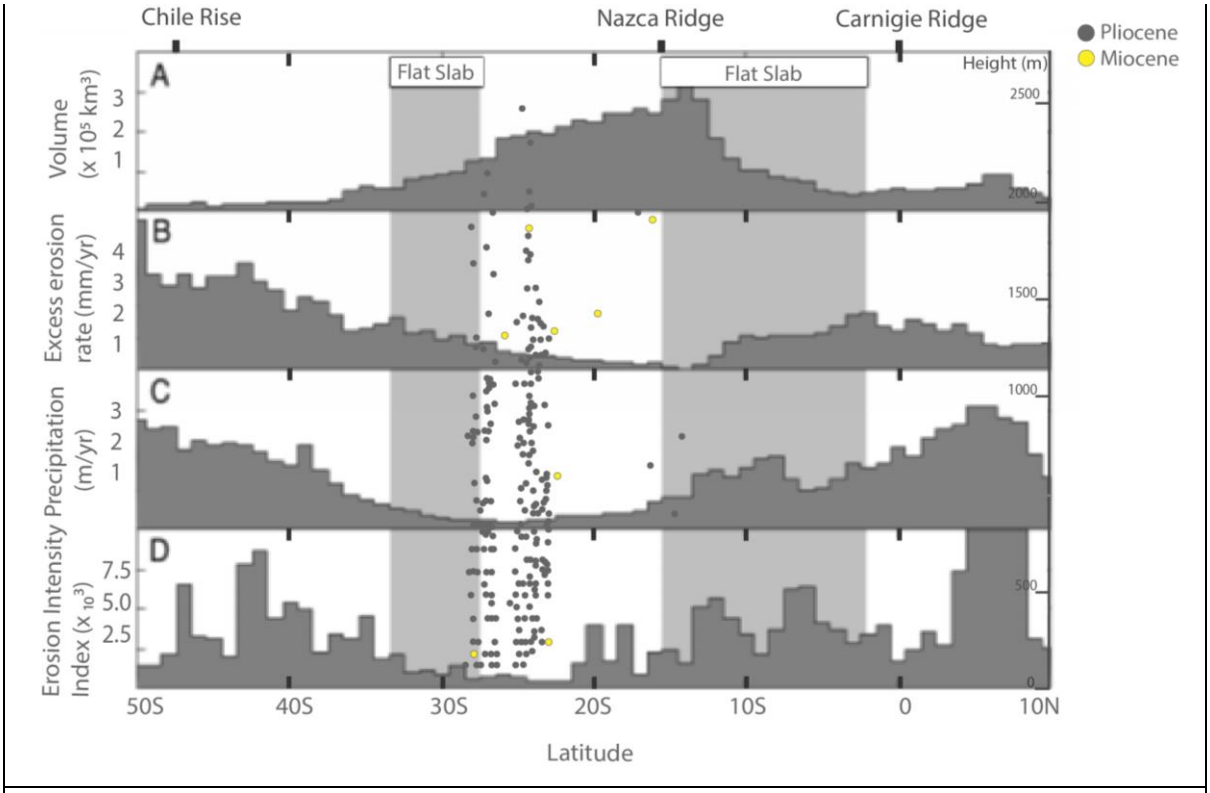


*b.*

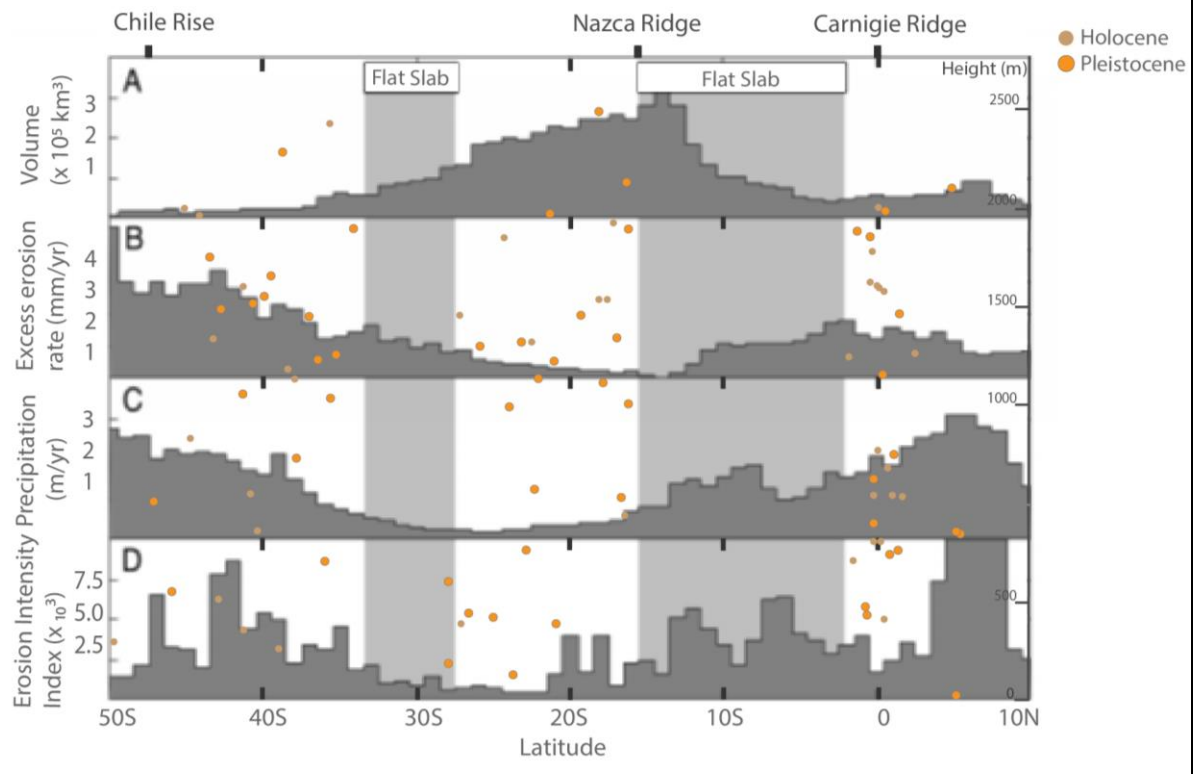


*Figure 4-19. Scatter plot for Volcanic edifice showing heights (right Y axis) against Latitude (m) (X axis), classified by Epoch (coloured dots). a. Miocene and Pliocene volcanoes. b. Holocene and Pleistocene volcanoes. Figure in in the background (grey) extracted from Montgomery et al., 2001 (for more details see Figure 4-18).*

## 4.5 Conclusions

I used volcanic edifice height to assess changes in the morphometry of volcanoes against climate, spatial location (altitude, longitude, elevation, regions in the Andes), erosion rates, tectonics, economic deposit type and finally, time. I use volcanic edifice height as a proxy for erosion rates and exposure time. I suggest that a shorter edifice has been exposed to either intense humid climatic conditions eroding volcanic deposits away, or the edifice has been exposed to a long period of restricted erosion rates, or both. The prior, assuming precipitation does not substantially affect the construction of volcanoes, and so the maximum height is reached.

My results in terms of volcanism and volcanic edifices show:

1. Erosion is highly dependent on climate, and there is a strong negative correlation between height and more humid climate for Pre-Quaternary edifices. This correspondence can be recognised during the Paleogene and even before that during the Cretaceous. This tendency is also independent of volcano edifice types. These results match with Karátson et al. (2010) conclusions that low erosion rates allow more than 50% of the original edifice volume to be conserved, even for Miocene edifices, as a result of the long-term arid climate which may have been in operation since 10-15 My ago, with the uplift of the Altiplano.
2. Young Quaternary volcanoes show different erosion-climate relation than older ones, because other processes affecting volcanic edifices are still in place. Some are very tall (>2200m) even in subtropical to tropical climates, while for the same climatic conditions, older edifices, prior to Pliocene times, have been completely eroded away. They are scattered along all latitudes, showing a variety of heights and growing in a wide range of elevations. Likely because they represent edifices under different growing stages being affected by high erosion rates because of their unconsolidated deposits and steeper slopes. If these new-born volcanic edifices were placed in high altitudes, they would be affected by modern erosion rates due to high precipitation.
3. Volcanic edifice height declines when precipitation rates and erosion intensity rise and correspondingly, the majority of volcanoes follow this tendency. Towards extreme latitudes (35$^{o}$S), volcanoes tend to be spatially scattered, show lower frequencies and a decreasing height. My findings convey with Montgomery et al. (2001) that is not likely that high topography can persist at high latitudes, due to the intersection of the perennial snowline.
4. Volcanoes close to the Chilean current coastline, in the Intermediate depression and Precordillera, are on average ~200m shorter than the ones located in Central Cordillera. The low number of volcanoes here compared to other places of the Andes, suggests a strong westward erosion increase.
5. The frequency of volcanoes along the Cretaceous volcanic arc are exceptionally low compared to other periods of time. Likely because tectonic erosion is that the Cretaceous volcanic arc has suffered a significant width reduction and the migration of the magmatism to the east.

The main findings in terms of economic deposits and enhanced exposure are:

1. There are an increasing number of outcropping economic deposits along the western Andean margin for Palaeocene up to Oligocene times. This trend is accentuated in the Arica Bend region, in Southern Peru, to the south of the Altiplano region and in the Precordillera. My results match with Horton (1999), who established the existence of a north–south erosion gradient along the west margin if the Andes, where high precipitation rates characterise northward of the Arica Bend region, dividing the low-erosion Altiplano–Puna plateau from the higher-erosion South Peruvian Cordillera.
2. The highest concentration of Mo-rich PCDs is located close to the Arica bend region. The Arica bend region (70.5ºS) has a relatively high number of porphyries, and the closer I get to the area the deeper into the crust I seem to move, finding more and more Mo-rich systems.
3. My results coincide with conclusions from Benjamin et al. (1987), Masek et al. (1994) and Gregory-Wodzicki (2000) suggesting that in the northern and southern Andes crystalline intrusion demonstrate deeper exhumation. A high concentration of economic deposits discovered are clear evidence of this highly eroded region, located between the Peruvian and Central Chile flat slabs, that particularly for Miocene PCDs, extends above the equator. The Peruvian flat slab area is the only region containing PCDs, which only belong to the Miocene epoch (23-5 Ma), while for Cretaceous and Palaeocene, PCDs concentrate closer to the Central Chile flat slab, expanding to the north up to Miocene times.
4. PCDs locate consistently in lower elevations compared to other regions in the Andes.
5. Tectonics play a major role in exposing PCDs in: (1) Precordillera, where intense reverse faulting in combination with high exhumation rates enhance the possibility of exposure; (2) southern Peru, where the Incapuquio fault system reveal economic deposits that develop in great depths next to well preserved volcanic edifices, and (3) major detachment scarps and material removal caused by rotational landslide, which again boost the chance of outcropping in the surface; (4) along the Chilean coastline, where tectonic erosion may be responsible of erasing any signs of Cretaceous arc (Cretaceous PCDs and volcanoes); (5) tectonic segments that isolate precisely areas with PCDs from the ones only with volcanoes, showing blocks exhumated into different levels.
6. There are no, or very few porphyries in sectors with high numbers of volcanoes, particularly in hyperarid an arid climate. Most porphyries seem to be are located preferentially: (1) in the centre of the segments defined by Sillitoe (1984), (2) in Precordillera and, (3) Mo-Cu porphyries are westwards in comparison to Cu-rich PCDs. This could be related to exhumated blocks, showing different levels of exposure, suggesting higher rates to centre of the blocks and closer to coastline.
7. As the number of pre-Pleistocene volcanoes drops with wetter conditions, the numbers of mineralised deposits rise, since erosional processes are unroofing deeper portions of the magmatic system. However, during the Palaeocene and Eocene in Central Cordillera, the tendency seems to

be the opposite. A sensible explanation would be that volcanic activity and therefore volcanic edifices growth, developed in Central Cordillera more intensely than in other areas.

8. For Palaeocene time, it is possible that undiscovered porphyries lie underneath paleosurfaces defined by Evenstar et al. (2017), particularly in the south of segment 7, where volcanic edifices have been completely eroded and some intrusive units are now outcropping. After the unroofing process during Palaeocene and Eocene, PCDs were preserved thanks to low erosion rates during and after Miocene times, due to climate change into hyperaridity.
9. Active river systems assist the exposure of PCDs, particularly if they are buried by a thick cover, either sedimentary or volcanic. If PCDs were covered by volcanic edifices, fluvial system would work as seen in the Camarones river region, decreasing height in volcanoes closer to rivers. Additionally, if the sector has also been affected by uplift, streams and rivers will create sharp incisions into gentle surfaces, facilitating the exposure of PCDs. Conclusions for Evenstar et al. (2020) fit very well with my results.

The Precordillera region exposes the most productive economic deposits in Chile and I suggest:

1. Longitudinal Valley and Precordillera development are the only regions experiencing extreme erosion while still growing. Since this feature is a unique characteristic of the region, it may have important implications for PCD exposure.
2. The Precordillera exhibits signs of greater exhumation and erosion rates compared to the Central Cordillera from Palaeocene to Oligocene times. I use PCDs, Au and Cu-rich porphyries as well as a deeper Mo-rich porphyry, particularly for the Eocene. These systems are restricted to the east of the Arica bend and found in lower elevations, suggesting that not only did exhumation happen at a higher rate, but also erosional processes. This is consistent with the subsequent drop in the numbers of deposits in this region. In contrast, PCDs in the Central Cordillera are more scattered and there is a relative trend of reducing elevation eastwards.
3. The Precordillera suffered high shortening rates, particularly during Palaeocene- Oligocene (Oncken et al., 2006), and the Eocene is a period of shortening within the arc (Incaic orogeny), with rapid formation of relief and with equally rapid erosion. Surprisingly, the Precordillera is the only region in the Andes involving this kind of intensity at the same time. I consider the prominent number of Eocene PCDs in the Precordillera to be evidence of this great exhumation process, combined with the intense reverse faulting in this elongated portion of the Andes, due to distinct compressive regimes. Another indication are abundant barren intrusive units of the same age are outcropping in the region (Dahlström unpublished).

# 5 Chapter 5: Summary and further work

In this study, I created 3 datasets. The largest, the Andean Volcanoes and Eruption Database (AVEDB), compiles volcanic edifices and eruptions in the Andes, in South America. It includes 5477 registers, which I use in an exploratory data analysis (EDA) in Chapter 2 to summarise their main characteristics and trends. I used *SPSS Statistics* software for the statistical analysis and chart creation. Additionally, I extracted a subset of 1239 volcanoes with edifice height values and assessed how volcanic edifices vary with: i) time, ii) volcano types, iii) climate conditions and iv) regions in the Andes (morphotectonic provinces). In order to make accurate comparisons between these groups and detect if there is a significant difference, I performed *ANOVA* and *Tukey* tests.

The second set of data, the Ignimbrite and Intrusive Database (IIDB), accounts for 2373 ignimbrite and intrusive samples. These data have not been used for any analysis in this thesis but present an opportunity for future studies.

The third set, designated as Porphyry Copper Deposits Database (PCDsDB), describes 593 mineralised deposits, such as Au, Cu and Mo enriched porphyries and epithermal deposits. I plotted the PCDsDB and AVEDB during relevant time periods in terms of copper fertility (Palaeocene, Eocene, Oligocene and Miocene). I differentiated between diverse types of mineralization within PCDs and epithermal deposits. Since they develop at different depths and I identified different levels of erosion and exposure in the Andes. Finally, I created maps in ArcGIS to identify patterns in the spatial distribution of edifices and PCDs for specific time periods.

My findings are valuable for exploration, demonstrating how the distribution and heights of volcanoes can be used as a rigorous methodology to recognise different levels of exhumation in different areas of the Andes and identifying the shallowest sectors for further exploration.

My model is powerful for indicating the most promising areas for finding PCDs close to the surface. It also qualitatively indicates differential erosion proportions and levels of exhumation and exposure for different tectonic blocks, identifies regional erosional trends by using volcanic edifices and PCDs with different mineralization types as a proxy, as well as changing climate conditions. For volcanoes, I use height as the main parameter, but I could add other dimensional constraints to assess the degree of erosion. Edifice height is easy to measure using tools such as Google Maps and does not require any field work during the statistical study, making it a low-cost technique and with easy application. Field work is recommended to provide more detailed evidence and test my hypotheses.

If other researchers would like to use this methodology, first they would need to select an area of regional scale. The second step is to do an extensive regional compilation of the geology, including lithology, geomorphology, structures, etc. After that, and most important, it is necessary to identify volcanic edifices and spatially locate them. Next comes the process of gathering information for volcanic edifices, such as eruption ages, volcano type, etc. The third step would be to measure volcanic edifices dimensions (height, crater, deposit diameter, etc). The fourth stage is collecting the information related to PCDs, such as ages, location, and in particular, different porphyries classified by mineralization. The fifth stage is to do an extensive investigation on the climate and major scale tectonics affecting the regions where volcanoes and

PCDs are. It is also important to look for local tectonic and structural trends, which could condition the exhumation and exposure of PCD. After all the information has been gathered and a quality control has been done, now is necessary to spatially plot the information in order to find patterns. On this stage, volcano age, the height and shape of volcanoes, age and mineralization type of PCDs, as well as structural domains, will indicate if regional erosion trends exist or if there are differences on the exhumation of tectonic blocks (Figure 4-4). Locally, it is essential to focus on the geomorphology, which plays a major role exposing or covering mineralised units in small- scale regions. Finally, using scatter plots, bar plots and statical analysis it is possible to understand the impact that climate and location may have on the erosion of volcanoes and PCDs conservation. After applying this method, the researcher should be able to select small to medium-scale areas and recommend them for further exploration. From an enormous territory such as the Andes, at the end of this study, I was able to select the Precordillera and the Arica bend region (Figure 4-13) as medium-scale prospective sectors, and small- scale areas, for specific time periods, in southern Peru (Figure 4-5) and Central Cordillera (Figure 4-2) for targeting porphyries close the surface. I was also able to indicate the conditions where the uncovering of PCDs was more likely, such as volcanoes close to fluvial systems in regions affected by tectonic exhumation and drier climates (Figure 4-3a; Figure 1-26) or places with strong structural controls and wet climates, where rotational slides where possible (Figure 1-21; Figure 1-26).

This analysis is designed and intended to be applied in exploration for epithermal deposits, Au, Cu mineralized body and Cu-Mo porphyries. However, this methodology does not distinguish enriched from barren porphyries, nor detect the intensity of the mineralization. Additionally, the datasets created in this thesis are a valuable source of information for future research by scientists from a range of fields. Economic geologists, volcanologists, climatologists and geomorphologists, and in particular for those looking to study the links between these subjects can take a huge advantage of the compilation created here.

There is plenty of potential for using both volcanoes and PCDs datasets in the future. For example, assessing the completeness of the PCDsDB and understanding how quickly PCDs tend to disappear from the geological archive. Further detailed study of volcanic edifices is also recommended, in order to obtain specific erosion rates per region and make more accurate predictions in terms of prospectivity and shallower areas to be explored. My technique can be complemented by thermometry to identify outcropping of intrusions that formed during fertile periods of time and improve understanding of the structural controls of the studied sectors, since PCDs are likely to be eroded or uncovered, unless they were selectively protected by faulting and differential uplift.

Additionally, the IIDB could be used for identifying areas that were part of an ignimbrite flare-up and discard them as potential places and times to find mineralised porphyries. These regions, for a constrained time window, suffered the development of calderas, a volcanic style that suppresses porphyry Cu formation because the all-important Cu-bearing magmatic fluids would be explosively discharged during silicic ignimbrite eruption and lost to the atmosphere (Sillitoe, 2018).

In conclusion, I have a developed a regional qualitative exploration tool that could be applied to other volcanic arcs beyond the Andes, into different tectonic conditions. A good place to apply it would be Japan

and South Korea, in the Pacific Rim. It could also be useful to different time windows, depending when the mineralization has occurred.

# 6 References


Aiuppa, A., Dongarrà, G., Valenza, M., Federico, C. & Pecoraino, G., 2003, in Volcanism and the Earth's Atmosphere Vol. 139, eds A. Robock & C. Oppenheimer, pp.41–54, American Geophysical Union, Washington DC.

Allard, P., Aiuppa, A., Loyer, H., Carrot, F., Gaudry, A., Pinte, G., Michel, A. and Dongarrà, G., 2000. Acid gas and metal emission rates during long-lived basalt degassing at Stromboli volcano. Geophysical Research Letters, 27(8), pp.1207-1210.

Allmendinger, R.W., Jordan, T.E., Kay, S.M., Isacks, B.L., 1997. The evolution of the Altiplano-Puna plateau of the Central Andes. Annu. Rev. Earth Planet. Sci. 25, 139–174.

Alpers, C.N. and Brimhall, G.H., 1988. Middle Miocene climatic change in the Atacama Desert, northern Chile: Evidence from supergene mineralization at La Escondida. Geological Society of America Bulletin, 100(10), pp.1640-1656.

Armijo, R., Lacassin, R., Coudurier-Curveur, A. and Carrizo, D., 2015. Coupled tectonic evolution of Andean orogeny and global climate. Earth-Science Reviews, 143, pp.1-35.

Arriagada, C., Roperch, P., Mpodozis, C. and Cobbold, P.R., 2008. Paleogene building of the Bolivian Orocline: Tectonic restoration of the central Andes in 2-D map view. Tectonics, 27(6).

Audétat, A., 2010. Source and evolution of molybdenum in the porphyry Mo (–Nb) deposit at Cave Peak, Texas. Journal of Petrology, 51(8), pp.1739-1760.

Bangs, N.L. and Cande, S.C., 1997. Episodic development of a convergent margin inferred from structures and processes along the southern Chile margin. Tectonics, 16(3), pp.489-503.

Barke, R., Lamb, S., 2006. Late Cenozoic uplift of the Eastern Cordillera, Bolivian Andes. Earth Planet. Sci. Lett. 249 (3–4), 350–367.

Barnes, J.B., Ehlers, T.A., 2009. End member models for Andean Plateau uplift. Earth Sci. Rev. 97 (1–4), 105–132.

Barr, D.A., Fox, P.E., Northcote, K.E. and Preto, V.A., 1976. The alkaline suite porphyry deposits: A summary. Canadian Institute of Mining and Metallurgy, 15, pp.359-367.

Barreiro, B.A. ed., 1984. Andean magmatism: chemical and isotopic constraints. Birkhäuser Boston.

Beck, S.L., Zandt, G., Myers, S.C., Wallace, T.C., Silver, P.G., Drake, L., 1996. Crustal-thickness variations in the Central Andes. Geology 24 (5), 407–410.

Behr, W.M. and Becker, T.W., 2018. Sediment control on subduction plate speeds. Earth and Planetary Science Letters, 502, pp.166-173.

Benjamin, M.T., Johnson, N.M., and Naeser, C.W., 1987, Recent rapid uplift in the Bolivian Andes: Evidence from fission-track dating: Geology, v. 15, p. 680–683.

BHP Copper Exploration 2017, BHP ArcGIS database extraction, BHP Billiton, Unpublished.

Birchfield, G.E. and Wertman, J., 1983. Topography, albedo-temperature feedback, and climate sensitivity. Science, 219(4582), pp.284-285.

Brandmeier, M., 2014. A remote sensing and geospatial statistical approach to understanding distribution and evolution of ignimbrites in the Central Andes with a focus on Southern Peru.

Brasse, H., Lezaeta, P., Rath, V., Schwalenberg, K., Soyer, W., Haak, V., 2002. The Bolivian altiplano conductivity anomaly. Journal of Geophysical Research: Solid Earth (1978–2012) 107 (B5), EPM 4-1-EPM 4-14.

Braxton, D.P., Cooke, D.R., Dunlap, J., Norman, M., Reiners, P., Stein, H. and Waters, P., 2012. From crucible to graben in 2.3 Ma: A high-resolution geochronological study of porphyry life cycles, Boyongan-Bayugo copper-gold deposits, Philippines. Geology, 40(5), pp.471-474.

Brown, S.K., Crosweller, H.S., Sparks, R.S.J., Cottrell, E., Deligne, N.I., Guerrero, N.O., Hobbs, L., Kiyosugi, K., Loughlin, S.C., Siebert, L. and Takarada, S., 2014. Characterisation of the Quaternary eruption record: analysis of the Large Magnitude Explosive Volcanic

Eruptions (LaMEVE) database. Journal of Applied Volcanology, 3(1), p.5.

Brozović, N., Burbank, D.W. and Meigs, A.J., 1997. Climatic limits on landscape development in the northwestern Himalaya. Science, 276(5312), pp.571-574.

Bunker E., n.d, Spence geochronology, University of Bristol, Unpublished.

Burt, D.M. and Sheridan, M.F., 1981. Model for the formation of uranium/lithophile element deposits in fluorine-rich volcanic rocks.

Capitanio, F., Faccenna, C., Zlotnik, S., Stegman, D., 2011. Subduction dynamics and the origin of Andean orogeny and the Bolivian orocline. Nature 480 (7375), 83–86.

Casella, George; Berger, Roger L. (2001). Statistical Inference (2nd ed.). Duxbury. ISBN 978-0-534-24312-8.

Cashman, K. and Blundy, J., 2000. Degassing and crystallization of ascending andesite and dacite. Philosophical Transactions of the Royal Society of London. Series A: Mathematical, Physical and Engineering Sciences, 358(1770), pp.1487-1513.

Castruccio, A., Diez, M. and Gho, R., 2017. The influence of plumbing system structure on volcano dimensions and topography. Journal of Geophysical Research: Solid Earth, 122(11), pp.8839-8859.

Cecilia Jamasmie 2016, Rio Tinto's Kennecott wins clean air lawsuit in the US, Mining.com, viewed September 2020, <http://www.mining.com/rio-tintos-kennecott-wins-clean-air-lawsuit-in-the-us/>.

Charrier, R., Baezar, O., Elgueta, S., Flynn, J.J., Gans, P., Kay, S.M., Muñoz, N., Wyss, A.R., y Zurita, E., 2002. Evidence for Cenozoic extensional basin development and tectonic inversion south of the flat-slab segment, southern Central Andes, Chile (33°-36°S.L.). Journal of South American Earth Sciences 15, 117–1139.

Chen, C.H., 1970. Geology and geothermal power potential of the Tatun volcanic region. Geothermics, 2, pp.1134-1143.

Chmielowski, J., Zandt, G., Haberland, C., 1999. The central Andean Altiplano–Puna magma body. Geophysical Research Letters 26 (6), 783–786.

Cimino, G., Del Duce, G., Kadonaga, L.K., Rotundo, G., Sisani, A., Stabile, G., Tirozzi, B. and Whiticar, M., 1999. Time series analysis of geological data. Chemical geology, 161(1-3), pp.253-270.

Clark, S.P. and Jäger, E., 1969. Denudation rate in the Alps from geochronologic and heat flow data. American Journal of Science, 267(10), pp.1143-1160.

Clayton, J.D. and Clapperton, C.M., 1997. Broad synchrony of a Late-glacial glacier advance and the highstand of palaeolake Tauca in the Bolivian Altiplano. Journal of Quaternary Science: Published for the Quaternary Research Association, 12(3), pp.169-182.

Clift, P. and Vannucchi, P., 2004. Controls on tectonic accretion versus erosion in subduction zones: Implications for the origin and recycling of the continental crust. Reviews of Geophysics, 42(2).

Cohen, K.M., Harper, D.A.T. and Gibbard, P.L., 2017. ICS International Chronostratigraphic Chart 2017/02.

Commission for the Geological Map of the World (2016), 'Tectonic Map of South America, Second edition', 1:5000000. Available at https://ccgm.org/img/cms/Explanatory%20Notes%20Tectonic%20Map%20South%20America_2016-web.pdf, (Accessed: November 2017).

Cox, D.P. and Singer, D.A., 1988. Distribution of gold in porphyry copper deposits (No. 88-46). US Geological Survey.

Creager, K.C., Chiao, L.Y., Winchester, J.P. and Engdahl, E.R., 1995. Membrane strain rates in the subducting plate beneath South America. Geophysical research letters, 22(16), pp.2321-2324.

Crosweller et al.: Global database on large magnitude explosive volcanic eruptions (LaMEVE). Journal of Applied Volcanology 2012 1:4.

Dahlström, S., Cooper, F., Blundy, J. and Condon, D., 2017. Exhumation of Andean granites: implications for porphyry copper formation and enrichment. Applied Earth Science, 126(2), pp.52-52.

De Bremond d'Ars, J., Jaupart, C. and Sparks, R.S.J., 1995. Distribution of volcanoes in active margins. Journal of Geophysical Research: Solid Earth, 100(B10), pp.20421-20432.

de Silva, S., Zandt, G., Trumbull, R., Viramonte, J.G., Salas, G. and Jiménez, N., 2006. Large ignimbrite eruptions and volcano-tectonic depressions in

the Central Andes: a thermomechanical perspective. Geological Society, London, Special Publications, 269(1), pp.47-63.

de Silva, S.L., 1989a. Altiplano–Puna volcanic complex of the central Andes. Geology 17, 1102–1106.

de Silva, S.L., 1989b. Geochronology and stratigraphy of the ignimbrites from the 21° 30′S to 23° 30′S portion of the Central Andes of Northern Chile. Journal of Volcanology and Geothermal Research 37, 93–131.

de Silva, S.L., 1991. Styles of zoning in central Andean ignimbrites; insights into magma chamber processes. Andean Magmatism and Its Tectonic Setting. Geol Soc Am, Special Paper 265, pp. 217–231.

de Silva, S.L., Francis, P.W., 1989. Correlation of large ignimbrites — two case studies from the central Andes of Northern Chile. Journal of Volcanology and Geothermal Research 37, 133–149.

de Silva, S.L., Francis, P.W., 1991. Volcanoes of the Central Andes. Springer, Berlin, Heidelberg, New York, pp. 1–216.

de Silva, S.L., Gosnold, W.D., 2007. Episodic construction of batholiths: insights from the spatiotemporal development of an ignimbrite flare-up. Journal of Volcanology and Geothermal Research 167 (1–4), 320–335.

Devlin, S., Isacks, B.L., Pritchard, M.E., Barnhart, W.D. and Lohman, R.B., 2012. Depths and focal mechanisms of crustal earthquakes in the central Andes determined from teleseismic waveform analysis and InSAR. Tectonics, 31(2).

Dewey, J.F. and Bird, J.M., 1970. Mountain belts and the new global tectonics. Journal of Geophysical Research, 75(14), pp.2625-2647.

Druitt, T.H., Young, S.R., Baptie, B., Bonadonna, C., Calder, E.S., Clarke, A.B., Cole, P.D., Harford, C.L., Herd, R.A., Luckett, R. and Ryan, G., 2002. Episodes of cyclic Vulcanian explosive activity with fountain collapse at Soufrière Hills Volcano, Montserrat. Memoirs-Geological Society of London, 21, pp.281-306.

Dunai, T.J., Gonzalez-Lopez, G.A., Juez-Larre, J., Carrizo, D., 2005. Preservation of (early) Miocene landscapes in the Atacama Desert, northern Chile. Geochim. Cosmochim. Acta 69 (10), A161.

Edlmann, K., Edwards, M.A., Qiao, X.J., Haszeldine, R.S. and McDermott, C.I., 2015. Appraisal of global CO 2 storage opportunities using the geomechanical facies approach. Environmental earth sciences, 73(12), pp.8075-8096.

Edmonds, M., Mather, T.A. and Liu, E.J., 2018. A distinct metal fingerprint in arc volcanic emissions. Nature Geoscience, 11(10), pp.790-794.

Ehlers, T.A., Poulsen, C.J., 2009. Influence of Andean uplift on climate and paleoaltimetry estimates. Earth Planet. Sci. Lett. 281 (3–4), 238–248.

England, P. and Molnar, P., 1990. Surface uplift, uplift of rocks, and exhumation of rocks. Geology, 18(12), pp.1173-1177.

Evenstar, L.A., Hartley, A.J., Archer, S.G., Neilson, J.E., 2015b. Climatic and halokinetic controls on alluvial–lacustrine sedimentation during compressional deformation, Andean forearc, northern Chile. Basin Res. 28, 634–657.

Evenstar, L.A., Mather, A.E. and Hartley, A.J., 2020. Using spatial patterns of fluvial incision to constrain continental-scale uplift in the Andes. Global and Planetary Change, p.103119.

Evenstar, L.A., Mather, A.E., Hartley, A.J., Stuart, F.M., Sparks, R.S.J. and Cooper, F.J., 2017. Geomorphology on geologic timescales: Evolution of the late Cenozoic Pacific paleosurface in Northern Chile and Southern Peru. Earth-Science Reviews, 171, pp.1-27.

Farías, M., 2007. Tectónica y erosión en la evolución del relieve de los Andes de Chile Central durante el Neógeno. Ph.D. Thesis, Universidad de Chile, Santiago, Chile.

Farías, M., Charrier, R., Comte, D., Martinod, J., Hérail, G., 2005. Late Cenozoic deformation and uplift of the western flank of the Altiplano: evidence from the depositional, tectonic, and geomorphologic evolution and shallow seismic activity (northern Chile at 19°30′S). Tectonics 24 (4), TC4001.

Franz, G., Lucassen, F., Kramer, W., Trumbull, R.B., Romer, R.L., Wilke, H.G., Viramonte, J.G., Becchio, R. and Siebel, W., 2006. Crustal evolution at the Central Andean continental margin: a geochemical record of crustal growth, recycling and destruction. In The Andes (pp. 45-64). Springer, Berlin, Heidelberg.

Gajardo, E. and Lomnitz, C., 1960. Seismic provinces of Chile. Proc of the 2nd world.

Gammons, C.H. and Williams-Jones, A.E., 1997. Chemical mobility of gold in the porphyry-epithermal environment. Economic Geology, 92(1), pp.45-59.

Garcia, M., Herail, G., 2005. Fault-related folding, drainage network evolution and valley incision during the Neogene in the Andean Precordillera of Northern Chile. Geomorphology 65 (3–4), 279–300.

García, M., Maksaev, V., Townley, B. and Dilles, J., 2017. Metallogeny, structural evolution, post-mineral cover distribution and exploration in concealed areas of the northern Chilean Andes. Ore Geology Reviews, 86, pp.652-672.

Garreaud, R.D., 2009. The Andes climate and weather. Advances in Geosciences, 22, p.3.

Garreaud, R.D., Molina, A. and Farias, M., 2010. Andean uplift, ocean cooling and Atacama hyperaridity: A climate modelling perspective. Earth and Planetary Science Letters, 292(1-2), pp.39-50.

Garzione, C.N., Hoke, G.D., Libarkin, J.C., Withers, S., MacFadden, B., Eiler, J., Ghosh, P., Mulch, A., 2008. Rise of the Andes. Science 320 (5881), 1304–1307.

Garzione, C.N., Molnar, P., Libarkin, J.C. and MacFadden, B.J., 2007. Reply to Comment on "Rapid late Miocene rise of the Bolivian Altiplano: Evidence for removal of mantle lithosphere" by Garzione et al. (2006), Earth Planet. Sci. Lett. 241 (2006) 543–556. Earth and Planetary Science Letters, 259(3-4), pp.630-633.

Garzione, C.N., Molnar, P., Libarkin, J.C. and MacFadden, B.J., 2006. Rapid late Miocene rise of the Bolivian Altiplano: Evidence for removal of mantle lithosphere. Earth and Planetary Science Letters, 241(3-4), pp.543-556.

Gaupp, R., Kött, A. and Wörner, G., 1999. Palaeoclimatic implications of Mio–Pliocene sedimentation in the high-altitude intra-arc Lauca Basin of northern Chile. Palaeogeography, Palaeoclimatology, Palaeoecology, 151(1-3), pp.79-100.

Gaupp, R., Kött, A., Wörner, G., 1999. Paleoclimatic implications of Mio –Pliocene sedimentation in the high-altitude intra-arc Lauca Basin of northern Chile. Palaeogeogr., Palaeoclimatol., Palaeoecol. 151, 79–100.

Gauthier, P.J. and Le Cloarec, M.F., 1998. Variability of alkali and heavy metal fluxes released by Mt. Etna volcano, Sicily, between 1991 and 1995. Journal of Volcanology and Geothermal Research, 81(3-4), pp.311-326.

Gauthier, P.J., Sigmarsson, O., Gouhier, M., Haddadi, B. and Moune, S., 2016. Elevated gas flux and trace metal degassing from the 2014–2015 fissure eruption at the Bárðarbunga volcanic system, Iceland. Journal of Geophysical Research: Solid Earth, 121(3), pp.1610-1630.

Global Volcanism Program, 2013. Volcanoes of the World, v. 4.7.0. Venzke, E (ed.). Smithsonian Institution. Downloaded 16 March 2017. https://doi.org/10.5479/si.GVP.VOTW4-2013.

Glodny, J., Echtler, H., Figueroa, O., Franz, G., Gräfe, K., Kemnitz, H., Kramer, W., Krawczyk, C., Lohrmann, J., Lucassen, F. and Melnick, D., 2006. Long-term geological evolution and mass-flow balance of the South-Central Andes. In The Andes (pp. 401-428). Springer, Berlin, Heidelberg.

Glodny, J., Gräfe, K., Echtler, H., Rosenau, M., 2008. Mesozoic to Quaternary continental margin dynamics in South-Central Chile (36°–42°S): the apatite and zircon fission track perspective. International. Journal of Earth Sciences 97, 1271–1291.

Gobierno de Chile Servicio de Geología y Minería Nacional (2003), 'Mapa Geológico de Chile: Versión Digital Publicación Geológica digital, No. 7, 2004 CD-ROM, versión 1.0, Base Geológica', 1:1.000.000, available at <http://www.ipgp.fr/~dechabal/Geol-millon.pdf>, downloaded: November 2017.

Gonzalez, E., 1990. Hydrocarbon resources in the coastal zone of Chile.

Goss, A.R., Kay, S.M., Mpodozis, C. and Singer, B.S., 2009. The Incapillo Caldera and Dome Complex (~ 28 S, central Andes): A stranded magma chamber over a dying arc. Journal of volcanology and geothermal research, 184(3-4), pp.389-404.

Graham, S.A., Chamberlain, C.P., Yue, Y., Ritts, B.D., Hanson, A.D., Horton, T.W., Waldbauer, J.R., Poage, M.A. and Feng, X., 2005. Stable isotope records of

Cenozoic climate and topography, Tibetan plateau and Tarim basin. American Journal of Science, 305(2), pp.101-118.

Grange, F., Hatzfeld, D., Cunningham, P., Molnar, P., Roecker, S.W., Suarez, G., Rodrigues, A. and Ocola, L., 1984. Tectonic implications of the microearthquake seismicity and fault plane solutions in southern Peru. Journal of Geophysical Research: Solid Earth, 89(B7), pp.6139-6152.

Gregory-Wodzicki, K.M., 2000, Uplift history of the central and northern Andes: A review: Geological Society of America Bulletin, v. 112, p. 1091–1105.

Gruen, G., Heinrich, C.A. and Schroeder, K., 2010. The Bingham Canyon porphyry Cu-Mo-Au deposit. II. Vein geometry and ore shell formation by pressure-driven rock extension. Economic Geology, 105(1), pp.69-90.

Grunder, A.L., Klemetti, E.W., Feeley, T.C. and McKee, C.M., 2008. Eleven million years of arc volcanism at the Aucanquilcha Volcanic Cluster, northern Chilean Andes: implications for the life span and emplacement of plutons. Earth and Environmental Science Transactions of the Royal Society of Edinburgh, 97(4), pp.415-436.

Guillaume, B., Martinod, J. and Espurt, N., 2009. Variations of slab dip and overriding plate tectonics during subduction: Insights from analogue modelling. Tectonophysics, 463(1-4), pp.167-174.

Gutscher, M.A., Malavieille, J., Lallemand, S., Collot, J.Y., 1999b. Tectonic segmentation of the North Andean margin: impact of the Carnegie Ridge collision. Earth Planet. Sci. Lett.168 (3), 255–270.

Guzmán, S., Grosse, P., Montero-López, C., Hongn, F., Pilger, R., Petrinovic, I., Seggiaro, R., Aramayo, A., 2014. Spatial–temporal distribution of explosive volcanism in the 25–28°S segment of the Andean Central Volcanic Zone. Tectonophysics 636, 170–189.

Hackney, R.I., Echtler, H.P., Franz, G., Götze, H.J., Lucassen, F., Marchenko, D., Melnick, D., Meyer, U., Schmidt, S., Tašárová, Z. and Tassara, A., 2006. The segmented overriding plate and coupling at the south-central Chilean margin (36–42 S). In The Andes (pp. 355-374). Springer, Berlin, Heidelberg.

Halter, W.E. and Webster, J.D., 2004. The magmatic to hydrothermal transition and its bearing on ore-forming systems.

Hargitai, H. and Kereszturi, Á. eds., 2015. Encyclopaedia of planetary landforms. Springer New York.

Hartley, A.J., Chong, G., Houston, J. and Mather, A.E., 2005. 150 million years of climatic stability: evidence from the Atacama Desert, northern Chile. Journal of the Geological Society, 162(3), pp.421-424.

Hartley, A.J., Evenstar, L., 2010. Cenozoic stratigraphic development in the north Chilean forearc: implications for basin development and uplift history of the Central Andean margin. Tectonophysics 495 (1–2), 67–77.

Hartley, A.J., May, G., 1998. Miocene gypcretes from the Calama Basin, northern Chile. Sedimentology 45 (2), 351–364.

Hartley, A.J., May, G., Chong, G., Turner, P., Kape, S.J., Jolley, E.J., 2000. Development of a continental forearc: a Cenozoic example from the Central Andes, northern Chile. Geology 28 (4), 331–334.

Hartley, A.J., Rice, C.M., 2005. Controls on supergene enrichment of porphyry copper deposits in the Central Andes: a review and discussion. Mineral. Deposita 40 (5), 515–525.

Hartley, A.J., Sempere, T., Wörner, G., 2007. A comment on “Rapid late Miocene rise of the Bolivian Altiplano: Evidence for removal of mantle lithosphere” by C.N. Garzione et al. [Earth Planet. Sci. Lett. 241 (2006) 543-556]. Earth Planet. Sci. Lett. 259 (3–4), 625–629.

Haschke, M. and Gunther, A., 2003. Balancing crustal thickening in arcs by tectonic vs. magmatic means. Geology, 31(11), pp.933-936.

Haschke, M.R., Scheuber, E., Günther, A. and Reutter, K.J., 2002. Evolutionary cycles during the Andean orogeny: repeated slab breakoff and flat subduction? Terra nova, 14(1), pp.49-55.

Hedenquist, J.W. and Lowenstern, J.B., 1994. The role of magmas in the formation of hydrothermal ore deposits. Nature, 370(6490), pp.519-527.

Hedenquist, J.W., Arribas, A. and Gonzalez-Urien, E., 2000. Exploration for epithermal gold deposits. Reviews in Economic Geology, 13(2), pp.45-77.

Hedenquist, J.W., Arribas, A. and Reynolds, T.J., 1998. Evolution of an intrusion-centered hydrothermal system; Far Southeast-Lepanto porphyry and epithermal Cu-Au deposits, Philippines. Economic Geology, 93(4), pp.373-404.

Heinrich, C.A., Driesner, T., Stefánsson, A. and Seward, T.M., 2004. Magmatic vapor contraction and the transport of gold from the porphyry environment to epithermal ore deposits. Geology, 32(9), pp.761-764.

Heinrich, C.A., Halter, W., Landtwing, M.R. and Pettke, T., 2005. The formation of economic porphyry copper (-gold) deposits: constraints from microanalysis of fluid and melt inclusions. Geological Society, London, Special Publications, 248(1), pp.247-263.

Hérail, G., Baby, P., Lopez, M., Oller, J. and López, O., 1990. Structure and kinematic evolution of Subandean thrust system of Bolivia. Colloques et séminaires-Institut français de recherche scientifique pour le développement en coopération, pp.179-182.

Hezarkhani, A., Williams-Jones, A.E. and Gammons, C.H., 1999. Factors controlling copper solubility and chalcopyrite deposition in the Sungun porphyry copper deposit, Iran. Mineralium deposita, 34(8), pp.770-783.

Hindle, D., Kley, J., Oncken, O. and Sobolev, S., 2005. Crustal balance and crustal flux from shortening estimates in the Central Andes. Earth and Planetary Science Letters, 230(1-2), pp.113-124.

Hinkley, T.K., Lamothe, P.J., Wilson, S.A., Finnegan, D.L. and Gerlach, T.M., 1999. Metal emissions from Kilauea, and a suggested revision of the estimated worldwide metal output by quiescent degassing of volcanoes. Earth and Planetary Science Letters, 170(3), pp.315-325.

Hoffmann-Rothe, A., Kukowski, N., Dresen, G., Echtler, H., Oncken, O., Klotz, J., Scheuber, E. and Kellner, A., 2006. Oblique convergence along the Chilean margin: partitioning, margin-parallel faulting and force interaction at the plate interface. In The Andes (pp. 125-146). Springer, Berlin, Heidelberg.

Hoke, G.D. and Garzione, C.N., 2008. Paleosurfaces, paleoelevation, and the mechanisms for the late Miocene topographic development of the Altiplano plateau. Earth and Planetary Science Letters, 271(1-4), pp.192-201.

Hong, S., Candelone, J.P., Soutif, M. and Boutron, C.F., 1996. A reconstruction of changes in copper production and copper emissions to the atmosphere during the past 7000 years. Science of the Total Environment, 188(2-3), pp.183-193.

Horton, B.K., 1999. Erosional control on the geometry and kinematics of thrust belt development in the central Andes. Tectonics 18 (6), 292–1293.

Horton, B.K., 2018. Sedimentary record of Andean mountain building. Earth-Science Reviews, 178, pp.279-309.

Houston, J. and Hartley, A.J., 2003. The central Andean west-slope rain shadow and its potential contribution to the origin of hyper-aridity in the Atacama Desert. International Journal of Climatology: A Journal of the Royal Meteorological Society, 23(12), pp.1453-1464.

Hu, J., Liu, L., Hermosillo, A. and Zhou, Q., 2016. Simulation of late Cenozoic South American flat-slab subduction using geodynamic models with data assimilation. Earth and Planetary Science Letters, 438, pp.1-13.

Huaman Rodrigo, M.D., 1985. Évolution tectonique cénozoïque et néotectonique du Piémont Pacifique dans la région d'Arequipa (Andes du Sud Pérou) (Doctoral dissertation, Paris 11).

Instituto Geográfico Nacional (ING), n.d, Volcanes Activos de la República Argentina, exported June 2017, <https://www.ign.gob.ar/NuestrasActividades/Geografia/DatosArgentina/VolcanesActivos>

Isacks, B.L., 1988. Uplift of the central Andean plateau and bending of the Bolivian orocline. Journal of Geophysical Research: Solid Earth, 93(B4), pp.3211-3231.

Ivanov, V.V., 1959. Present-day hydrothermal activity within the Kurile-Kamchatka Island arc and its relation to volcanicity. Bulletin Volcanologique, 20(1), pp.137-154.

Jordan, T.E., Burns, W.M., Veiga, R., Pángaro, F., Copeland, P., Kelley, S. and Mpodozis, C., 2001. Extension and basin formation in the southern Andes caused by increased convergence rate: A mid-Cenozoic trigger for the Andes. Tectonics, 20(3), pp.308-324.

Jordan, T.E., Kirk-Lawlor, N.E., Blanco, P.N., Rech, J.A., Cosentino, N.J., 2014. Landscape

modification in response to repeated onset of hyperarid paleoclimate states since 14 Ma, Atacama Desert, Chile. Geol. Soc. Am. Bull. 94, 341–361.

Juez-Larré, J., Kukowski, N., Dunai, T.J., Hartley, A.J., Andreissen, P.A.M., 2010. Thermal and exhumation history of the Coastal Cordillera arc of northern Chile revealed by thermochronological dating. Tectonophysics 495, 48–66.

Karátson, D., Favalli, M., Tarquini, S., Fornaciai, A. and Wörner, G., 2010. The regular shape of stratovolcanoes: a DEM-based morphometrical approach. Journal of Volcanology and Geothermal Research, 193(3-4), pp.171-181.

Karátson, D., Telbisz, T. and Wörner, G., 2012. Erosion rates and erosion patterns of Neogene to Quaternary stratovolcanoes in the Western Cordillera of the Central Andes: an SRTM DEM based analysis. Geomorphology, 139, pp.122-135.

Karger, D.N., Conrad, O., Böhner, J., et al. 2017 Climatologies at high resolution for the earth's land surface areas. Sci. Dat.

Kay, S.M., Coira, B. and Viramonte, J., 1994. Young mafic back arc volcanic rocks as indicators of continental lithospheric delamination beneath the Argentine Puna plateau, central Andes. Journal of Geophysical Research: Solid Earth, 99(B12), pp.24323-24339.

Kay, S.M., Coira, B.L., Caffe, P.J., Chen, C.H., 2010. Regional chemical diversity, crustal and mantle sources and evolution of central Andean Puna plateau ignimbrites. Journal of Volcanology and Geothermal Research 198 (1–2), 81–111.

Kay, S.M., Mpodozis, C. and Coira, B., 1999. Neogene magmatism, tectonism, and mineral deposits of the Central Andes (22 to 33 S latitude). In Geology and ore deposits of the Central Andes (Vol. 7, pp. 27-59). Lancaster, USA: Society of Economic Geologists.

Kay, S.M., Mpodozis, C., Tittler, A. and Cornejo, P., 1994. Tertiary magmatic evolution of the Maricunga mineral belt in Chile. International Geology Review, 36(12), pp.1079-1112.

Keigwin, L.D., 1980. Palaeoceanographic change in the Pacific at the Eocene–Oligocene boundary. Nature, 287(5784), pp.722-725.

Keith, J.D., 1979. Miocene volcanism hosting porphyry- molybdenum and epithermal vein mineralization, southwestern Utah and Nevada [abs.]: Geol. Soc. America. In Abstracts with Programs (Vol. 11, p. 455).

Kelleher, J., Sykes, L. and Oliver, J., 1973. Possible criteria for predicting earthquake locations and their application to major plate boundaries of the Pacific and the Caribbean. Journal of Geophysical Research, 78(14), pp.2547-2585.

Kesler, S.E. and Wilkinson, B.H., 2006. The role of exhumation in the temporal distribution of ore deposits. Economic Geology, 101(5), pp.919-922.

Klein, A.G., Seltzer, G.O., Isacks, B.L., 1999. Modern and last glacial maximum snowlines in the Peruvian–Bolivian Andes. Quaternary Science Reviews 18, 63–84.

Klemm, L.M., Pettke, T., Heinrich, C.A. and Campos, E., 2007. Hydrothermal evolution of the El Teniente deposit, Chile: Porphyry Cu-Mo ore deposition from low-salinity magmatic fluids. Economic Geology, 102(6), pp.1021-1045.

Kley, J., 1999. Geologic and geometric constraints on a kinematic model of the Bolivian orocline. Journal of South American Earth Sciences, 12(2), pp.221-235.

Kober, F., Ivy-Ochs, S., Schlunegger, F., Baur, H., Kubik, P.W. and Wieler, R., 2007. Denudation rates and a topography-driven rainfall threshold in northern Chile: Multiple cosmogenic nuclide data and sediment yield budgets. Geomorphology, 83(1-2), pp.97-120.

Kober, F., Schlunegger, F., Ivy-Ochs, S. and Wieler, R., 2002, August. The dependency of cosmogenic nuclides to climate and surface uplift in transient landscapes. In Geochimica et Cosmochimica Acta (Vol. 66, No. 15 A, pp. A408-A408). The Boulevard, Langford Lane, Kidlington, Oxford OX5 1GB, England: Pergamon-Elsevier Science Ltd.

Kudrass, H.R., Von Rad, U., Seyfied, H., Andruleit, H., Hinz, K. and Reichert, C., 1998. Age and facies of sediments of the northern Chilean continental slope-Evidence for intense vertical movements. Crustal Investigations Off-and Onshore Nazca/CINCA, pp.170-196.

Kutzbach, J.E., Guetter, P.J., Ruddiman, W.F. and Prell, W.L., 1989. Sensitivity of climate to late Cenozoic uplift in southern Asia and the American west: numerical experiments. Journal of Geophysical Research: Atmospheres, 94(D15), pp.18393-18407.

Laerd statistics n.d., One-way ANOVA in SPSS Statistics, Lund Research Ltd, viewed on 5th September 2020, <https://statistics.laerd.com/spss-tutorials/one-way-anova-using-spss-statistics.php>

Lallemand, S.E., Schnürle, P. and Malavieille, J., 1994. Coulomb theory applied to accretionary and non-accretionary wedges: Possible causes for tectonic erosion and/or frontal accretion. Journal of Geophysical Research: Solid Earth, 99(B6), pp.12033-12055.

Lamb, S. and Davis, P., 2003. Cenozoic climate change as a possible cause for the rise of the Andes. Nature, 425(6960), pp.792-797.

Lamb, S., 2016. Cenozoic uplift of the Central Andes in northern Chile and Bolivia – reconciling paleoaltimetry with the geological evolution. Can. J. Earth Sci. 53 (11), 1227–1245.

Lamb, S., Hoke, L., 1997. Origin of the high plateau in the Central Andes, Bolivia, South America. Tectonics 16 (4), 623–649.

Langbein, W.B. and Schumm, S.A., 1958. Yield of sediment in relation to mean annual precipitation. Eos, Transactions American Geophysical Union, 39(6), pp.1076-1084.

Larson, J.L., and Pitman, W.C., 1972, World-wide correlation of Mesozoic magnetic anomalies, and its implications: Geological Society of America Bulletin, v. 83, p. 3645-3662.

Lenters, J.D. and Cook, K.H., 1995. Simulation and diagnosis of the regional summertime precipitation climatology of South America. Journal of Climate, 8(12), pp.2988-3005.

Lindsay, J.M., Schmitt, A.K., Trumbull, R.B., de Silva, S.L., Siebel, W., Emmermann, R., 2001b. Magmatic evolution of the La Pacana caldera system, Central Andes, Chile: compositional variation of two cogenetic, large-volume felsic ignimbrites. Journal of Petrology 42 (3), 459–486.

Llambías, E.J. and EJ, L., 1972. Estructura del Grupo Volcánico Farallón Negro Catamarca, República Argentina.

Llambías, E.J. and EJ, L., 1972. Estructura del Grupo Volcánico Farallón Negro Catamarca, República Argentina.

Lowenstern, J.B. and Sinclair, W.D., 1996. comb-layered quartz at the Cretaceous Logtung W-Mo deposit, Yukon Territory, Canada. In The Third Hutton Symposium on the Origin of Granites and Related Rocks (Vol. 315, p. 291). Geological Society of America.

Maksaev, V. and Zentilli, M., 1999. Fission track thermochronology of the Domeyko Cordillera, northern Chile: Implications for Andean tectonics and porphyry copper metallogenesis. Exploration and Mining Geology, 8(1/2), pp.65-90.

Maksaev, V., Townley, B., Palacios, C., Camus, F., 2007. Metallic ore deposits. In: Gibbons, W., Moreno, T. (Eds.), The Geology of Chile. The Geological Society, London, pp. 179–199.

Malamud, B.D., 2004. Tails of natural hazards. Physics World, 17(8), p.25.

Mamani, 2010. Geochemical variations in igneous rocks of the Central Andean orocline (13°S to 18°S): Tracing crustal thickening and magma generation through time and space.

Margirier, A., Audin, L., Carcaillet, J., Schwartz, S. and Benavente, C., 2015. Tectonic and climatic controls on the Chuquibamba landslide (western Andes, southern Peru). Earth Surface Dynamics, 3(2), pp.281-289.

Masek, J.G., Isacks, B.L., Gubbels, T.L., and Fielding, E.J., 1994, Erosion and tectonics at the margins of continental plateaus: Journal of Geophysical Research, v. 99, p. 13 941–13 956.

Mather, T.A., Witt, M.L.I., Pyle, D.M., Quayle, B.M., Aiuppa, A., Bagnato, E., Martin, R.S., Sims, K.W.W., Edmonds, M., Sutton, A.J. and Ilyinskaya, E., 2012. Halogens and trace metal emissions from the ongoing 2008 summit eruption of Kīlauea volcano, Hawaii. Geochimica et Cosmochimica Acta, 83, pp.292-323.

McInnes, I.A., Evans, N.J., Fu, F.Q., Garwin, S., Belousova, E., Griffin, W.L., Bertens, A., Sukarna, D., Permanadewi, S., Andrew, R.L. and Deckart, K., 2005. Super porphyry copper and gold deposits. A global perspective, 1, pp.27-42.

McQuarrie, N., Horton, B.K., Zandt, G., Beck, S. and DeCelles, P.G., 2005. Lithospheric evolution of the Andean fold–thrust belt, Bolivia, and the origin of the central Andean plateau. Tectonophysics, 399(1-4), pp.15-37.

Meagher, C 2017, Constancia Mine Form 43-101F1 Technical Report, Hudbay, downloaded March 2019, < https://s23.q4cdn.com/405985100/files/doc_downloads/tech_reports/peru/ConstanciaTechReport_032918.pdf>.

Meinert, L.D., 2007. Mineral Deposits of Canada: A Synthesis of Major Deposit Types, District Metallogeny, the Evolution of Geological Provinces and Exploration Methods. Wayne D. Goodfellow, Editor. 1,068 Pp. Geological Association of Canada, Mineral Deposits Division, Special Publication No. 5. 2007. Hardcover. ISBN-13: 978-1-897095-24-9. Price: members CDN 60.00, non-members CDN 80.00. Economic Geology, 102(7), pp.1355-1355.

Meissner, R. and Mooney, W., 1998. Weakness of the lower continental crust: a condition for delamination, uplift, and escape. Tectonophysics, 296(1-2), pp.47-60.

Montgomery, D.R., Balco, G. and Willett, S.D., 2001. Climate, tectonics, and the morphology of the Andes. Geology, 29(7), pp.579-582.

Mortimer, C., E, F., Saric, Nicolas, 1974. K-Ar ages from tertiary lavas of the northernmost Chilean Andes. Geol. Rundsch. 63, 484–493.

Moune, S., Gauthier, P.J. and Delmelle, P., 2010. Trace elements in the particulate phase of the plume of Masaya Volcano, Nicaragua. Journal of Volcanology and Geothermal Research, 193(3-4), pp.232-244.

Mpodozis, C. and Cornejo, P., 2012. Cenozoic tectonics and porphyry copper systems of the Chilean Andes. Society of Economic Geologists Special Publication, 16, pp.329-360.

Mueller RD, Roest WR, Royer JY, Gahagan LM, Sclater JG (1997) Digital isochrons of the world's ocean floor. J Geophys Res 102: 3211–3214.

Mullineaux, D.R., 1996. Pre-1980 tephra-fall deposits erupted from Mount St. Helens, Washington (No. 1563). US Geological Survey.

Münchmeyer, C., 1996. Exotic deposits—products of lateral migration of supergene solutions from porphyry copper deposits. Soc. Econ. Geol. Special Publication 5, 43–58.

Murakami, H., Seo, J.H. and Heinrich, C.A., 2010. The relation between Cu/Au ratio and formation depth of porphyry-style Cu– Au ± Mo deposits. Mineralium Deposita, 45(1), pp.11-21.

Myers B. 2008, Geologic Mapping in Southern Washington Cascades: Eruptive history for the Cascades, USGS, viewed April 2018, <http://vulcan.wr.usgs.gov/Projects/Mapping/SoWA_Cascades/summary.html>.

Nakamura, H., Sumi, K., Katagiri, K. and Iwata, T., 1970. The geological environment of Matsukawa geothermal area, Japan. Geothermics, 2, pp.221-231.

NASA Black Tusk 2008, Map of the Cascadia Volcanic Arc, NASA World Wind, viewed April 2018, <https://commons.wikimedia.org/wiki/File:Cascade_Volcanic_Arc.jpg>.

NASA Earth Observatory n.d, Comparison of Chaitén and Mount St. Helens, NASA Earth Observatory, viewed April 2018, <https://earthobservatory.nasa.gov/images/8790/comparison-of-chaiten-and-mount-st-helens>.

New, M., Lister, D., Hulme, M. and Makin, I., 2002. A high-resolution data set of surface climate over global land areas. Climate research, 21(1), pp.1-25.

Newhall, C.G. and Self, S., 1982. The volcanic explosivity index (VEI) an estimate of explosive magnitude for historical volcanism. Journal of Geophysical Research: Oceans, 87(C2), pp.1231-1238.

Oncken, O., Hindle, D., Kley, J., Elger, K., Victor, P. and Schemmann, K., 2006. Deformation of the central Andean upper plate system—Facts, fiction, and constraints for plateau models. In The Andes (pp. 3-27). Springer, Berlin, Heidelberg.

Ouimet, W.B., Whipple, K.X., Royden, L.H., Sun, Z. and Chen, Z., 2007. The influence of large landslides on river incision in a transient landscape: Eastern margin of the Tibetan Plateau (Sichuan, China). Geological Society of America Bulletin, 119(11-12), pp.1462-1476.

Oxford University Press, 2021, Volcano, downloaded April 2021, < https://www.oxfordlearnersdictionaries.com/definition/english/volcano>.

Pacey, A., 2016. The characteristics, geochemistry and origin of propylitic alteration in the Northparkes porphyry Cu-Au system (Doctoral dissertation, Imperial College London).

Pardo-Casas, F., and Molnar, P., 1987, Relative motion of the Nazca (Farallon) and South American plates since Late Cretaceous time: Tectonics, v. 6, p. 233-248.

Parrish, Randall R.; Noble, Stephen R., 2003. Zircon U-Th-Pb Geochronology by Isotope Dilution – Thermal Ionization Mass Spectrometry (ID-TIMS). In Zircon (eds. J. Hanchar and P. Hoskin). Reviews in Mineralogy and Geochemistry, Mineralogical Society of America. 183-213.

Paterson, J.T. and Cloos, M., 2005. Grasberg porphyry Cu–Au deposit, Papua, Indonesia: 1. Magmatic history. Super porphyry copper and gold deposits: A global perspective, 2, pp.313-329.

Peacock, S.M., 1996. Thermal and petrologic structure of subduction zones. Subduction: top to bottom, 96, pp.119-133.

Perelló, J., Carlotto, V., Zárate, A., Ramos, P., Posso, H., Neyra, C., Caballero, A., Fuster, N., Muhr, R., 2003. Porphyry-style alteration and mineralization of the middle Eocene to early Oligocene Andahuaylas-Yauri belt, Cuzco region, Peru. Econ. Geol. 98, 1575–1605.

Perkins, J.P., Ward, K.M., de Silva, S., Zandt, G., Beck, S.L., Finnegan, N.J., 2016. Surface uplift in the Central Andes driven by growth of the Altiplano Puna Magma Body. Nat. Commun. 7, 13185.

Pfeiffer T 2004, Illustrated Volcano Glossary, Volcano discovery viewed February 2019, <https://www.volcanodiscovery.com/photoglossary/fissure-vent.html>.

Philip, H. and Ritz, J.F., 1999. Gigantic paleolandslide associated with active faulting along the Bogd fault (Gobi-Altay, Mongolia). Geology, 27(3), pp.211-214.

Philip, H., Ritz, J.-F., 1999. Gigantic paleolandslide associated with active faulting along the Bogd fault (Gobi– Altay, Mongolia). Geology 27, 211 – 214.

Placzek, C.J., Quade, J. and Patchett, P.J., 2011. Isotopic tracers of paleohydrologic change in large lakes of the Bolivian Altiplano. Quaternary Research, 75(1), pp.231-244.

Placzek, C.J., Quade, J., Patchett, P.J., 2006. Geochronology and stratigraphy of late Pleistocene lake cycles on the southern Bolivian Altiplano: implications for causes of tropical climate change. Geological Society of America Bulletin 118, 515–532.

Pollard, P.J., Taylor, R.G. and Peters, L., 2005. Ages of intrusion, alteration, and mineralization at the Grasberg Cu-Au deposit, Papua, Indonesia. Economic Geology, 100(5), pp.1005-1020.

Potro, R., Díez, M., Blundy, J., Camacho, A.G., Gottsmann, J., 2013. Diapiric ascent of silicic magma beneath the Bolivian Altiplano. Geophysical Research Letters 40 (10), 2044–2048.

Presnell, R.D., 1997. Structural controls on the plutonism and metallogeny in the Wasatch and Oquirrh Mountains, Utah. Soc Econ Geol Guidebook, 29, pp.1-14.

Pyle, D., 2000. Sizes of volcanic eruptions. In: Sigurdsson, H., Houghton, B., McNutt, S., Rymer, H., Stix, J. (Eds.), Encyclopedia of Volcanoes. Academic Press, London, UK.

Rech, J.A., Currie, B.S., Jordan, T.E., Riquelme, R., Lehmann, S.B., Kirk-Lawlor, N.E., Li, S. and Gooley, J.T., 2019. Massive middle Miocene gypsic paleosols in the Atacama Desert and the formation of the Central Andean rain-shadow. Earth and Planetary Science Letters, 506, pp.184-194.

Redmond, P.B. and Einaudi, M.T., 2010. The Bingham Canyon porphyry Cu-Mo-Au deposit. I. Sequence of intrusions, vein formation, and sulfide deposition. Economic Geology, 105(1), pp.43-68.

Reutter, K.J., Scheuber, E. and Chong, G., 1996. The Precordilleran fault system of Chuquicamata, northern Chile: Evidence for reversals along arc-parallel strike-slip faults. Tectonophysics, 259(1-3), pp.213-228.

Richards, J.P. and Tosdal, R.M. eds., 2001. Structural controls on ore genesis. Society of Economic Geologists.

Richards, J.P., 2003. Tectono-magmatic precursors for porphyry Cu-(Mo-Au) deposit formation. Economic Geology, 98(8), pp.1515-1533.

Riller, U. and Oncken, O., 2003. Growth of the Central Andean Plateau by tectonic segmentation is controlled by the gradient in crustal shortening. The Journal of Geology, 111(3), pp.367-384.

Riquelme, R., Darrozes, J., Maire, E., Hérail, G., Soula, J.C., 2008. Long-term denudation rates from the Central Andes (Chile) estimated from a Digital Elevation Model using the Black Top Hat function and Inverse Distance Weighting: implications for the Neogene climate of the Atacama Desert. Revista Geológica de Chile 35 (1), 105–121.

Rodda, P., 1976, Geology of northern and central Viti Levu: Fiji Mineral Resources Div. Bull. 3, 160 p.

Roedder, Edwin, 1971, Fluid inclusion studies on the porphyry-type ore deposits at Bingham, Utah, Butte, Montana, and Climax, Colorado: Econ. Geology, v. 66, p. 98-120.

Roman, A. and Jaupart, C., 2014. The impact of a volcanic edifice on intrusive and eruptive activity. Earth and Planetary Science Letters, 408, pp.1-8.

Rosenbaum, G. and Lister, G.S., 2005. The Western Alps from the Jurassic to Oligocene: spatio-temporal constraints and evolutionary reconstructions. Earth-Science Reviews, 69(3-4), pp.281-306.

Rosenbaum, G., Giles, D., Saxon, M., Betts, P.G., Weinberg, R.F. and Duboz, C., 2005. Subduction of the Nazca Ridge and the Inca Plateau: Insights into the formation of ore deposits in Peru. Earth and Planetary Science Letters, 239(1-2), pp.18-32.

Ross, J.L.S., Fierz, M.D.S.M., Nepomuceno, P.L.M. and de Melo, M.A., 2019. Macroformas do Relevo da América do Sul. Revista Do Departamento De Geografia, 38, pp.58-69.

Rougier, J., Sparks, R.S.J., Cashman, K.V. and Brown, S.K., 2018. The global magnitude–frequency relationship for large explosive volcanic eruptions. Earth and Planetary Science Letters, 482, pp.621-629.

Ruddiman, W.F. and Kutzbach, J.E., 1989. Forcing of late Cenozoic northern hemisphere climate by plateau uplift in southern Asia and the American West. Journal of Geophysical Research: Atmospheres, 94(D15), pp.18409-18427.

Salisbury, M.J., Jicha, B.R., de Silva, S.L., Singer, B.S., Jimenez, N.C., Ort, M.H., 2011. (40)Ar/(39)Ar chronostratigraphy of Altiplano–Puna volcanic complex ignimbrites reveals the development of a major magmatic province. Geological Society of America Bulletin 123 (5–6), 821–840.

Sasso, A.M. and Clark, A.H., 1998. SOC ECON GEOL NEWSL. Soc. Econ. Geol. Newsl., 34, p.8.

Savin, S.M., 1977. The history of the Earth's surface temperature during the past 100 million years. Annual review of earth and planetary sciences, 5(1), pp.319-355.

Savin, S.M., Douglas, R.G. and Stehli, F.G., 1975. Tertiary marine paleotemperatures. Geological Society of America Bulletin, 86(11), pp.1499-1510.

Schildgen, T.F., Balco, G. and Shuster, D.L., 2010. Canyon incision and knickpoint propagation recorded by apatite 4He/3He thermochronometry. Earth and Planetary Science Letters, 293(3-4), pp.377-387.

Schildgen, T.F., Ehlers, T.A., Whipp Jr, D.M., van Soest, M.C., Whipple, K.X. and Hodges, K.V., 2009. Quantifying canyon incision and Andean Plateau surface uplift, southwest Peru: A thermochronometer and numerical modeling approach. Journal of Geophysical Research: Earth Surface, 114(F4).

Schildgen, T.F., Hodges, K.V., Whipple, K.X., Pringle, M.S., Van Soest, M. and Cornell, K., 2009. Late Cenozoic structural and tectonic development of the western margin of the central Andean Plateau in southwest Peru. Tectonics, 28(4).

Schildgen, T.F., Hodges, K.V., Whipple, K.X., Pringle, M.S., Van Soest, M. and Cornell, K., 2009. Late Cenozoic structural and tectonic development of the western margin of the central Andean Plateau in southwest Peru. Tectonics, 28(4).

Schildgen, T.F., Hodges, K.V., Whipple, K.X., Reiners, P.W. and Pringle, M.S., 2007. Uplift of the western margin of the Andean plateau revealed from canyon incision history, southern Peru. Geology, 35(6), pp.523-526.

Schmitz, M., Heinsohn, W.-D., Schilling, F., 1997. Seismic, gravity and petrological evidence for partial melt beneath the thickened central Andean crust (21–23 S). Tectonophysics 270 (3), 313–326.

Schöpa, A., Annen, C., Dilles, J.H., Sparks, R.S.J. and Blundy, J.D., 2017. Magma emplacement rates and porphyry copper deposits: thermal modeling of the Yerington Batholith, Nevada. Economic Geology, 112(7), pp.1653-1672.

Sébrier, M., Lavenu, A., Fornari, M. and Soulas, J.P., 1988. Tectonics and uplift in Central Andes (Peru, Bolivia and northern Chile) from Eocene to present. Géodynamique, 3(1-2), pp.85-106.

Sébrier, M., Mercier, J.L., Mégard, F., Laubacher, G. and Carey-Gailhardis, E., 1985. Quaternary normal and reverse faulting and the state of stress in the central Andes of south Peru. Tectonics, 4(7), pp.739-780.

Seedorff, E. and Einaudi, M.T., 2004. Henderson porphyry molybdenum system, Colorado: I. Sequence and abundance of hydrothermal mineral assemblages, flow paths of evolving fluids, and evolutionary style. Economic Geology, 99(1), pp.3-37.

Sempere, T., Hérail, G., Oller, J. and Bonhomme, M.G., 1990. Late Oligocene-early Miocene major tectonic crisis and related basins in Bolivia. Geology, 18(10), pp.946-949.

Sepulchre, P., Schuster, M., Ramstein, G., Krinnezr, G., Girard, J.F., Vignaud, P. and Brunet, M., 2008. Evolution of Lake Chad Basin hydrology during the mid-Holocene: A preliminary approach from lake to climate modelling. Global and Planetary Change, 61(1-2), pp.41-48.

Servicio Nacional de Geología y Minería (SERNAGEOMIN), 2015, Ranking de los 90 volcanes activos de Chile, <http://sitiohistorico.sernageomin.cl/archivos/Ranking-de-Volcanes.pdf>

Shackleton, N.J. and Brenchley, P., 1984. Fossils and Climate.

Shackleton, N.J., 1975. Late Cenozoic oxygen and carbon isotopic ranges at DSDP Site 284: Implications for glacial history of the northern hemisphere and antarctica. Init. Reps. Deep Sea Drilling Project, 29, pp.801-807.

Shannon, J.R., Walker, B.M., Carten, R.B. and Geraghty, E.P., 1982. Unidirectional solidification textures and their significance in determining relative ages of intrusions at the Henderson Mine, Colorado. Geology, 10(6), pp.293-297.

Sheffels, B.M., 1995. Is the bend in the Bolivian Andes an orocline?

Shinohara, H., Kazahaya, K. and Lowenstern, J.B., 1995. Volatile transport in a convecting magma column: Implications for porphyry Mo mineralization. Geology, 23(12), pp.1091-1094.

Siebert, L., Simkin, T. and Kimberly, P., 2011. Volcanoes of the World. Univ of California Press.

Sillitoe, R., 1988. Epochs of intrusion-related copper mineralization in the Andes. J. South Am. Sci. 1, 89–108.

Sillitoe, R., 2005. Supergene oxidized and enriched porphyry copper and related deposits. Econ. Geol. 100th Anniversary Volume, 723–768.

Sillitoe, R.H. and Bonham, H.F., 1984. Volcanic landforms and ore deposits. Economic Geology, 79(6), pp.1286-1298.

Sillitoe, R.H., 1973. The tops and bottoms of porphyry copper deposits. Economic Geology, 68(6), pp.799-815.

Sillitoe, R.H., 1974. Tectonic segmentation of the Andes: implications for magmatism and metallogeny. Nature, 250(5467), pp.542-545.

Sillitoe, R.H., 1981. Regional aspects of the Andean porphyry copper belt in Chile and Argentina. Trans. Inst. Mining Metal. Sec. B, 90, pp.B15-B36.

Sillitoe, R.H., 1984. Philippine porphyry copper deposits: Geologic setting and characteristics. United Nations ESCAP, CCOP. Technical Publication, 14, p.89.

Sillitoe, R.H., 1995. Exploration of porphyry copper lithocaps. In Pacrim Congress 1995'Exploring the Rim' (pp. 527-532). Aust. Inst. Mining Metall.

Sillitoe, R.H., 1997. Characteristics and controls of the largest porphyry copper-gold and epithermal gold deposits in the circum-Pacific region. Australian Journal of Earth Sciences, 44(3), pp.373-388.

Sillitoe, R.H., 2000. Gold-rich porphyry deposits: descriptive and genetic models and their role in exploration and discovery. Reviews in Economic Geology, 13, pp.315-345.

Sillitoe, R.H., 2010. Porphyry copper systems. Economic geology, 105(1), pp.3-41.

Sillitoe, R.H., 2018. Why no porphyry copper deposits in Japan and South Korea?. Resource geology, 68(2), pp.107-125.

Sillitoe, R.H., Perelló, J., 2005. Andean copper province: tectonomagmatic settings, deposit types,

metallogeny, exploration, and discovery. Econ. Geol. 100, 845– 890.

Silver, P.G., Russo, R.M. and Lithgow-Bertelloni, C., 1998. Coupling of South American and African plate motion and plate deformation. Science, 279(5347), pp.60-63.

Simakin, A. and Talbot, C., 2001. Tectonic pumping of pervasive granitic melts. Tectonophysics, 332(4), pp.387-402.

Simmon R. 2010, Chaitén Volcano Lava Dome, Chile: Reduced volcanic emissions and clear skies over southern Chile on March 3, 2010, revealed Chaitén volcano's new lava dome, NASA, downloaded April 2018, <https://visibleearth.nasa.gov/images/45265/chaitacn-volcano-chile>.

Smith, G.A., Landis., CA, 1995. Intra-arc basins. Tectonics of Sedimentary Basins: Recent Advances. Cambridge: Blackwell, pp.263-298.

Sobolev, S.V., Babeyko, A.Y., Koulakov, I. and Oncken, O., 2006. Mechanism of the Andean orogeny: insight from numerical modeling. In The Andes (pp. 513-535). Springer, Berlin, Heidelberg.

Somoza, R., 1998. Updated Nazca (Farallon)—South America relative motions during the last 40 My: implications for mountain building in the central Andean region. Journal of South American Earth Sciences, 11(3), pp.211-215.

Stauder, W., 1973. Mechanism and spatial distribution of Chilean earthquakes with relation to subduction of the oceanic plate. Journal of Geophysical Research, 78(23), pp.5033-5061.

Stefánsson, A. and Seward, T.M., 2004. Gold (I) complexing in aqueous sulphide solutions to 500 C at 500 bar. Geochimica et Cosmochimica Acta, 68(20), pp.4121-4143.

Tassara, A. and Yáñez, G., 1996. Thermomechanic segmentation of the Andes (15-50 S): a flexural analysis approach.

Tassara, A., Yáñez, G., 2003. Relación entre el espesor elástico de la litósfera y la segmentación tectónica del margen andino (15–47°S). Revista Geológica de Chile 30, 159–186.

Thomas, R., Vaughan, I. and Lello, J., 2013. Data analysis with R statistical software. A guidebook for scientists. Eco-explore.

Thorpe, R.S., 1984. The tectonic setting of active Andean volcanism. In Andean Magmatism (pp. 4-8). Birkhäuser Boston.

Thouret, J.C., Wörner, G., Singer, B., Gunnell, Y., Zhang, X., Souriot, T., 2007. Landscape evolution on the western Andean slope in southern Peru: incision of deepest Andean canyons during Miocene uplift of the Central Andes. Earth and Planetary Science Letters 263, 151–166.

Trumbull, R.B., Riller, U., Oncken, O., Scheuber, E., Munier, K. and Hongn, F., 2006. The time-space distribution of Cenozoic volcanism in the South-Central Andes: a new data compilation and some tectonic implications. In The Andes (pp. 29-43). Springer, Berlin, Heidelberg.

Tsang, D.P., Wallis, S.R., Yamamoto, K., Takeuchi, M., Hidaka, H., Horie, K. and Tattitch, B.C., 2018. Zircon U–Pb geochronology and geochemistry of the Cerro Colorado porphyry copper deposit, northern Chile. Ore Geology Reviews, 93, pp.114-140.

University of Leeds n.d., Stepwise linear regression, School of Geography - University of Leeds, viewed on 5th September 2020, <http://www.geog.leeds.ac.uk/courses/other/statistics/spss/stepwise/>

Urrego, D.H., Silman, M.R. and Bush, M.B., 2005. The Last Glacial Maximum: stability and change in a western Amazonian cloud forest. Journal of Quaternary Science: Published for the Quaternary Research Association, 20(7-8), pp.693-701.

USGS n.d., Mount St Helens eruptive history from 1400 years ago to 1990, USGS, viewed April 2018,<http://vulcan.wr.usgs.gov/Volcanoes/MSH/Publications/MSHPPF/MSH_past_present_future.html>

Van Zalinge, M., Sparks, R., Cooper, F., Condon, D., 2016a. Early Miocene large-volume ignimbrites of the Oxaya Formation, Central Andes. J. Geol. Soc. 173 (5), 716–733.

Van Zalinge, M., Sparks, S., Evenstar, L., Cooper, F., Aslin, J., Condon, D., 2016b. Using ignimbrites to quantify structural relief growth and understand deformation processes: implications for the

development of the Western Andean Slope, northernmost Chile. Lithosphere 8, L593-1.

Victor, P., Oncken, O. and Glodny, J., 2004. Uplift of the western Altiplano plateau: Evidence from the Precordillera between 20 and 21 S (northern Chile). Tectonics, 23(4).

Vietor, T. and Echtler, H., 2006. Episodic Neogene southward growth of the Andean subduction orogen between 30 S and 40 S—plate motions, mantle flow, climate, and upper-plate structure. In The Andes (pp. 375-400). Springer, Berlin, Heidelberg.

Vila, T., Sillitoe, R.H., Betzhold, J. and Viteri, E., 1991. The porphyry gold deposit at Marte, northern Chile. Economic Geology, 86(6), pp.1271-1286.

von Huene, R. and Ranero, C.R., 2003. Subduction erosion and basal friction along the sediment-starved convergent margin off Antofagasta, Chile. Journal of Geophysical Research: Solid Earth, 108(B2).

Von Huene, R. and Scholl, D.W., 1991. Observations at convergent margins concerning sediment subduction, subduction erosion, and the growth of continental crust. Reviews of Geophysics, 29(3), pp.279-316.

Vry, V.H., Wilkinson, J.J., Seguel, J. and Millán, J., 2010. Multistage intrusion, brecciation, and veining at El Teniente, Chile: Evolution of a nested porphyry system. Economic Geology, 105(1), pp.119-153.

Ward, C. W., 1979, The geology and hydrothermal alteration of the Tongonan geothermal field, in New Zealand Geothermal Workshop, 1979, Proc.: Univ. Auckland Geothermal Inst. Centre Continuing Education, pt. 1, p. 113-125.

Weiland, R.J. and Cloos, M., 1996. Pliocene-Pleistocene asymmetric unroofing of the Irian fold belt, Irian Jaya, Indonesia: Apatite fission-track thermochronology. Geological Society of America Bulletin, 108(11), pp.1438-1449.

Westra, G., 1982. The Mount Hope stockwork molybdenum de-posit labs. I: Geol Soc. In America Abstracts with Programs (Vol. 14, p. 646).

Whipple, K.X., 2009. The influence of climate on the tectonic evolution of mountain belts. Nature geoscience, 2(2), pp.97-104.

White, D.E. and Waring, G.A., 1963. Volcanic Emanations: Chemical Analyses of Volcanic Gases, Volcanic Sublimates [etc.]. US Government Printing Office.

Wilkinson, B.H. and Kesler, S.E., 2007. Tectonism and exhumation in convergent margin orogens: Insights from ore deposits. The Journal of Geology, 115(6), pp.611-627.

Willett, S., Beaumont, C. and Fullsack, P., 1993. Mechanical model for the tectonics of doubly vergent compressional orogens. Geology, 21(4), pp.371-374.

Willett, S.D., 1999. Orogeny and orography: The effects of erosion on the structure of mountain belts. Journal of Geophysical Research: Solid Earth, 104(B12), pp.28957-28981.

Williams-Jones, A.E. and Heinrich, C.A., 2005. 100th Anniversary special paper: vapor transport of metals and the formation of magmatic-hydrothermal ore deposits. Economic Geology, 100(7), pp.1287-1312.

Wolfe, J.A. and Hopkins, D.M., 1967. Climatic changes recorded by Tertiary land floras in northwestern North America. In Tertiary correlations and climatic changes in the Pacific (Vol. 25, pp. 67-76). 11th Pacific Sci. Symp.

Wolfe, J.A., 1971. Tertiary climatic fluctuations and methods of analysis of Tertiary floras. Palaeogeography, Palaeoclimatology, Palaeoecology, 9(1), pp.27-57.

Wolfe, J.A., 1978. A paleobotanical interpretation of Tertiary climates in the Northern Hemisphere: Data from fossil plants make it possible to reconstruct Tertiary climatic changes, which may be correlated with changes in the inclination of the earth's rotational axis. American scientist, 66(6), pp.694-703.

Wood, C.A., McLaughlin, G. and Francis, P., 1987. Segmentation of volcano rich arcs. Transactions of the American Geophysical Union (EOS), 68, p.1519.

Woodruff, F., Savin, S.M. and Douglas, R.G., 1981. Miocene stable isotope record: a detailed deep Pacific Ocean study and its paleoclimatic implications. Science, 212(4495), pp.665-668.

Worcester P. 1935, Mining A Mountain, pp.63-64, Popular Mechanics.

Wörner, G., Hammerschmidt, K., Henjes-Kunst, F., Lezaun, J. and Wilke, H., 2000. Geochronology (40Ar/39Ar, K-Ar and He-exposure ages) of Cenozoic magmatic rocks from northern Chile (18-22 S): implications for magmatism and tectonic evolution of the central Andes. Revista geológica de Chile, 27(2), pp.205-240.

Wörner, G., Uhlig, D., Kohler, I., Seyfried, H., 2002. Evolution of the West Andean Escarpment at 18°S (N. Chile) during the last 25 Ma: uplift, erosion and collapse through time. Tectonophysics 345 (1–4), 183–198.

Yáñez, G. and Cembrano, J., 2004. Role of viscous plate coupling in the late Tertiary Andean tectonics. Journal of Geophysical Research: Solid Earth, 109(B2).

Yáñez, G., Cembrano, J., Pardo, M., Ranero, C. and Selles, D., 2002. The Challenger–Juan Fernández–Maipo major tectonic transition of the Nazca–Andean subduction system at 33–34 S: geodynamic evidence and implications. Journal of South American Earth Sciences, 15(1), pp.23-38.

Yanites, B.J. and Kesler, S.E., 2015. A climate signal in exhumation patterns revealed by porphyry copper deposits. Nature Geoscience, 8(6), pp.462-465.

Yogodzinski, G.M., Rubenstone, J.L., Kay, S.M. and Kay, R.W., 1993. Magmatic and tectonic development of the western Aleutians: An oceanic arc in a strike-slip setting. Journal of Geophysical Research: Solid Earth, 98(B7), pp.11807-11834.

Yuan, X., Sobolev, S., Kind, R., 2002. Moho topography in the central Andes and its geodynamic implications. Earth and Planetary Science Letters 199 (3), 389–402.

Yuan, X., Sobolev, S., Kind, R., Oncken, O., Bock, G., Asch, G., Schurr, B., Graeber, F., Rudloff, A., Hanka, W., 2000. Subduction and collision processes in the Central Andes constrained by converted seismic phases. Nature 408 (6815), 958–961.

Zachos, J., Pagani, M., Sloan, L., Thomas, E. and Billups, K., 2001. Trends, rhythms, and aberrations in global climate 65 Ma to present. science, 292(5517), pp.686-693.

Zandt, G., Beck, S., Ruppert, S., Ammon, C., Rock, D., Minaya, E., Wallace, T., Silver, P., 1996. Anomalous crust of the Bolivian Altiplano, Central Andes: constraints from broadband regional seismic waveforms. Geophysical Research Letters 23 (10), 1159–1162.

Zandt, G., Leidig, M., Chmielowski, J., Baumont, D., Yuan, X., 2003. Seismic detection and characterization of the Altiplano–Puna magma body, central Andes. Pure and Applied Geophysics 160 (3–4), 789–807 (Sc).

# 7 Appendices

## 7.1 Appendix I

The Andean Volcanoes and Eruption Database (AVEDB) is a compilation of volcanic centres and eruptions along the South American Andes extracted from diverse sources with a total of 5477 records. It is presented in Microsoft Excel format and the design is explained below.

### 7.1.1 Database design

In this dataset there are 63 data columns with information, which remain the same for the AVEDB as well as for the IIDB and they are described in detail below.

For empty numerical or string records in the AVEDB, values of -99 and NP were assigned respectively. For consistency, some transformations were made (e.g., change in co-ordinate system, units, references). If the original information provided by the source was considered particularly important, then, the raw data were kept in columns in the DB with the suffix 'Source' (e.g., Age Class Source)

#### *7.1.1.1 General fields*

- *ID*
  Each record was assigned with a unique identificatory number.
- *Sample ID*
  Samples collected in the field were assigned a name by each author.
- *Unit sampled*
  When provided by the source, a short and simple description of the unit where the sample was collected is given.
- *Unit filter*
  With the aim of easily identifying different components of this set, data were classified in 4 broad categories: ignimbrites, intrusive units, volcanoes and eruptions (Figure 7-1).

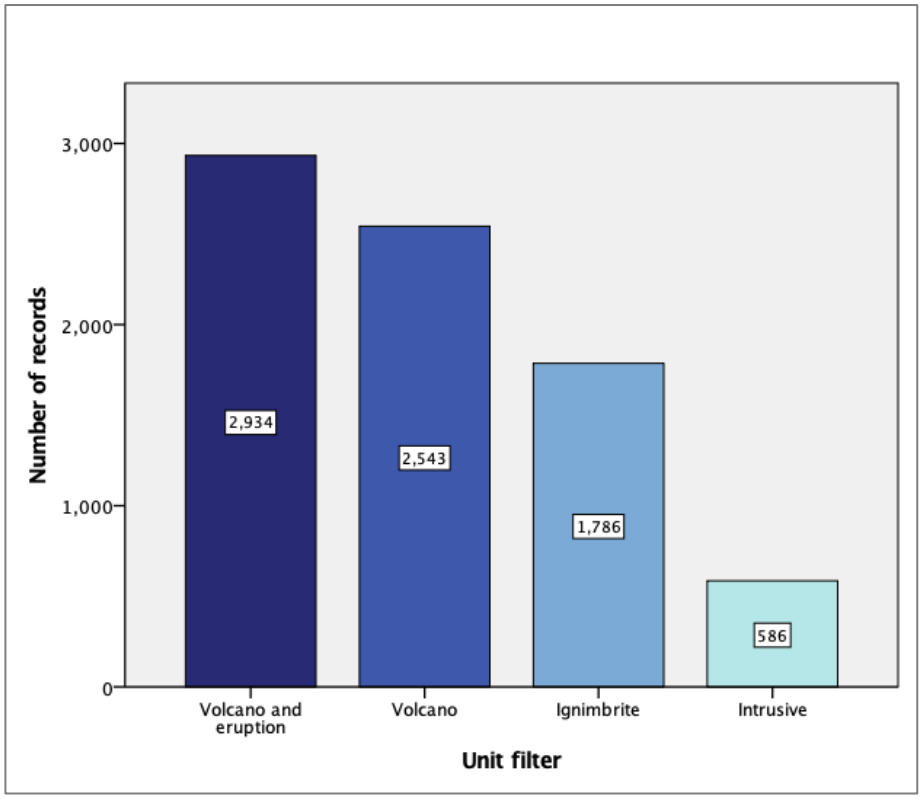


*Figure 7-1. Histogram showing 4 categories for "Unit filter" field.*

- *IAVCEI ID and Volcano ID number* provide a unique identification number for each volcano. ID numbers between 351002 to 355150 were assigned by the International Association of Volcanology and Chemistry of the Earth's Interior (IAVCEI). The Smithsonian is responsible for these volcano numbers. This information is only provided by LaMEVE DB, SGVP and NOA's programmes.

- *Volcano name: Volcano name and Alternative name*

  This field includes primary and, sometimes, alternative volcano names. In some cases, different authors use similar names (e.g., Quevar Volcanic complex/ Quevar stratovolcano). In other cases, the volcano has an official name, but a completely different name is also used (e.g., Ramadas / La Pava). Lastly, the spelling of the volcano name can vary according to the author's nationality, although the name remains similar (e.g., Vulsini / Volsini).

- *Volcano location: Country, region and coordinates (Latitude DD, Longitude DD, Elevation(m))*

  The first two fields specify the country and region where the volcanic edifice/ volcanic deposit is located.

  - *Country* records belong to 6 countries in South America, Argentina, Bolivia, Colombia, Chile, Ecuador and Peru (**Error! Reference source not found.**).
  - *Region* field is the result of different sources feeding the AVEDB:

- LaMEVE assigns number codes for countries and regions. In AVEDB these codes were replaced by the name of the region following LaMEVE specifications. (15: South America).
- It could represent provinces (i.e., Rio Negro in Argentina or II Region in Chile).
- It could also indicate a referenced location (i.e., 2 km from La Bandera area), or a city, a geographic or geological feature (i.e., Arica, Cardones Valley, Caldera south rim).
- When no information was provided, the field was completed with "South America".

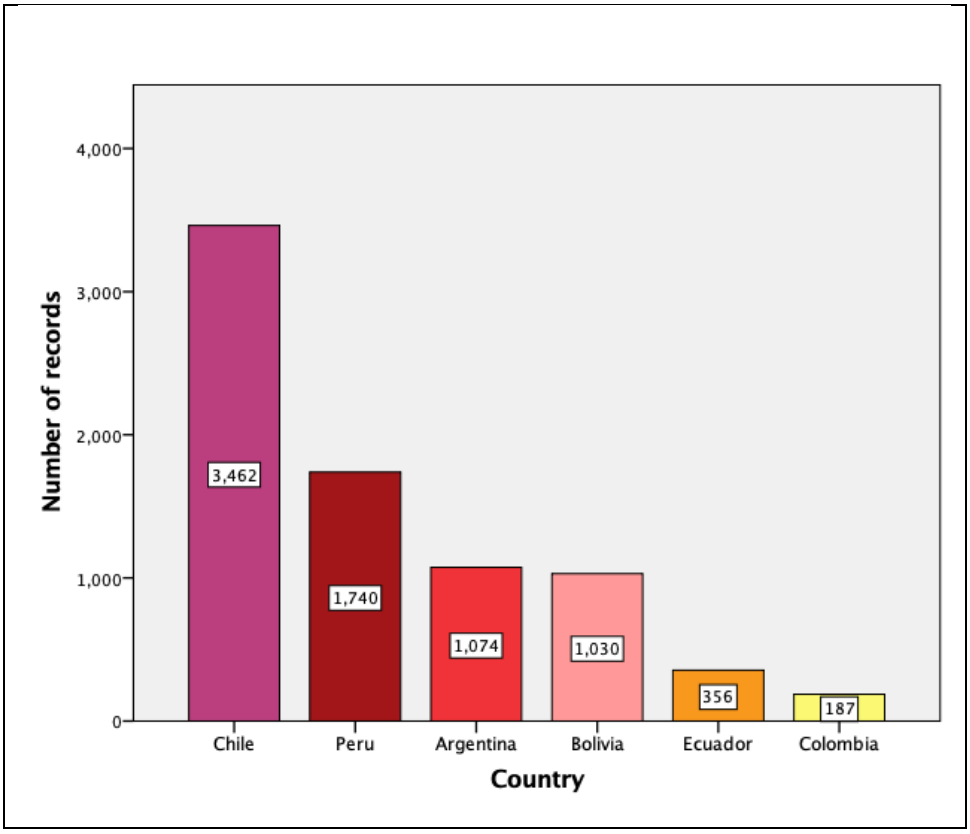


*Figure 7-2. Histogram showing "Country" categories and the number or records.*

The last three fields, *Latitude DD, Longitude DD, Elevation(m)* above the sea level, indicate the location of the feature. For edifices this is the centre of the base of the volcano (i.e., not the summit). It was necessary to unify the coordinate systems of the sources. For example, for northern Chile, a local coordinate system called PSAD19S (Provisional South American Datum 1956) is usually used. It is a projected coordinate system for South America that extents between 72°W and 66°W, in the southern hemisphere. While southern Argentina uses a local datum called Campo Inchauspe. For that reason, a unique coordinate system that could be applied for all South America was defined for this study which is WGS84 given in Decimal degrees (DD). The latitude and longitude are located at the centre of the volcanic edifice.

Regarding elevation, any record was kept as in the original source, except for volcanoes.

If no elevation data were provided by the original source, the parameter was calculated as followed:

a. For intrusive samples (Haschke et al., 2002), elevation is not a representative parameter, since it is only showing the altitude where the sample was collected, thus I have assigned a -99 value.
b. Elevation was extracted from a Digital Elevation Model (DEM) in ArcGIS for any datapoint except volcanoes.
c. If the record is a volcano with no altitude information, I have obtained the edifice base altitude using Google Earth profiles.
d. If the record is a volcano with altitude information, I have corroborated how the estimation was made, since some authors have estimated the elevation on the summit of the volcanic edifice. If that was the case, I have recalculated elevation as follow: Elevation (m) = volcano summit elevation - volcano height.

#### *7.1.1.2 Volcanoes parameters*

- *Volcano type*

  Volcano edifices and its deposits were classified using the categories described in Table 7-1 and shown in Figure 7-3.

  A unification was needed since the different sources have different names for the same type o volcano (i.e., Stratovolcano = Composite volcano = Volcanic complex = Complex Composite Volcano or Lava dome = Dome).

*Table 7-1: Volcano type classification.*

| Volcano type | Database | Description |
|---|---|---|
| Breached Cone | AVEDB | Stratovolcano with broad amphitheatre or valleys cutting from the summit through flanks. |
| Caldera | IIDB | Volcanic crater (its diameter has several times the vent dimension) generated by the collapse of the central portion of a volcano or by explosions during eruptions. |
| Dome | AVEDB | Extrusive lava dome. |
| Fissure vent | AVEDB | Linear volcanic vent through which lava erupts, usually without any major explosive activity. (Pfeiffer, 2004) |
| Ignimbrite Shield | IIDB | Low shield often cut by radial valleys and topped by domes. |
| Intrusive units (stocks, dykes, porphyry) | IIDB | Intrusive bodies are not volcanoes but are included in the IIDB. |
| Lava flow | AVEDB | Lava flow without an obvious source. |
| Maar | AVEDB | Circular volcanic crater produced by a phreatomagmatic eruption, often filled with a shallow water body. |
| Monogenetic centre | AVEDB | Group of small volcanoes, each of which erupts only once. |
| Pyroclastic deposit | AVEDB | Deposit of ash and magma fragments from an explosive eruption. |
| Scoria cone | AVEDB | Simple scoria cone formed around the vent, consisting of loose pyroclastic debris after an explosive eruption. |
| Shield Volcano | AVEDB | Constructed from basaltic low viscosity lava flows, they have a broad profile due to the cumulative built up of flows over time, erupting from vents or fissures on the surface of the volcano. |
| Stratovolcano | AVEDB | Simple composite volcano, most common type in the Andes. |
| Central volcano and domes | AVEDB | Focal point for volcanic activity and normally is the largest edifices within the system. They are generally at the centre of a volcano cluster. They could be a proper volcano edifice or a dome. |
| Volcanic Centre | AVEDB | Also called “volcanic field”, they are characterised by many cinder cones or other volcanic features that have not been independently recognised as separate volcanoes. |

| | | |
|---|---|---|
| | | They could be scattered over a large area, if many short-lived volcanoes are built rather than a major volcano with frequent eruptions. |
| Subglacial | AVEDB | Volcanic edifice constructed in whole or in part by eruption beneath ice. Although eruptions may start subglacially initially, many subglacial volcanoes culminate subaerially, having melted their way completely through the overlying ice. (Smellie, 2014) |

*a.*

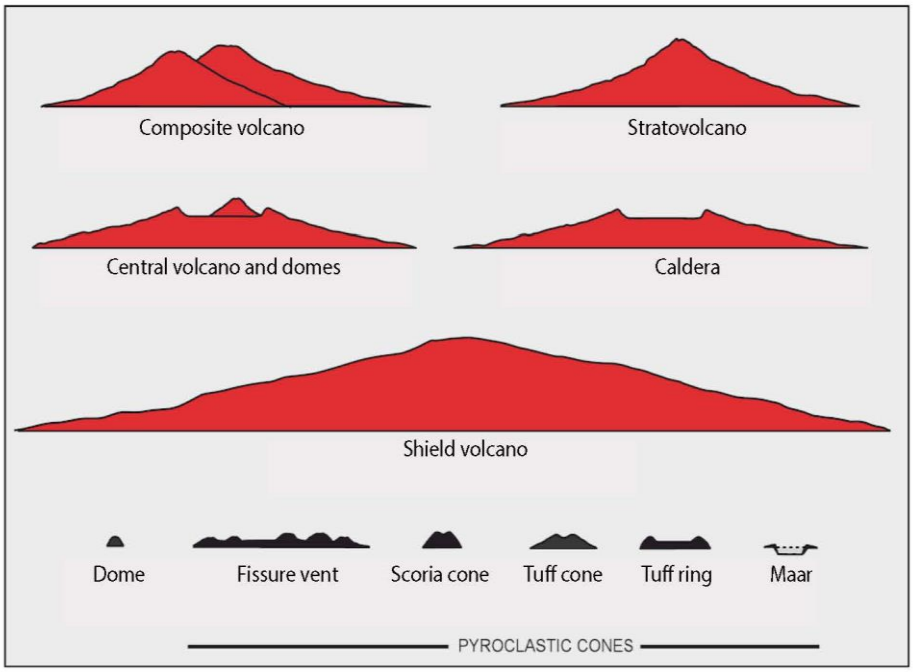


*b.*

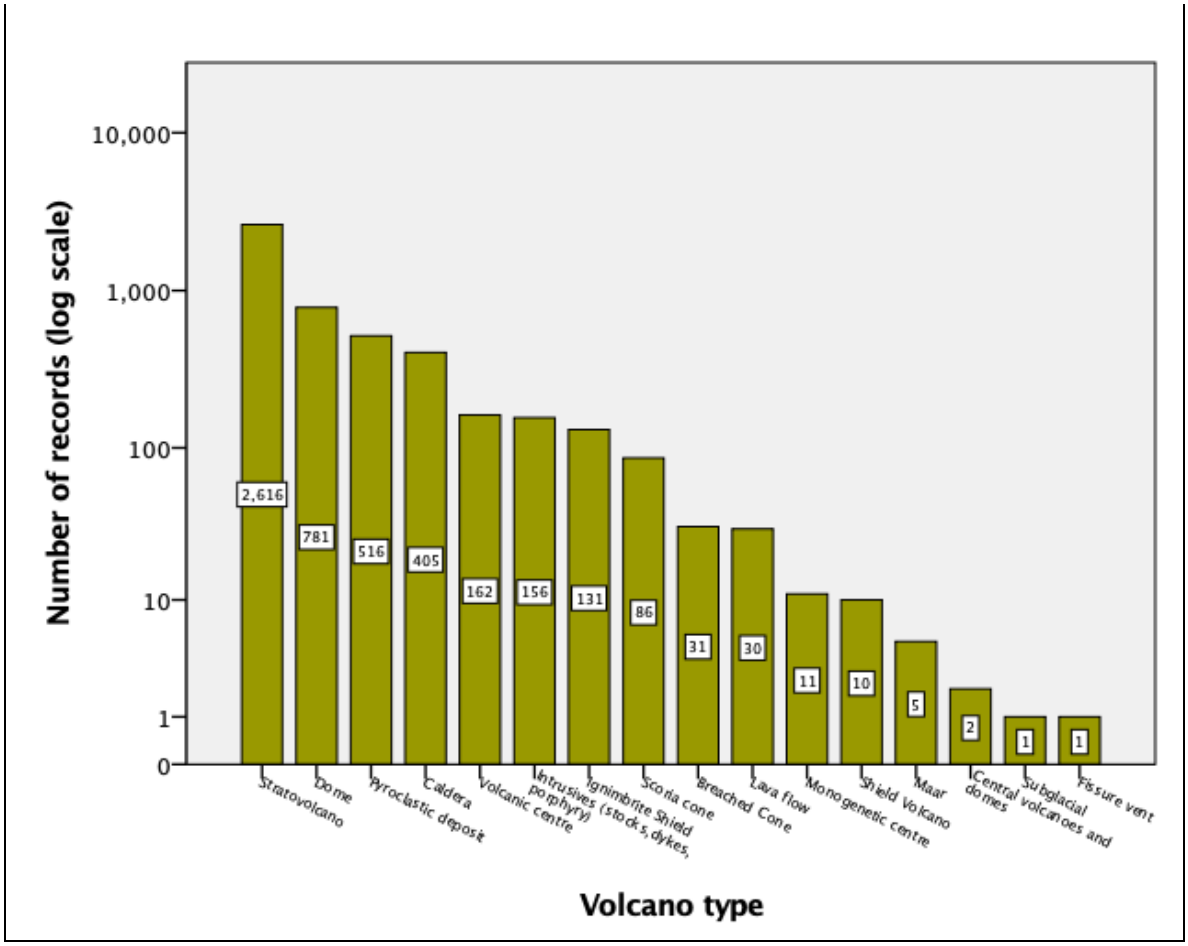


*Figure 7-3. a. Volcano classification modified from Volcanoes of the World, Siebert et al. (2010). b. Histogram showing "Volcano type" categories.*

- *Volcano Activity Status*

  The level of activity of the volcano was classified into the following categories (Figure 7-4) respecting the epochs and time ranges in **Error! Reference source not found.**:

  - *Active:* Available age records of magmatic or phreatomagmatic events in the last 100 years, considering the present as the year 2020 (0.0001Ma).
  - *Fumarolic stage:* characterised by steam and volcanic gas, or fume, reaching the surface. Temperatures are near the boiling point of water. This category is assigned only if there is no explicit evidence for Holocene nor Pleistocene eruptive activity. (Siebert et al., 2010)
  - *Latent:* evidence of very recent activity or age records of Holocene activity prior 100 years from present. (2020-0.01Ma)
  - *Dormant:* No age records of Holocene, although it may include some evidence of Holocene eruption. It also includes age records for Pleistocene activity. (0.01Ma-1.5Ma)
  - *Cenozoic active:* Age records of eruptions 1.5Ma- 60Ma.
  - *Mesozoic active:* Age records of eruptions 60Ma- 201.3Ma.
  - *Palaeozoic active:* Age records of eruptions 201.3Ma - 541Ma.

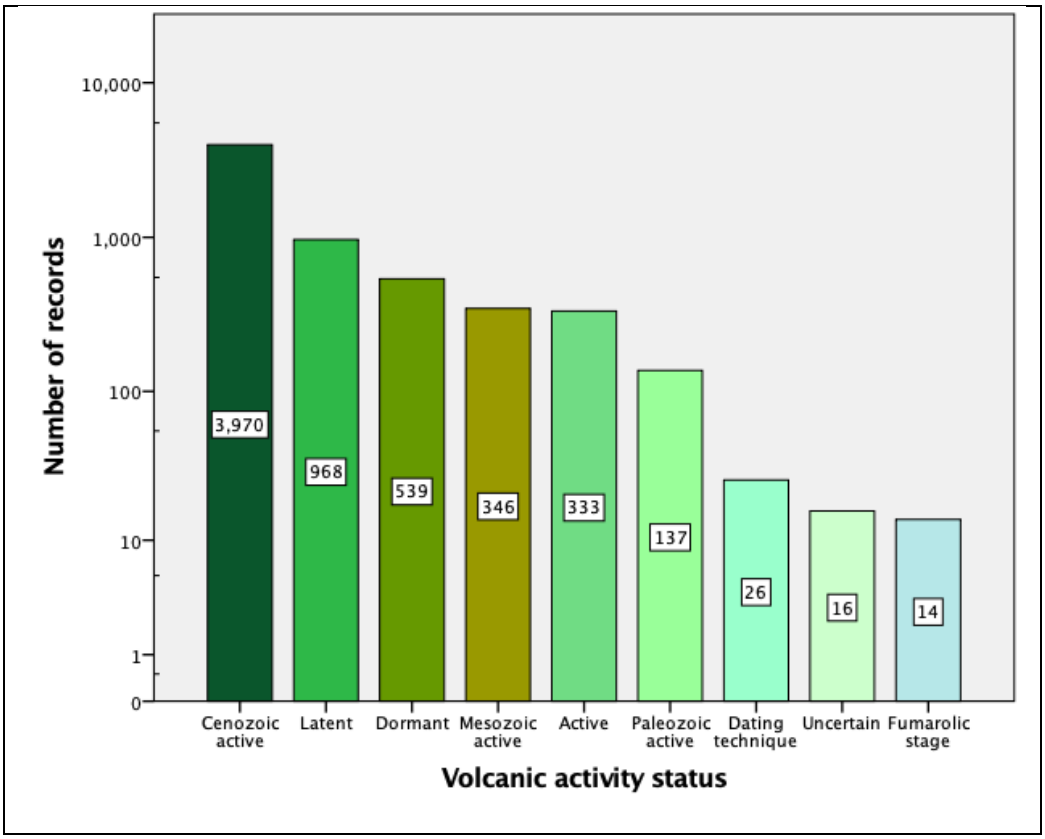


*Figure 7-4. Histogram showing the volcanic activity status records.*

- *Volcano height (m)*

- *Volcano Volume ($km^3$)* was extracted from sources with different approaches for volcano volume calculation. In Volcanoes of the Andes book (De Silva et al., 1991), volume was calculated by modelling the edifice as a steep cone on an apron of debris with an assumed 3º slope even if the volcanic centre is not conical. Brandmeier et al. (2014) calculated volume based on a series of GIS-based maps of individual outflow sheets and assigned an average thickness to each volcanic unit. Guzmán et al. (2014) determined an aerial extent of the deposits for assessment of the intensity of volcanic activity, and then they assumed a proportional volume.
  Other sources, such as *Volcanes Activos de la República Argentina-ING* and *Ranking de los 90 volcanes activos de Chile* did not explain how volcano volume was calculated. For more extensive details, see the original source documents.

- *Cone Diameter (km)* is the basal diameter of the volcano and it is a topographic parameter derived from an estimation of the change of slope from gentle surrounding to steeper slopes of the volcanic edifice. In this study, cone diameter values were calculated using the Google Earth profile tool, delimiting the margin of the edifice where the rate of change in the slope is highest.

- *Crater Diameter (km)* is the average diameter of a central or summit depression (De Silva et al., 1991). When no crater diameter was given by the author, but the caldera diameter or any of its axes could be measured, these values were added into this field.

  Values '0' means no crater was recognised or detected and value 0.25 means there may be a small crater, but a meaningful estimation cannot be made.

- *Volcano size*

  I have classified the volcanic edifices as large, medium or small, following Castruccio (2017), as outlined in **Error! Reference source not found.**.

*Table 7-2: Volcano size classification of Castruccio (2017).*

| Volcano size | Volcano Volume ($km^3$) | Volcano height (m) | Cone Diameter (km) |
|---|---|---|---|
| Large | > 100 $km^3$ | > 2,000 m | > 24 km |
| medium | 100 $km^3$ < > 50 $km^3$ | 2,000 m < > 1,800 m | 24 km < > 14 km |
| small | <50 $km^3$ | < 1,800 m | < 14 km |

According to Castruccio et al. (2017), the vent and how the plumbing system is connected at depth, will influence the shape and size of volcanoes. Therefore, it is possible to infer the properties of the plumbing system using the volcano dimensions. As shown in Figure 7-5, basal radius, maximum volcano height and maximum volume are regulated by the depth and size of the magma chamber, in turn, these parameters will influence the lifetime of the volcano.

Castruccio et al. (2017) found:

- Large volcanoes present heights greater than 2000 m; basal radius bigger than 12 km; and volume over 100 $km^3$. They are associated with basaltic systems with intermediate to deep and large magma chambers.
- Small volcanoes show heights shorter than 1800 m, basal radius smaller than 7 km and volume of 50 $km^3$ or lees. They are associated to more evolved systems and shallower magma chambers.

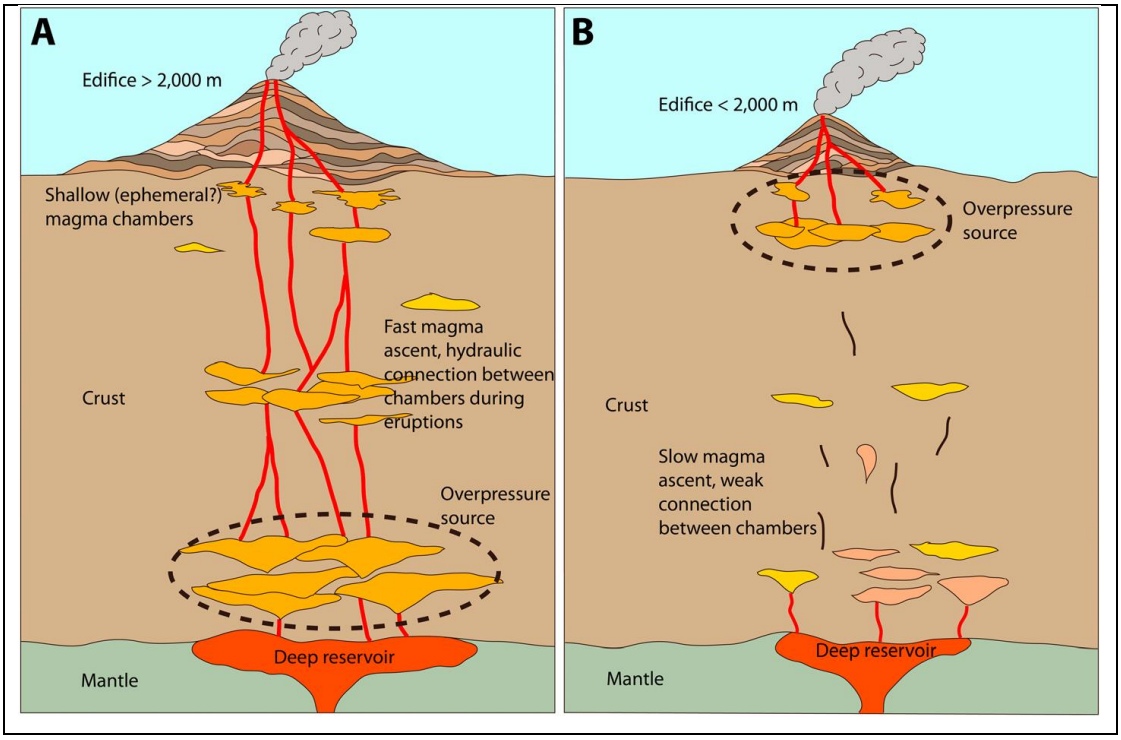


*Figure 7-5. Cartoon from Castruccio et al. (2017), showing two size of volcano and the implication in their plumbing system: a) large volcanoes are fed by a deep overpressured magma source and b) smaller volcanoes only connected to shallow magma chambers.*

- *Erosion Status* indicates the morphological state of erosion of the volcanic edifice. The five categories (**Error! Reference source not found.**; Figure 7-6) are estimated by comparison with radiometrically dated volcanoes and take into account that pyroclastic deposits erode faster than lava flows (De Silva et al., 1991).

*Table 7-3: Erosion status classification for volcanoes edifices* (De Silva et al., 1991).

| Erosion status | Description |
|---|---|
| 1 | Fresh, young cones, often dark, and pristine lava flows and summit crater visible, sharp profile. Not glaciated. |
| 2 | Small gullies on flanks, lavas visible and crater may exist, but degraded; cone still sharp, dark apron gone. Moraines present. |
| 3 | Individual lava flows barely visible, no crater, well established gullies; constructional surfaces dwindling; planezes initiated. |
| 4 | No lava flows visible, deeply incised gullies, large planezes little original cone surface left. Considerable relief; major “U-shaped” glacial valleys. |
| 5 | Barely recognisable, low relief; radial symmetry the only clue to volcanic origin. |

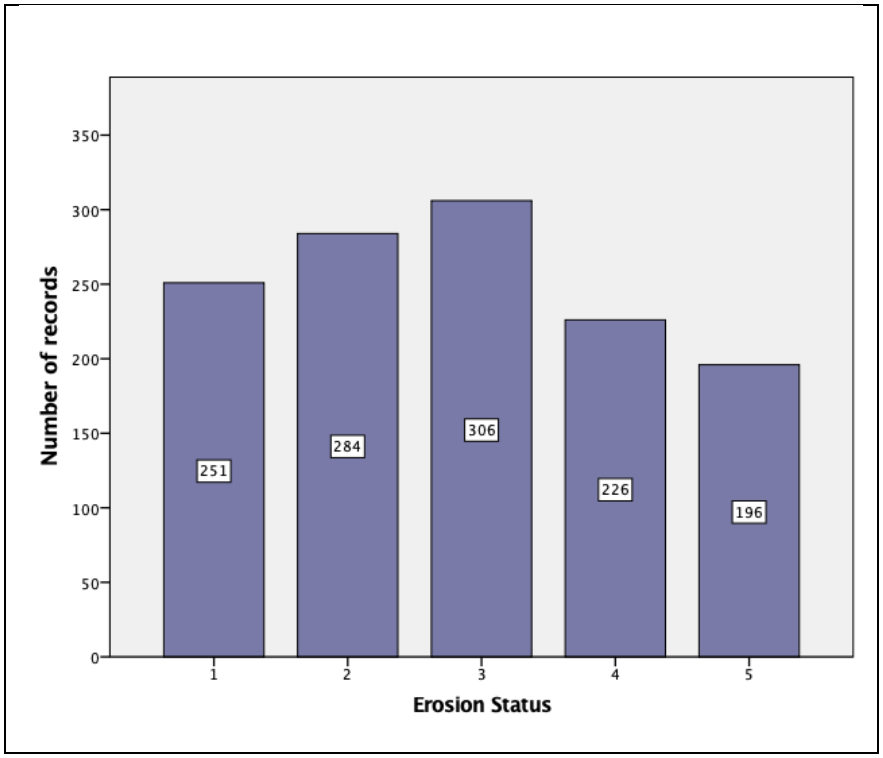


*Figure 7-6. Erosion status histogram and its categories.*

### *7.1.1.3 Eruption parameters*

- *Deposit Diameter (km)* provides a measure of the extent of volcanic products derived directly from the volcano, such as lavas and mudflows. It is often a subjective measurement, obtained by measuring a dark halo of material surrounding the volcano thought to correspond to the extent of the deposit (De Silva et al., 1991). Records for this field were mainly extracted from the sources, the rest of the values were calculated in this study using the Google Earth profile tool.

- *Flow length (km)* is the length of the longest distinct lava flow on the volcano (De Silva et al., 1991). Records for this field were mainly extracted from the sources, the rest of the values were calculated in this study using Google Earth profile tool.

- *Area ($km^2$)* represents the areal extent of pyroclastic deposits. These values were extracted from Guzmán et al. (2014) who mapped the units using LANDSAT images. Some missing values were complemented with information extracted from Volcanes Activos de la República Argentina.

- *Bulk Volume ($km^3$)*
  Bulk Volume is the combined volume of tephra fall, ignimbrite and primary intra-caldera material volumes. Lava flow volumes are not included because eruption magnitude values traditionally only

include explosive phases. See LaMEVE DB for more information on values and calculations. No new calculations were performed for this field in this study.

- *Bulk DRE Volume ($km^3$)*

  DRE stands for Dense Rock Equivalent and represents the unvesiculated erupted magma volume from explosive eruptions (as for Bulk Volume). It was extracted from literature or calculated by Crosweller et al. (2012) in the LaMEVE DB. No new calculations were performed for this field in this study.

- *Magnitude*

  Magnitude is the preferred measure of eruption size used in the LaMEVE database and the one used for this study. It is calculated using the formula of Pyle et al. (2000) as follows:

$$\boldsymbol{M = log10(erupted\ mass\ in\ kg)^{-7}}$$

  However, for eruptions with an assigned Volcanic Explosivity Index (VEI; Newhall et al., 1982) value but no volume data or magnitude reported in the literature, eruption magnitude is assigned according to the relationship found between these two variables as done by Crosweller et al. (2012) (Figure 7-7**Error! Reference source not found.**). It is a quantitative parameter rather than a qualitative indicator that can be used to estimate magnitude-frequency relationships. The largest explosive eruptions on Earth are ~M=9, comparable to the magnitude of the largest earthquakes, and the smallest ones are M=1 (Newhall et al., 1982).

  The only source that provides magnitude of eruption values is the LaMEVE DB and no new calculations were performed in this study.

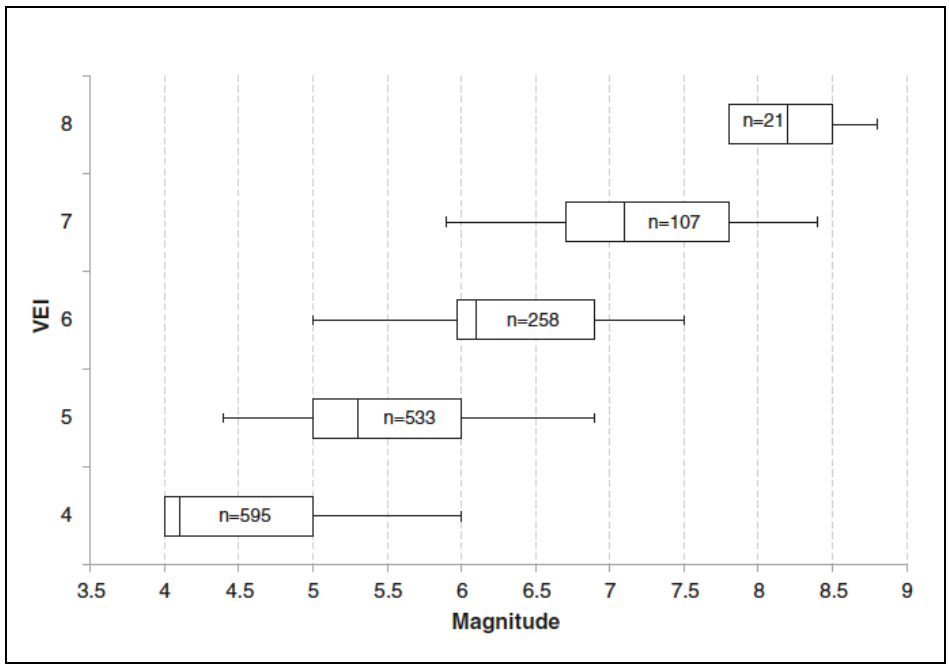

*Figure 7-7. Figure from Crosweller et al. (2012). Box and whisker plot of VEI classification versus Magnitude for global and historic eruptions in the LaMEVE database, the boxes represent a range between 5$^{th}$ and 95$^{th}$ percentiles, median is represented by the dividing line within the boxes. Whiskers indicate minimum/maximum values and 'n' inside the boxes stands for the number of eruption records at that VEI.*

- *Rock type from source* indicates rock types (e.g., Plutonic) and compositions (e.g., Dacite-Andesite) as written in the original sources.

- *Dominant Rock type*

  The dominant rock type categories were standardised into '*Composition'* field using the terms shown in **Error! Reference source not found.**. Figure 7-8 shows the distribution of the different eruption compositions.

*Table 7-4: Rock name classified as per composition.*

| Composition | Rock names |
|---|---|
| Basaltic | Mafic composition |
| | Basalt |
| | Basalt- Basaltic andesite |
| | Basaltic andesite |
| | Trachybasalt |
| | Nepheline |
| | Picro-Bassalt |
| Andesitic | Intermediate composition |
| | Andesite |
| | Diorite |
| | Shoshonite |
| | Latite |
| | Monzonite |
| | Monzodiorite |
| | Monzogabbro |
| | Trachyandesite |
| Dacitic | Dacite |
| | Dacite-Rhyolite |
| | Dacite-Andesite |
| | Dacite-Rhyodacite |
| | Granodiorite |
| Rhyolitic | Felsic composition |
| | Rhyolite |
| | Rhyolite-Rhyodacite |
| | Granite |
| | Vitrophyre |
| | Glass |

| | |
|---|---|
| | Aplite |
| | Macusanite |
| Trachytic | Trachyte |
| | Trachydacite |
| Phonolitic | Phonolite |
| | Phonotephrite |

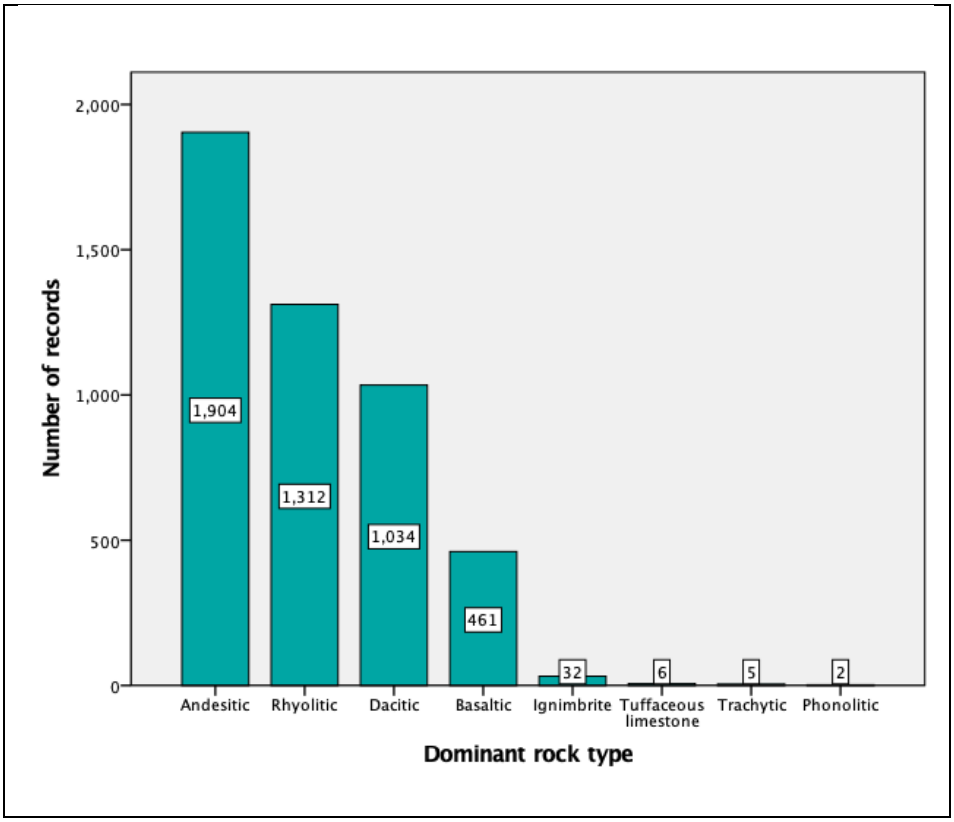


*Figure 7-8. Histogram plot of dominant rock composition of the different eruptive events.*

### *7.1.1.4 Ages and dating*

Authors state the age when a volcanic eruption took place in different ways. LaMEVE DB for example, record all the eruptions dates as number of years before or after a reference date, considering the "present" to be 1950. Consequently, years from 1950 until today are represented with negative values. In addition, the error for each data point is given in number of years. Other datasets (e.g., Brandmeier et al. and Trumbull et al.) provide ages in millions of years from now backwards (i.e., 15 Ma). In the case of the VOTW DB, the dates are given in the year when the eruption started (i.e., 1810 AC) and negative values, represent eruptions that took place BC (e.g., -200 BC). For the Guzmán et al. (2014) dataset, a range of age was given (e.g., 2.08–2.72 Ma). For other sources (Smithsonian Global Volcanism Program, Chilean Geological Map), only epochs were given, according to the international stratigraphic chart.

Because of the variability in how eruption ages were established and reported, a transformation was needed in order to bring all the ages to the same starting point. For this study, the origin date was set to be the year

2020 and all the ages were re-calculated to that initial point in time. In the same way, the scale was changed from years into millions of years (Ma).

For age ranges, the transformation was to calculate an average between the maximum and minimum ages. Similarly, for epochs, the average age between the beginning and the end of the epoch was used.

**Error! Reference source not found.** summarises the age recalculation done.

*Table 7-5: Eruption age recalculations.*

| Date | LaMEVE (years) | VOTW (years) | SGVP | Geological map of Chile | Guzmán et al. (2014) | Brandmeier et al. (2014) | Trumbull et al. (2006) | This study | |
|---|---|---|---|---|---|---|---|---|---|
| | | | | | | | | Age Classes | Age (Ma) |
| 1 Ma | 1002950 | -1000000 | Pleistocene | Pleistocene | | 1 Ma | 1 Ma | Pleistocene (0.01-1.5 Ma) | 1 Ma |
| 1000 BC | 2950 | -1000 | Holocene | Holocene | | 0.001 Ma | 0.001 Ma | Holocene | 0.001 Ma |
| 0 | 1950 | 0 | Holocene | Holocene | | | | Holocene | 0.00202 Ma |
| 1950 AC | 0 | 1950 | Holocene | Holocene | | | | Holocene | 0.00195 Ma |
| 2020 AC | -70 | 2020 | Holocene | Holocene | | | | Holocene | 0 Ma |
| | | | | | 3.7–5.1 Ma | | | Lower Pliocene (3.1-5) | 4.4 Ma |

The fields related to age created are:

- *Last known eruption*: the last known and recorded eruption according to the original source. Units may vary.

- *Year source*: the age/date when the eruption has happened, exactly as given as in the original source.

- *Error source (A)* represents the estimated error in the eruption age, given in number of years, as obtained in the original source. While in the LaMEVE DB the error is given in number of years respect to the absolute age, the GSVP defines an uncertain period from when the eruption started (Start Year Uncertainty).

- *Age (Ma)*

- *Error (Ma)*

- *Age class source* represents the epoch when the eruption took place, extracted from the original source.

- *Age epoch* represents the epoch when the eruption took place, transformed following the 2017 international stratigraphic chart time periods. The year range for each category can be seen in **Error! Reference source not found.**.

  When no absolute age is known, but a class age was provided, it was transformed into the upper age class (i.e., Age class source: Eocene, in this study Age class: Upper Eocene (35-41)). When instead of providing an age epoch, the author only gave the period, then the Age Class field was assigned a code

corresponding to the upper epoch (i.e., Period provided by author: Quaternary, Epoch assigned in this study: Holocene).

Because absolute ages are important in this study, if the age was not provided but there was an epoch available, then a transformation was applied in order to obtain a value for the field Age (Ma). I calculated the middle point between the beginning and the end of the age range. **Error! Reference source not found.** shows recalculated ages in My.

*Table 7-6: Age classes and age periods.*

| Age-Period | Age-Epoch | Age range (Ma) | Recalculated age (Ma) | Recalculated age (Ma) |
|---|---|---|---|---|
| Holocene | Holocene (0-0.01) | 0-0.01 | 0.0005 | 0.0005 |
| Pleistocene | Pleistocene (0.01-1.5) | 0.01-1.5 | 0.755 | 0.755 |
| Pliocene | Upper Pliocene (1.5-3) | 1.5-3 | 1.58 | 3.25 |
| | Lower Pliocene (3.1-5) | 3.1-5 | 3.26 | |
| Miocene | Upper Miocene (5-10) | 5-10 | 5.25 | 14 |
| | Mid-Miocene (10-15) | 10-15 | 10.50 | |
| | Lower Miocene (15-23) | 15-23 | 15.75 | |
| Oligocene | Upper Oligocene (23-29) | 23-29 | 24.15 | 29 |
| | Lower Oligocene (29-35) | 29-35 | 30.45 | |
| Eocene | Upper Eocene (35-41) | 35-41 | 36.75 | 39.025 |
| | Lower Eocene (41-56) | 41-56 | 43.05 | |
| Palaeocene | Upper Palaeocene (56-61) | 56-61 | 58.80 | 60.025 |
| | Lower Palaeocene (61-66) | 61-66 | 64.05 | |
| Cretaceous | Upper Cretaceous (66-100.5) | 66-100.5 | 69.30 | 85.765 |
| | Lower Cretaceous (100.5-145) | 100.5-145 | 105.53 | |
| Jurassic | Upper Jurassic (145-163.5) | 145-163.5 | 152.25 | 173.15 |
| | Middle Jurassic (163.5-174.1) | 163.5-174.1 | 171.68 | |
| | Lower Jurassic (174.1-201.3) | 174.1-201.3 | 182.81 | |
| Triassic | Triassic (201.3-251.9) | 201.3-251.9 | 211.37 | 226.6 |
| Palaeozoic | Permian (251.9-298.9) | 251.9-298.9 | 264.50 | 380.785 |
| | Carboniferous (298.9-358.9) | 298.9-358.9 | 313.85 | |
| | Devonian (358.9-419.2) | 358.9-419.2 | 376.85 | |
| | Silurian (419.2-443.8) | 419.2-443.8 | 440.16 | |
| | Ordovician (443.8-485.4) | 443.8-485.4 | 465.99 | |
| | Cambrian (485.4-541.0) | 485.4-541.0 | 509.67 | |
| Precambrian | Precambrian (541-4600) | 541-4600 | 568.05 | 2570.5 |

- *Age period* is a simplification for epochs and periods ages. If a volcano/ eruption or sample was assigned as Upper Eocene in the *Age epoch* field, in this category it is Eocene.

- *Period by arc*

- *Age by arc (Ma)*

  After a volcano/sample was given a period age according to the arc where it is located, an age in My was assigned, using **Error! Reference source not found.**. Empty cells were filled in with data from *Age (Ma)*. This field is the most complete compilation of ages within the AVED).

- *Age period* represents the final compilation for age periods after recalculations and spatial location estimation.

*a.*

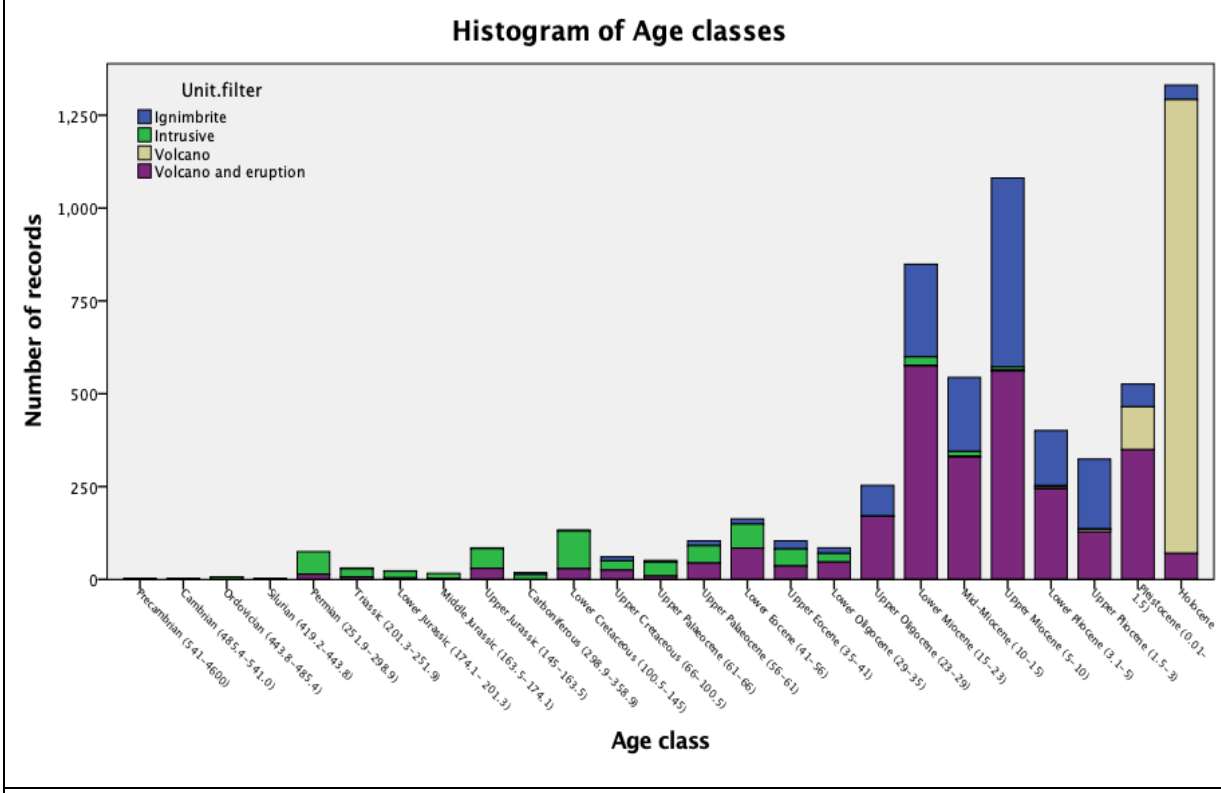


*b.*

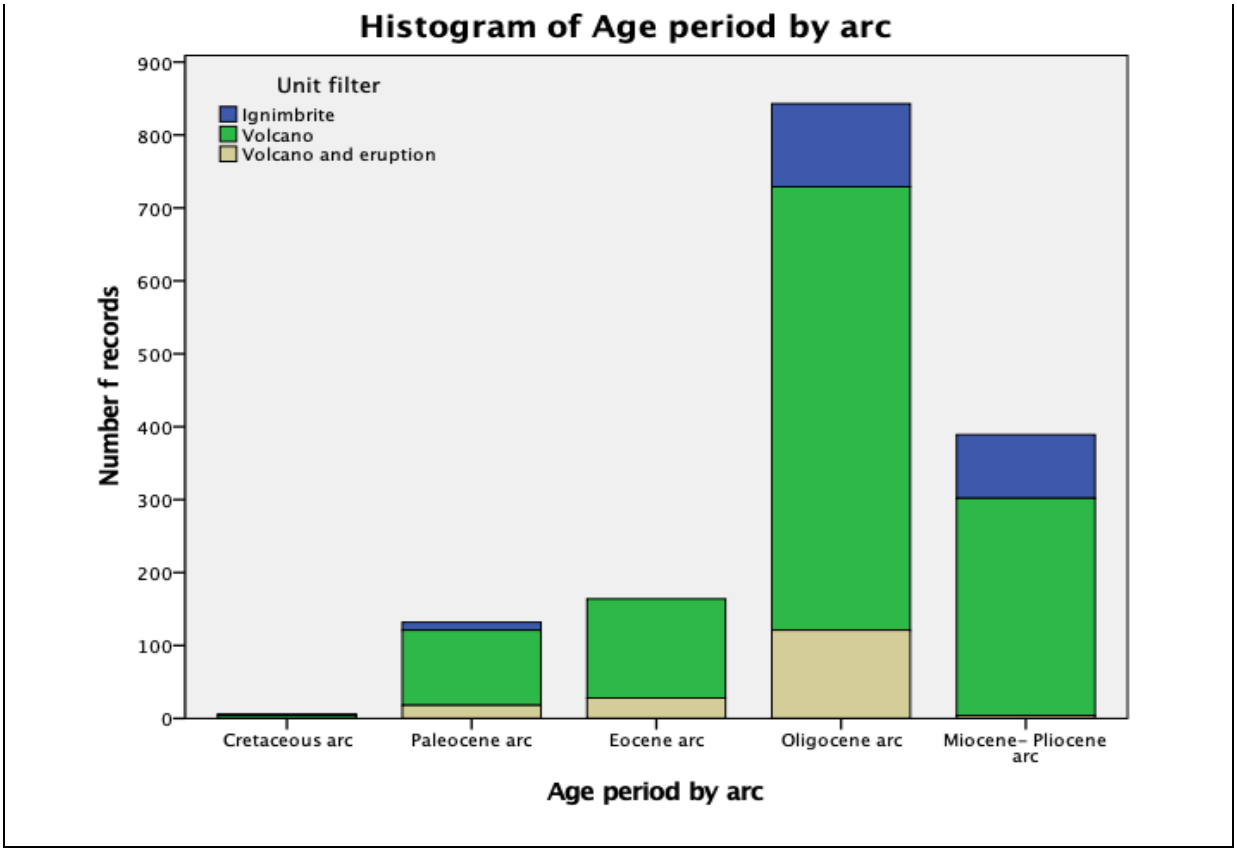


*Figure 7-9. Comparison between the number of registers with ages from literature against ages assigned by the location within magmatic arcs. a. Histogram of age classes coming from different sources. b. Histogram of the age periods for datapoints located in different magmatic arcs.*

- *Uncertainty source* refers to the age certainty of the record, provided by the original source. No unification of the data is applied in this field, it corresponds to the raw data coming directly from the source.

- *Dating method*

  The different categories of dating methods in the compiled data are described below and summarised in **Error! Reference source not found.**.

  For recent eruptions, including those with only an approximate date, two categories exist: *Anthropology* and *Historical observations*.

  The most commonly used dating techniques for eruptions are Argon- Argon ($^{40}Ar$-$^{39}Ar$), Potassium-Argon (*K-Ar*), stratigraphy (*varve count*), *tephrochronology* and radiocarbon ($^{14}C$).

  The first two deliver absolute dates in My with an associated uncertainty (*Error Source(A)* and *Error 2020(Ma)*), while *Varve count* and *Tephrochronology* offer an unprecise relative date, constrained by dated stratigraphic layers on top and bottom of the one being studied.

Radiocarbon dating works well for eruptions that occurred up to 50,000 years. However, radiocarbon years are not equivalent to standard calendar years because of fluctuations in atmospheric $^{14}C$ and thus a calibration must be applied to determine the actual eruption date (Crosweller et al., 2012). Although this kind of error will not affect the results of this study, this type of dating has been classified as corrected or uncorrected by Crosweller et al. (2012). For details on the calibration method, refer to the LaMEVE dataset compilation.

Lastly, Fission Track *(FT)* is useful for a geological range between 0.1Ma to 2000 Ma, while Rubidium-Strontium *(Rb-Sr)* and Uranium- Lead *(U-Pb)* from about 1 My to billions of years (Parrish et al., 2003).

Regrettably, in some cases although ages were provided, no dating method was indicated, and those samples were classified as *Uncertain*.

*Table 7-7: Dating methods and codes.*

| **Dating method** | Material | Code method |
|---|---|---|
| **Anthropology** | | Anthropology |
| **Argon–argon** | | Ar-Ar |
| | Alunite | Ar-Ar Alu |
| | Biotite | Ar-Ar Bt |
| | Sanidine | Ar-Ar Snd |
| | Sericite | Ar-Ar Ser |
| | Amphibole | Ar-Ar Amph |
| | Feldspar | Ar-Ar Feld |
| | Glass or Matrix | Ar-Ar G/M |
| | Hornblende | Ar-Ar Hornb |
| | Muscovite | Ar-Ar Muscov |
| | Plagioclase | Ar-Ar Plag |
| | Zircon | Ar-Ar Zirc |
| | Ash or Pumice | Ar-Ar Ash/Pum |
| | Total rock | Ar-Ar Total Rock |
| **Radiocarbon** | Not given | $^{14}C$ |
| | Organic material | $^{14}C$ Organic mat |
| | Radiocarbon (uncorrected) | $^{14}C$ (uncorrected) |
| | Radiocarbon (corrected) | $^{14}C$ (corrected) |
| **Fission track** | Not given | FT |
| | Apatite | FT Apat |
| | Zircon | FT Zirc |
| **Historical observations** | | Historical obs |
| **Potassium-Argon** | Biotite | K-Ar Bt |
| | Alunite | K-Ar Alu |

| | | |
|---|---|---|
| | Sanidine | K-Ar Snd |
| | Sericite | K-Ar Ser |
| | Amphibole | K-Ar Amph |
| | Feldspar | K-Ar Feld |
| | Glass or Matrix | K-Ar G/M |
| | Hornblende | K-Ar Hornb |
| | Muscovite | K-Ar Muscov |
| | Plagioclase | K-Ar Plag |
| | Ash or Pumice | K-Ar Ash/Pum |
| | Total rock | K-Ar Total Rock |
| | Organic material | K-Ar Organic mat |
| **Rubidium-Strontium** | Not given | Rb-Sr |
| | Biotite | Rb-Sr Bt |
| | Muscovite | Rb-Sr Muscov |
| | Glass or Matrix | Rb-Sr G/M |
| | Ash or Pumice | Rb-Sr Ash/Pum |
| | Mineral isochronology | Rb-Sr Min isochron |
| | Total rock | Rb-Sr Total Rock |
| **Surface Exposure** | | Surface Exposure |
| **Tephrochronology** | | Tephrochron |
| **Uranium-series** | | Uranium-series |
| **Uncertain** | | Uncertain |
| **Varve Count** | | Varve Count |
| **Uranium- Lead** | Zircon | U-Pb Zirc |

- *Data Uncertainty* (Figure 7-10) gives a qualitative indication of how reliable age records are depending on the dating method used.
  Homogenization of the data was needed, since several names existed referring to the same activity status (e.g., Fumarole = Fumarolic = Solfataric = Hot spring).

1. *Anthropology:* this class includes volcanoes with undated (but recent) activity described in aboriginal legends as well as activity dated by buried artefacts (Siebert et al., 2010).
2. *Dating techniques:* samples and units dated using any of the methodology listed in **Error! Reference source not found.**.
3. *Discredited eruptions:* eruptive events that, although once were established in the volcanological literature, they have later been discredited (Siebert et al., 2010).
4. *Fumarole:* characterises a volcano that has not had any eruption during the Holocene period, although shows thermal and superficial activity. Fumarole is a synonym of the Pleistocene, Pleistocene Geyser and Thermal features classifications assigned in previous editions of Volcanoes of the World (Siebert et al., 2010).

5. *Historical:* is a synonym of "active" an "erupting", assigned by other authors. It is used for eruptions that were documented during or shortly after the event.
6. *Holocene:* this group include volcanoes mapped as Holocene or Postglacial; it also includes those where the original author indicates uncertainty exists. Some subjectivity is involved, and inclusion may depend on the field experience of the original *author* (Siebert et al., 2010).
7. *Uncertain:* indicates the report of an historical eruption is of uncertainty validity (Siebert et al., 2010).

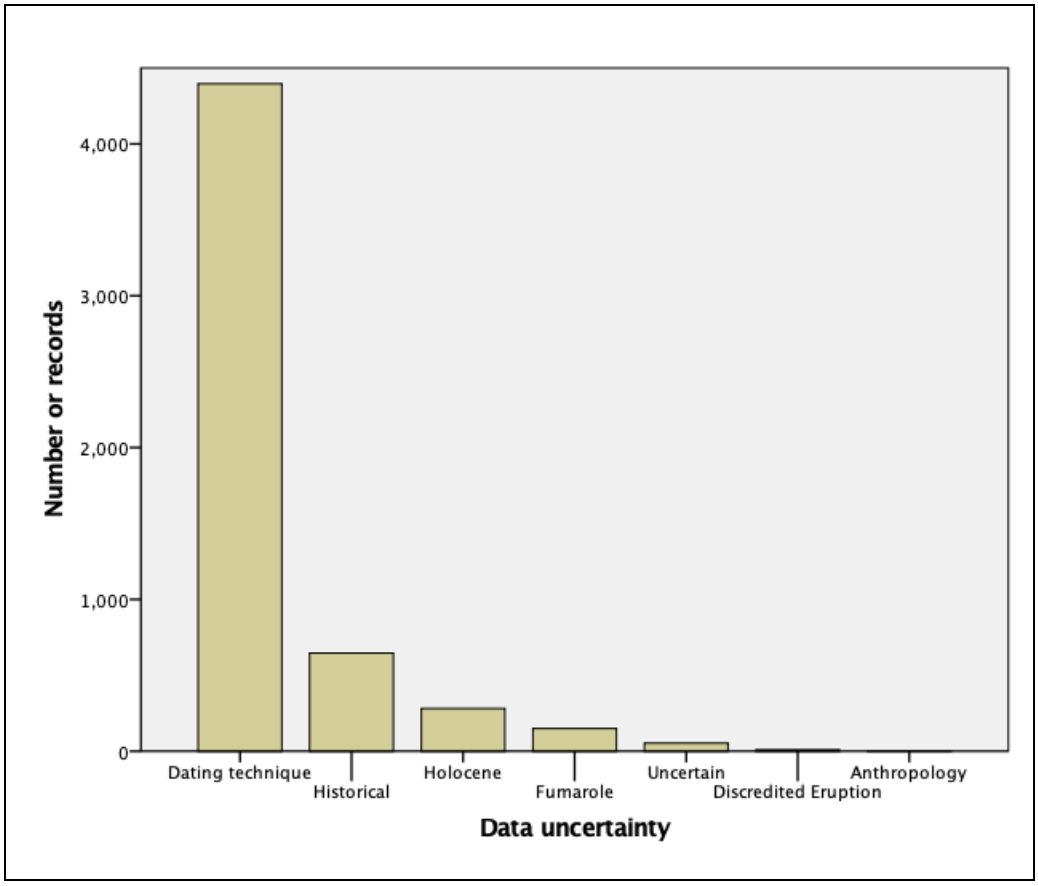


*Figure 7-10. Histogram showing categories of Data uncertainty field.*

### *7.1.1.5 Ignimbrite parameters*

Ignimbrite data were mainly extracted from four sources: Haschke et al. (2012), Guzmán et al. (2014), Brandmeier et al. (2016) and Crosweller et al. (2012) (LaMEVE DB). Except for Crosweller et al. (2012), who collected data worldwide, these studies focused their work on the ignimbrite flare-up in Northern Chile, Argentina and Southern Peru. Ignimbrite refers to both pyroclastic flow and pyroclastic surge deposits.

In order to calculate the deposit volume, Guzmán et al. (2014) used the areal extent of the deposits for assessment of the intensity of volcanic activity, assuming it is proportional to volume. They categorised the

data using Area ($km^2$), where large is >100 $km^2$, moderate is between 100–10 $km^2$ and small <10 $km^2$. In addition, they also used pumice volume (%) and crystal content (%).
All parameter values range between absent, low, moderate, and high according to the original source author.

- *IGN Welding degree*
  This property affects how well the pyroclastic material is conserved and how dense the rock is.

- *IGN Pumice content* indicates the volume (%) of pumice fragments contained in the rock, where high >30%, moderate is between 30–10% and low <10% (Guzmán et al., 2014).

- *IGN Crystal content* specifies the quantity of crystals confined to the unit. Categories are high (>30 vol.%), moderate (30–10 vol.%) and low content (<10 vol.%) (Guzmán et al., 2014).

- *IGN DRE Volume ($km^3$)* represents the unvesiculated erupted magma volume. It was extracted from literature or calculated by Crosweller et al. (2012) in the LaMEVE DB.

- *IGN Volume ($km^3$)* was extracted from literature or calculated by Crosweller et al. (2012) in the LaMEVE DB.

#### *7.1.1.6 Tectonic parameters*

- *Crust thickness*
  Thickness crust of >25km was extracted from the Smithsonian (SGVP) datasets, while thickness >50 km come from Thorpe (1984) (

  Figure *7-11*).

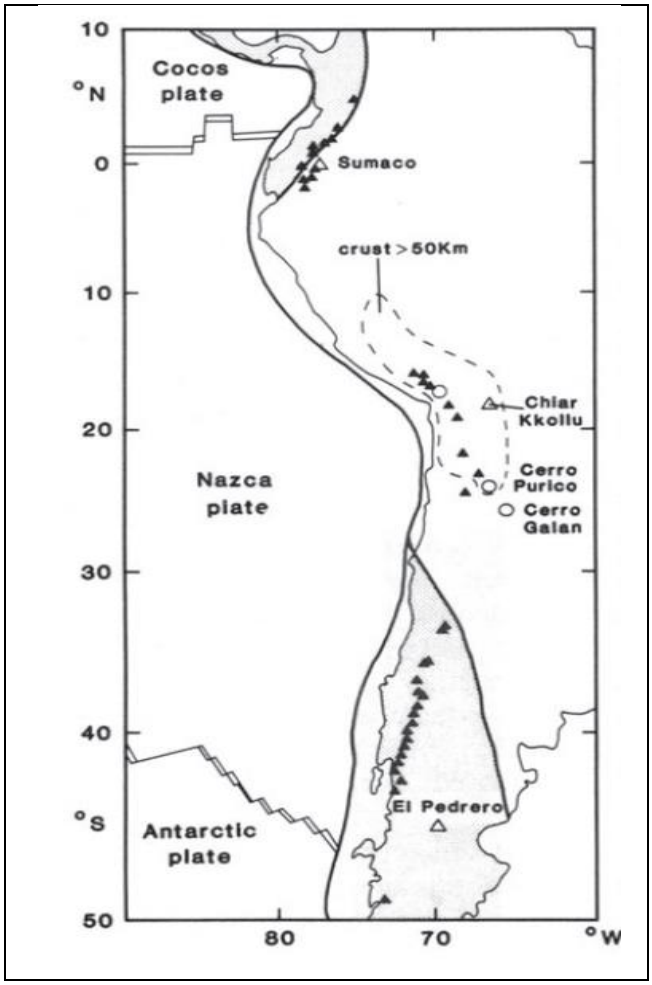


*Figure 7-11. Figure from Thorpe (1984) showing a map of western South America indicating the tectonic plates configuration related to active volcanism and the thickness of the crust.- ▲ - active calc-alkaline basalt-andesite, dacite volcanoes (MacDonald, 1972); - Δ - some alkaline volcanoes; - ○ - volcanic areas. The location of crust with thickness over 50 km is shown by a dotted line.*

- *Tectonic settings*

  The *Tectonic Map of South America* (Cordani et al., 2016) was used to establish which tectonic setting (Figure 7-12), each data point corresponds to and specify the codes used in the AVEDB. (**Error! Reference source not found.**).

| *a.* |
|---|

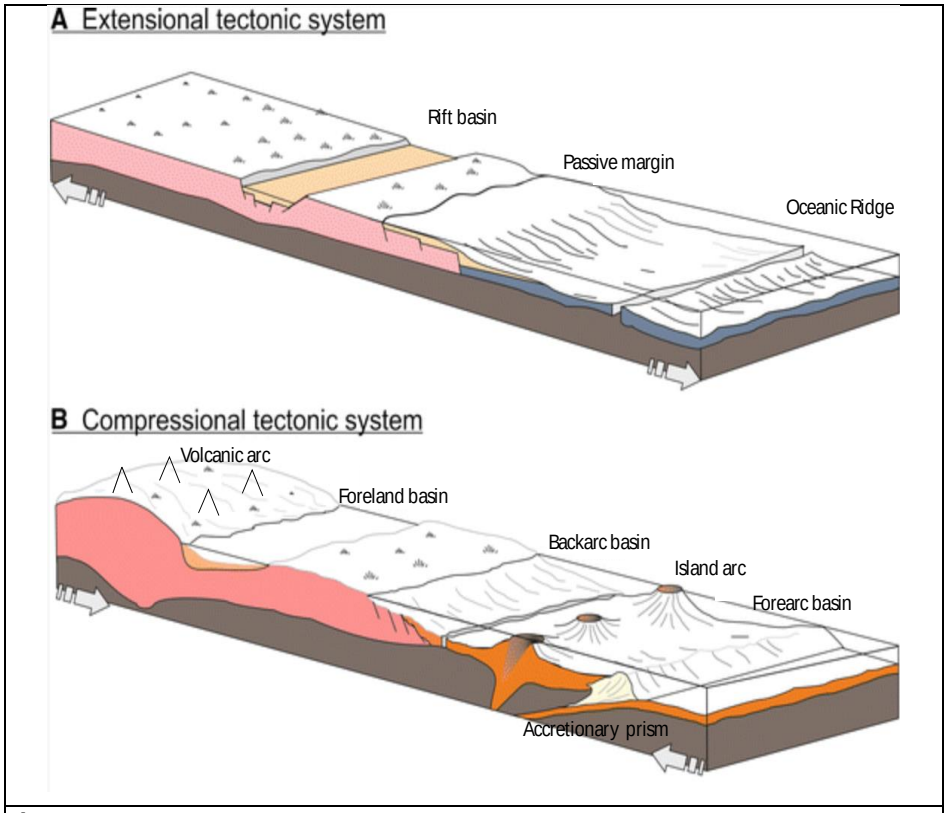


*b.*

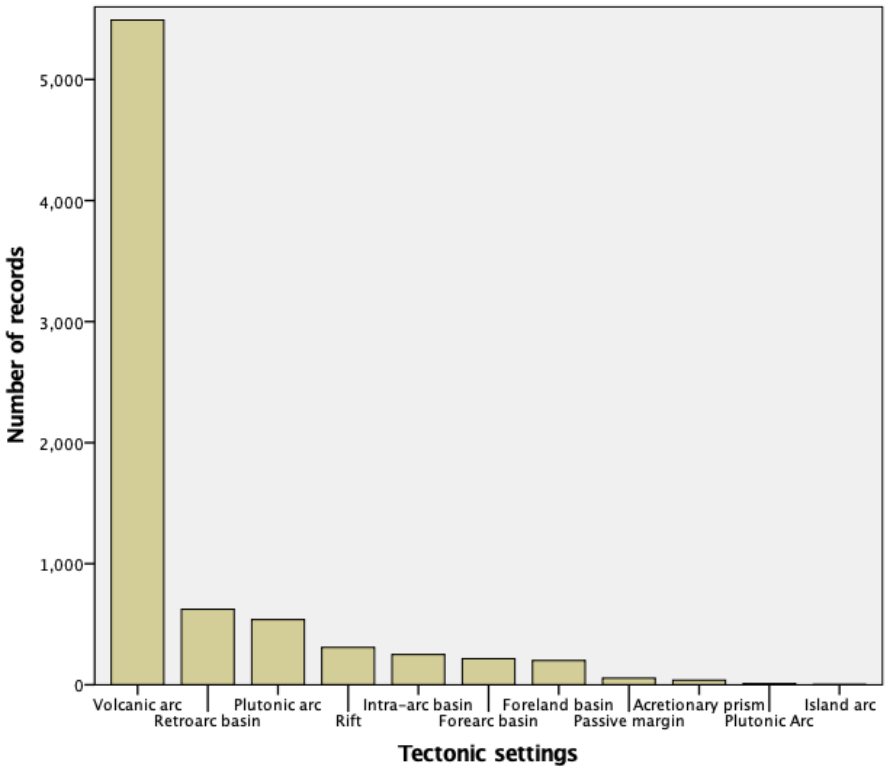


*Figure 7-12. a. Schematic of the basin types generated under the two main tectonic settings. Modified from Edlmann K. et al., 2015. b. Histogram of Tectonic settings where volcanoes and its deposits are spatial distributed.*

- *Tectonic margins*

  Tectonic margins describe the type of boundary between tectonic plates. For this study three are recognised (**Error! Reference source not found.**).

  - *Convergent boundary*
  - *Divergent boundary*
  - *Transform boundary*

*Table 7-8: Tectonic settings and margins.*

| Tectonic settings | Tectonic margins |
|---|---|
| Accretionary prism | Convergent boundary |
| Forearc basin | Convergent boundary |
| Foreland basin | Convergent boundary |
| Intra-arc basin | Convergent boundary |
| Island arc | Divergent boundary |
| Passive margin | Intraplate |
| Plutonic arc | Convergent boundary |
| Retroarc basin | Convergent boundary |
| Rift | Divergent boundary |
| Volcanic arc | Convergent boundary |

- *Volcanic zone*

  From the Cenozoic to present time and due to the subduction of the Nazca plate under South America, four main areas have been recognised where volcanism has developed, and volcanoes have distributed along the Andes. Those zones are: NVZ (Northern Volcanic Zone), which include northern Peru, Ecuador and Colombia and is located between 10ºN to 10ºS; CVZ (Central Volcanic Zone) from 10º- 28ºS, comprises southern Peru, northern Chile and southwestern Bolivia and Argentina; SVZ (Southern Volcanic Zone) in central Chile and Argentina between 32º to 45ºS. Finally, AVZ (Austral Volcanic zone) below 46°S.

  In addition to these volcanic zones, data were classified into different flat slab areas obtained from Jiashun H. et al. (2016) (Figure 7-13).

- *Volcanic Segments Wood*

  Nine volcanic segments were defined by Wood et al. (1987) within the CVZ area, eruptions and volcanoes were classified accordingly (A-I). (Figure 7-14a).

- *Tectonic Segments Sillitoe*

  Eruptions and volcanoes were classified according their locations between the 16 tectonic segments defined by Sillitoe (1974). (Figure 7-14b).

*a.*


*b.*

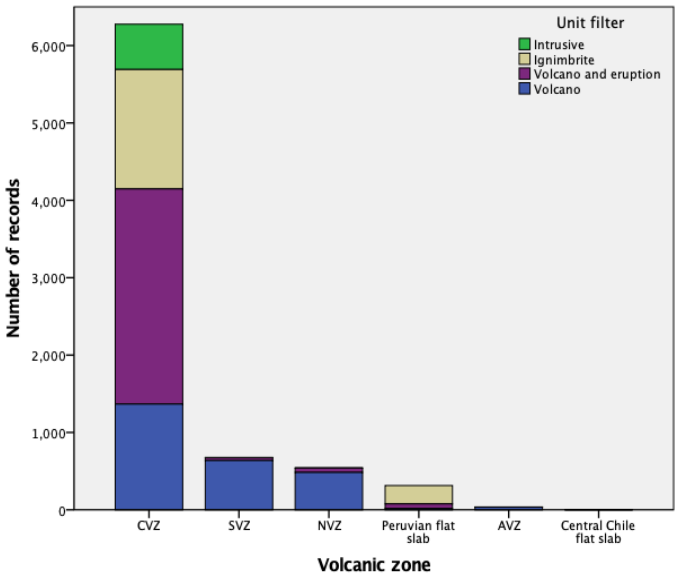


*Figure 7-13. Volcanic zones and flat slab areas present in the Andes showed in a. map of South America and b. histogram.*

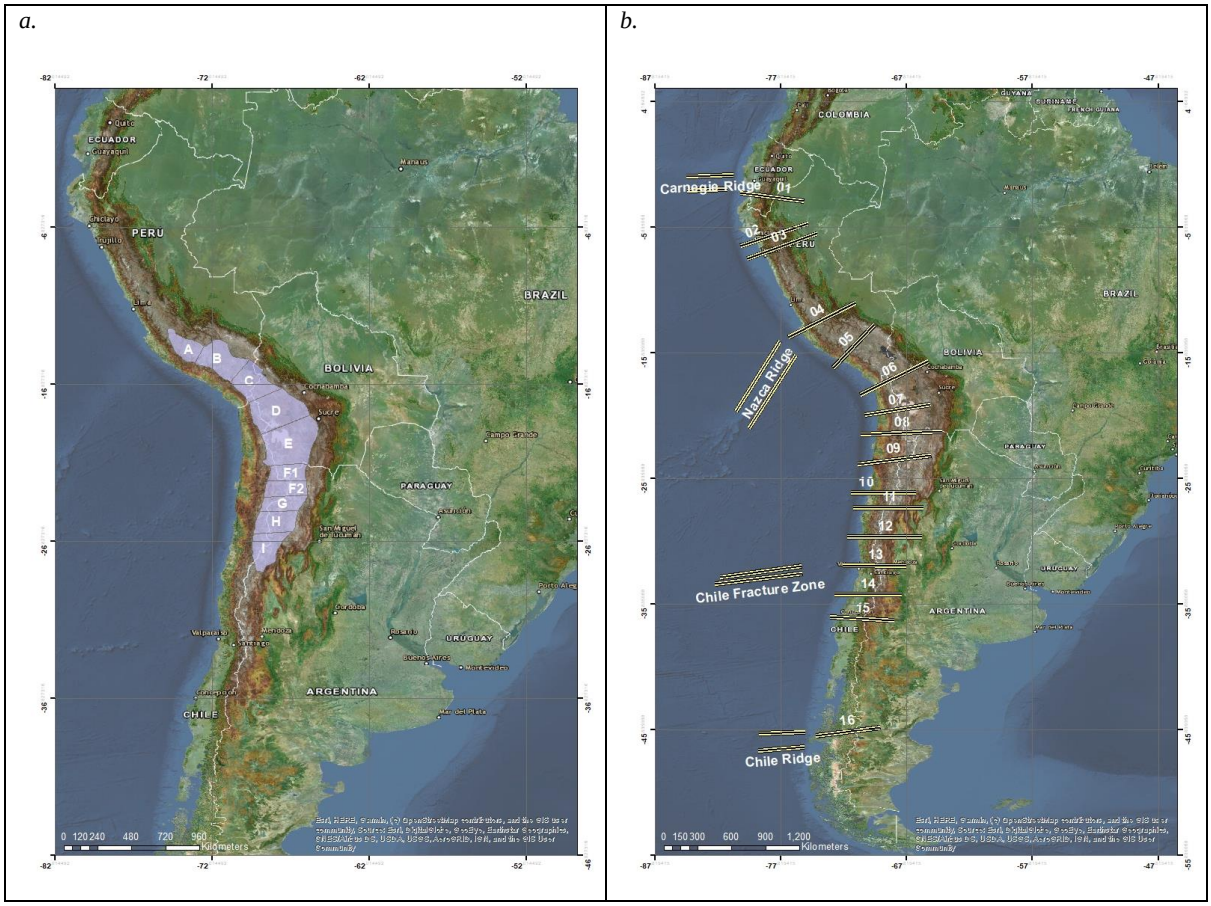


*Figure 7-14. a. Volcanic segments defined by Wood et al. (1987). b. Tectonic segments in the Andes, outlined by Sillitoe (1974).*

### *7.1.1.7 Morphotectonic provinces*

- *Geomorphology*

  Datapoints were classified according their location in the Andes, following a morphotectonic map from Ross (2015) (Figure 7-15).

*a.*

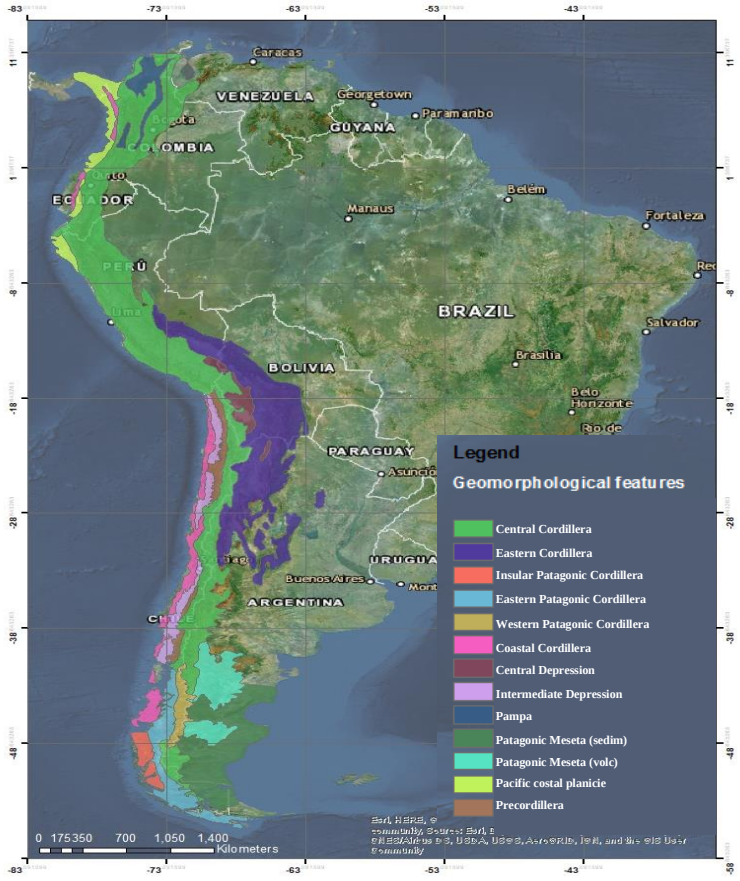


*b.*

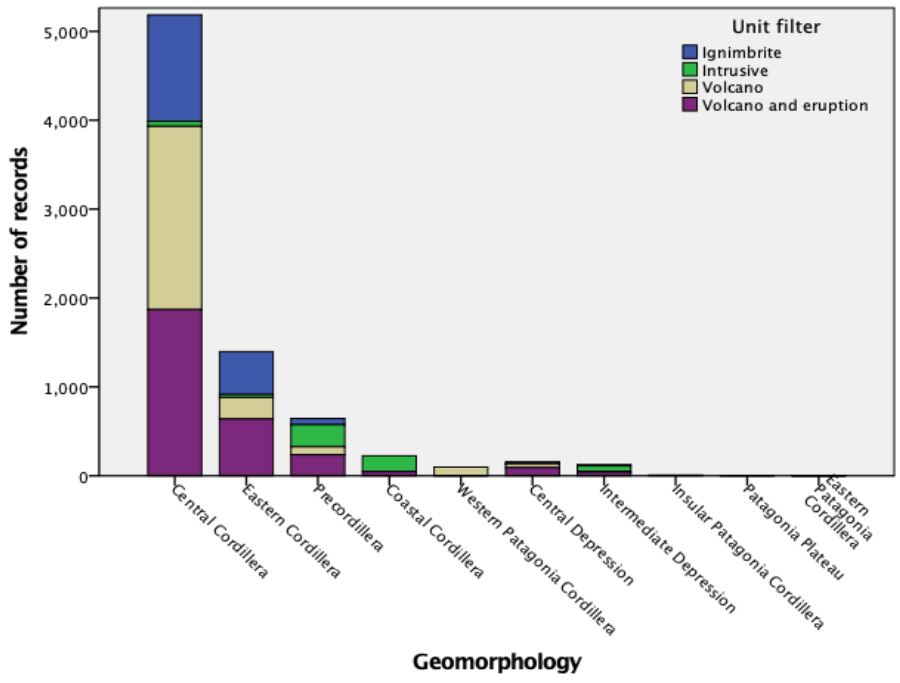


*Figure 7-15. Morphotectonic provinces in the Andes. a. Showed in a map modified from Ross J. L. S., 2015 and b. Histogram showing the distribution of the datapoints.*

- *Denudation Rate*

  Karátson et al. (2011), after performing morphometric modelling of volcanoes located in Central Volcanic zone, defined erosion patterns and erosion rates for volcanic edifices within different areas in the CVZ. Erosion rate is defined as the meters in height removed from a volcano edifice by erosion in a certain period of time in My. Since at least Late Miocene, typical erosion rates of 10-20 m/Ma have been obtained for the Altiplano–Puna Plateau. Every datapoint was classified according to values obtained by Karátson et al. (2010) (Figure 7-16).

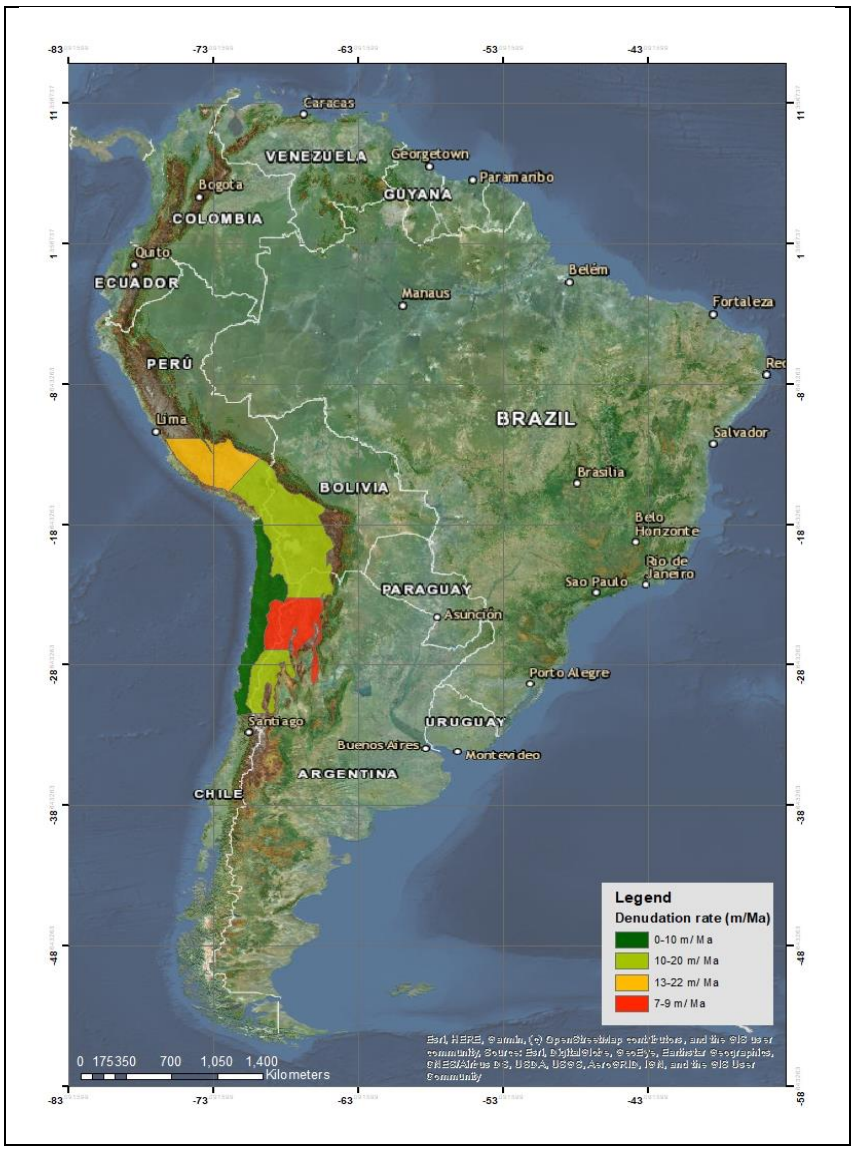


*Figure 7-16. Denudation rates mapped in ArcGIS from Karátson et al. (2011).*

- *Annual Precipitation (mm)* was extracted for each particular point (volcano/ sample) from a Raster image called CHELSA. The Climatologies at high resolution for the Earth's land surface (CHELSA) dataset includes high spatial resolution for monthly climatology of mean precipitation, including a period between 1979-2013. CHELSA is essentially a statistical downscaling of the precipitation

algorithm using geographic predictors (Figure 7-17a). These high-resolution pixel-based images count with a precipitation value for each point in the image and was obtained from: https://climatedataguide.ucar.edu/climate-data/chelsa-high-resolution-land-surface-temperature-and-precipitation.

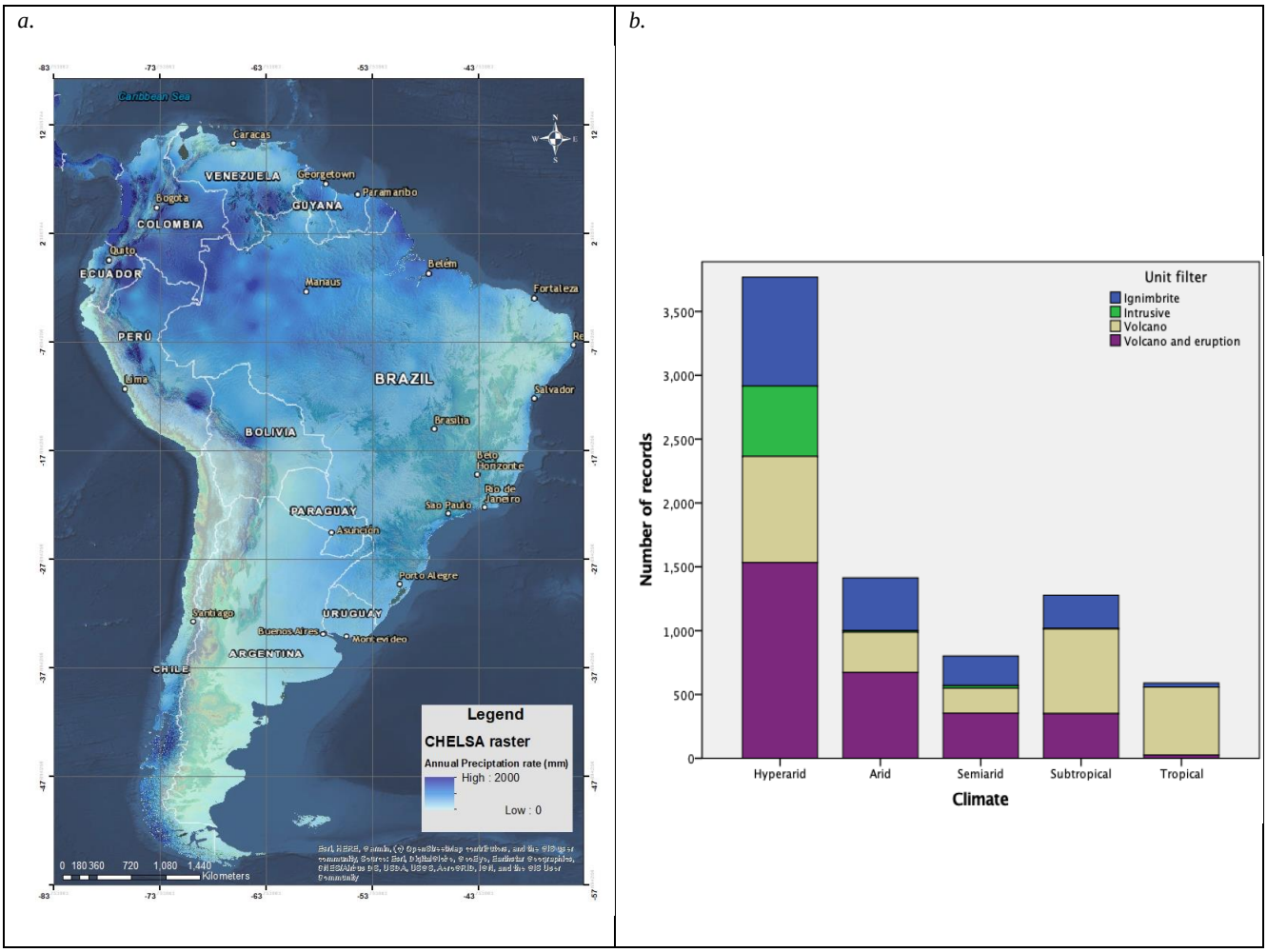


*Figure 7-17. a. CHELSA raster image showing modern annual precipitation (mm). b. Histogram of climate distribution according to the location of datapoints.*

- *Climate*

- *DEM values (m)*

  DEM stands for Digital Elevation Model. Elevation above sea level (m) was extracted for each datapoint (volcano/ sample) from a DEM raster image for South America (1km resolution). The software used was ArcGIS. If no elevation value was included in the DEM where a data point was located, ArcGIS did not assign an elevation value.

- *Slope (degrees)*

  Slope calculation was performed using ArcGIS software and the same DEM raster image used to extract elevation values. To calculate the slope, a 3 by 3 cell neighbourhood plane is fitted around each processing cell using the Least Squares Method (Figure 7-18a). Gradients vary between 0°-30° (Figure 7-18b).

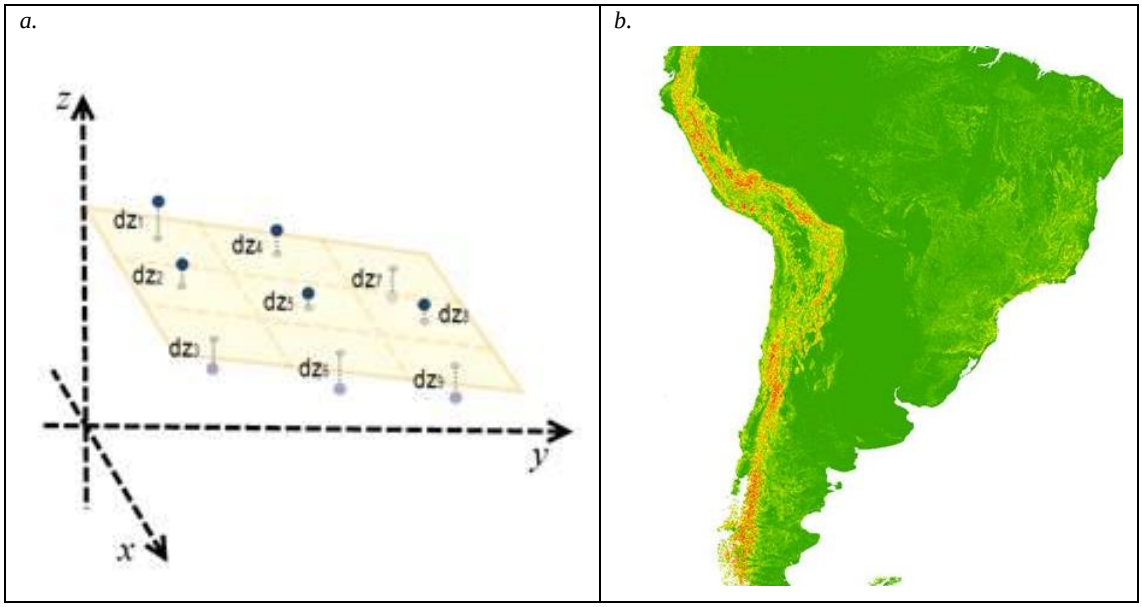


*Figure 7-18. a. Plane used to calculate slope where a 3 by 3 cell (elevation value) is fitted around each processing cell. b. Slope calculated raster image for South America.*

### *7.1.1.8 Sources*

This field show the provenances of the information feeding the Excel Master DB.

- *Source ArcGIS*

  Information in this field corresponds to data extracted from ArcGIS shapefiles and then adapted to fit in the master table.

- *Source*

  Represented by a short code, values correspond to published databases and literature from different authors. Table 2-1 show the codes and the name of the original study, along with the author's name and publication year.

- *Reference from source*

If any author included the references where information they used for their own compilation was extracted, it would be in this field.

- *Export date*
  Considering that online databases such as the Smithsonian ones or LaMEVE could be updated, the extraction date, month and year, is included here as a reference.

## 7.2 Appendix II

The Ignimbrite and Intrusive database (IIDB) is a compilation of ignimbrites and intrusive samples along the South American Andes extracted from diverse sources with a total of 2373 records. It is presented in Microsoft Excel format.

## 7.3 Appendix III

The Porphyry Copper Deposits dataset (PCDsDB) is the result of an extraction of the Cu Atlas BHP dataset. It includes a total of 593 PCDs, skarns and epithermal deposits, with Au, Mo and Cu as commodities, located in South America. It is presented in Microsoft Excel format.
Following, the explanation of the design of the dataset.

### 7.3.1 Database design

The PCDs dataset counts with 99 data fields.

#### *7.3.1.1 General fields*

- *Cu Atlas ID*
  Each record was assigned a unique identificatory number.
- *Property SNL ID*
  Samples collected in the field were assigned a name by each author.
- *Names: Main name, name2, name3*
  Each deposit is identified by a primary name, '*Main name'. S*ometimes, alternative names are provided.
- *Cluster name*
- *Location: Coordinates (Latitude DD, Longitude DD, SNL Coordinate accuracy, Distance from), Country, Region, and State/Province.*
  The first two fields specify the exact coordinates in the space where the deposit is located. It corresponds to WGS84 given in Decimal degrees (DD). *SNL Coordinate accuracy (exact,*

*approximate, best guess)*, states how accurate the location of the deposit is. This information has been extracted from SNL. *Distance from*, refers to the distance (km) from the main and closer cities. *Country*, records belong to 13 countries in America: Argentina, Brazil, Bolivia, Canada, Colombia, Chile, Ecuador, Haiti, Mexico, Nicaragua, Panama, Peru, USA and Venezuela.
*Region* has 2 categories: Latin America and Caribbean and United States and Canada.

#### *7.3.1.2 Sources*

This field show the provenances of the information feeding the Excel Master DB.

- *Info Source*
  Information in this field corresponds to data extracted from SNL (public data or subscription needed to access the system) or internal BHP data.
- *Validated BHP*
  If the information was validated by a geologist, the field will be filled with YES.
- *Last SNL Update*
  SNL is a platform being updated regularly, therefore information could change depending on the update date. For that reason, extraction date is included, on the following format DD/MM/YYYY.
- *SNL comments: SNL comments2, SNL comments3, SNL comments4*
  Different comments from SNL source, and in a variety of topics are added here.
- *SNL summary: SNL summa1, SNL summa2, SNL summa1*
  Contains a summary of the main technical characteristics of the deposit, such as host rock, alteration mineralization, depth, cover, etc.
- *Internal Comments: Internal Comments2*
  Similar to SNL comments, although in this case, comments and new information has been added by BHP geologists.
- *Data quality*
  Quality of extracted information may vary from excellent, very good, good, moderate, poor, very poor, no data, unreliable, unknown.
- *Literature reference: Literature ref2, Literature ref3*
  Extracted information count with different kind of sources: publications and reviews in journals, private and public reports, technical reports, websites, book, PhD thesis, SNL platform.

#### *7.3.1.3 Project details*

These fields state the characteristics of the project/ mine.

- *Project Stage* indicates how advanced into the Exploration/Production pipeline the project is. It could be at the beginning stage (*Satellite, Target outline, Grassroots, Exploration, Advanced Exploration*). It could be a growth project (*Prefeas/Scoping, Feasibility started, Feasibility,*

*Feasibility Complete*). It could be an advance project (*Reserves Development, Construction Planned, Construction Started, Expansion*) or the project could be already in operation (*Preproduction, Limited Production, Operating, Residual Production*) or a closed operation (*Closed*).

- *Owner (Owner name1, Owner name2, Owner name3, Owner Website)*
  Previous and actual owners of the projects/ assets and the current owner website.
- *Full Work History (Full Work History2, Full Work History 3, Full Work History4)* describes the whole history of the deposit, since its discovery to production stages, if any, including land information, owners, social and economic context, etc.
- *Discovery (Discovery year, Discovery method, Discovery method2, Discovery method3, Drilling method, Internal Fu)*
  Fields comprise all details related to the discovery of the deposit, including year, exploration techniques applied and drilling method (*DD*, stands for diamond drilling, *RC* stands for Reverse Circulation methodology).

#### *7.3.1.4 Deposit details*

The following fields hold the information regarding deposit and commodity type as long as production calculations per metal.

- *Deposit type*: porphyry deposits, epithermal and skarns.
- *Commodity: Primary Commodity, Other Commodities, Other Commodities2, Other Commodities3* refers to the metals extracted from the deposit. Includes: Cu, Au, Ag, Mo, Ni and Zn. Other commodities refer to sub- products resulting after the extraction of the primary commodity.
- *Production: Cu Production (tonnes), Au production (Kg), Mo Production (tonnes)* considers the total metal production in tonnes or Kg (depending on the commodity) during the beginning of extraction process, up to the dataset update date.
- *Resources and Reserves: Total Reserves (tonnes), Total Reserves and resources (tonnes), Cu grade (%), Au Grade (g/tn), Mo grade (%), Ag grade (g/tn), Contained Cu (tonnes), ASOFDATE* takes into consideration how much metal left to be mined is still in the deposit. The resources are what is proven whereas reserves are an estimation. In addition, grades for different metals are provided; this indicates how much metal there is (in percentage or as grams per tonne of extracted material).

#### *7.3.1.5 Geology details*

- *Geologic terrane* defines a specific belt with potential to hold mineralization within a region (i.e., Laramide).
- *Postmineral Cover* refers to the depth in metres of postmineral cover on top of the deposit.
- *Lithology (Host rock lithology, ore lithology)*

Host rock returns the lithology where the porphyry was intruded and the ore lithology refers to the porphyry itself.

- *Alteration: Main Hypogene Alteration and Other Hypogene Alteration.*
- *Veins: Main veins and Other veins.*
- *Mineralization mineralogy: Hypogene Cu mineral, Supergene Cu mineral, Oxide Cu mineral.*
- *Mineralization: Dominant mineralization type, type of enrichment.*
- *Structural Geology: Local structures, Local structure orientation, Regional structural, Regional structural orientation.*

#### *7.3.1.6 Ages and dating*

- *Age Range* states the age range of the ore deposit.
- *Mineral Systems: Mineral system1 Age, Mineral system1 Method, Mineral system1 Mineral*
  These fields describe in detail methodologies applied to obtain ages, mineral dated and genetical process to be dated (*Alteration, Hypogene Alteration, Intermineral porphyry, Late Porphyry, Mineralised intrusion, Mineralization*).

## 7.4 Appendix IV

This dataset is the result of the combination between the AVEDB, IIDB and PCDs datasets. It contains: 1239 volcanoes, 507 PCDs and epithermal deposits, and finally, 18 dated ignimbrite deposits extracted from the IIDB, that resulted from eruptions from active volcanoes. It is presented in Microsoft Excel format and it is called *Descriptive_Stats_Height1239+BHPPCDsEpith*.

## 7.5 Appendix V

These 4 datasets are subsets of the AVEDB after filtering and eliminating duplicated values. It contains only one volcano dimension parameter value per volcanic edifice. They are presented in Microsoft Excel format and are called:

i. *Descriptive Stats_Height_1239records*: 1239 volcanoes with height values,
ii. *Descriptive Stats_VolcVolume_1139records*: 1139 volcanic edifices with volcano volume records,
iii. *Descriptive Stats_ConeDiam_1162records*: 1162 volcanoes with cone diameter information and
iv. *Descriptive Stats_CratDiam_1162records*: 1162 edifices with crater diameters.